



City Research Online

City, University of London Institutional Repository

Citation: Gargaro, R.J. (1991). Thermally-driven shallow cavity flows. (Unpublished Doctoral thesis, City, University of London)

This is the accepted version of the paper.

This version of the publication may differ from the final published version.

Permanent repository link: <https://openaccess.city.ac.uk/id/eprint/28500/>

Link to published version:

Copyright: City Research Online aims to make research outputs of City, University of London available to a wider audience. Copyright and Moral Rights remain with the author(s) and/or copyright holders. URLs from City Research Online may be freely distributed and linked to.

Reuse: Copies of full items can be used for personal research or study, educational, or not-for-profit purposes without prior permission or charge. Provided that the authors, title and full bibliographic details are credited, a hyperlink and/or URL is given for the original metadata page and the content is not changed in any way.

Thermally-driven shallow cavity flows

R.J. Gargaro

A thesis submitted for the degree of
Doctor of Philosophy

City University
Department of Mathematics
London

29th March 1991

Abstract

Buoyancy driven flows in enclosures, due to temperature gradients, have been studied since the eighteenth century for both scientific and practical reasons alike. Thus numerous analytical, numerical and experimental studies of two-dimensional rectangular cavities have been undertaken. A simple generic problem has been studied in order to make progress in understanding the physical nature of these motions. In such cavity flows, three parameters are found to be important, a Rayleigh number R based on the height of the cavity and the temperature difference across the end walls, the Prandtl number σ of the fluid and the aspect ratio (length/height).

Thermal convection in a shallow laterally heated cavity with conducting boundaries is considered in Chapter 2. The companion problem for adiabatic boundaries is studied in Chapter 3. Chapters 4-7 are concerned with the boundary-layer structure that emerges near the ends of the cavity as the Rayleigh number increases. On the horizontal walls two stages of development are identified, a horizontal boundary layer where the flow is independent of the temperature field and a longer scale on which buoyancy becomes significant. The horizontal boundary layer is considered in Chapters 4 and 5 and the horizontal buoyancy layer is studied in Chapters 6 and 7.

Contents

		Page
Chapter 1	Introduction	1
Chapter 2	Thermal convection in a shallow laterally heated cavity with conducting boundaries	7
	2.1 Introduction	7
	2.2 Formulation of the problem	8
	2.3 Core region	11
	2.4 End region	12
	2.5 Numerical results	15
	2.6 Asymptotic results for large R_1	16
	2.7 Discussion	21
Chapter 3	Thermal convection in a shallow laterally heated cavity with adiabatic boundaries	32
	3.1 Introduction	32
	3.2 Formulation and the solution for $R_1 = R/L = O(1)$	33
	3.3 The end zone structure for $R_1 \gg 1$	37
	3.4 Solution to the vertical boundary layer equation	40
	3.5 Separation of the vertical boundary layer	42
	3.6 Outer structure and horizontal layers	44
Chapter 4	The horizontal boundary layer $x = O(1)$: asymptotic solution	57
	4.1 Introduction	57
	4.2 Formulation	57
	4.3 Solution for small x	59
	4.4 Solution for large x	67

Chapter 5	The horizontal boundary layer $x = 0(1)$: numerical solution	82
	5.1 Introduction	82
	5.2 Solution for $0 < x < 1$	82
	5.3 Solution for $x > 1$	88
	5.4 Summary and comparison with analytical results	91
Chapter 6	The horizontal buoyancy layer $x = 0(R_1^{2/5})$: asymptotic solution	122
	6.1 Introduction	122
	6.2 Formulation	122
	6.3 Solution for small x_3	125
	6.4 Solution for large x_3	135
	6.5 Summary	137
Chapter 7	The horizontal buoyancy layer $x = 0(R_1^{2/5})$: numerical solution	156
	7.1 Introduction	156
	7.2 Solution for $0 < x_3 < 1$	156
	7.3 Solution for $x_3 > 1$	160
	7.4 Numerical results	163
	7.5 Discussion	168
Appendix 1	Numerical scheme for the vertical boundary-layer equations	245
Appendix 2	Numerical scheme for the horizontal boundary-layer $x < 1$	250
Appendix 3	Numerical scheme for the horizontal boundary-layer $x > 1$	256
Appendix 4	Numerical scheme for the buoyancy layer $x_3 < 1$	260
Appendix 5	Numerical scheme for the buoyancy layer $x_3 > 1$	265

CHAPTER 1

Introduction

Convective motions driven by temperature gradients not aligned with the gravitational field were first studied in connection with large-scale geophysical disturbances (Hadley (1735); Jeffreys (1925); Defant (1961); Stern (1975)). The lateral extent of the flow is a key factor in many modern applications including certain crystal growing techniques (Hurle (1966); Hurle et al (1974); Gill (1974)), cooling systems for nuclear reactors (Boyack and Kearney (1972)), dispersion of pollutants in river estuaries (Cormack et al (1974a)), and in solar energy collectors (Bejan and Rossie (1981)).

Due to the wide range of applications, a simple generic problem has been studied in order to make progress in understanding the physical nature of these motions. Numerous analytical, numerical and experimental studies of two dimensional rectangular cavities have been undertaken where the flow is driven by heating from the side. Typically the sidewalls are held at different constant temperatures. Reviews of the work have been reported by Catton (1978) and Ostrach (1972).

In two-dimensional cavity flows, three parameters are important, a Rayleigh number R based on the height of the cavity and the temperature difference across the end walls, the Prandtl number σ of the fluid and the aspect ratio L (length/height).

Cavity flows driven by lateral heating have been investigated experimentally by Rossby (1965), Imberger (1974), Ostrach et al (1980), Bejan et al (1981), Simpkins and Dudderar (1981) and Simpkins and Chen (1986). In these flows driven by

horizontal temperature gradients the fluid near the hot wall becomes less dense causing it to rise and flow across the upper half of the cavity to the top of the cold wall. There it cools and descends to the bottom of the wall, and it then completes the circuit along the bottom half of the cavity. For the simplest thermal boundary conditions, the movement of fluid around the cavity is achieved in such a way that there is an odd symmetry about the centre (Gill 1966). Numerical studies of this motion have been discussed, for example, by Quon (1972), Cormack et al (1974b), Shiralkar and Tien (1981) and Kuo et al (1986).

Much of the analytical work on these flows is based on Gill's (1966) paper, where it was first shown that for high Rayleigh numbers and finite aspect ratios, boundary layers on the end walls give rise to a stratified core region, in accordance with earlier experimental studies in tall cavities (Eckert and Carlson (1961), Elder (1965)). Gill derived an approximate solution to the boundary layer equations using a modified Oseen method with the mass flux in layers adjacent to the horizontal surfaces vanishingly small. This assumption known as the 'mass-flux hypothesis' was questioned by Quon (1972, 1977). Modifications to the core flow structure when the mass-flux hypothesis is relaxed have been discussed by Blythe and Simpkins (1977). Recent numerical calculations (Winters (1983), Haldenwang and Labrosse (1986), Gaskell and Wright (1987)) suggested that the mass flux hypothesis may be incorrect for a Newtonian fluid, although consistent asymptotic structures have been found for porous media (Blythe, Daniels and Simpkins 1981, 1982). Experiments by Bejan et al (1981) for relatively shallow cavities revealed that in the boundary layer regime $R \gg 1$, intrusion jets adjacent to the horizontal boundaries penetrated the core

from the trailing edges of the end walls (the bottom of the cold wall, the top of the hot wall) where there were also 'sharp temperature gradients. The central region of the core, sandwiched between these intrusion jets, was found to be almost stagnant. A later experiment by Simpkins and Chen (1986) confirmed Bejan's result and thus an alternative structure to the mass-flux hypothesis was suggested, with all the fluid entrained in the vertical boundary layer being expelled into jets on the horizontal surfaces of the cavity, leaving an almost stagnant core.

For a shallow cavity and Rayleigh numbers $R \ll L$ flow throughout the cavity consists of a Hadley cell driven by the constant horizontal temperature gradient set up between the end walls (Cormack et al 1974a). Non-linear convective effects first become significant at the ends of the cavity where the flow is turned when $R_1 = R/L = O(1)$. For small σ in this limit the Hadley cell is susceptible to a variety of instabilities (Hart 1972). For Rayleigh numbers greater than some critical value $R_1 = R_{1c}(\sigma)$ the parallel core flow is destroyed and replaced by stationary multiple cells (Daniels et al 1987). This stationary transverse mode of instability forms an integral part of the steady motion in the cavity, appearing as an imperfect bifurcation of the nonlinear flow in the end regions. The ensuing motion is difficult to treat analytically because the nonlinear effects become important throughout the cavity for $R_1 > R_{1c}(\sigma)$. Daniels et al (1987) showed that this type of behaviour occurs for $\sigma \leq 0.12$ for a cavity with insulated horizontal walls. For cavities with conducting horizontal walls this behaviour is relevant for $\sigma \leq 0.27$ and is discussed in Chapter 2. For large

Prandtl numbers the question remains as to what form the basic steady motion takes as $R_1 \rightarrow \infty$. The main purpose here is to find the form of the end-zone solution near the cold wall as $R_1 \rightarrow \infty$. An integral constraint has important consequences for the flow structure, involving an unusually large constant contribution $O(L^{-1}R_1^{7/5})$ to the local temperature field, in order to maintain the necessary heat balance. This in turn leads to the suggestion, alluded to earlier, of a structure rather different from the 'mass-flux hypothesis' structure, with all the fluid entrained by vertical boundary layers expelled into wall jets on the horizontal surfaces of the cavity.

The plan of the thesis is as follows. Chapter 2 investigates the structure of the flow in a shallow cavity driven by lateral heating which has conducting boundaries. The range of Prandtl numbers and Rayleigh numbers for which multicellular convection occurs is determined, as is the lateral extent of the end zones for general Prandtl numbers, σ , and Rayleigh numbers, R_1 .

Chapter 3 describes the corresponding flow structure when the horizontal boundaries are insulated. The structure of the end-zone as $R_1 \rightarrow \infty$ is considered in detail, in particular a vertical boundary layer on the end wall. The susceptibility of this vertical boundary layer to separate from the end wall is discussed suggesting a possible way in which the isotherms and streamlines in the vertical boundary layer are carried around into a horizontal boundary layer. A complete asymptotic description of the corner is not attempted due to its likely complexity.

Chapter 4 formulates the problem for the horizontal boundary layer, or wall jet, where the horizontal coordinate x is comparable with the cavity height. The solution for small x , where the flow has to adjust to the new temperature condition on the insulated horizontal surface, is described. The large x solution is also found, extending the work of Glauert (1956) to include the temperature field.

Chapter 5 contains the full numerical solution of the $x = 0(1)$ region. The numerical scheme is based on the asymptotic structures described in Chapter 4, incorporating the work of Smith (1974), but extending it to include temperature.

As x increases the flow enters a new regime when $x = 0(R_1^{2/5})$ and the buoyancy term, absent to a first approximation in the $x = 0(1)$ region, reappears in the vorticity equation. In Chapter 6 asymptotic solutions are found for small x_3 and large x_3 , where x_3 is the horizontal boundary layer coordinate for this region. Buoyancy couples the vorticity and heat equations and the jet structure in the $x = 0(1)$ region develops into a boundary layer with a forcing velocity at the outer edge of the layer. The problem is now dependent on two parameters, the Prandtl number σ and the effective forcing velocity ϵ , a consequence of the recirculating inviscid zone above the horizontal boundary layers. It is shown that buoyancy produces an adverse pressure gradient whose effect becomes apparent downstream as the inertial and viscous terms weaken, and reverse flow is predicted to occur for certain ranges of σ and ϵ .

Chapter 7 contains a numerical investigation of the boundary layer analysed in Chapter 6. It is shown that for only a restricted range of ϵ is a straightforward development downstream possible. For low values of ϵ , a singularity is seen to develop in the boundary layer leading to the breakdown of the numerical scheme. The implication for the overall structure of the flow in the cavity is discussed in the final section.

CHAPTER 2

Thermal convection in a shallow laterally heated cavity with conducting boundaries

2.1 Introduction

This chapter investigates the structure of the flow in a two dimensional rectangular cavity driven by lateral heating. The end walls are maintained at fixed but different temperatures which generate steady two dimensional motions within the cavity. The horizontal boundaries are assumed to be conducting. The companion problem for insulated boundaries has already been discussed by Daniels et al (1987).

The aspect ratio L is assumed to be large so that the cavity is shallow while the Rayleigh number R based on height is $O(L)$. In this range nonlinear effects become significant in the end zones. For $R \ll L$ the flow is conduction - dominated everywhere with a parallel two-way flow generated throughout most of the cavity by a linear temperature field set up between the vertical end walls. The local solution near the vertical walls satisfies the full nonlinear Boussinesq equations when $R_1 = O(1)$ and involves eigensolutions that generally decay away into the core region; these eigensolutions are involved in turning the flow in the end region, but one is associated with a stationary transverse mode of instability (Hart (1972), (1983a)) which can present itself at low Prandtl numbers. The parallel core flow is then destroyed by this spatial oscillation, and as the Rayleigh number increases the instability is forced into the system as a smooth transition emanating from the ends of the cavity. This chapter determines the overall flow structure in the cavity and the range of Prandtl numbers and Rayleigh numbers for which this

imperfect bifurcation occurs. It also determines the lateral extent of the end zones for general Prandtl numbers and Rayleigh numbers. A complete numerical solution of the nonlinear end zone problem has not been attempted.

2.2 Formulation of the problem

The flow domain is a rectangular cavity of height h and length l . The end walls are maintained at fixed but different temperatures which generate steady two dimensional motions within the cavity. The governing equations for the flow, taking buoyancy into consideration, are the Navier-Stokes equations,

$$u^* \frac{du^*}{dx^*} + w^* \frac{dw^*}{dz^*} = -\frac{1}{\rho^*} \frac{dp^*}{dx^*} + \nu \left(\frac{d^2 u^*}{dx^{*2}} + \frac{d^2 u^*}{dz^{*2}} \right) \quad (2.2.1)$$

$$u^* \frac{dw^*}{dx^*} + w^* \frac{dw^*}{dz^*} = -\frac{1}{\rho^*} \frac{dp^*}{dz^*} + \nu \left(\frac{d^2 w^*}{dx^{*2}} + \frac{d^2 w^*}{dz^{*2}} \right) - g \quad (2.2.2)$$

the heat equation,

$$u^* \frac{dT^*}{dx^*} + w^* \frac{dT^*}{dz^*} = \kappa \left(\frac{d^2 T^*}{dx^{*2}} + \frac{d^2 T^*}{dz^{*2}} \right) \quad (2.2.3)$$

and the continuity equation

$$\frac{d}{dx^*} (\rho^* u^*) + \frac{d}{dz^*} (\rho^* w^*) = 0 \quad (2.2.4)$$

where (x^*, z^*) are Cartesian co-ordinates, x^* in the direction along the horizontal boundaries and z^* in the direction up the end walls with the origin at the bottom of the cold wall ($x^* = 0$). u^* and w^* are the velocity components in the directions x^* and z^* respectively and T^* is the temperature with $T^* = T_0^*$ on the cold wall; p^* is the pressure, ρ^* is the density, ν is the kinematic viscosity, κ is the thermal diffusivity and g is the acceleration due to gravity (see figure 2.1). It is assumed that

$$\rho^* = \rho_0 (1 - \beta(T^* - T_0^*)) \quad (2.2.5)$$

where ρ_0 is the density at $T^* = T_0^*$ and β is the coefficient of thermal expansion. In line with the Oberbeck-Boussinesq approximation the variation of density with temperature is assumed to only affect the buoyancy term in (2.2.2).

Re-scaling the variables as follows

$$u^* = \bar{u} \frac{K}{h}, w^* = \bar{w} \frac{K}{h}, T^* = T_0^* + \bar{T} \Delta T', x^* = \bar{x} h, z^* = \bar{z} h, p^* = \bar{p} - \rho_0 g z^* + \rho_0 \frac{K^2}{h^2} \bar{p} \quad (2.2.6)$$

where $T_0^* + \Delta T'$ is the temperature of the hot wall, equations (2.2.1)-(2.2.4) become

$$\bar{u} \frac{d\bar{u}}{d\bar{x}} + \bar{w} \frac{d\bar{u}}{d\bar{z}} = -\frac{d\bar{p}}{d\bar{x}} + \sigma \left(\frac{d^2 \bar{u}}{d\bar{x}^2} + \frac{d^2 \bar{u}}{d\bar{z}^2} \right) \quad (2.2.7)$$

$$\bar{u} \frac{d\bar{w}}{d\bar{x}} + \bar{w} \frac{d\bar{w}}{d\bar{z}} = -\frac{d\bar{p}}{d\bar{z}} + \sigma \left(\frac{d^2 \bar{w}}{d\bar{x}^2} + \frac{d^2 \bar{w}}{d\bar{z}^2} \right) + \sigma R \bar{T} \quad (2.2.8)$$

$$\frac{d\bar{u}}{d\bar{x}} + \frac{d\bar{w}}{d\bar{z}} = 0 \quad (2.2.9)$$

$$\bar{u} \frac{d\bar{T}}{d\bar{x}} + \bar{w} \frac{d\bar{T}}{d\bar{z}} = \frac{d^2 \bar{T}}{d\bar{x}^2} + \frac{d^2 \bar{T}}{d\bar{z}^2} \quad (2.2.10)$$

By eliminating the pressure from (2.2.7) and (2.2.8) and by introducing a stream function $\bar{\psi}$ defined by

$$\bar{u} = \frac{d\bar{\psi}}{d\bar{z}}, \quad \bar{w} = -\frac{d\bar{\psi}}{d\bar{x}} \quad (2.2.11)$$

equations (2.2.7)-(2.2.10) may be reduced to

$$\bar{\nabla}^4 \bar{\psi} - R \frac{d\bar{T}}{d\bar{x}} = \frac{1}{\sigma} \frac{d(\bar{\nabla}^2 \bar{\psi}, \bar{\psi})}{d(\bar{x}, \bar{z})} \quad (2.2.12)$$

$$\bar{\nabla}^2 \bar{T} = \frac{d(\bar{T}, \bar{\psi})}{d(\bar{x}, \bar{z})} \quad (2.2.13)$$

where $\bar{\nabla}^2$ is the Laplacian operator.

The non-dimensional parameters are the Prandtl number

$$\sigma = \frac{\nu}{\kappa} \quad (2.2.14)$$

and the Rayleigh number

$$R = \frac{\beta g \Delta T' h^3}{\nu K} \quad (2.2.15)$$

The rigid walls are impermeable and at constant temperature so that

$$\bar{\Psi} = \frac{d\bar{\Psi}}{d\bar{x}} = \bar{T} = 0 \quad \text{on } \bar{x} = 0 \quad (2.2.16)$$

and

$$\bar{\Psi} = \frac{d\bar{\Psi}}{d\bar{x}} = 0, \quad \bar{T} = 1 \quad \text{on } \bar{x} = L \quad (2.2.17)$$

where

$$L = l/h \quad (2.2.18)$$

is the cavity aspect ratio. The horizontal walls are rigid and conducting, so that

$$\bar{\Psi} = \frac{d\bar{\Psi}}{d\bar{z}} = 0, \quad \bar{T} = \frac{\bar{z}}{L} \quad \text{on } \bar{z} = 0, 1. \quad (2.2.19)$$

Gill (1966) noted that the governing equations and boundary conditions possess the centrosymmetry properties

$$\begin{aligned} \bar{\Psi}(\bar{x}, \bar{z}; L, R, \sigma) &= \bar{\Psi}(L-\bar{x}, 1-\bar{z}; L, R, \sigma), \\ \bar{T}(\bar{x}, \bar{z}; L, R, \sigma) &= 1 - \bar{T}(L-\bar{x}, 1-\bar{z}; L, R, \sigma), \end{aligned} \quad (2.2.20)$$

which allows half the flow domain to be considered.

This chapter is concerned with the limit $L \rightarrow \infty$ such that

$$R_1 = R/L = O(1) \quad (2.2.21)$$

for which the flow contains strong nonlinear effects in end regions near the vertical walls.

2.3 Core region

Away from the ends of the cavity appropriate independent variables are

$$\xi = \bar{x}/L, \quad z = \bar{z} \quad (2.3.1)$$

Expanding formally the stream function and the temperature,

$$\bar{\psi}(\bar{x}, \bar{z}; R_1, L, \sigma) = \bar{\psi}_0(\xi, z; R_1, \sigma) + L^{-1} \bar{\psi}_1(\xi, z; R_1, \sigma) + O(L^{-2})$$

$$\bar{T}(\bar{x}, \bar{z}; R_1, L, \sigma) = \bar{T}_0(\xi, z; R_1, \sigma) + L^{-1} \bar{T}_1(\xi, z; R_1, \sigma) + O(L^{-2}) \quad (2.3.2)$$

and substituting into (2.2.13) gives at $O(1)$,

$$\frac{d^4 \bar{\psi}_0}{dz^4} - R_1 \frac{d\bar{T}_0}{d\xi} = 0 \quad (2.3.3)$$

$$\frac{d^2 \bar{T}_0}{dz^2} = 0. \quad (2.3.4)$$

The use of Gill's centrosymmetry relations and the boundary conditions (2.2.17) gives

$$\bar{T}_0 = \xi, \quad \bar{\psi}_0 = \frac{R_1}{24} z^2 (1-z)^2. \quad (2.3.5)$$

At $O(L^{-1})$ using the expressions found for \bar{T}_0 and $\bar{\psi}_0$

$$\frac{d^2 \bar{T}_1}{dz^2} = \frac{R_1}{12} z(1-z)(1-2z) \quad (2.3.6)$$

$$\frac{d^4 \bar{\psi}_1}{dz^4} = R_1 \frac{d\bar{T}_1}{d\xi}. \quad (2.3.7)$$

Using the same conditions as above gives

$$\bar{\psi}_1 = 0, \quad \bar{T}_1 = R_1 \left(\frac{z^5}{120} - \frac{z^4}{48} + \frac{z^3}{72} - \frac{z}{720} \right). \quad (2.3.8)$$

Further terms associated with inverse powers of L in (2.3.2) are zero so that

$$\bar{\psi} = R_1 F(z), \quad \bar{T} = \xi + L^{-1} R_1 G(z) \quad (2.3.9)$$

to within corrections which are exponentially small as $L \rightarrow \infty$

(see Section 2.4) and where $F(z) = \frac{z^2}{24}(1-z)^2$ and

$$G(z) = \frac{z^5}{120} - \frac{z^4}{48} + \frac{z^3}{72} - \frac{z}{720}. \quad (2.3.10)$$

The results (2.3.9) are only valid if a consistent solution can be found in end-regions near each vertical wall. Regions in (R_1, σ) parameter space for which parallel core structures exist are determined in later sections.

2.4 End Region

At each end of the cavity is an approximately square region in which the flow is turned. The flow has a structure near $\bar{x} = 0$ defined by

$$\begin{aligned} \bar{\psi}(\bar{x}, \bar{z}; R_1, L, \sigma) &= \Psi(x, z; R_1, \sigma) + \dots \\ \bar{T}(\bar{x}, \bar{z}; R_1, L, \sigma) &= L^{-1} T(x, z; R_1, \sigma) + \dots \end{aligned} \quad (2.4.1)$$

where

$$x = \bar{x}, \quad z = \bar{z}. \quad (2.4.2)$$

ψ and T satisfy (2.2.12) and (2.2.13) with (ψ, T, x, z, R_1) replacing $(\bar{\psi}, \bar{T}, \bar{x}, \bar{z}, R)$. Boundary conditions in this end region are

$$\psi = \frac{\partial \psi}{\partial x} = T = 0 \quad \text{on} \quad x = 0 \quad (2.4.3)$$

$$\psi = \frac{\partial \psi}{\partial z} = 0, \quad T = x \quad \text{on} \quad z = 0, 1. \quad (2.4.4)$$

The end region solution matches with the core solution given that ψ and T have the following limiting behaviours

$$\psi \sim R_1 F(z) + O(e^{-\alpha x}) \quad (2.4.5)$$

$$T \sim x + R_1 G(z) + O(e^{-\alpha x}) \quad (2.4.6)$$

as $x \rightarrow \infty$, where $\text{Re}(\alpha) > 0$. A full numerical solution of this nonlinear problem is not attempted but some of its main properties will be discussed.

The decaying parts of the stream function and temperature in (2.4.5) and (2.4.6) have the forms

$$\begin{aligned} \phi(z; R_1, \sigma) \exp(-\alpha(R_1, \sigma)x), \\ \theta(z; R_1, \sigma) \exp(-\alpha(R_1, \sigma)x), \end{aligned} \quad (2.4.7)$$

respectively, where ϕ , θ and α are determined by the sixth order boundary value problem

$$\phi^{(6)} + 2\alpha^2 \phi'' + \alpha^4 \phi + \alpha R_1 \theta = \alpha R_1 (F''' \phi - F'(\phi'' + \alpha^2 \phi)) / \sigma \quad (2.4.8)$$

$$\theta'' + \alpha^2 \theta - \phi' = \alpha R_1 (G' \phi - F' \theta) \quad (2.4.9)$$

with

$$\theta = \phi = \phi' = 0 \text{ on } z = 0, 1. \quad (2.4.10)$$

The decomposition (2.4.7) follows from the fact that the decaying parts of ψ and T satisfy a pair of linear equations whose coefficients depend only on z , implying that the dependence on x is of exponential form.

The forms in (2.4.7) will be generated by the conditions (2.4.3) so that the end region will have a solution consistent with the core region solution only if a triply infinite set of eigenvalues α with $\text{Re}(\alpha) > 0$ exists. If the eigenvalue $\alpha(R_1, \sigma)$ corresponds to the eigenfunctions $\phi(z; R_1, \sigma)$ and $\theta(z; R_1, \sigma)$, the boundary value problem implies that $-\alpha(R_1, \sigma)$ corresponds to $\phi(1-z; R_1, \sigma)$ and $-\theta(1-z; R_1, \sigma)$. Also if α is complex then the complex conjugate $\alpha^*(R_1, \sigma)$ corresponds to $\phi^*(z; R_1, \sigma)$

and $\theta^*(z; R_1, \sigma)$. Attention can therefore be restricted to the first quadrant of the α plane.

The roots can be counted by reference to the structure at $R_1 = 0$, which is not dependent on the Prandtl number, and which has a triply infinite set of eigenvalues with $\text{Re}(\alpha) > 0$. At $R_1 = 0$, (2.4.8) becomes

$$\phi^{iv} + 2\alpha^2 \phi'' + \alpha^4 \phi = 0 \quad (2.4.11)$$

with $\phi = \phi' = 0$ on $z = 0, 1$ and (2.4.9) becomes

$$\theta'' + \alpha^2 \theta - \phi' = 0 \quad (2.4.12)$$

with $\theta = 0$ on $z = 0, 1$.

Equations (2.4.11) and (2.4.12) indicate that there are real eigenvalues defined by trivial solutions of (2.4.11), that is, $\phi = 0$ for all α , and from (2.4.12)

$$\alpha = n\pi, \quad \theta = \sin n\pi z, \quad n = 1, 2, \dots \quad (2.4.13)$$

Complex eigenvalues are found from the non-trivial solutions of (2.4.11) and occur in two non-combining even and odd groups

$$\phi = \sin \alpha z - \alpha z \cos \alpha z + (\alpha \cot \alpha - 1) z \sin \alpha z \quad (2.4.14)$$

where α is the solution of

$$\sin^2 \alpha - \alpha^2 = 0. \quad (2.4.15)$$

The even eigenfunctions correspond to the solutions of $\sin \alpha + \alpha = 0$, tabulated by Robbins and Smith (1948)

$$\alpha = 4.2124 + 2.2507i, 10.713 + 3.1032i, \dots \quad (2.4.16)$$

and the odd ones to the solutions of $\sin \alpha - \alpha = 0$, tabulated by Hillman and Salzer (1943)

$$\alpha = 7.4977 + 2.7687i, 13.900 + 3.3522i, \dots \quad (2.4.17)$$

2.5 Numerical results

A fourth order Runge-Kutta scheme with Newton iteration was used to solve the eigenvalue problem numerically. Solutions were calculated for fixed σ by incrementing R_1 using the value of α at the previous R_1 as an initial estimate. By use of this method the roots could be traced from the known values at $R_1 = 0$.

Figures 2.2 and 2.3 show the first few branches of the real and complex eigenvalues for infinite Prandtl number; each branch maintains a positive real part for all values of R_1 , which indicates that the end-region solution matches in a consistent manner to the core region solution. The decay of the real eigenvalues as $R_1 \rightarrow \infty$ indicates the expansion of the end region into the core at large R_1 .

Figure 2.4 shows the first few branches of the real eigenvalues at various finite Prandtl numbers; for $\sigma = 1$ there is little change from the infinite Prandtl number case and for $\sigma = 0.1$ the decay of the eigenvalues as $R_1 \rightarrow \infty$ is still apparent.

Figure 2.5 shows the first complex branch at Prandtl numbers of 0.1 and 1.0. For the $\sigma = 0.1$ branch the real part of α becomes zero at a critical value of $R_1 = R_{1c}$ and the root bifurcates into two imaginary branches for $R_1 > R_{1c}$. This type

of bifurcation occurs for $\sigma \leq \sigma_c \approx 0.27$ with $\text{Re}(\alpha)$ zero for $R_1 > R_{1c}(\sigma)$. Spatial oscillations from the end zone then enter the core and $R_{1c}(\sigma)$ may be identified with the critical Rayleigh number for the transverse mode of stationary instability of the parallel core flow, first examined by Hart (1972). Figure 2.6 shows the critical Grashof number

$$Gr_c = R_{1c} / \sigma \quad (2.5.1)$$

as a function of σ .

2.6 Asymptotic results for large R_1

(i) Decaying roots

The real branches in figures 2.2 and 2.4 have the asymptotic form

$$\alpha \sim \alpha_0 / R_1 \text{ as } R_1 \rightarrow \infty, \quad (2.6.1)$$

where α_0 is the eigenvalue defined by the boundary value problem

$$\phi^{iv} + \alpha_0 \theta = (\alpha_0 / \sigma) (F''' \phi - F' \phi''), \quad (2.6.2)$$

$$\theta'' - \phi' = \alpha_0 (G' \phi - F' \theta), \quad (2.6.3)$$

with

$$\phi = \phi' = \theta = 0 \text{ on } z = 0, 1. \quad (2.6.4)$$

Numerical solutions calculated by a Runge-Kutta scheme are shown in figure 2.7. Real solutions exist for all Prandtl numbers, and the leading branches approach the limiting values

$$\alpha_0 = 1852, 11052, 30919 \text{ as } \sigma \rightarrow \infty, \quad (2.6.5)$$

found by taking the right hand side of (2.6.2) equal to zero. Wholly imaginary roots exist for $\sigma < 0.24$.

(ii) Finite roots

Numerical calculations suggest that asymptotic solutions exist in which α remains finite as $R_1 \rightarrow \infty$ and purely imaginary solutions may correspond to the upper branches of the neutral curves in figure 2.5. For such solutions

$$\alpha \sim i\bar{\alpha}, \phi = \bar{\phi}(z), \theta \sim \bar{\theta}(z) \text{ as } R_1 \rightarrow \infty, \quad (2.6.6)$$

where $\bar{\alpha}$ is real. Substitution into (2.4.9) gives

$$\bar{\theta} = G' \bar{\phi} / F' \quad (2.6.7)$$

and therefore (2.4.8) yields

$$\bar{\phi}'' + ((\sigma G' - F'F''') / (F'^2 - \bar{\alpha}^2)) \bar{\phi} = 0. \quad (2.6.8)$$

A local solution of (2.4.8) and (2.4.9) consistent with (2.4.10), close to the lower surface of the cavity, requires that

$$\bar{\phi} = O(z^\lambda), \bar{\theta} = O(z^{\lambda-1}) \text{ as } z \rightarrow 0 \quad (2.6.9)$$

where $\lambda = \frac{1}{2} \{1 + (1 + \frac{4\sigma}{5})^{1/2}\}$. It is also required that $\bar{\phi} = 0$ at $z = 1$. From (2.6.8) it can be shown that

$$\bar{\phi} \sim K_{\pm} |z - \frac{1}{2}|^{\frac{1}{2}(1 \pm \delta)} \text{ as } |z - \frac{1}{2}| \rightarrow 0 \quad (2.6.10)$$

where K_{\pm} are arbitrary constants, and

$$\delta = (1 - 14\sigma/5)^{1/2}. \quad (2.6.11)$$

It may be argued that for $\sigma < 5/14$ the stronger of the two singularities must be avoided i.e. $K_- = 0$. If the reverse were true then a solution subject to (2.6.9) would have to be

constructed in $z < \frac{1}{2}$ with $K_- \neq 0$ and the symmetry of (2.6.8) implies a similar behaviour would occur in $z > \frac{1}{2}$. The structure near $z = \frac{1}{2}$ is then a critical layer defined by

$$z = \frac{1}{2} + (R_1 \bar{\alpha})^{-1/3} \tilde{z} \quad (2.6.12)$$

$$\left. \begin{aligned} \phi &\sim (R_1 \bar{\alpha})^{-1/6(1-\sigma)} \bar{\Phi}(\tilde{z}) \\ \theta &\sim (R_1 \bar{\alpha})^{1/6(1-\sigma)} \Theta(\tilde{z}) \end{aligned} \right\} \quad (2.6.13)$$

where it is assumed that $\bar{\phi} = 0(1)$. Substitution back into (2.4.8) and (2.4.9) gives

$$576\sigma \bar{\Phi}^{vi} - 24i\tilde{z}(1+\sigma)\bar{\Phi}^{iv} - 48i\bar{\Phi}^{iii} - \tilde{z}^2\bar{\Phi}'' - \frac{7}{10}\sigma\bar{\Phi} = 0, \quad (2.6.14)$$

which is independent of $\bar{\alpha}$. The solution of (2.6.14) must satisfy

$$\bar{\Phi} \sim K_- (\tilde{z})^{1/2(1-\sigma)} \quad \text{as } |\tilde{z}| \rightarrow \infty. \quad (2.6.15)$$

Daniels, Blythe and Simpkins (1987) considered a similar problem to (2.6.14) and (2.6.15) and were able to show that non-zero solutions would not generally exist, contradicting the original assertion and suggesting that the outer solution must satisfy

$$K_- = 0. \quad (2.6.16)$$

Figure 2.8 shows the numerical solution of (2.6.8) subject to (2.6.9) and (2.6.16). To distinguish between the two singular forms in (2.6.10), the solution is rewritten as

$$\bar{\phi} = Z^{(1/2)(1-\sigma)} f(\mathcal{Y}) \quad (2.6.17)$$

where

$$Z = \frac{1}{2} - z, \quad \mathcal{Y} = Z^\sigma \quad (2.6.18)$$

$$f'' + \mathcal{Y}^{2(1-\sigma)/\sigma} \mathcal{Y}^{-2} \left\{ \frac{16(1-\sigma)^2 [2\mathcal{Y}^{2/\sigma} - 1]}{7(1-4\mathcal{Y}^{2/\sigma})^2} + \frac{24}{(1-4\mathcal{Y}^{2/\sigma})} - \bar{\alpha}^2 \right\} f = 0. \quad (2.6.19)$$

The boundary conditions derived from (2.6.9) and (2.6.16) are

$$f = 0 \text{ at } \eta = 0, 2^{-\gamma} \quad (2.6.20)$$

The numerical solution was computed from $\zeta = 0$ to $\zeta = 2^{-\gamma}$ using an additional initial condition $f' = 1$ at $\zeta = 0$; iterative adjustment of $\bar{\alpha}$ enabled a solution to be found for any Prandtl number $0 < \sigma < 5/14$. The influence of the central singularity can be seen by replacing (2.6.16) by

$$K_{\pm} = 0. \quad (2.6.21)$$

The resulting upper branch of figure 2.8 is obtained by use of the conditions

$$f = 1, f' = 0 \text{ at } \eta = 0, f = 0 \text{ at } \eta = 2^{-\gamma}. \quad (2.6.22)$$

The form of the solution for $\bar{\alpha}$, on the lower branch of figure 2.8, can be found analytically for small Prandtl number, where

$$\bar{\alpha} \sim \sigma \bar{\alpha}_0 \text{ as } \sigma \rightarrow 0. \quad (2.6.23)$$

The corresponding eigenfunction is

$$\bar{\phi} = \bar{\phi}_0 + \sigma \bar{\phi}_1 + \sigma^2 \bar{\phi}_2 + \dots \quad (2.6.24)$$

and substitution into (2.6.8) gives at leading order

$$F' \bar{\phi}_0'' - F'' \bar{\phi}_0 = 0. \quad (2.6.25)$$

The boundary conditions on $\bar{\phi}_0$ obtained from (2.6.9) and (2.6.16)

are

$$\bar{\phi}_0 = O(z) \text{ as } z \rightarrow 0 \quad (2.2.26)$$

and

$$\bar{\phi}_0 \sim K_+ |z - \frac{1}{2}| \quad \text{as } |z - \frac{1}{2}| \rightarrow 0 \quad (2.6.27)$$

giving, without loss of generality,

$$\bar{\phi}_0 = F'. \quad (2.6.28)$$

At order σ

$$F' \bar{\phi}_1'' + G' - F''' \bar{\phi}_1 = 0 \quad (2.6.29)$$

and the boundary conditions on $\bar{\phi}_1$ are

$$\bar{\phi}_1 = O(z \log_e z) \quad \text{as } z \rightarrow 0 \quad (2.6.30)$$

and

$$\bar{\phi}_1 \sim \frac{-7}{10} K_+ |z - \frac{1}{2} \log_e |z - \frac{1}{2}| | \quad \text{as } |z - \frac{1}{2}| \rightarrow 0. \quad (2.6.31)$$

Writing

$$\bar{\phi}_1 = F' H(z), \quad (2.6.32)$$

(2.6.29) reduces to

$$\frac{d}{dz} [F'^2 H'] = -G' \quad (2.6.33)$$

and use of (2.6.30) and (2.6.31) gives

$$H = \frac{1}{10} \log_e \frac{z^2(1-z)^2}{(\frac{1}{2}-z)^7} + \text{constant}. \quad (2.6.34)$$

At order σ^2

$$F'^2 \bar{\phi}_2'' + G' \bar{\phi}_1' - F' F''' \bar{\phi}_2 - F'^3 \bar{\alpha}_0^2 = 0 \quad (2.6.35)$$

and the boundary conditions on $\bar{\phi}_2$ are

$$\bar{\phi}_2 = O(z \log_e^2 z) \quad \text{as } z \rightarrow 0 \quad (2.6.36)$$

and

$$\bar{\alpha}_2 \sim \frac{1}{2} \left(\frac{7}{10}\right)^2 K_+ |z - \frac{1}{2}| \log_e |z - \frac{1}{2}| \quad \text{as } |z - \frac{1}{2}| \rightarrow 0. \quad (2.6.37)$$

A consistent solution of (2.6.35) exists only if

$$\int_0^{1/2} (\bar{\alpha}_0^2 F'^2 - G'H) dz = 0, \quad (2.6.38)$$

which gives

$$\bar{\alpha}_0 = \frac{1}{5} \sqrt{483} \approx 4.37545.$$

This result compares well with the numerical solution, as shown in table 2.1 and figure 2.8.

2.7 Discussion

Convective motions driven by a horizontal temperature gradient in a shallow cavity with conducting walls have been analysed for the limit $L \rightarrow \infty$ with $R_1 = R/L = O(1)$, over a range of Rayleigh numbers R_1 and Prandtl numbers σ .

The numerical solution to the relevant eigenvalue problem indicates the existence of a critical Prandtl number $\sigma \approx 0.27$ below which the parallel core flow is destroyed by multiple eddies which are forced into the core if the Grashof number $Gr = R_1/\sigma$ is greater than the critical value $Gr_c(\sigma)$ shown in figure 2.6. As $\sigma \rightarrow 0$ the results show that Gr_c approaches a value of about 8×10^3 consistent with, but a little higher than, the critical Grashof number of 7980 for $\sigma < 0.02$ found by Hart (1972). Figure 2.6 shows that the results also compare well with the work done by Kuo, Korpela, Chait and Marcus (1986) whose stability analysis was based on the use of Chebychev polynomials and

collocation. The insulating boundaries case was studied by Daniels, Blythe and Simpkins (1987) and their results for the critical Grashof number as a function of Prandtl number are also included in figure 2.6. The Gr_c curves for the insulating and conducting boundaries approach the same limit as $\sigma \rightarrow 0$, consistent with Hart's (1972) arguments that the critical Grashof number should be the same because the thermal contributions become negligible in this limit.

At general Prandtl number, the decay of the end zone solution is reduced as the Rayleigh number is increased, causing the structure set out in Sections 2.3 and 2.4 to break down. Figure 2.7 identifies the e - folding decay length

$$x \sim \alpha_0^{-1} R_1 \quad (2.7.1)$$

associated with this process, with $\alpha_0 \approx 1.8 \times 10^3$ for $\sigma \geq 0.2$.

TABLE 2.1

Numerical solution of (2.6.19), (2.6.20) for small σ

σ	$\bar{\alpha}$	$\bar{\alpha}/\sigma$
0.20	0.98708	4.93542
0.15	0.71227	4.74846
0.10	0.46044	4.60443
0.05	0.22447	4.48946
0.01	0.04413	4.41296

Asymptotic $\bar{\alpha}/\sigma = 4.39545$

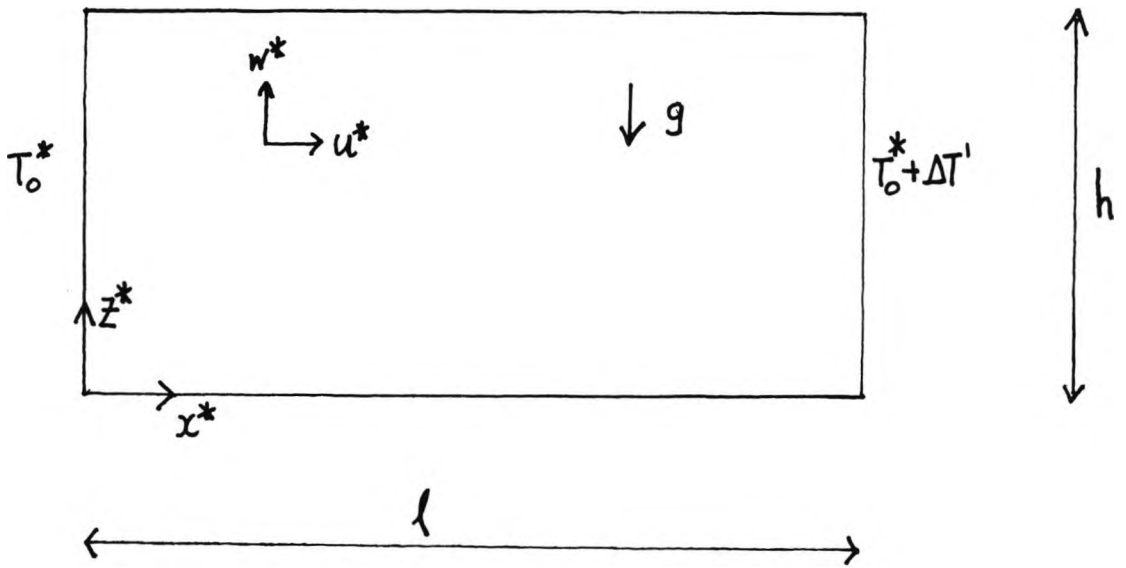


Figure 2.1 Flow domain of Problem.

Figure 2.2 First three branches of the real eigenvalue α for infinite Prandtl number.

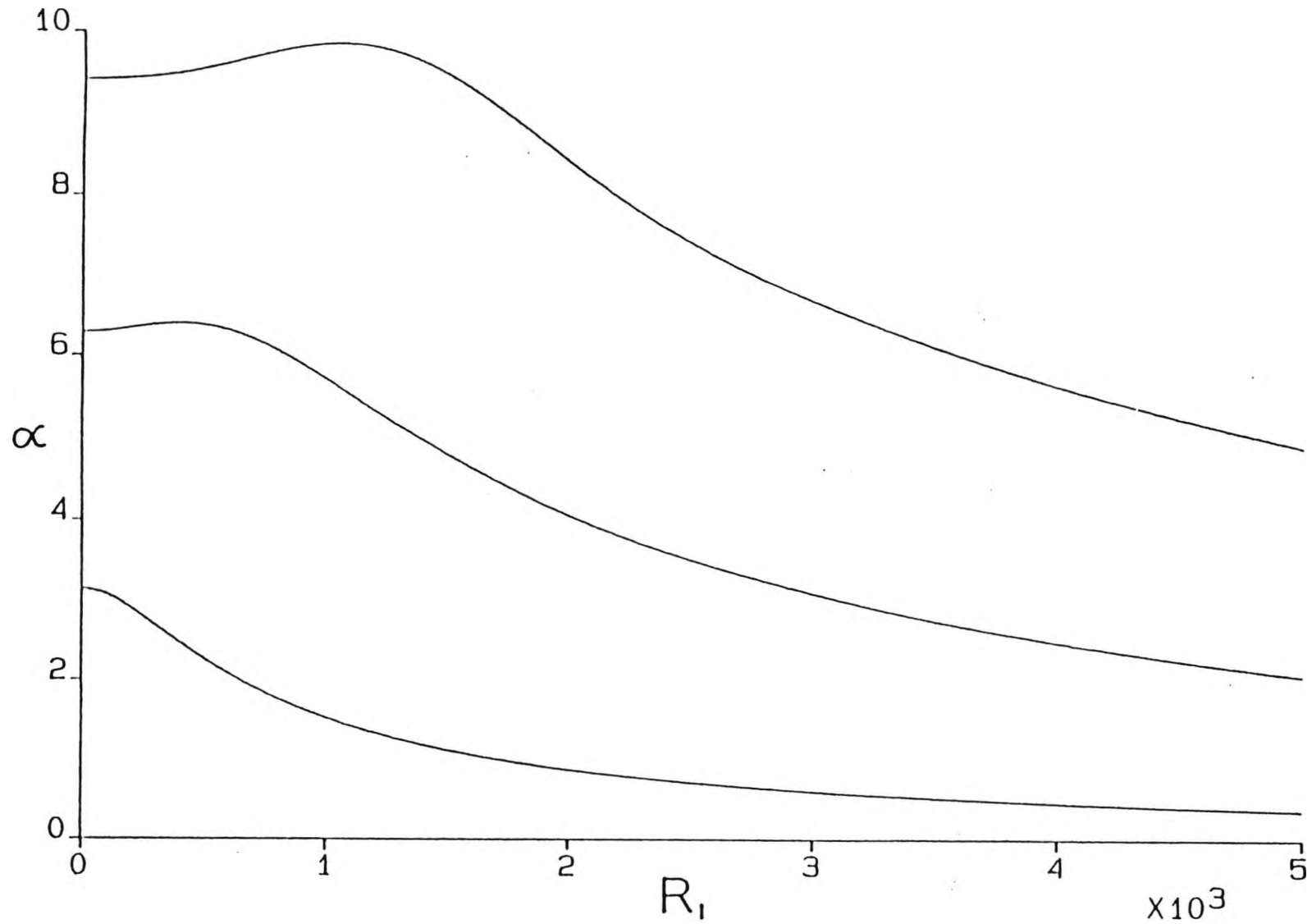


Figure 2.3 First three branches a, b, c of the complex eigenvalue α for infinite Prandtl number,
 ——— real part, - - - - - imaginary part.

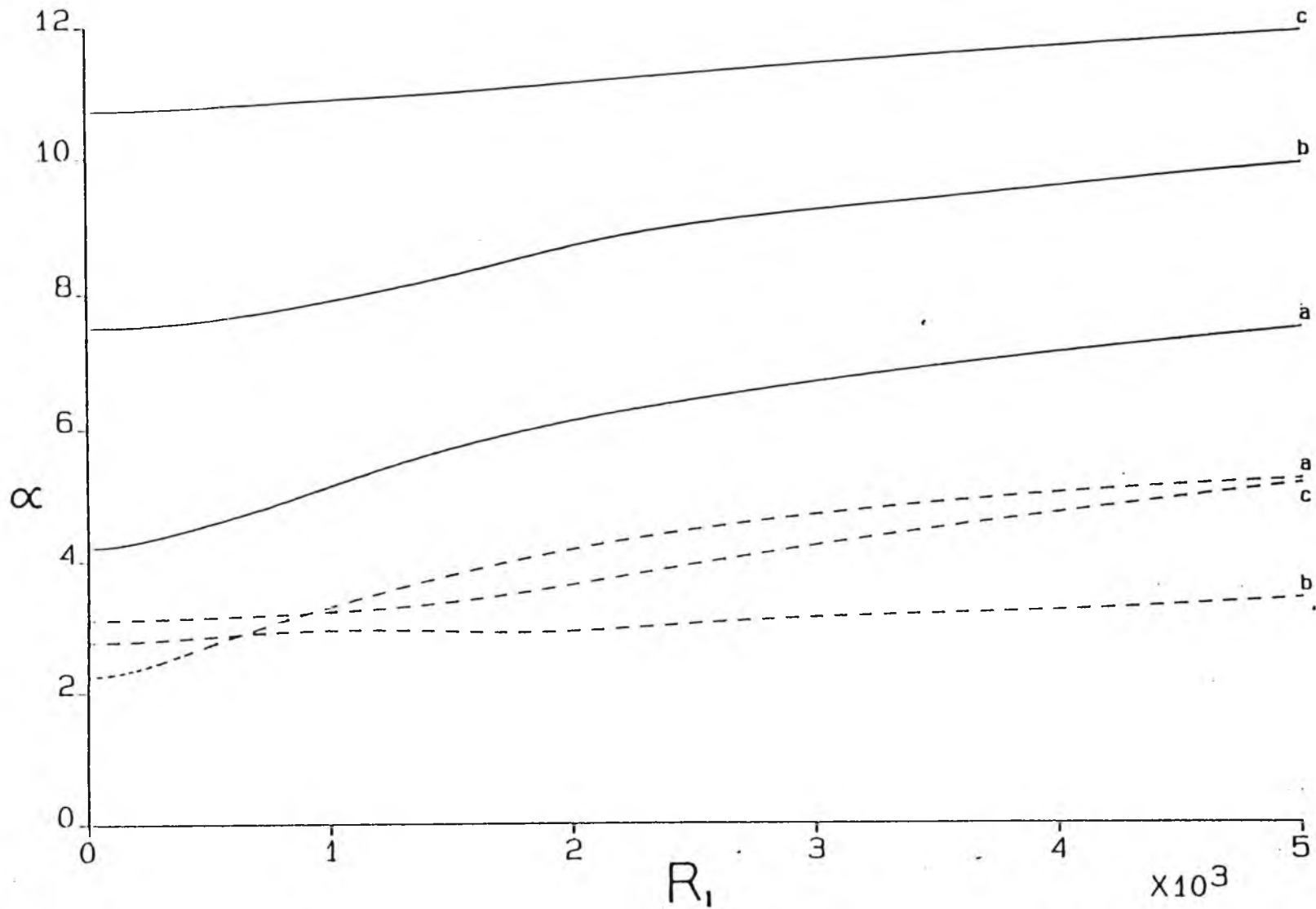


Figure 2.4 First three branches of the real eigenvalue α for $\sigma = 0.1$, - - - - - and $\sigma = 1$, ——— .

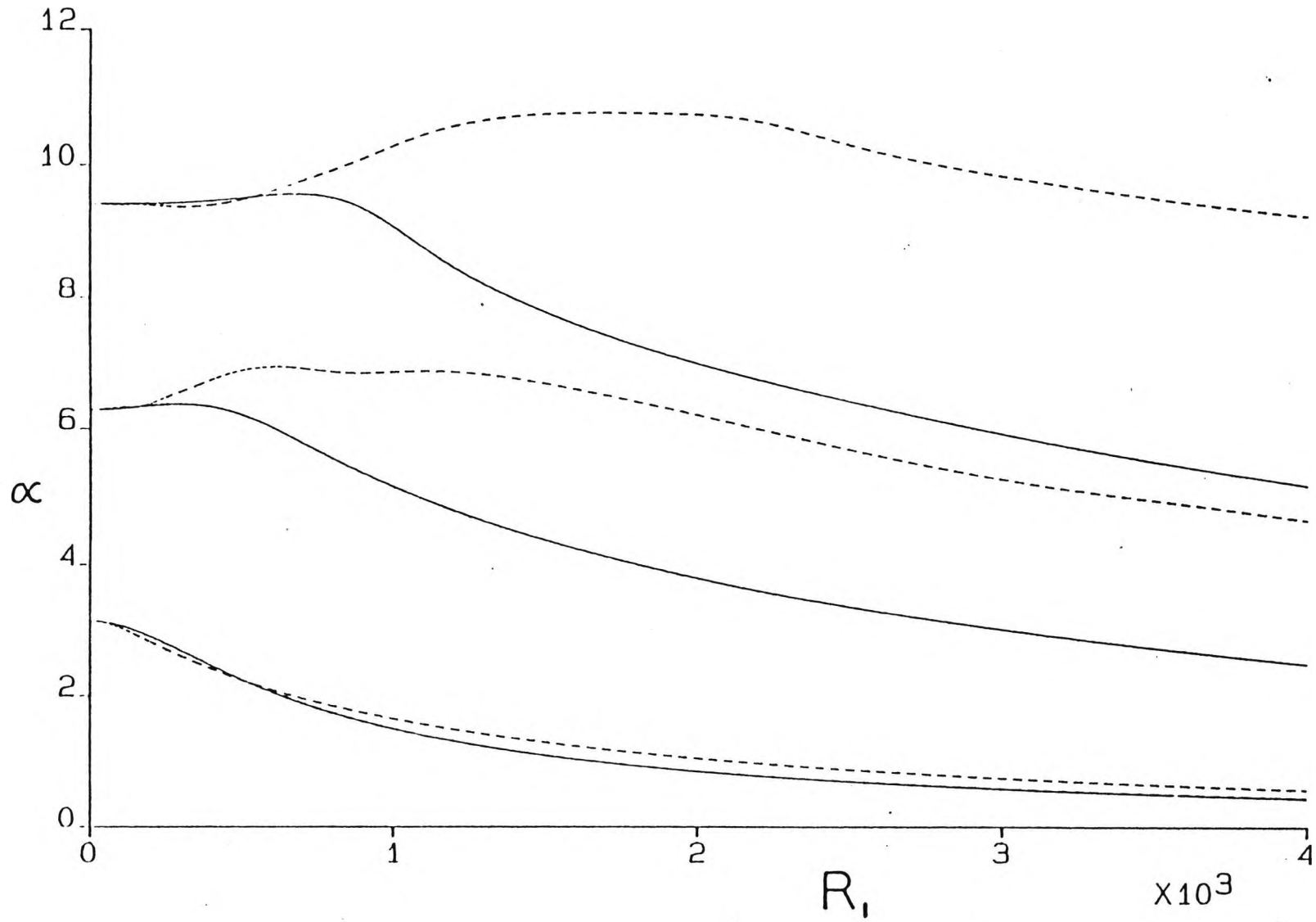
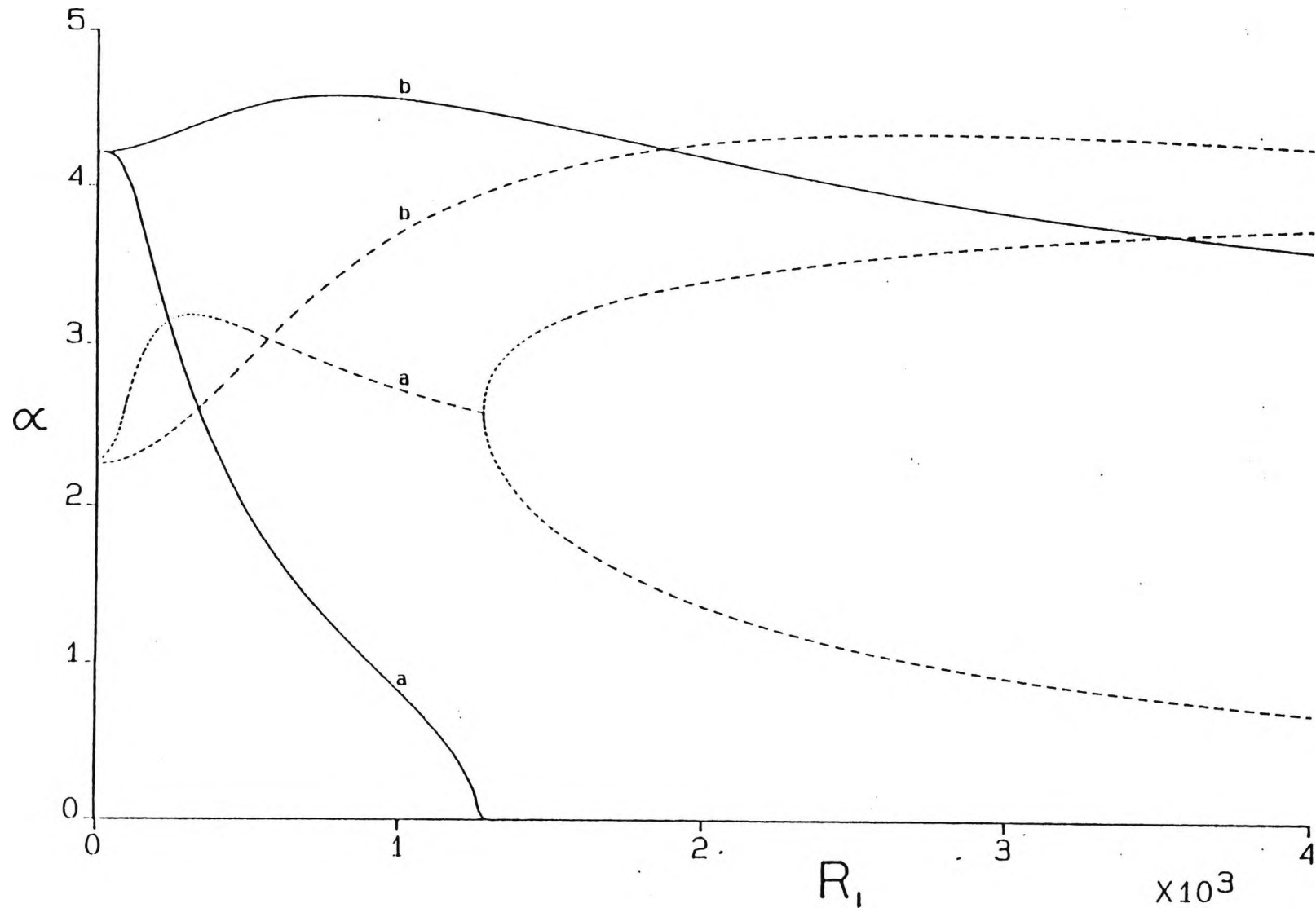


Figure 2.5 Complex eigenvalues α for finite Prandtl number, $\frac{\sigma}{Pr}$, Real part, -----, Imaginary part; (a) $\sigma = 0.1$, (b) $\sigma = 1.0$.



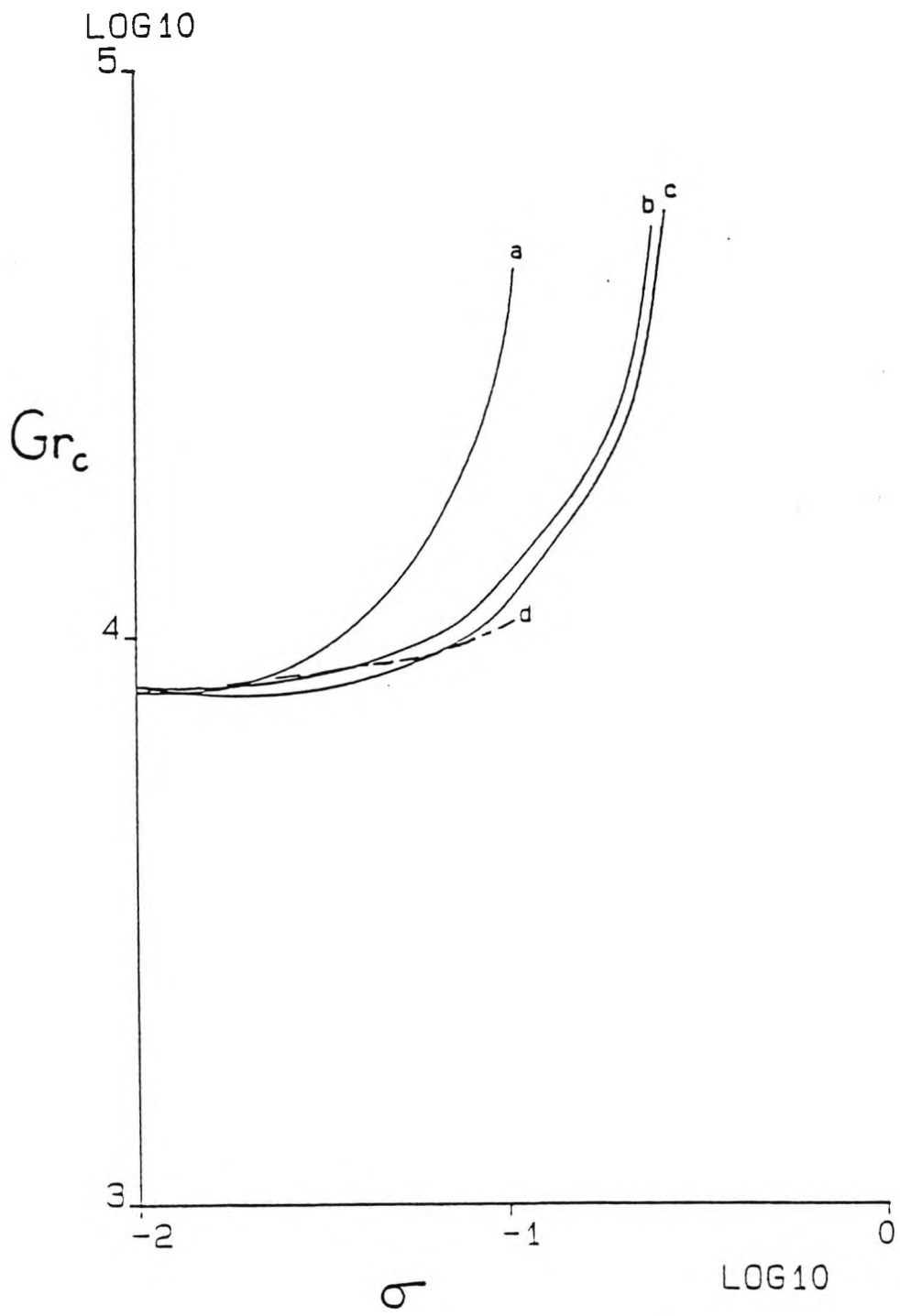


Figure 2.6 Comparison of critical Grashof numbers.
 a) Daniels et al (1987), b) Present Work,
 c) Kuo et al (1986), d) Hart (1972).

Figure 2.7 Eigenvalues α_0 as a function of Prandtl number, —, Real part, - - - -, Imaginary part.

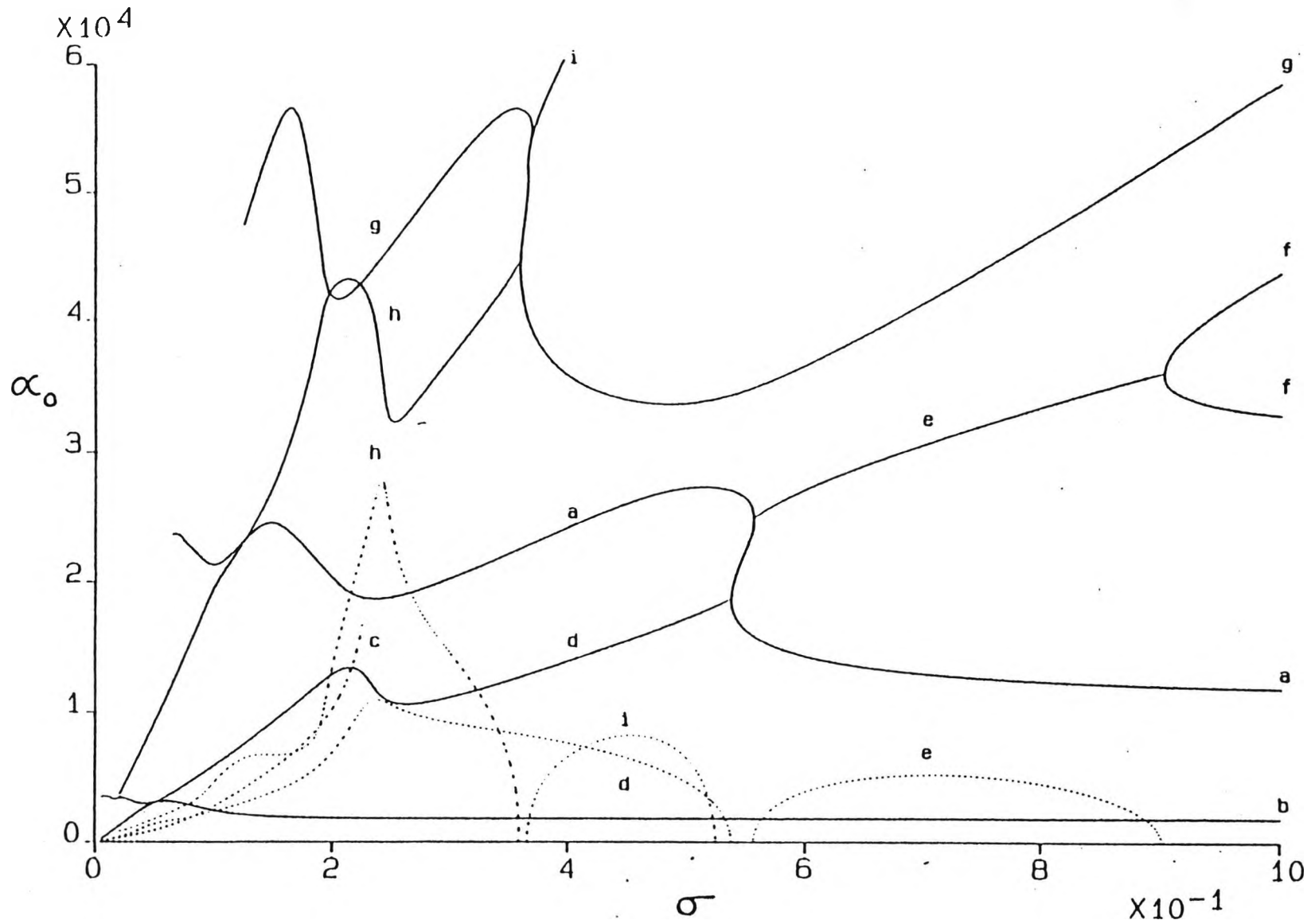
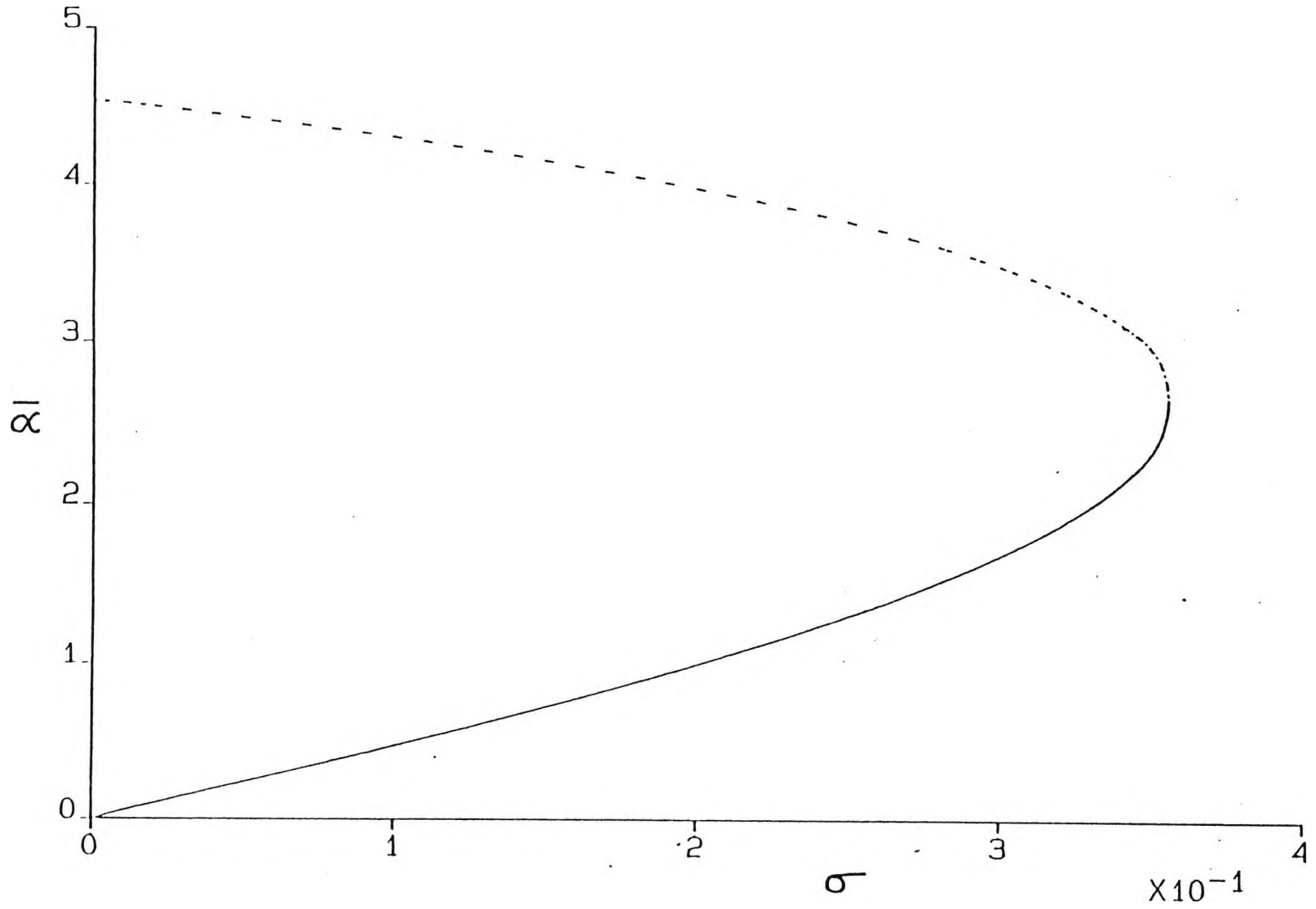


Figure 2.8 Eigenvalues $\bar{\alpha}$ for $0 < \sigma < 5/14$.



CHAPTER 3

Thermal convection in a shallow laterally heated cavity with adiabatic boundaries

3.1 Introduction

In this chapter the structure of the flow in a shallow laterally heated cavity with adiabatic horizontal surfaces is considered. As mentioned in Chapter 1 the problem was studied by Daniels et al (1987) and in Section 3.2 the main results for Rayleigh numbers $R_1 = R/L = O(1)$ are reviewed. The overall structure is similar to that described in detail in Chapter 2 for the case of conducting boundaries.

Section 3.3 describes the structure of the flow in the end-zone at the cold wall as $R_1 \rightarrow \infty$, discussed by Daniels et al (1987a), it details the relevant scalings for a vertical boundary layer adjacent to the end wall and sets out the resulting boundary layer equations. A similarity solution is found numerically in Section 3.4 and compared with previous results obtained by Ostrach (1952) and Kuiken (1968). Section 3.5 shows that the vertical boundary layer is susceptible to separation of the type described by Smith and Duck (1977) suggesting a possible way in which the isotherms and streamlines in the vertical boundary layer are carried around the lower corner into a horizontal boundary layer. A complete asymptotic description of the corner is likely to be extremely complicated and is not attempted. Finally, Section 3.6 gives a summary of the overall end-zone structure for $R_1 \gg 1$ proposed by Daniels et al (1987a) and this forms the basis for a study of the horizontal boundary layer structure in Chapters 4-7.

3.2 Formulation and the solution for $R_1 = R/L = O(1)$

The governing equation for the flow, from Chapter 2 are

$$\bar{\nabla}^4 \bar{\psi} = R \frac{\partial \bar{T}}{\partial \bar{x}} + \frac{1}{\sigma} \frac{\partial (\bar{\nabla}^2 \bar{\psi}, \bar{\psi})}{\partial (\bar{x}, \bar{z})} \quad (3.2.1)$$

$$\bar{\nabla}^2 \bar{T} = \frac{\partial (\bar{T}, \bar{\psi})}{\partial (\bar{x}, \bar{z})} \quad (3.2.2)$$

The boundary conditions on the rigid walls are

$$\bar{\psi} = \frac{\partial \bar{\psi}}{\partial \bar{x}} = \bar{T} = 0 \quad \text{on } \bar{x} = 0 \quad (3.2.3)$$

$$\bar{\psi} = \frac{\partial \bar{\psi}}{\partial \bar{x}} = 0, \quad \bar{T} = 1 \quad \text{on } \bar{x} = L \quad (3.2.4)$$

$$\bar{\psi} = \frac{\partial \bar{\psi}}{\partial \bar{z}} = \frac{\partial \bar{T}}{\partial \bar{z}} = 0 \quad \text{on } \bar{z} = 0, 1. \quad (3.2.5)$$

The boundary conditions and governing equations are consistent with Gill's (1966) centrosymmetry relations

$$\bar{\psi}(\bar{x}, \bar{z}) = \bar{\psi}(L - \bar{x}, 1 - \bar{z}) \quad (3.2.6)$$

$$\bar{T}(\bar{x}, \bar{z}) = 1 - \bar{T}(L - \bar{x}, 1 - \bar{z})$$

which allow one half of the flow domain to be considered.

For $L \gg 1$, and

$$R_1 = R/L = O(1) \quad (3.2.7)$$

Daniels et al (1987) outlined the formal asymptotic flow structure. The core region where

$$\xi = \bar{x}/L, \quad \bar{z} = \bar{z} \quad (3.2.8)$$

is dominated by lateral conduction associated with a Hadley circulation so that

$$\bar{T} = \xi + L^{-1} \left\{ (\xi - \frac{1}{2}) C_1(R_1, \sigma) + R_1 F_1(\bar{z}) \right\} + O(L^{-2}) \quad (3.2.9)$$

and

$$\bar{\psi} = R_1 \left\{ 1 + L^{-1} c_1(R_1, \sigma) \right\} F_1'(z) + O(L^{-2}) \quad (3.2.10)$$

as $L \rightarrow \infty$, with

$$F_1(z) = \frac{1}{120} z^5 - \frac{1}{48} z^4 + \frac{1}{72} z^3 - \frac{1}{440} \cdot \quad (3.2.11)$$

$c_1(R_1, \sigma)$ is a constant contribution determined by matching with solutions near the end walls.

Near the cold wall, the solution adjusts to the boundary conditions on the wall in an approximately square zone where $x = \bar{x}$, $z = \bar{z}$ are $O(1)$. Here,

$$\bar{T} = L^{-1} T(x, z) + \dots, \quad \bar{\psi} = \psi(x, z) + \dots \quad (3.2.12)$$

Substitution into (3.2.1) and (3.2.2) gives

$$\nabla^4 \psi = R_1 \frac{\partial T}{\partial x} + \frac{1}{\sigma} \frac{\partial(\nabla^2 \psi, \psi)}{\partial(x, z)} \quad (3.2.13)$$

and

$$\nabla^2 T = \frac{\partial(T, \psi)}{\partial(x, z)} \quad (3.2.14)$$

respectively.

It is also noted that the pressure field in the end zone may be expanded as

$$\bar{p} = p(x, z) + \dots \quad (3.2.15)$$

where

$$u \frac{du}{dx} + w \frac{dw}{dz} = -\frac{dp}{dx} + \sigma \nabla^2 u, \quad (3.2.16)$$

$$u \frac{dw}{dx} + w \frac{dw}{dz} = -\frac{dp}{dz} + \sigma \nabla^2 w + \sigma R_1 T. \quad (3.2.17)$$

From (3.2.3) and (3.2.5) the equations are to be solved subject to

$$\psi = \frac{d\psi}{dx} = T = 0 \quad \text{on } x=0 \quad (3.2.18)$$

$$\psi = \frac{d\psi}{dz} = \frac{dT}{dz} = 0 \quad \text{on } z=0, 1 \quad (3.2.19)$$

and to match with the core solution

$$T \sim x + c + R_1 F_1(z) \quad (3.2.20)$$

$$\psi \sim R_1 F_1'(z) \quad (3.2.21)$$

as $x \rightarrow \infty$.

The core temperature is determined to $O(L^{-1})$ through the matching requirement

$$c_1 = -2c. \quad (3.2.22)$$

The value of c can only be determined by solving the end zone problem (3.2.13)-(3.2.21).

In order to be consistent with the parallel core flow the end zone solution must have the form

$$\psi \sim R_1 F_1'(z) + \operatorname{Re} \sum_{\alpha} \phi(z; R_1, \sigma) \exp \{ -\alpha(R_1, \sigma) x \} \quad (3.2.23)$$

$$T \sim x + c + R_1 F_1(z) + \operatorname{Re} \sum_{\alpha} \theta(z; R_1, \sigma) \exp \{ -\alpha(R_1, \sigma) x \} \quad (3.2.24)$$

as $x \rightarrow \infty$ where $\operatorname{Re}(\alpha) > 0$. Substitution into (3.2.13) and (3.2.14) yields the sixth-order boundary value problem for ϕ , θ and α :

$$\phi^{iv} + 2\alpha^2 \phi'' + \alpha^4 \phi + \alpha R_1 \sigma = \frac{\alpha R_1}{\sigma} \{ F_1^{iv} \phi - F_1'' (\phi'' + \alpha^2 \phi) \} \quad (3.2.25)$$

$$\theta'' + \alpha^2 \theta - \phi' = \alpha R_1 (F_1' \phi - F_1'' \theta) \quad (3.2.26)$$

$$\text{with } \phi = \phi' = \theta' = 0 \text{ at } z = 0, 1. \quad (3.2.27)$$

Daniels et al (1987) solved the above eigenvalue problem using a fourth-order Runge-Kutta scheme and Newton iteration. When $R_1 = o(1)$ the vorticity and energy equations uncouple and the non-trivial solutions of the reduced system for ϕ are associated with the same complex eigenvalues as in the conducting case (see Chapter 2). Studies of the complex solution branch for various values of σ show that as in the conducting case $\text{Re}(\alpha) = 0$ at finite $R_1 > R_{1c}$ if σ is sufficiently low, and beyond this bifurcation point spatial oscillations penetrate the core from the end zones. Figure 2.6 shows a graph of the critical Grashof number $\text{Gr}_c = R_{1c}/\sigma$ as a function of σ . The limiting value of $\text{Gr}_c \approx 7950$ at $\sigma = 0$ is consistent with $\text{Gr}_c \approx 7880$ found by Hart (1972) and $\text{Gr}_c \approx 8000$ found in Chapter 2 for the conducting boundaries case. As $\sigma \rightarrow 0$ the limiting values of Gr_c for the insulating and conducting boundaries cases are believed to be the same as thermal effects become negligible in this limit (Hart (1972)). Similar results for the transverse modes of stationary instability have been found by Hart (1983a). For $\sigma > \sigma_c \approx 0.12$ it appears that the parallel core flow could exist for all R_1 when the horizontal boundaries are insulated. Altering the horizontal boundary condition from adiabatic to conducting has the effect of increasing σ_c to approximately 0.27.

Numerical studies for flows in shallow cavities have been described by Hart (1983b), who solved the end zone problem

numerically for low values of σ , and by Drummond and Korpela (1987), who solved the Oberbeck-Boussinesq equations using a finite difference technique and the Du Fort-Frankel method, again with attention focussed on small σ . Their examples of the flow field near Gr_c illustrate the emergence of multicellular flow. Solutions of the end zone problem involving higher σ have not previously been considered in any detail, although currently a numerical investigation is under way to calculate the parameter c for a whole range of σ and R_1 (Daniels and Wang (1990)).

3.3 The end zone structure for $R_1 \gg 1$

At general R_1 , integration of the energy equation (3.2.14) using (3.2.19) gives an expression for the horizontal heat transfer balance

$$\int_0^1 \left(\frac{\partial T}{\partial x} + \psi \frac{\partial T}{\partial z} \right) dz = Q_1 \quad (3.3.1)$$

where Q_1 is a constant.

If we assume the parallel flow structure ($\sigma > \sigma_c$) and use the form (3.2.20) and (3.2.21) as $x \rightarrow \infty$, Q_1 can be evaluated as

$$Q_1 = R_1^2 Q_0 + 1 \quad (3.3.2)$$

where

$$Q_0 = \int_0^1 F_1'^2 dz = \frac{1}{362,880} \quad (3.3.3)$$

The convective term $\psi \frac{\partial T}{\partial z}$ is the major contribution to the left hand side of (3.3.1) at large x when $R_1 \gg 1$. At the wall ($\psi = 0$) the conduction term $\frac{\partial T}{\partial x}$ dominates requiring that locally

$$T = O(x R_1^2). \quad (3.3.4)$$

In the vertical boundary layer a balance between conduction and convection in the energy equation, and a balance between viscosity and buoyancy in the vorticity equation requires that

$$x\Psi = O(1), \quad \Psi = O(R_1 T x^3) \quad (3.3.5)$$

which together with (3.3.4) implies the following scalings for the layer:

$$x = R_1^{-3/5} x_1, \quad z = z, \quad T \sim R_1^{7/5} T_1, \quad \Psi \sim R_1^{3/5} \Psi_1 \quad (R_1 \rightarrow \infty). \quad (3.3.6)$$

Other possible scalings appear to lead to contradictions. The scalings (3.3.6) differ from the $O(R_1)$ scalings for T and Ψ that might have been expected from the forms (3.2.20) and (3.2.21), a consequence of which is that the order $R_1^{7/5}$ temperature field outside the vertical boundary layer must be constant, with

$$C(R_1, \sigma) = R_1^{7/5} C_0(\sigma) + \dots \quad (R_1 \rightarrow \infty). \quad (3.3.7)$$

The governing equations and boundary conditions in the vertical boundary layer are therefore

$$\frac{\partial^4 \Psi_1}{\partial x_1^4} = \frac{\partial T_1}{\partial x_1} + \frac{1}{\sigma} \left[\frac{\partial^3 \Psi_1}{\partial x_1^3} \frac{\partial \Psi_1}{\partial z} - \frac{\partial^3 \Psi_1}{\partial x_1^2 \partial z} \frac{\partial \Psi_1}{\partial x_1} \right] \quad (3.3.8)$$

and

$$\frac{\partial^2 T_1}{\partial x_1^2} = \frac{\partial(T_1, \Psi_1)}{\partial(x_1, z)} \quad (3.3.9)$$

with

$$T_1 \rightarrow C_0, \quad \frac{\partial \Psi_1}{\partial x_1} \rightarrow 0 \quad \text{as } x_1 \rightarrow \infty \quad (3.3.10)$$

$$\Psi_1 = \frac{\partial \Psi_1}{\partial x_1} = T_1 = 0 \quad \text{on } x_1 = 0. \quad (3.3.11)$$

A solution to (3.3.8)-(3.3.11) is the similarity form

$$T_1 = c_0 g(\eta), \quad \psi_1 = c_0^{1/4} (1-z)^{3/4} f(\eta) \quad (3.3.12)$$

where $\eta = \frac{c_0^{1/4} x_1}{(1-z)^{1/4}}$, as discussed by Squire, see Goldstein

(1938). Here

$$f''' + \sigma^{-1} \left(\frac{3}{4} f f'' - \frac{1}{2} f'^2 \right) - g + 1 = 0 \quad (3.3.13)$$

$$g'' + \frac{3}{4} f g' = 0 \quad (3.3.14)$$

with

$$f = f' = g = 0 \quad (\eta = 0); \quad g \rightarrow 1, \quad f' \rightarrow 0 \quad (\eta \rightarrow \infty). \quad (3.3.15)$$

The boundary conditions at $\eta = 0$ follow from the end wall conditions (3.3.11), and the conditions at $\eta = \infty$ from (3.3.10) which is based on the assumption that there is no vertical external flow of magnitude $R_1^{6/5}$. By integrating (3.3.14) using

(3.3.15) an expression for g can be found:

$$g = \frac{\int_0^1 \exp \left\{ -\frac{3}{4} \int_0^1 f d\eta \right\} d\eta}{\int_0^\infty \exp \left\{ -\frac{3}{4} \int_0^1 f d\eta \right\} d\eta} \quad (3.3.16)$$

The wall heat transfer can be approximated to within $\frac{1}{2}\%$ by the formula

$$\gamma = g'(0) = \frac{3}{4} \sigma^{1/4} \left\{ 2.436 + 4.884 \sigma^{1/2} + 4.952 \sigma \right\}^{-1/4} \quad (3.3.17)$$

for all values of σ (Ostrach (1952)), and agrees with a numerical solution outlined in Section 3.4 (see table 3.2 below). The heat transferred through the cold wall from the vertical boundary layer

$$R_1^2 \int_0^1 \frac{\partial T_1}{\partial x_1}(0, z) dz \quad (3.3.18)$$

is the dominant contribution to the left hand side of the integral constraint (3.3.1) at $x = 0$. Using (3.3.12)

$$c_0^{5/4} \gamma = 3/4 Q_0 \quad (3.3.19)$$

so that $c_0 = \left(\frac{3Q_0}{4\gamma}\right)^{4/5}$.

At the base of the vertical boundary layer the wall heat transfer has been converted to a convective transfer

$$R_1^2 \int_0^{\infty} \psi_1 \frac{\partial T_1}{\partial x_1}(x_1, 0) dx_1 = \frac{4}{3} R_1^2 c_0^{5/4} \gamma \quad (3.3.21)$$

which is carried with the isotherms and streamlines around the lower corner into a horizontal boundary layer (see Section 3.6). This conversion to a horizontal transfer

$$\int \psi \frac{\partial T}{\partial z} dz \sim \frac{4}{3} R_1^2 c_0^{5/4} \gamma \quad (3.3.22)$$

near the base of the cavity accomplishes the transfer of (negative) heat energy, via a horizontal boundary layer structure, into the main outer part of the end zone where $x = 0(R_1)$. The integration on the left hand side of (3.3.22) is taken across the horizontal boundary layer region to be discussed in Section 3.6.

3.4 Solution of the vertical boundary layer equations

To solve the problem (3.3.13)-(3.3.15) we obtain a system of first order differential equations for discretization by setting

$$A = f, \quad B = \frac{dA}{d\eta}, \quad C = \frac{dB}{d\eta}, \quad D = g, \quad E = \frac{dD}{d\eta}. \quad (3.4.1)$$

Substitution into (3.3.13) and (3.3.14) yields

$$\frac{dC}{d\eta} + \frac{1}{\sigma} \left[\frac{3}{4} AC - \frac{1}{2} B^2 \right] - D + 1 = 0 \quad (3.4.2)$$

$$\frac{dE}{d\eta} + \frac{3}{4} AE = 0. \quad (3.4.3)$$

The three first order equations in (3.4.1) are approximated by

$$B_{j-\frac{1}{2}} = \frac{A_j - A_{j-1}}{h_j}, \quad C_{j-\frac{1}{2}} = \frac{B_j - B_{j-1}}{h_j}, \quad E_{j-\frac{1}{2}} = \frac{D_j - D_{j-1}}{h_j} \quad (3.4.4)$$

where $\eta_j = \eta_{j-1} + h_j$. Also (3.4.2) and (3.4.3) become

$$C_j \frac{C_j - C_{j-1}}{h_j} + \frac{1}{\sigma} \left[\frac{3}{4} (AC)_{j-\frac{1}{2}} - \frac{1}{2} (B^2)_{j-\frac{1}{2}} \right] - D_{j-\frac{1}{2}} + 1 = 0 \quad (3.4.5)$$

$$\text{and} \quad E_j \frac{E_j - E_{j-1}}{h_j} + \frac{3}{4} (AE)_{j-\frac{1}{2}} = 0. \quad (3.4.6)$$

The equations are centred on $\eta_{j-1/2}$. The centred averages taken for the nonlinear terms are

$$AC = \frac{1}{2} (A_j C_j + A_{j-1} C_{j-1}), \quad B^2 = \frac{1}{2} (B_j^2 + B_{j-1}^2), \quad AE = \frac{1}{2} (A_j E_j + A_{j-1} E_{j-1}). \quad (3.4.7)$$

The boundary conditions, from (3.3.15) are

$$A_0 = 0, \quad B_0 = 0, \quad D_0 = 0; \quad D_N = 1, \quad B_N = 0 \quad (3.4.8)$$

for N sufficiently large. From (3.4.5) and (3.4.6) we obtain

$$C_j - C_{j-1} + \frac{h_j}{\sigma} \left\{ \frac{3}{4} (A_j C_j + A_{j-1} C_{j-1}) - \frac{1}{4} (B_j^2 + B_{j-1}^2) \right\} - \frac{h_j}{2} (D_j + D_{j-1}) + h_j = 0 \quad (3.4.9)$$

and

$$E_j - E_{j-1} + \frac{3}{4} h_j \left\{ A_j E_j + A_{j-1} E_{j-1} \right\} = 0 \quad (3.4.10)$$

respectively.

A Newton iteration scheme is used to solve the problem and details are given in Appendix 1. In the computations the meshwidth h was 0.01 or 0.02 and the tolerance for which the Newton increments were deemed sufficiently small was set to 0.0001. The effect of the size of h on the values of f and g (A and D) is presented in table 3.1.

Graphs of f , f' and g against η which show that for larger σ there is a wider and stronger jet but a thinner thermal boundary layer are shown in figures 3.1, 3.2 and 3.3 respectively for Prandtl numbers of 0.028 (mercury), 0.1, 0.72 (air), 8.1 (water) and 17.2 (ethylalcohol). The main properties of the solution are summarised in table 3.2.

The system (3.3.13)-(3.3.15) has been previously considered by Ostrach (1952) and Kuiken (1968), the latter for large σ only. Figure 3.4 shows that the present solution and Kuiken's temperature solution for $\sigma = 2$ are in good agreement. However there is some disagreement with the velocity solution (figure 3.5) and the present solution is more in line with Ostrach's work at this Prandtl number. This is due to the Prandtl number being too low for the validity of Kuiken's asymptotic solution, a fact which is further confirmed in figure 3.6 for $\sigma = 10$ where the two solutions are virtually indistinguishable from each other.

3.5 Separation of the vertical boundary layer

In this section the separation of the wall jet in the vertical boundary layer on the end wall is investigated. This problem was considered by Smith and Duck (1977) who showed that separation was possible within a double-deck structure which in the present context is of vertical extent $z = O(R_1^{-18/35})$. The double-deck consists of a main deck of width $x = O(R_1^{-3/5})$ which spans the vertical boundary layer and a viscous sublayer of width $x = O(R_1^{-27/35})$. The double-deck itself is located close to the lower corner of the cavity at $z = z_0$ where $z_0 \ll 1$.

In the main deck the velocity and temperature profiles at the base of the vertical boundary layer $-w = O(R_1^{6/5})$, $T = O(R_1^{7/5})$ remain unchanged to leading order but contain corrections of relative order $R^{-6/35}$; there are corresponding perturbations of order $R_1^{33/35}$ and $R_1^{72/35}$ to the horizontal velocity and pressure fields u and p respectively. Corresponding solutions for w , T , u and p in the viscous sublayer are of order $R_1^{36/35}$, $R_1^{43/35}$, $R_1^{27/35}$ and $R_1^{72/35}$ respectively.

Continuity of pressure across the boundary layer leads to a relationship between the inviscid displacement of the main deck and the pressure field in the lower deck which is sufficient to allow a numerical computation of the lower deck solution, first carried out by Smith and Duck (1977). A solution exists in which the pressure increases as z decreases and leads to separation of the flow from the wall within the lower deck, with a slowly moving upward flow close to the wall. Because of the short length scale of the interaction, buoyancy effects are of minor significance and the temperature field does not influence the leading order velocity field in the double deck. The flow during interaction is therefore precisely that calculated by Smith and Duck (1977), incorporating the order of magnitude arguments of Smith (1976).

Smith and Duck argued that during the interaction, the fluid near to the wall forms a sublayer caused by the induced pressure gradient, whilst the majority of the boundary layer behaves in an inviscid manner. Upstream of the separation point the sublayer pressure rises slightly, causing a decrease in the skin friction, leading to the expansion of the sublayer. The resulting movement

of the fluid in the inviscid region induces a pressure fall across the jet, but as the pressure at the edge of the jet remains unchanged, the transverse pressure gradient reinforces the pressure rise at the wall and so the process is mutually reinforcing. If the arguments put forward by Smith & Duck (1977) are valid in the present context, the separation (followed by an eddy of reversed flow) is most likely to occur within the double deck at a distance $z_0 = O(R_1^{-9/35})$ from the corner. The isotherms and streamlines are swept around the corner into a horizontal boundary layer to be discussed in Section 3.6.

3.6 Outer structure and horizontal layers

The core solution and the governing equations in the end zone of the cavity suggest a main outer horizontal length scale for the end zone where $x = O(R_1)$. Therefore we define

$$x = R_1 X \tag{3.6.1}$$

and expect that

$$\begin{aligned} T_1 &\sim c(R_1, \sigma) + R_1 \Theta(X, z), \\ \Psi_1 &\sim R_1 \Psi(X, z) \quad \text{as } R_1 \rightarrow \infty \end{aligned} \tag{3.6.2}$$

where $c(R_1, \sigma)$ is defined in (3.3.7) and from (3.2.13) and (3.2.14) Θ and Ψ satisfy the horizontal boundary layer equations

$$\frac{\partial^4 \bar{\Psi}}{\partial z^4} = \frac{\partial \Theta}{\partial X} + \frac{1}{\sigma} \left[\frac{\partial^3 \bar{\Psi}}{\partial z^2 \partial X} \frac{\partial \bar{\Psi}}{\partial z} - \frac{\partial^3 \bar{\Psi}}{\partial z^3} \frac{\partial \bar{\Psi}}{\partial X} \right] \tag{3.6.3}$$

$$\frac{\partial^2 \Theta}{\partial z^2} = \frac{\partial(\Theta, \Psi)}{\partial(X, z)}. \tag{3.6.4}$$

These must be solved subject to the full horizontal conditions

$$\bar{\Psi} = \frac{\partial \bar{\Psi}}{\partial z} = \frac{\partial \Theta}{\partial z} = 0 \quad \text{on } z = 0, 1 \tag{3.6.5}$$

and the required outer behaviour

$$\Theta \sim X + F_1(z), \quad \bar{\Psi} \sim F_1(z) \quad \text{as } X \rightarrow \infty. \quad (3.6.6)$$

Here any constant contribution to Θ is considered part of $c(R_1, \sigma)$ and the solution must satisfy the integral property

$$\int_0^1 \bar{\Psi} \frac{d\Theta}{dz} dz = Q_0 \quad (\text{all } X). \quad (3.6.7)$$

As $X \rightarrow 0$ the governing equations (3.6.3) and (3.6.4) are first modified within a region where horizontal diffusion becomes significant. Here x, z are appropriate local variables and

$$T \sim c(R_1, \sigma) + R_1 \tilde{\Theta}(x, z) \quad (3.6.8)$$

$$\Psi \sim R_1 \tilde{\Psi}(x, z) \quad (3.6.9)$$

giving the inviscid convection - dominated system

$$\frac{d(\tilde{\Theta}, \tilde{\Psi})}{d(x, z)} = 0, \quad d(\nabla^2 \tilde{\Psi}, \tilde{\Psi}) + \sigma \frac{d\tilde{\Theta}}{dx} = 0. \quad (3.6.10)$$

Adjacent to the end wall it must be anticipated that $\tilde{\Psi} = 0$ in which case the inviscid zone must accommodate a re-circulating flow in which

$$\begin{aligned} \tilde{\Theta} &= \tilde{G}(\tilde{\Psi}) \\ \nabla^2 \tilde{\Psi} &= \sigma z \tilde{G}'(\tilde{\Psi}) + \tilde{W}(\tilde{\Psi}) \end{aligned} \quad (3.6.11)$$

where \tilde{G} and \tilde{W} are continuous single-valued functions of $\tilde{\Psi}$.

This in turn implies that there is no net contribution to the heat transfer (3.6.7) in the main body of the outer zone, $0 < z < 1$, as $X \rightarrow 0$. Instead, the net heat transfer at $X = 0$ implied by (3.6.7) must be supplied by a region where vertical diffusion is retained in (3.6.3) and (3.6.4). Such a balance, together with the vorticity equation and the requirement from (3.6.7) that $\Theta \Psi \sim 1$ implies scalings $z \sim X^{1/2}$, $\Psi \sim X^{1/2}$,

$\theta \sim X^{-1/2}$ as $X \rightarrow 0$ for a region near the lower wall of the cavity. This region represents the final asymptotic stage of a horizontal boundary layer initiated in the corner of the cavity at the base of the cold wall and is discussed in detail in Chapter 6.

Assuming that the profiles for the stream function and temperature are preserved as the fluid turns the corner from the vertical boundary layer, the initial profile for the horizontal boundary layer is defined by the solution to the system (3.3.13)-(3.3.15). In this horizontal boundary layer region where $x = O(1)$ the buoyancy term in the vorticity equation is too small to influence the flow field and since $u = O(R_1)$ in the inviscid zone above, the flow in the boundary layer, of speed $O(R_1^{6/5})$, has a jet like structure. This wall jet is fully discussed in Chapters 4 and 5. It emerges that there exists an intermediate region between the horizontal boundary layer where $x = O(1)$ and the main outer zone where $x = O(R_1)$. In this region near the ~~base~~^{base} of the cavity where $x = O(R_1^{2/5})$ the buoyancy term, absent at $x = O(1)$ in the vorticity equation, reappears and in addition the flow is partially driven by the external velocity of the inviscid zone above. This second stage of the horizontal boundary layer is analysed in Chapter 6 and a full numerical solution is presented in Chapter 7.

A diagram of the proposed overall structure for the end zone is shown in figure 3.7. The description is by no means complete in terms of the number of asymptotic regions that must develop in the limit as $R_1 \rightarrow \infty$, but is believed to contain the main ingredients of the process by which heat is transferred through the end zone. The remainder of the thesis is concerned with

testing the validity of the horizontal boundary layer structure at the base of the cavity. Although this is important in determining the consistency of the model overall, within the context of thermal boundary layer theory the problems are of significant interest in their own right.

TABLE 3.1

Effect of meshwidth on values of $f(\eta)$ and $g(\eta)$, $\sigma = 0.72$.

η	(a)	(b)	(c)
0.12	(f) 0.006055	0.006052	0.006041
	(g) 0.046482	0.046482	0.006480
0.48	0.083929	0.083919	0.083878
	0.185433	0.185430	0.185419
1.0	0.291876	0.291860	0.291794
	0.379155	0.379148	0.379122
2.0	0.739069	0.739057	0.739009
	0.683159	0.683152	0.683120
4.0	1.205203	1.205209	1.205234
	0.944906	0.944905	0.944903
8.0	1.321254	1.321208	1.321293
	0.998911	0.998919	0.998911

a) $h = 0.01$ b) $h = 0.02$ c) $h = 0.04$

TABLE 3.2

Comparison of wall heat transfers

Prandtl number σ	γ (computed)	γ (from 3.3.17)	K/σ (computed)
0.028	0.226	0.226	9.7319
0.1	0.289	0.290	3.41633
0.72	0.387	0.387	0.6116
8.1	0.461	0.462	0.0645
17.2	0.478	0.474	0.0313

Figure 3.1 Graph of f against η for $\sigma = 0.028$ (a),
0.1(b), 0.72(c), 8.1(d), 17.2(e).

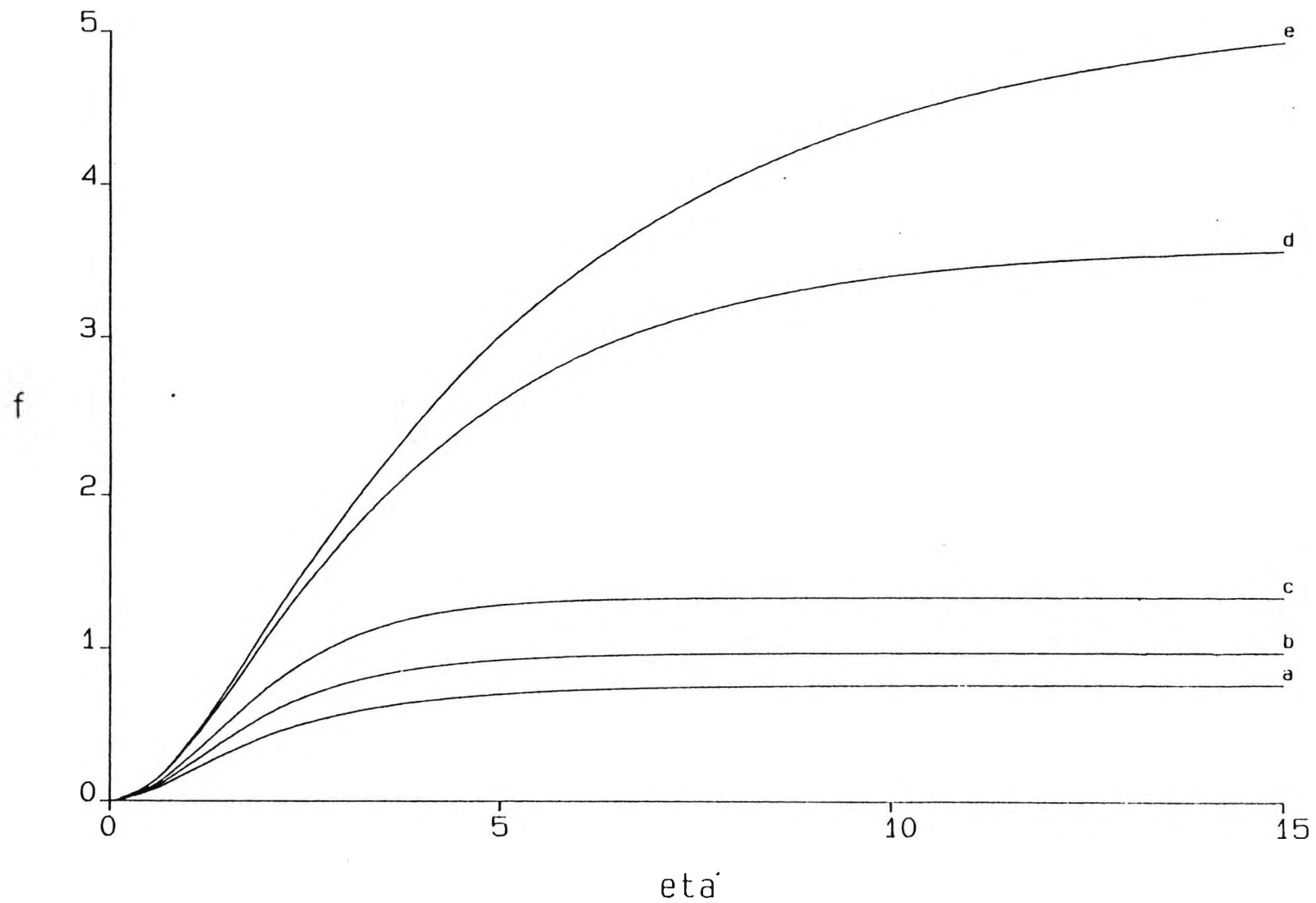


Figure 3.2 Graph of f' against η for $\sigma = 0.028$ (a),
0.1(b), 0.72(c), 8.1(d), 17.2(e).

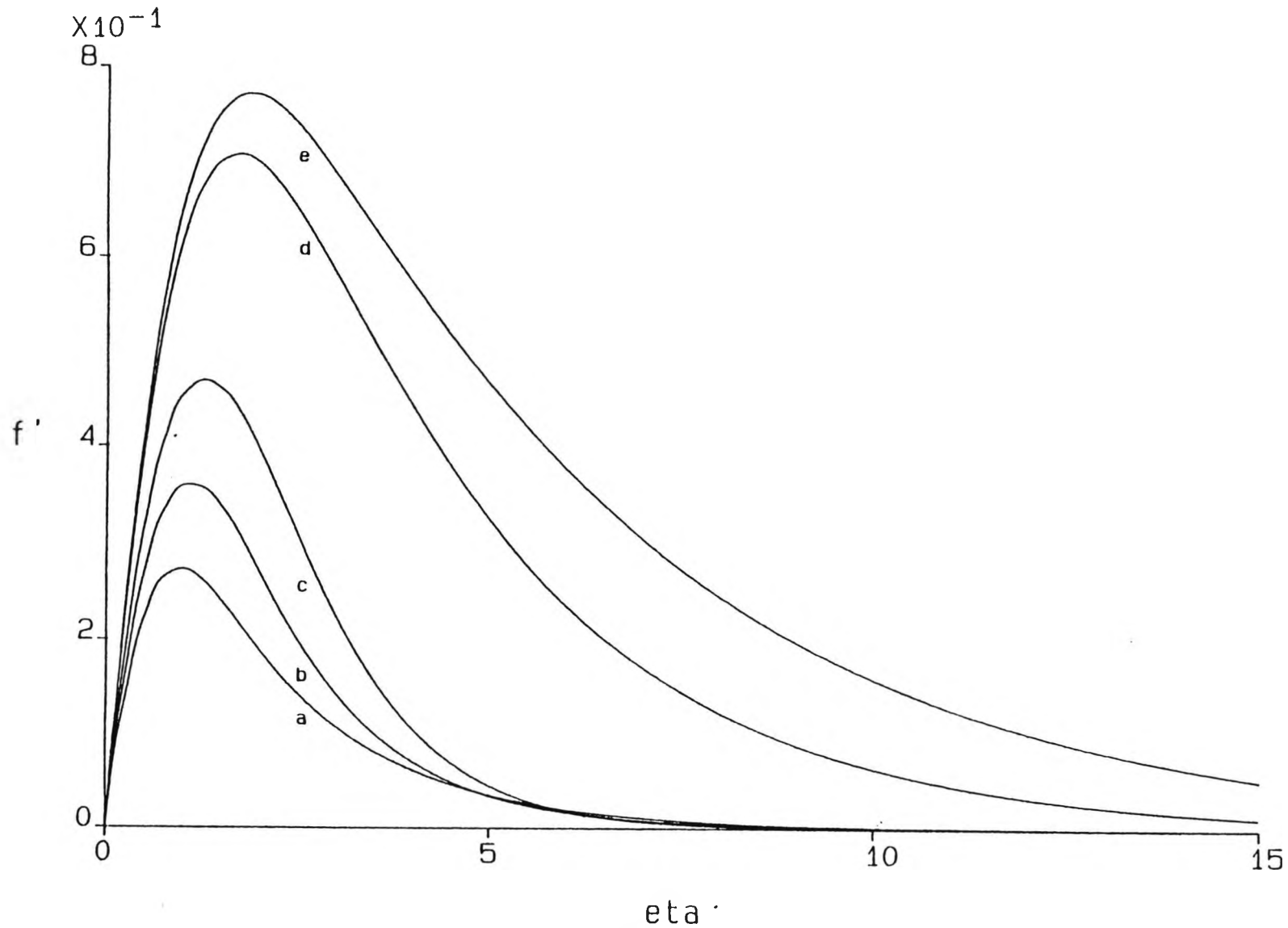


Figure 3.3 Graph of g against η for $\sigma = 0.028$ (a),
0.1(b), 0.72(c), 8.1(d), 17.2(e).

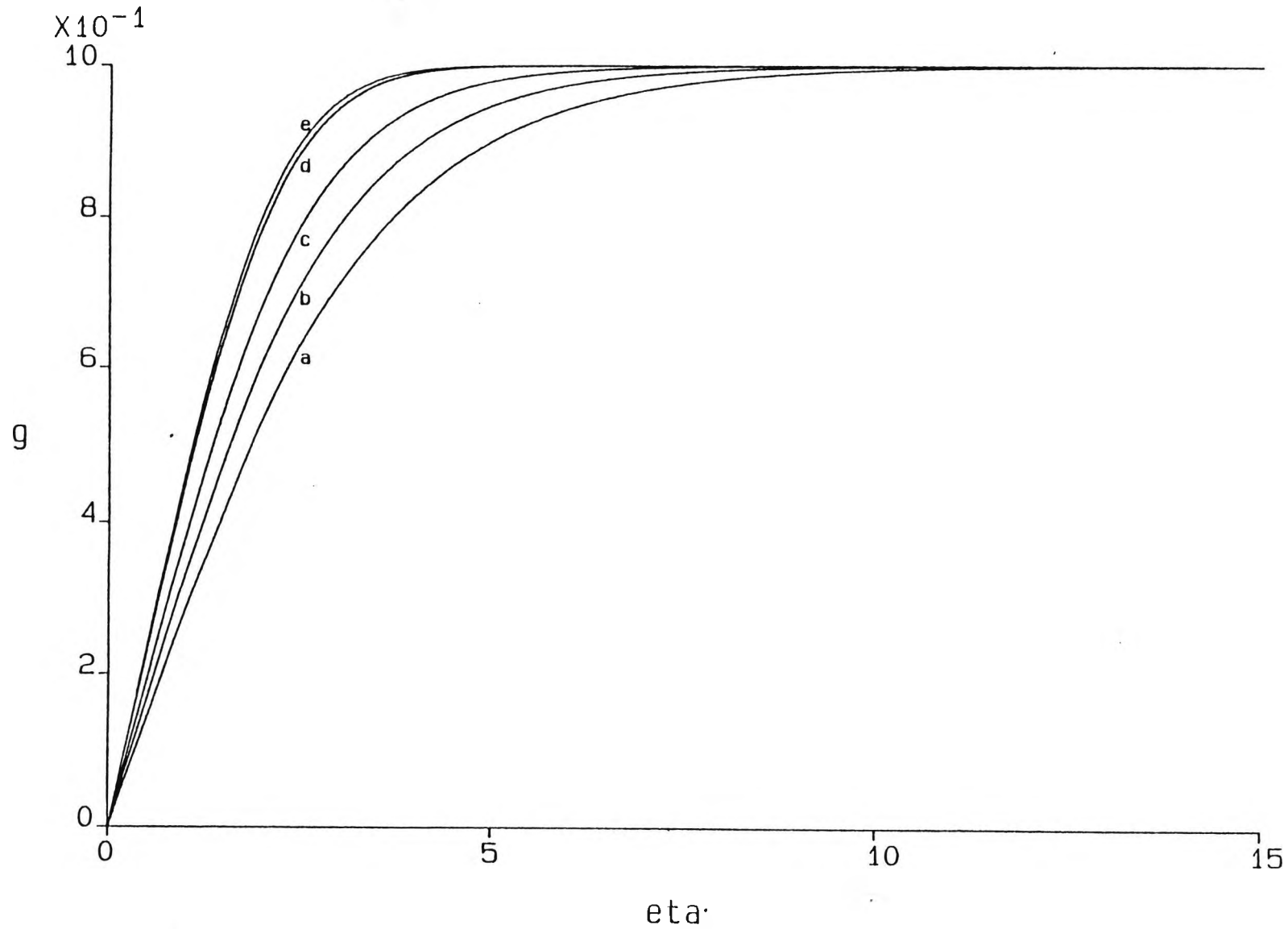


Figure 3.4 Comparison of present solution (a) and Kiukem solution (b) for temperature at $\sigma = 2$.

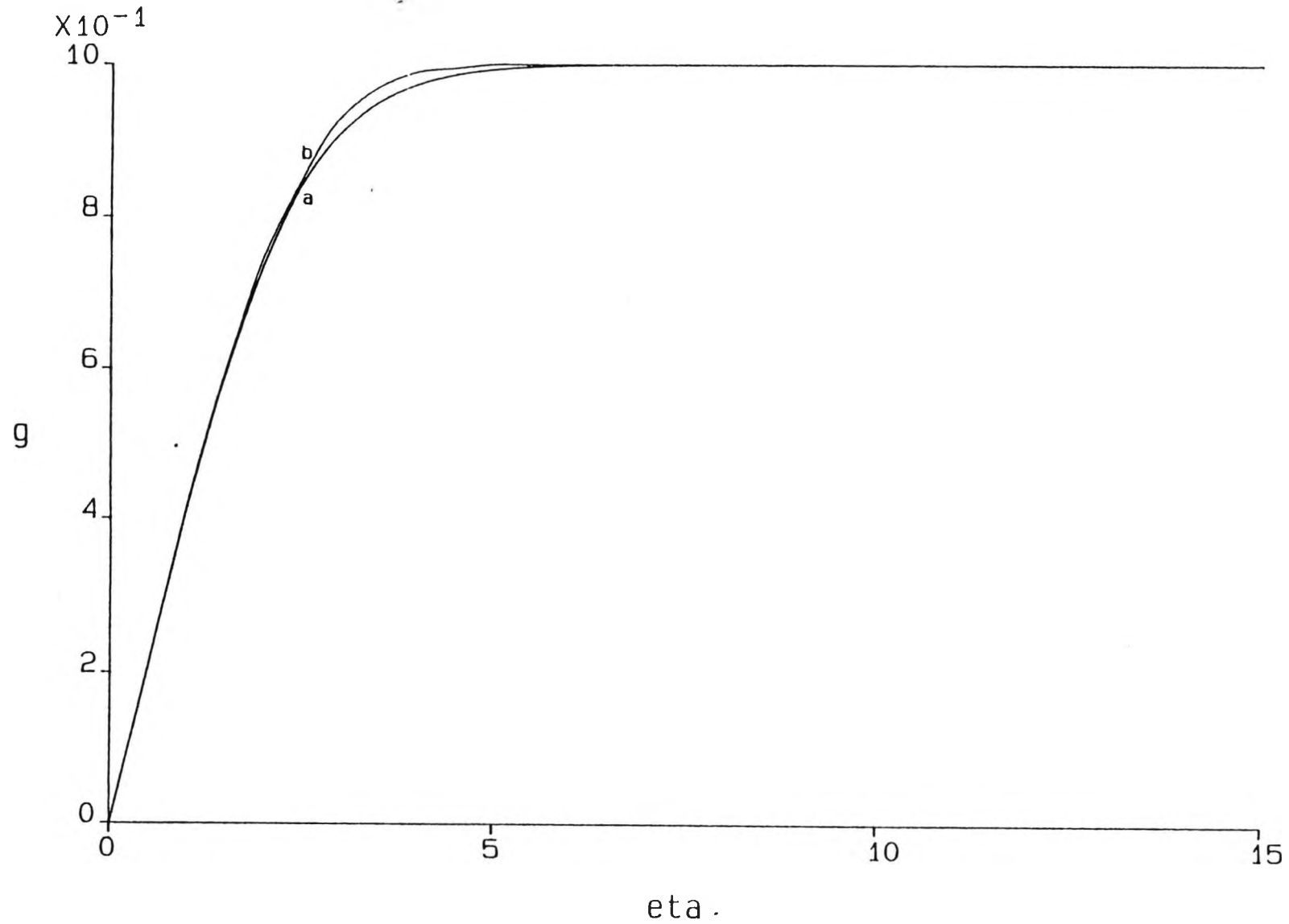
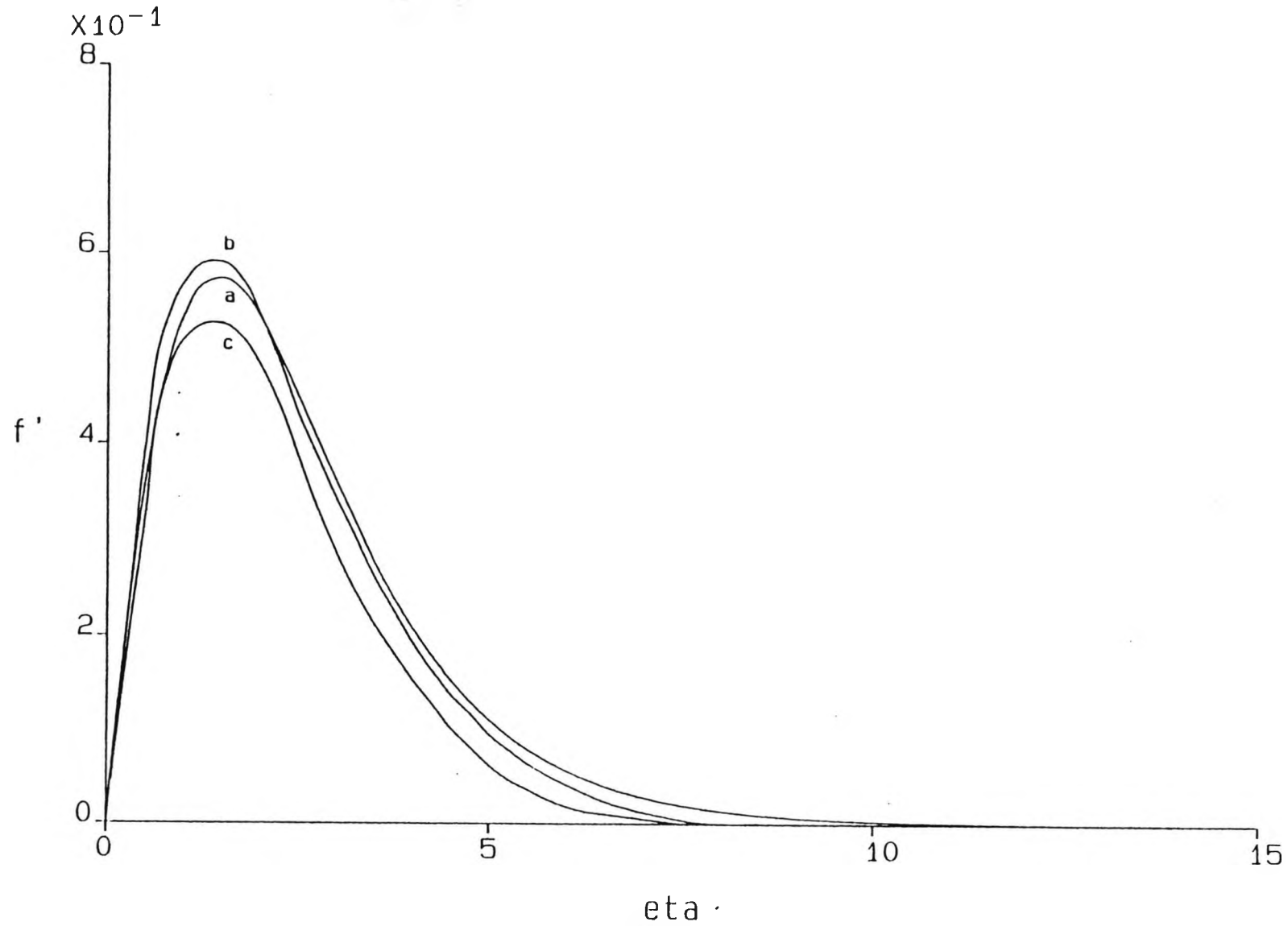
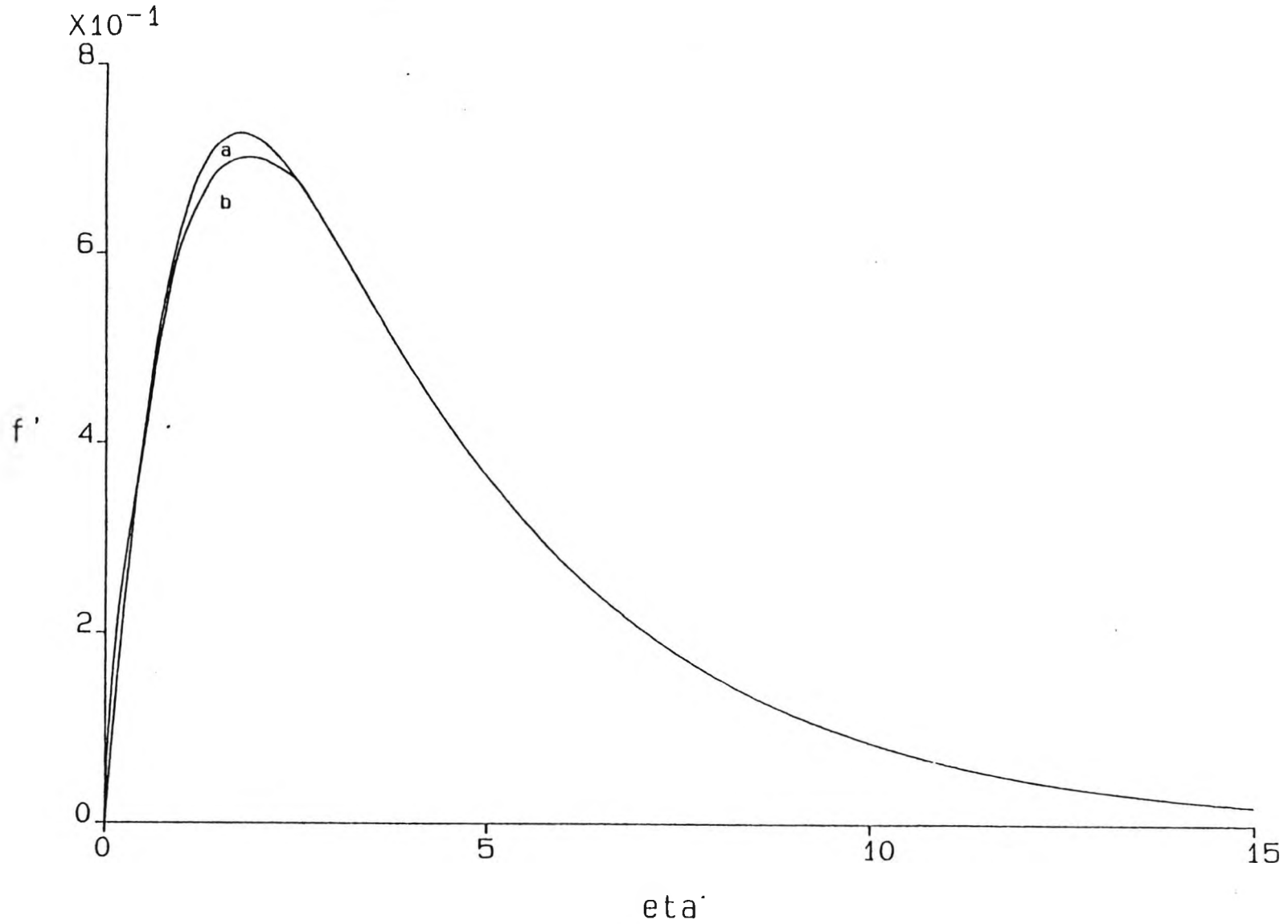


Figure 3.5 Comparison of present solution (a), Ostrach solution (b) and Kuiker solution (c) for velocity at $\sigma = 2$.



54

Figure 3.6 Comparison of present solution (a) with Kuiken solution (b) for velocity at $\sigma = 10$.



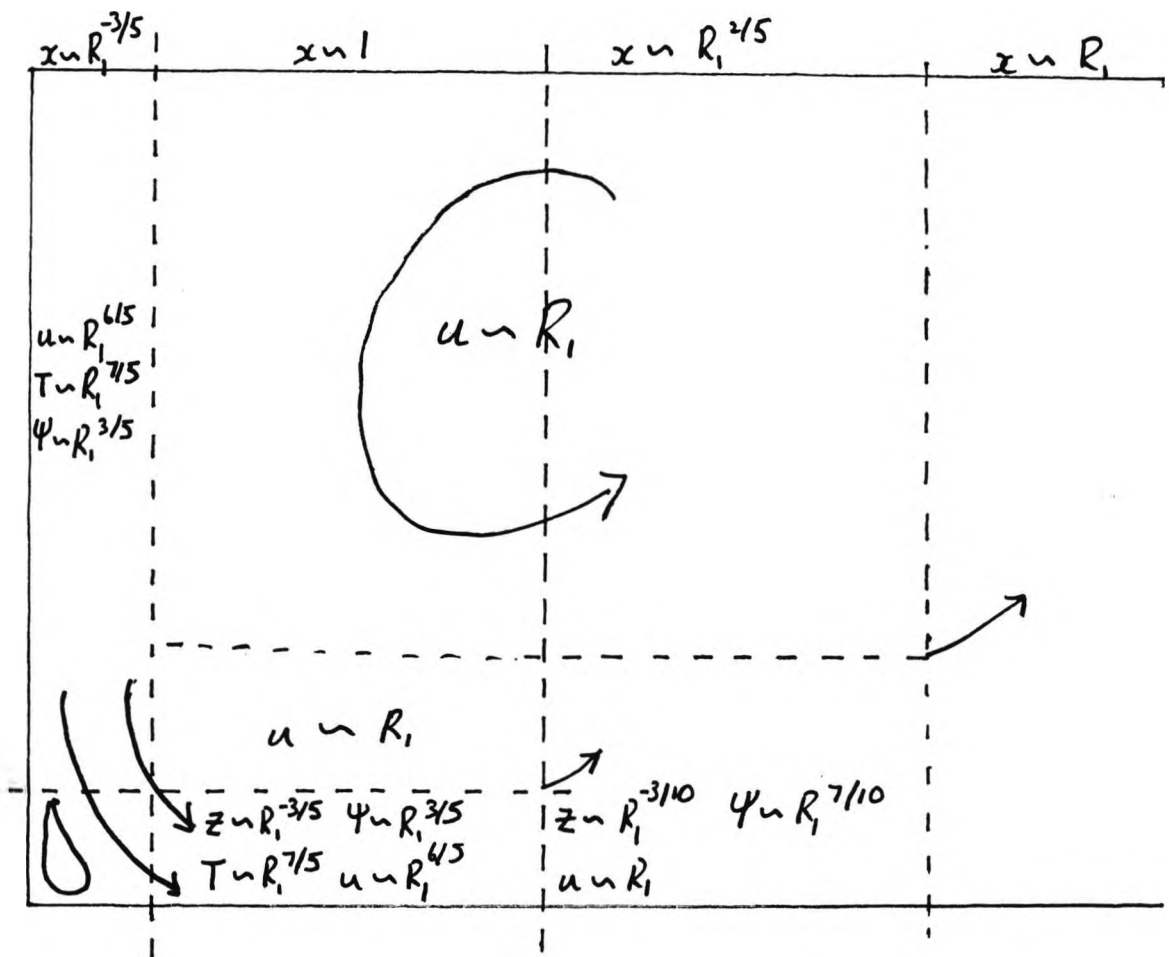


Figure 3.7 Proposed overall structure for end-zone.

CHAPTER 4

The horizontal boundary layer $x = 0(1)$:
asymptotic solution

4.1 Introduction

As described in Chapter 3, the isotherms and streamlines in the vertical boundary layer on the end wall are turned around the lower corner into a horizontal boundary layer. This chapter deals with the horizontal boundary layer for $x = 0(1)$. In Section 4.2 the horizontal boundary layer equation and boundary conditions are derived together with two integral constraints which are a feature of the flow. The solution for small x (where the flow has to adjust to the new boundary condition for the temperature on the insulated horizontal wall) is considered in Section 4.3. The fourth section outlines the form the flow assumes as $x \rightarrow \infty$, extending the work of Glauert (1956) to include the temperature field.

4.2 Formulation

The solution in the vertical boundary layer suggests the following scalings for the horizontal boundary layer

$$T \sim R_1^{7/5} c_0 T_2, \quad \psi \sim R_1^{3/5} \sigma c_0^{1/4} \Psi_2, \quad \phi \sim R_1^{12/5} \sigma p_2, \\ x = x, \quad z = R_1^{-3/5} c_0^{-1/4} z_2 \quad (R_1 \rightarrow \infty) \quad (4.2.1)$$

The horizontal velocity is $O(R_1)$ in the inviscid region above the horizontal boundary layer, whilst it is $O(R_1^{6/5})$ within it, so that the layer has a jet-like structure with zero external flow and pressure gradient. Since, from (3.2.17), $\frac{\partial p_2}{\partial z_2} = 0$, the pressure p_2 is constant everywhere, and from (3.2.16), (3.2.14) we obtain

$$\frac{\partial \Psi_2}{\partial z_2} \frac{\partial^2 \Psi_2}{\partial x \partial z_2} - \frac{\partial \Psi_2}{\partial x} \frac{\partial^2 \Psi_2}{\partial z_2^2} = \frac{\partial^3 \Psi_2}{\partial z_2^3} \quad (4.2.2)$$

and

$$\frac{\partial \Psi_2}{\partial z_2} \frac{\partial T_2}{\partial x} - \frac{\partial \Psi_2}{\partial x} \frac{\partial T_2}{\partial z_2} = \frac{1}{\sigma} \frac{\partial^2 T_2}{\partial z_2^2} \quad (4.2.3)$$

respectively.

These are to be solved subject to

$$\Psi_2 = \frac{\partial \Psi_2}{\partial z_2} = \frac{\partial T_2}{\partial z_2} = 0 \quad \text{on } z_2 = 0 \quad (4.2.4)$$

$$\frac{\partial \Psi_2}{\partial z_2} \rightarrow 0, \quad T_2 \rightarrow 1 \quad \text{as } z_2 \rightarrow \infty. \quad (4.2.5)$$

with initial profiles

$$T_2 = g(z_2), \quad \Psi_2 = \frac{1}{\sigma} f(z_2) \quad \text{on } x = 0. \quad (4.2.6)$$

Note that the temperature c_0 at the edge of the horizontal boundary layer has been scaled out of the problem through the transformations (4.2.1).

The initial conditions (4.2.6) at $x = 0$ are taken to be the solution to the vertical boundary layer equations solved in Chapter 3. Since these depend implicitly on σ a single calculation of the velocity field for all Prandtl numbers is not possible, even though the momentum field is uncoupled from the temperature, allowing the former to be calculated first.

Glauert (1956) showed that the momentum equation (4.2.2) and boundary conditions (4.2.4), (4.2.5) admit an integral relation involving the velocity

$$u_2 = \frac{\partial \Psi_2}{\partial z_2}, \quad (4.2.7)$$

$$P = \int_0^\infty u_2 \left[\int_{z_2}^\infty u_2^2 dz_2 \right] dz_2 = \text{constant}. \quad (4.2.8)$$

This constraint was interpreted physically by Glauert as the flux of exterior momentum flux being constant along the boundary layer.

By rewriting (4.2.3) as

$$\frac{d}{dx} \left[\psi_2 \frac{dT_2}{dz_2} \right] = \frac{d}{dz_2} \left[\frac{dT_2}{dx} \psi_2 - \frac{1}{\sigma} \frac{dT_2}{dz_2} \right] \quad (4.2.9)$$

and integrating with respect to z_2 from 0 to ∞ , making use of (4.2.4), (4.2.5), we also obtain

$$\frac{d}{dx} \int_0^{\infty} \psi_2 \frac{dT_2}{dz_2} dz_2 = 0 \quad (4.2.10)$$

or

$$Q = \int_0^{\infty} \psi_2 \frac{dT_2}{dz_2} dz_2 = \text{constant.} \quad (4.2.11)$$

The values of P and Q are determined from the initial profiles at $x = 0$ and in particular, $Q = Q_0 / c_0^{5/4} \sigma$, where Q_0 is the constant defined by (3.3.3). Integration using the functions f and g determined in Section 3.4 and based on Simpson's rule give the results for P and Q shown in table 4.1.

4.3 Solution for small x

At $x = 0$, the start of the horizontal boundary layer, the stream function and temperature are solutions of the vertical boundary layer equations (3.3.13)-(3.3.15) where the temperature is zero on the (cold) end wall. The boundary condition on the horizontal wall however is $\frac{\partial T_2}{\partial z_2} = 0$. A two-region solution is therefore generated consisting of an outer region where the solution coincides with the vertical boundary layer solution to a leading approximation and of an inner region, near the wall where this solution is adjusted to take account of the new boundary

condition.

(i) Outer Region

The stream function and the temperature are expanded as follows

$$\Psi_2 = \Psi_{20}(z_2) + x^{2/3} \Psi_{21}(z_2) + \dots \quad \text{as } x \rightarrow 0 \quad (4.3.1)$$

$$T_2 = T_{20}(z_2) + x^{2/3} T_{21}(z_2) + \dots \quad \text{as } x \rightarrow 0 \quad (4.3.2)$$

where the $x^{2/3}$ terms are a consequence of matching with the inner region solution (see section (ii) below). Substitution into (4.2.2) and (4.2.3) gives at $O(x^{-1/3})$

$$\frac{\partial \Psi_{20}}{\partial z_2} \frac{\partial \Psi_{21}}{\partial z_2} - \Psi_{21} \frac{\partial^2 \Psi_{20}}{\partial z_2^2} = 0 \quad (4.3.3)$$

and

$$\frac{\partial \Psi_{20}}{\partial z_2} T_{21} - \Psi_{21} \frac{\partial T_{20}}{\partial z_2} = 0 \quad (4.3.4)$$

respectively. Hence,

$$\Psi_{21} = c_2 \frac{\partial \Psi_{20}}{\partial z_2}, \quad T_{21} = c_2 \frac{\partial T_{20}}{\partial z_2} \quad (4.3.5)$$

where c_2 is a constant.

The profiles T_{20} and $\sigma \psi_{20}$ are the solutions $g(z_2)$ and $f(z_2)$ to the vertical boundary layer equations the forms of which for small values of the argument are given by

$$f(\eta) = K\eta^2 - \frac{1}{6}\eta^3 + \frac{1}{24}\gamma\eta^4 + \frac{1}{120}\frac{K^2}{\sigma}\eta^5 + \dots \quad \text{as } \eta \rightarrow 0 \quad (4.3.7)$$

$$g(\eta) = \gamma\eta - \frac{1}{16}K\gamma\eta^4 + \frac{1}{160}\gamma\eta^5 + \dots \quad \text{as } \eta \rightarrow 0. \quad (4.3.8)$$

where K and γ are the known constants already given in table 3.2 for various prandtl numbers. Therefore

$$\psi_2 = \left[\frac{K}{\sigma} z_2^2 - \frac{1}{6\sigma} z_2^3 + \frac{1}{24} \frac{\gamma}{\sigma} z_2^4 + \dots \right] + C_2 x^{2/3} \left[\frac{2K}{\sigma} z_2 - \frac{1}{2\sigma} z_2^2 + \frac{1}{6\sigma} \gamma z_2^3 + \dots \right] + \dots \text{ as } z_2 \rightarrow 0 \quad (4.3.9)$$

and

$$T_2 = \left[\gamma z_2 - \frac{1}{16} K \gamma z_2^4 + \frac{1}{160} \gamma z_2^5 + \dots \right] + C_2 x^{2/3} \left[\gamma - \frac{1}{4} K \gamma z_2^3 + \dots \right] + \dots \text{ as } z_2 \rightarrow 0. \quad (4.3.10)$$

(ii) Inner Region

Following the structure of the outer region, we expand the stream function and temperature as

$$\psi_2(x, z_2) = x^{2/3} f_{20}(\eta_2) + x f_{21}(\eta_2) + \dots \text{ as } x \rightarrow 0 \quad (4.3.11)$$

$$T_2(x, z_2) = x^{1/3} T_{20}(\eta_2) + x^{2/3} T_{21}(\eta_2) + \dots \text{ as } x \rightarrow 0 \quad (4.3.12)$$

where

$$\eta_2 = \frac{z_2}{x^{1/3}} = O(1). \quad (4.3.13)$$

As $\eta_2 \rightarrow \infty$ the inner region solution must match with the outer region solution as $z_2 \rightarrow 0$. Therefore

$$f_{20}(\eta_2) \sim \frac{K}{\sigma} \eta_2^2 \text{ as } \eta_2 \rightarrow \infty \quad (4.3.14)$$

$$f_{21}(\eta_2) \sim \frac{-1}{6\sigma} \eta_2^3 + 2C_2 \frac{K}{\sigma} \eta_2 \text{ as } \eta_2 \rightarrow \infty \quad (4.3.15)$$

$$T_{20}(\eta_2) \sim \gamma \eta_2 \text{ as } \eta_2 \rightarrow \infty \quad (4.3.16)$$

$$T_{21}(\eta_2) \sim C_2 \gamma \text{ as } \eta_2 \rightarrow \infty. \quad (4.3.17)$$

Substituting (4.3.11) and (4.3.13) into (4.2.2) we obtain at $O(x^{-1/3})$

$$\frac{1}{3} f_{20}'^2 - \frac{2}{3} f_{20} f_{20}'' = f_{20}''' \quad (4.3.18)$$

with wall conditions

$$f_{20} = f_{20}' = 0 \quad \text{at} \quad \eta_2 = 0 \quad (4.3.19)$$

and at $0(1)$

$$f_{20}' f_{21}' - f_{21} f_{20}'' - \frac{2}{3} f_{20} f_{21}'' = f_{21}''' \quad (4.3.20)$$

with wall conditions

$$f_{21} = f_{21}' = 0 \quad \text{at} \quad \eta_2 = 0. \quad (4.3.21)$$

The solution of (4.3.18) subject to (4.3.19) and (4.3.14) is simply

$$f_{20} = \frac{K}{\sigma} \eta_2^2 \quad (4.3.22)$$

so that the leading order velocity field is unchanged across the inner region. Hence (4.3.20) becomes

$$\frac{2K}{\sigma} (\eta_2 f_{21}' - f_{21} - \frac{1}{3} \eta_2 f_{21}'') = f_{21}''' \quad (4.3.23)$$

If we let

$$\eta_2 = \left(\frac{2K}{\sigma}\right)^{-1/3} \hat{\eta}_2, \quad f_{21} = \left(\frac{1}{2K}\right) \hat{f}_{21}, \quad c_2 = \frac{\sigma^{2/3}}{(2K)^{5/3}} \hat{c}_2 \quad (4.3.24)$$

then (4.3.23) becomes

$$\hat{\eta}_2 \hat{f}_{21}' - \hat{f}_{21} - \frac{1}{3} \hat{\eta}_2^2 \hat{f}_{21}'' = \hat{f}_{21}''' \quad (4.3.25)$$

which is to be solved subject to

$$\begin{aligned} \hat{f}_{21} = \hat{f}_{21}' = 0 \quad \text{at} \quad \hat{\eta}_2 = 0 \\ \hat{f}_{21} \sim -\frac{1}{6} \hat{\eta}_2^3 + \hat{c}_2 \hat{\eta}_2 \quad \text{as} \quad \hat{\eta}_2 \rightarrow \infty. \end{aligned} \quad (4.3.26)$$

The above system was solved numerically using a fourth order Runge-Kutta scheme and the value of \hat{c}_2 was found to be -1.427 .

Results for f_{20} and f_{21} are presented in figures 4.1 and 4.2 for various Prandtl numbers.

The existence of the required solution for \hat{f}_{21} can be confirmed analytically by setting

$$\hat{f}_{21} = \hat{\eta}_2 \hat{u}_2(\hat{\eta}_2) \quad (4.3.27)$$

so that (4.3.22) becomes

$$\frac{1}{3} \hat{\eta}_2^2 \hat{u}_2' - \frac{1}{3} \hat{\eta}_2^3 = \hat{\eta}_2 \hat{u}_2''' + 3 \hat{u}_2'' \quad (4.3.28)$$

Writing $\hat{u}_2' = \hat{\beta}_2$ (4.3.29)

$$\hat{\eta}_2 \hat{\beta}_2'' + (3 + \frac{1}{3} \hat{\eta}_2^3) \hat{\beta}_2' - \frac{1}{3} \hat{\eta}_2^2 \hat{\beta}_2 = 0 \quad (4.3.30)$$

and then letting $\hat{\beta}_2 = (\frac{3}{\hat{\eta}_2^2} + \hat{\eta}_2) \hat{V}_2(\hat{\eta}_2)$ (4.3.31)

gives

$$\hat{V}_2'' [9 \hat{\eta}_2 + 3 \hat{\eta}_2^4] + \hat{V}_2' [-9 + 18 \hat{\eta}_2^3 + \hat{\eta}_2^6] = 0 \quad (4.3.32)$$

which may be rewritten as

$$\frac{\hat{V}_2''}{\hat{V}_2'} = \frac{1}{\hat{\eta}_2} - \frac{1}{3} \hat{\eta}_2^2 - \frac{6 \hat{\eta}_2^2}{3 + \hat{\eta}_2^3} \quad (4.3.33)$$

Integration of (4.3.33) gives

$$\hat{V}_2' = \frac{-\hat{a}_2 \hat{\eta}_2}{(3 + \hat{\eta}_2^3)^2} \exp \left[-\frac{\hat{\eta}_2^3}{9} \right] \quad (4.3.34)$$

where \hat{a}_2 is a constant.

A second integration gives

$$\hat{V}_2 = \hat{a}_2 \left[\int_{\hat{\eta}_2}^{\infty} \frac{\hat{\eta}_2}{(3 + \hat{\eta}_2^3)^2} \exp \left[-\frac{\hat{\eta}_2^3}{9} \right] d\hat{\eta}_2 \right] + \hat{b}_2 \quad (4.3.35)$$

where \hat{b}_2 is a constant.

Thus from (3.3.31)

$$\hat{\beta}_2 = \left(\frac{3}{\hat{\eta}_2^2} + \hat{\eta}_2 \right) \left(\hat{a}_2 \hat{I}_2(\hat{\eta}_2) + \hat{b}_2 \right) \quad (4.3.36)$$

$$\text{where } \hat{I}_2(\hat{\eta}_2) = \int_{\hat{\eta}_2}^{\infty} \frac{\hat{\eta}_2}{(3 + \hat{\eta}_2^3)^2} \exp\left(-\frac{\hat{\eta}_2^3}{9}\right) d\hat{\eta}_2 \quad (4.3.37)$$

and hence using (4.3.29) and integrating (4.3.36)

$$\hat{u}_2 = -\hat{a}_2 \int_{\hat{\eta}_2}^{\infty} \left(\frac{3}{\hat{\eta}_2^2} + \hat{\eta}_2\right) \hat{I}_2(\hat{\eta}_2) d\hat{\eta}_2 + \hat{b}_2 \left(-\frac{3}{\hat{\eta}_2} + \frac{1}{2} \hat{\eta}_2^2\right) + \hat{d}_2 \quad (4.3.38)$$

where \hat{d}_2 in a constant.

Thus from (4.3.27) we finally get

$$\hat{f}_{21} = -\hat{a}_2 \hat{\eta}_2 \int_{\hat{\eta}_2}^{\infty} \left(\frac{3}{\hat{\eta}_2^2} + \hat{\eta}_2\right) \hat{I}_2(\hat{\eta}_2) d\hat{\eta}_2 + \hat{b}_2 \left(-3 + \frac{1}{2} \hat{\eta}_2^3\right) + \hat{d}_2 \hat{\eta}_2. \quad (4.3.39)$$

Comparison with (4.3.26) gives

$$\hat{b}_2 = -\frac{1}{3}, \quad \hat{d}_2 = \hat{c}_2. \quad (4.3.40)$$

Defining

$$\hat{J}_2(\hat{\eta}_2) = \hat{\eta}_2 \int_{\hat{\eta}_2}^{\infty} \left[\frac{3}{\hat{\eta}_2^2} + \hat{\eta}_2\right] \hat{I}_2(\hat{\eta}_2) d\hat{\eta}_2 \quad (4.3.41)$$

we have

$$\hat{f}_{21} = -\hat{a}_2 \hat{J}_2(\hat{\eta}_2) + 1 + \hat{c}_2 \hat{\eta}_2 - \frac{1}{6} \hat{\eta}_2^3 \quad (4.3.42)$$

$$\text{and since } \hat{f}_{21} = \hat{f}'_{21} = 0 \quad \text{at } \hat{\eta}_2 = 0 \quad (4.3.43)$$

$$\hat{a}_2 = \frac{1}{\hat{J}_2(0)} \quad (4.3.44)$$

and

$$\hat{c}_2 = \frac{\hat{J}'_2(0)}{\hat{J}_2(0)}. \quad (4.3.45)$$

Thus

$$\hat{f}_{21} = \left(1 - \frac{\hat{J}_2(\hat{\eta}_2)}{\hat{J}_2(0)}\right) + \frac{\hat{J}'_2(0)}{\hat{J}_2(0)} \hat{\eta}_2 - \frac{1}{6} \hat{\eta}_2^3. \quad (4.3.46)$$

Substituting (4.3.11)-(4.3.13) into (4.2.3) we find that at $0(x^{1/3})$

$$\frac{1}{3} f'_{20} \tau_{20} - \frac{2}{3} f_{20} \tau'_{20} = \frac{1}{\sigma} \tau_{20}'' \quad (4.3.47)$$

and at $0(1)$

$$\frac{2}{3} f_{20}' \tau_{21} + \frac{1}{3} f_{21}' \tau_{20} - \frac{2}{3} f_{20} \tau_{21}' - f_{21} \tau_{20}' = \frac{1}{\sigma} \tau_{21}'' \quad (4.3.48)$$

Recalling (4.3.22), equation (4.3.47) becomes

$$\frac{2K_1}{3} [\gamma_2 \tau_{20} - \gamma_2^2 \tau_{20}'] = \tau_{20}'' \quad (4.3.49)$$

and (4.3.48) is now

$$\frac{1}{3} [2K_1 \gamma_2 (2\tau_{21} - \gamma_2 \tau_{21}') + \sigma (f_{21}' \tau_{20} - 3 f_{21} \tau_{20}')] = \tau_{21}'' \quad (4.3.50)$$

The boundary conditions at the wall from (4.2.4) are

$$\tau_{20}' = \tau_{21}' = 0 \quad \text{at} \quad \gamma_2 = 0. \quad (4.3.51)$$

If we let

$$\gamma_2 = \left(\frac{2K}{3}\right)^{-1/3} \bar{\gamma}_2, \quad \tau_{20} = \delta \left(\frac{2K}{3}\right)^{-1/3} \bar{\tau}_{20}(\bar{\gamma}_2) \quad (4.3.52)$$

then (4.3.49) becomes

$$\bar{\gamma}_2 \bar{\tau}_{20} - \bar{\gamma}_2^2 \bar{\tau}_{20}' = \bar{\tau}_{20}'' \quad (4.3.53)$$

which is to be solved subject to

$$\bar{\tau}_{20}' = 0 \quad \text{at} \quad \bar{\gamma}_2 = 0$$

$$\bar{\tau}_{20} \sim \bar{\gamma}_2 \quad \text{as} \quad \bar{\gamma}_2 \rightarrow \infty. \quad (4.3.54)$$

The systems for $\bar{\tau}_{20}$ and $\bar{\tau}_{21}$ were solved numerically using a fourth order Runge-Kutta scheme. The η_2^2 behaviour of τ_{21} as $\eta_2 \rightarrow \infty$ was eliminated in the solution by solving twice and subtracting out the quadratic behaviour. Results for τ_{20} and τ_{21} are presented in figures 4.3 and 4.4 for several Prandtl numbers.

The existence of the required solution for $\bar{\tau}_{20}$ can be confirmed analytically by setting

$$\bar{\tau}_{20} = \bar{\eta}_2 \bar{u}_2(\bar{\eta}_2). \quad (4.3.55)$$

Substitution into (4.3.53) gives

$$\bar{\eta}_2 \bar{u}_2'' = -(2 + \bar{\eta}_2^3) \bar{u}_2' \quad (4.3.56)$$

which on integration gives

$$\bar{u}_2' = \frac{-\bar{b}_2}{\bar{\eta}_2^2} \exp\left(-\frac{1}{3} \bar{\eta}_2^3\right) \quad (4.3.57)$$

where \bar{b}_2 is a constant.

A second integration produces

$$\bar{u}_2 = \bar{b}_2 \int_{\bar{\eta}_2}^{\infty} \frac{1}{\bar{\eta}_2} \exp\left(-\frac{1}{3} \bar{\eta}_2^3\right) d\bar{\eta}_2 + \bar{d}_2 \quad (4.3.58)$$

where \bar{d}_2 is a constant.

Hence from (4.3.55)

$$\bar{\tau}_{20} = \bar{b}_2 \bar{\eta}_2 \int_{\bar{\eta}_2}^{\infty} \frac{1}{\bar{\eta}_2^2} \exp\left(-\frac{1}{3} \bar{\eta}_2^3\right) d\bar{\eta}_2 + \bar{d}_2 \bar{\eta}_2 \quad (4.3.59)$$

and consequently, after integration by parts

$$\bar{\tau}_{20}' = \bar{d}_2 - \bar{b}_2 \int_{\bar{\eta}_2}^{\infty} \bar{\eta}_2 \exp\left(-\frac{1}{3} \bar{\eta}_2^3\right) d\bar{\eta}_2. \quad (4.3.60)$$

Using the boundary conditions

$$\bar{\tau}_{20}' = 0 \quad \text{at} \quad \bar{\eta}_2 = 0, \quad \bar{\tau}_{20}' \rightarrow 1 \quad \text{as} \quad \bar{\eta}_2 \rightarrow \infty. \quad (4.3.61)$$

given by (4.3.51) and (4.3.16), the result (4.3.59) becomes

$$\bar{\tau}_{20} = \bar{\eta}_2 \left\{ 1 + \frac{\int_{\bar{\eta}_2}^{\infty} \frac{1}{\bar{\eta}_2^2} \exp\left(-\frac{1}{3} \bar{\eta}_2^3\right) d\bar{\eta}_2}{\int_0^{\infty} \bar{\eta} \exp\left(-\frac{1}{3} \bar{\eta}^3\right) d\bar{\eta}} \right\}. \quad (4.3.62)$$

In summary, leading and second order terms in both inner and outer expansions of the solution as $x \rightarrow 0$ have been determined. Knowledge of the constant c_2 completes the outer solution (4.3.5) which involves order $x^{2/3}$ corrections to both the velocity and temperature fields. The leading order velocity field is unchanged across the inner region but the wall temperature has been shown to increase like $x^{1/3}$ with

$$T_2(x, 0) \sim x^{1/3} \gamma \left(\frac{2K}{3} \right)^{-1/3} \quad \text{as } x \rightarrow 0. \quad (4.3.63)$$

The skin friction decreases sharply, with

$$u_{2,z_2}(x, 0) \sim \frac{2K}{\sigma} + x^{1/3} f_{21}'(0) \quad \text{as } x \rightarrow 0 \quad (4.3.64)$$

while at the edge of the jet

$$\psi_2(x, \infty) \sim \sigma^{-1} f(\infty) + o(x^{2/3}) \quad \text{as } x \rightarrow 0. \quad (4.3.65)$$

4.4 Solution for large x

The momentum problem was first studied by Glauert (1956) and following his method we solve using a similarity variable

$$\eta_2 = \frac{1}{4} \frac{z_2}{x^{3/4}} \quad (4.4.1)$$

with

$$\psi_2 = x^{1/4} \phi_2(\eta_2) + \dots \quad (x \rightarrow \infty) \quad (4.4.2)$$

as suggested by the integral constraint (4.2.8).

Substitution into (4.2.2) gives

$$\phi_2''' + \phi_2 \phi_2'' + 2 \phi_2'^2 = 0 \quad (4.4.3)$$

which is to be solved subject to the boundary conditions derived from (4.2.4) and (4.2.5)

$$\phi_2(0) = 0, \quad \phi_2'(0) = 0, \quad \phi_2'(\infty) = 0. \quad (4.4.4)$$

Equation (4.4.3) is reducible to

$$\phi_2^{-1/2} \phi_2' + \frac{2}{3} \phi_2^{3/2} = \text{constant} \quad (4.4.5)$$

after two integrations (Glauert (1956)). The constant here is taken to be $(2/3)K_2^{3/2}$, so that ϕ_2 may be written in the form

$$\phi_2 = K_2 g_2 (\zeta_2)^2 \quad (4.4.6)$$

and substitution into (4.4.5) leads to

$$g_2' = \frac{K_2}{3} (1 - g_2^3) \quad (4.4.7)$$

which when integrated gives

$$\zeta_2 = \frac{1}{K_2} \left[\log_e \frac{\sqrt{1+g_2^2+g_2^4}}{1-g_2} + \sqrt{3} \tan^{-1} \left(\frac{\sqrt{3}g_2}{2+g_2} \right) \right]. \quad (4.4.8)$$

Substitution of (4.4.1)-(4.4.2) into the integral constraint (4.2.8) gives

$$P = \frac{1}{4} \int_0^\infty \phi_2' \left\{ \int_{\zeta_2}^\infty \phi_2'^2 d\zeta_2 \right\} d\zeta_2 \quad (4.4.9)$$

which, with the use of (4.4.6) and (4.4.7) becomes

$$P = \frac{2}{3} K_2^4 \int_0^1 g_2 \left\{ \int_{g_2}^1 (\bar{g}_2^{-2} - \bar{g}_2^{-5}) d\bar{g}_2 \right\} dg_2 \quad (4.4.10)$$

and on integration

$$P = \frac{K_2^4}{40}. \quad (4.4.11)$$

This fixes K_2 in solution (4.4.6).

Graphs of ϕ_2/K_2 and $\phi_2'/\frac{2}{3}K_2^2$ against $K_2\zeta_2$ are presented in figures 4.5 and 4.6 respectively.

To find a solution for the temperature we write

$$T_2 = 1 + x^m \theta_2(\xi_2) + \dots \quad \text{as } x \rightarrow \infty \quad (4.4.12)$$

and consequently require that

$$\theta_2 \rightarrow 0 \quad \text{as } \xi_2 \rightarrow \infty. \quad (4.4.13)$$

Substitution of (4.4.2) and (4.4.12) into the integral constraint (4.2.1) shows that

$$m = -\frac{1}{4}. \quad (4.4.14)$$

Substitution of (4.4.12) with (4.4.14) into (4.2.3) gives

$$\frac{1}{\sigma} \theta_2'' = -(\phi_2' \theta_2 + \phi_2 \theta_2'). \quad (4.4.15)$$

Integration of (4.4.15) using the wall condition

$$\theta_2' = 0 \quad \text{on } \xi_2 = 0 \quad (4.4.16)$$

derived from (4.2.4), gives

$$\frac{1}{\sigma} \theta_2' = -\phi_2 \theta_2. \quad (4.4.17)$$

A second integration yields

$$\theta_2 = \theta_0 \exp \left[-\sigma \int_0^{\xi_2} \phi_2 d\xi_2 \right] \quad (4.4.18)$$

where $\theta_0 = \theta_2(0)$ is an arbitrary constant.

Use of (4.4.6) and (4.4.7) enables us to rewrite (4.4.18) as

$$\theta_2 = \theta_0 \exp \left[-\sigma \int_0^{g_2} \frac{3g_2^2}{1-g_2^3} dg_2 \right] \quad (4.4.19)$$

which is easily simplified to

$$\theta_2 = \theta_0 (1-g_2^3)^\sigma. \quad (4.4.20)$$

Substitution of (4.4.2) and (4.4.12) with (4.4.14) into the integral constraint (4.2.11) gives

$$Q = -3\theta_0 K_2 \sigma \int_0^1 (1-g_2^3)^{\sigma-1} g_2^4 dg_2 \quad (4.4.21)$$

Substituting $p_2 = 1 - g_2^3$, equation (4.4.21) becomes

$$Q = -\theta_0 K_2 \sigma \int_0^1 p_2^{\sigma-1} (1-p_2)^{2/3} dp_2 \quad (4.4.22)$$

or

$$Q = -\theta_0 K_2 \sigma \frac{\Gamma(\sigma)\Gamma(5/3)}{\Gamma(\sigma + 5/3)}$$

This fixes θ_0 in solution (4.4.20).

Graphs of θ_2/θ_0 and $\theta_2'/\theta_0 K_2$ against $K_2 \zeta_2$ are presented in figures 4.7 and 4.8 respectively.

To find higher order terms in the stream function and temperature solutions it is noted that an 'origin shift'

$$\psi_2 = (x+d_2)^{1/4} \phi_2(\hat{\zeta}_2) \quad (4.4.23)$$

$$T_2 = (x+d_2)^{-1/4} \theta_2(\hat{\zeta}_2) \quad (4.4.24)$$

may be applied, where

$$\hat{\zeta}_2 = \frac{1}{4} \frac{z_2}{(x+d_2)^{3/4}}, \quad d_2 = \text{constant}, \quad (4.4.25)$$

without changing the equations (4.4.3) and (4.4.15) for ϕ_2 and θ_2 . Thus (4.4.23) and (4.4.24) are also exact solutions to the boundary layer equations. Expanding (4.4.23) and (4.4.24) by a Taylor expansion

$$\psi_2 = x^{1/4} \phi_2(\zeta_2) + \frac{1}{4} d_2 x^{-3/4} [\phi_2(\zeta_2) - 3\zeta_2 \phi_2'(\zeta_2)] + \dots \quad (4.4.26)$$

$$T_2 = 1 + x^{-1/4} \theta_2(\zeta_2) - \frac{1}{4} d_2 x^{-5/4} [\theta_2(\zeta_2) + 3\zeta_2 \theta_2'(\zeta_2)] + \dots \quad (4.4.27)$$

provides the likely form of the solutions as $x \rightarrow \infty$. The above

results may be recovered by formally writing

$$\psi_2 = x^{1/4} \phi_{21}(\zeta_2) + x^{-3/4} \phi_{22}(\zeta_2) + \dots \quad (4.4.28)$$

$$T_2 = x^{-1/4} \theta_{21}(\zeta_2) + x^{-5/4} \theta_{22}(\zeta_2) + \dots \quad (4.4.29)$$

and substituting into (4.2.2) and (4.2.3). Then

$$\phi_{21}''' + 2\phi_{21}'' + \phi_{21}\phi_{21}'' = 0; \quad \phi_{21} = \phi_{21}' = 0 \quad (\zeta_2 = 0), \quad \phi_{21}'(\infty) = 0 \quad (4.4.30)$$

and

$$\phi_{22}''' + 8\phi_{21}'\phi_{22}' - 3\phi_{22}\phi_{21}'' + \phi_{21}\phi_{22}'' = 0 \quad (4.4.31)$$

$$\phi_{22} = \phi_{22}' = 0 \quad (\zeta_2 = 0), \quad \phi_{22}'(\infty) = 0$$

$$\text{so that we may write } \phi_{21} = \phi_2 \quad (4.4.32)$$

and it is easily confirmed that

$$\phi_{22} = \frac{1}{4} d_2 (\phi_2 - 3\zeta_2 \phi_2') \quad (4.4.33)$$

where d_2 is an arbitrary constant equivalent to that appearing in (4.4.23).

From the equations and boundary conditions for the temperature

$$\frac{1}{\sigma} \theta_{21}'' + \phi_{21}' \theta_{21} + \phi_{21} \theta_{21}' = 0; \quad \theta_{21}'(0) = 0, \quad \theta_{21}(\infty) = 0 \quad (4.4.34)$$

and

$$\frac{1}{\sigma} \theta_{22}'' + 5\phi_{21}' \theta_{22} + \phi_{22}' \theta_{21} - 3\phi_{22} \theta_{21}' + \phi_{21} \theta_{22}' = 0; \quad (4.4.35)$$

$$\theta_{22}'(0) = 0, \quad \theta_{22}(\infty) = 0$$

so that we may write $\theta_{21} = \theta_2$ (4.4.36)

and it is easily verified that

$$\theta_{22} = -\frac{1}{4} d_2 (\theta_2 + 3 \int_2 \theta_2') \quad (4.4.37)$$

confirming the form for the temperature in (4.4.27).

Thus in this ^{sub-}section we have shown that for large x the jet takes on the Glauert similarity form with the velocity decreasing to order $x^{-1/2}$. The temperature rises to its constant external value across the entire layer to within a correction of order $x^{-1/4}$.

TABLE 4.1

Values of P and Q for various σ

σ	c_0	P	Q
0.72	6.05×10^{-5}	0.648698	0.717354
8.1	5.26×10^{-5}	0.004291	0.075912
17.2	5.11×10^{-5}	0.000928	0.036692

Figure 4.1 Graph of f_{20} against η_2 for Prandtl numbers
a) 0.028, b) 0.1, c) 0.72, d) 8.1, e) 17.2.

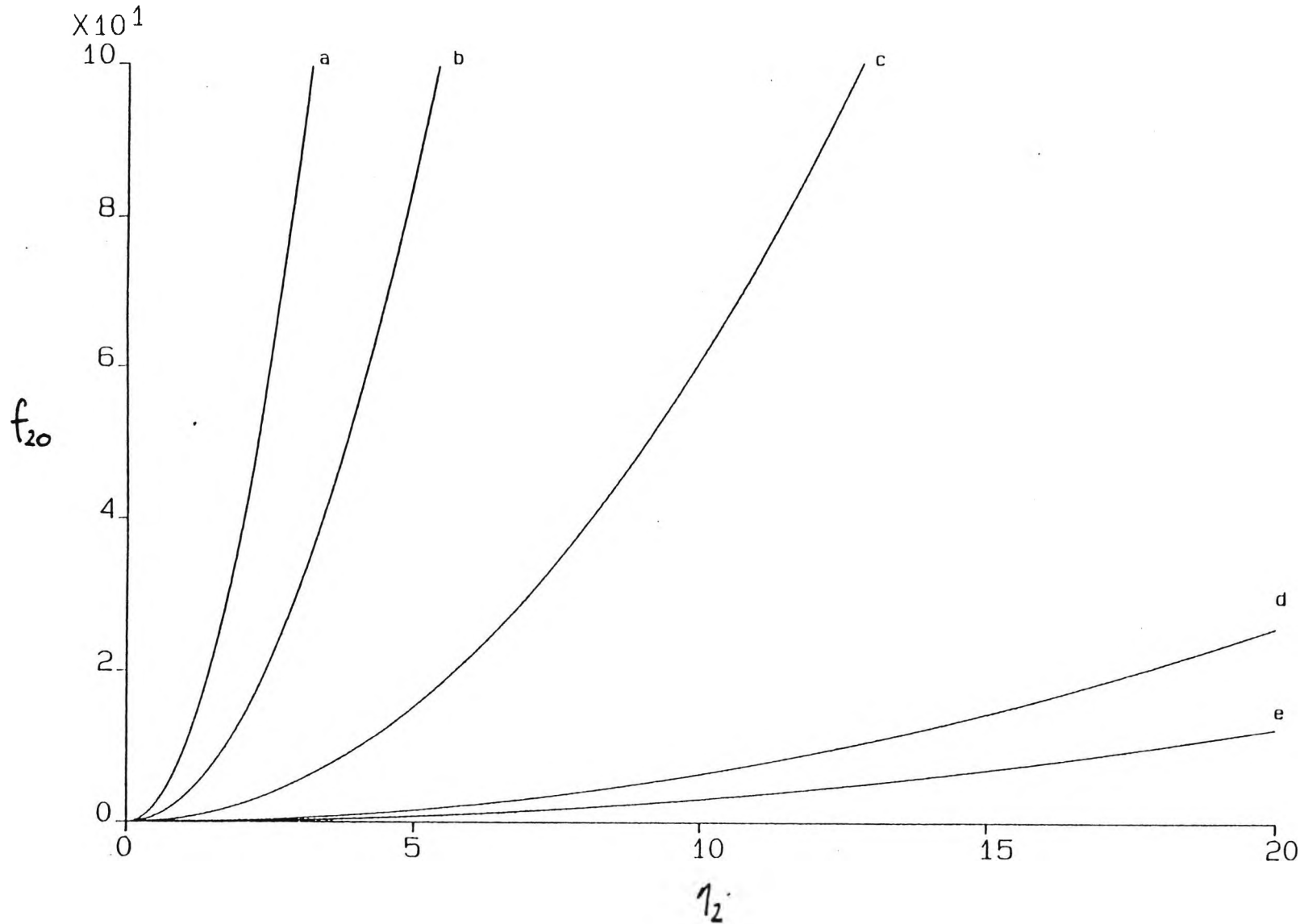


Figure 4.2 Graph of f_{21} for Prandtl numbers a) 0.028 and e) 17.2.

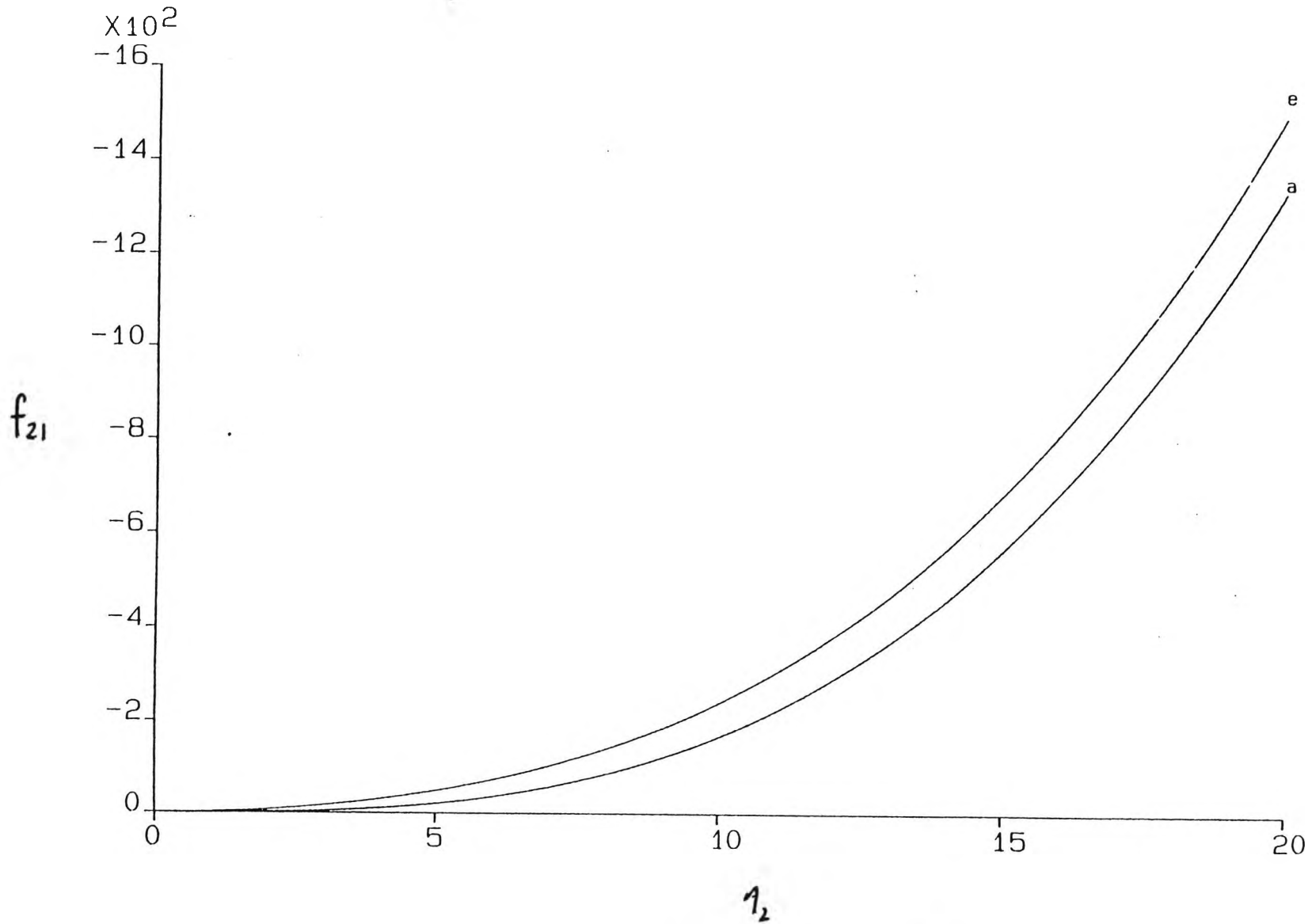


Figure 4.3 Graph of τ_{20} against η_2 for Prandtl numbers
a) 0.028, c) 0.72 and e) 17.2.

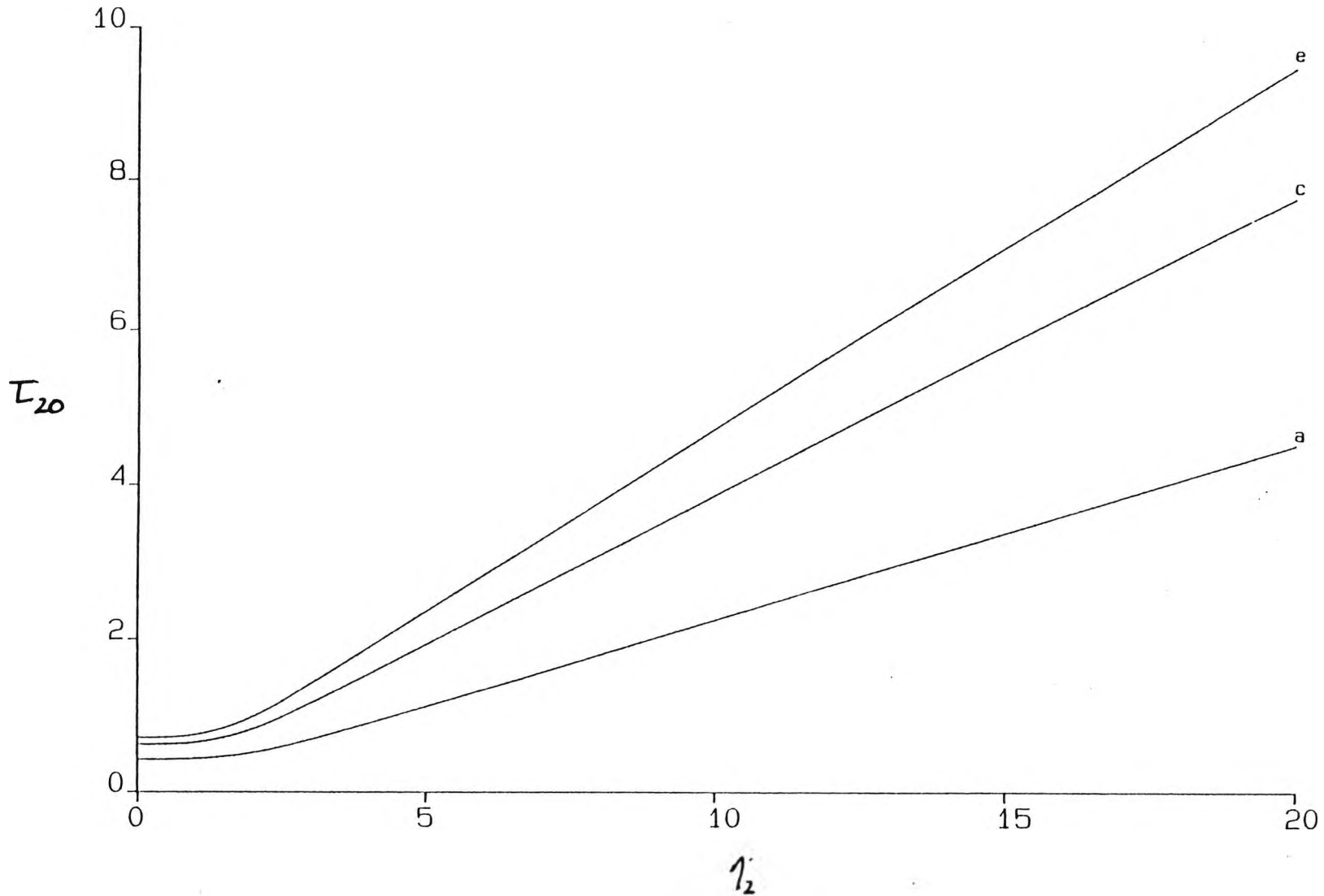


Figure 4.4 Graph of τ_{21} against η_2 for Prandtl numbers
d) 8.1 and e) 17.2.

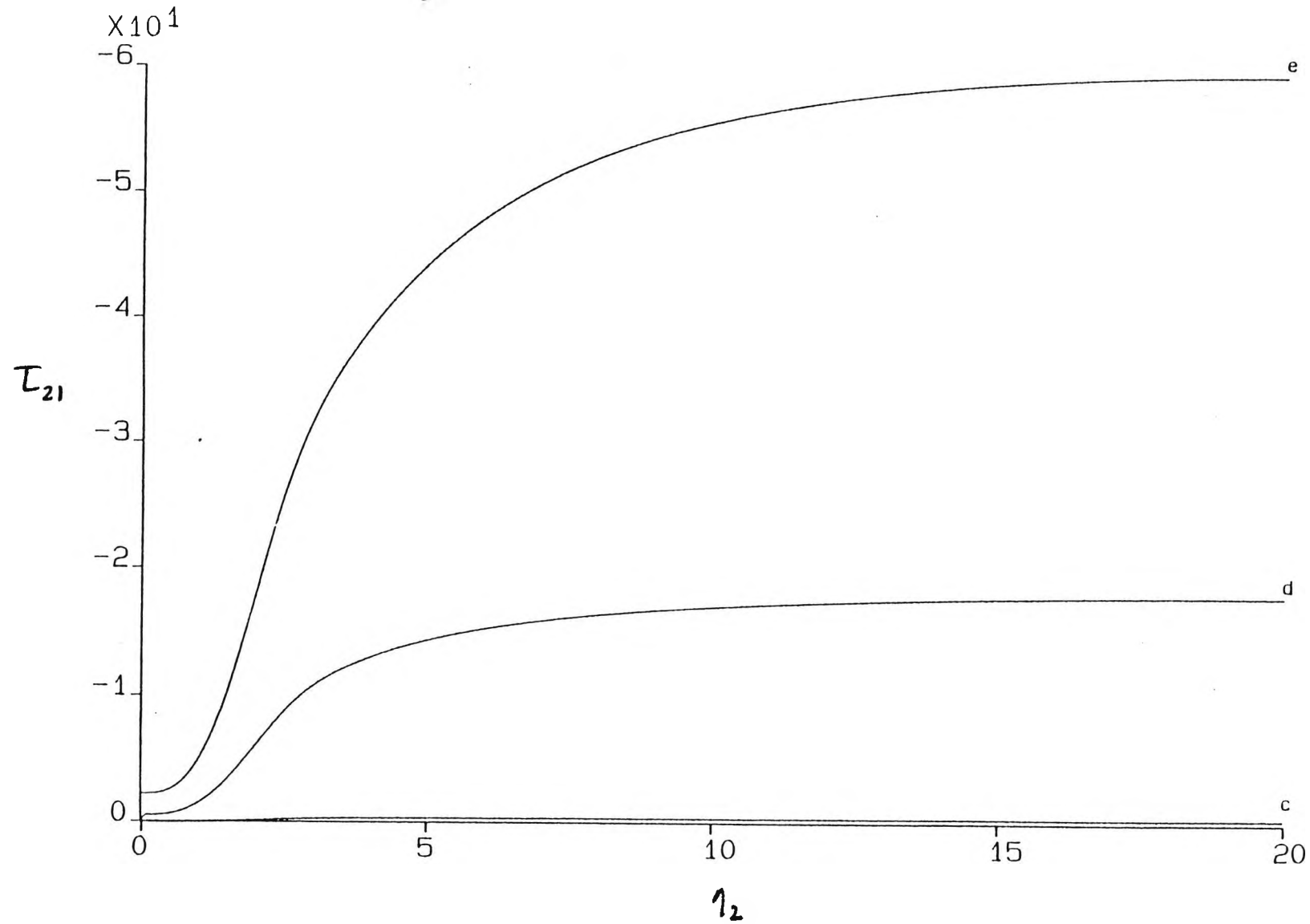


Figure 4.5 Graph of ϕ_2/K_2 against $K_2\zeta_2$.

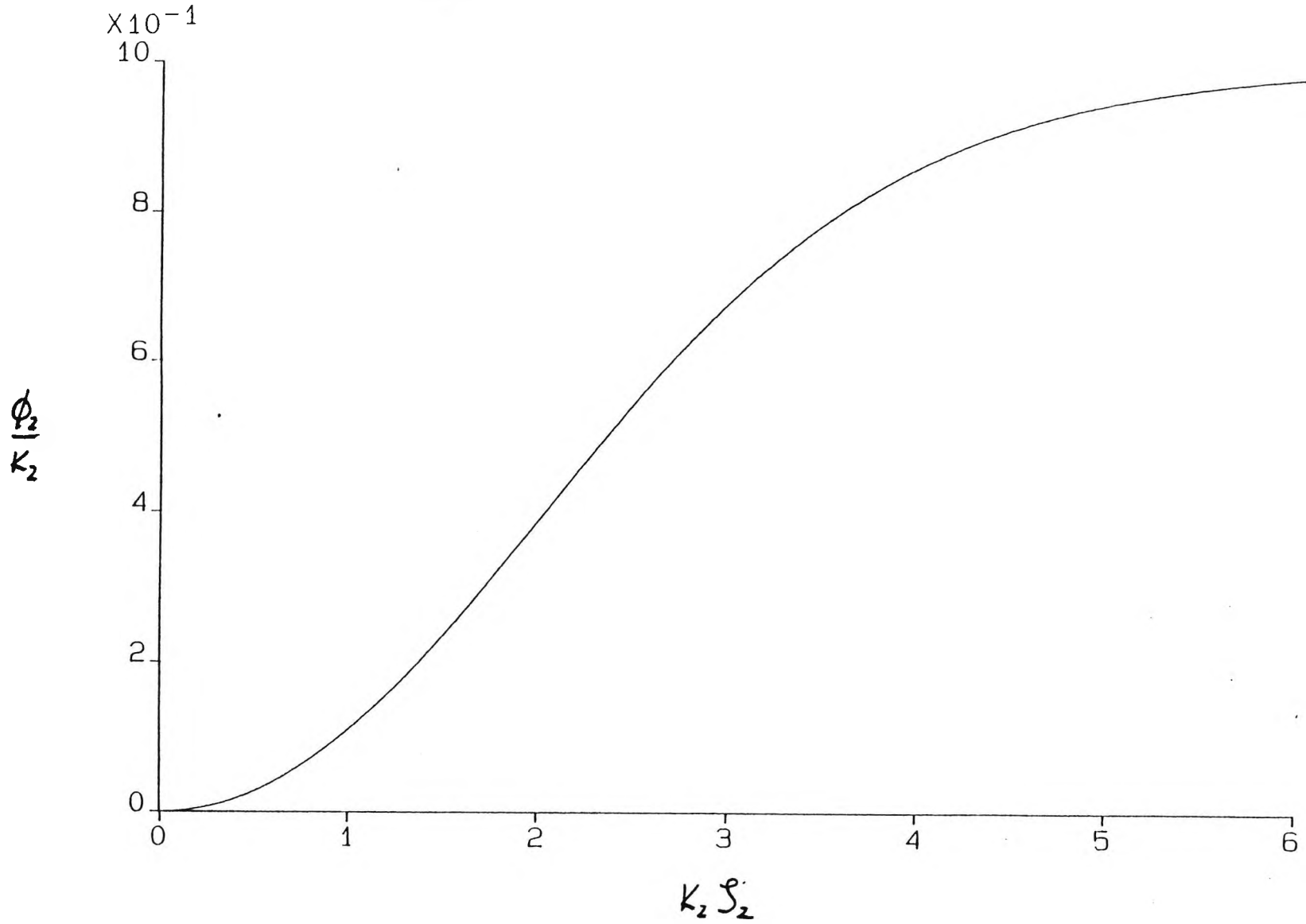


Figure 4.6 Graph of $\phi_2' / \frac{2}{3}K_2^2$ against $K_2\zeta_2$.

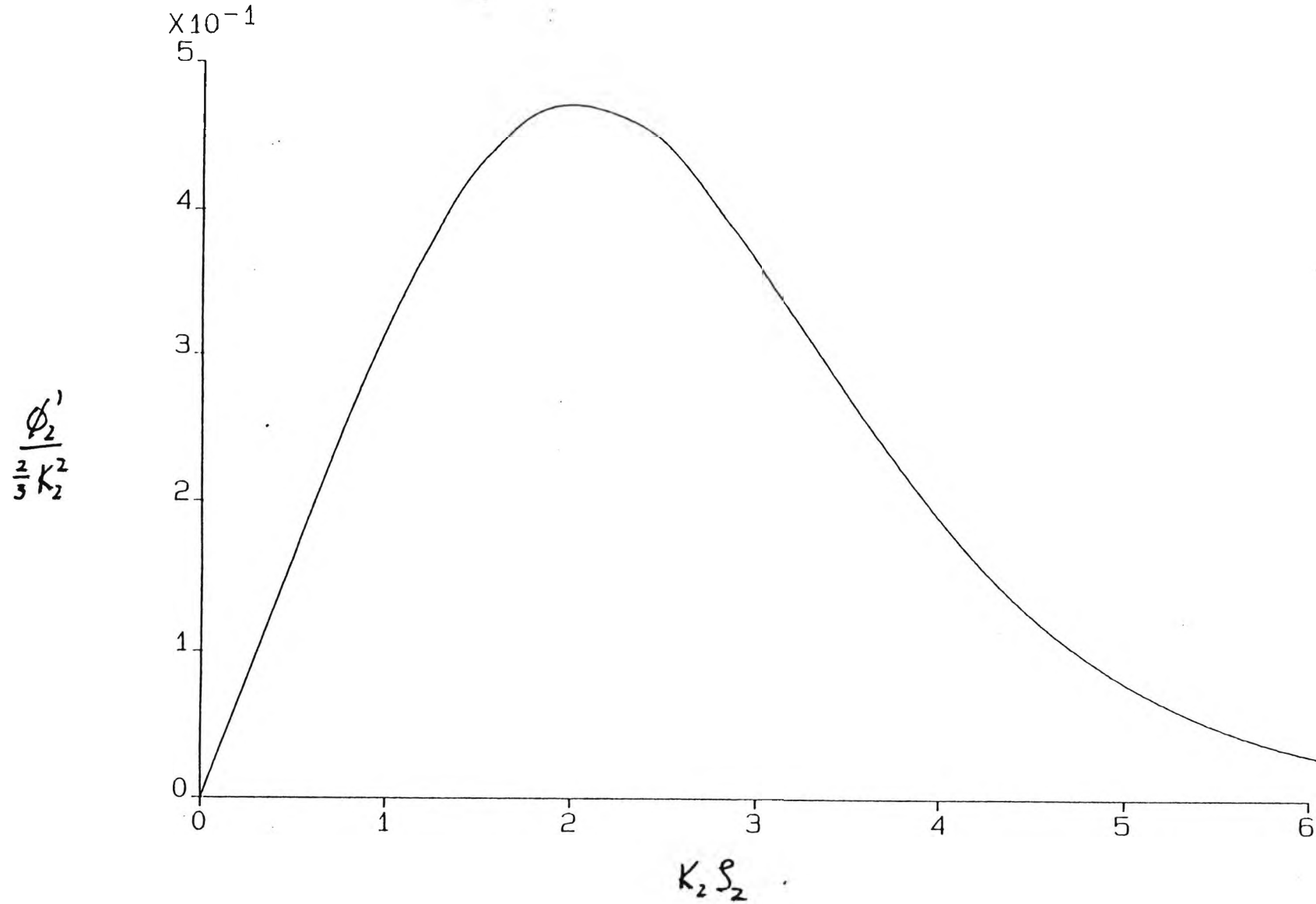


Figure 4.7 Graph of θ_2/θ_0 against $K_2\zeta_2$ for Prandtl numbers a) 0.028, b) 0.1, c) 0.72 and d) 8.1.

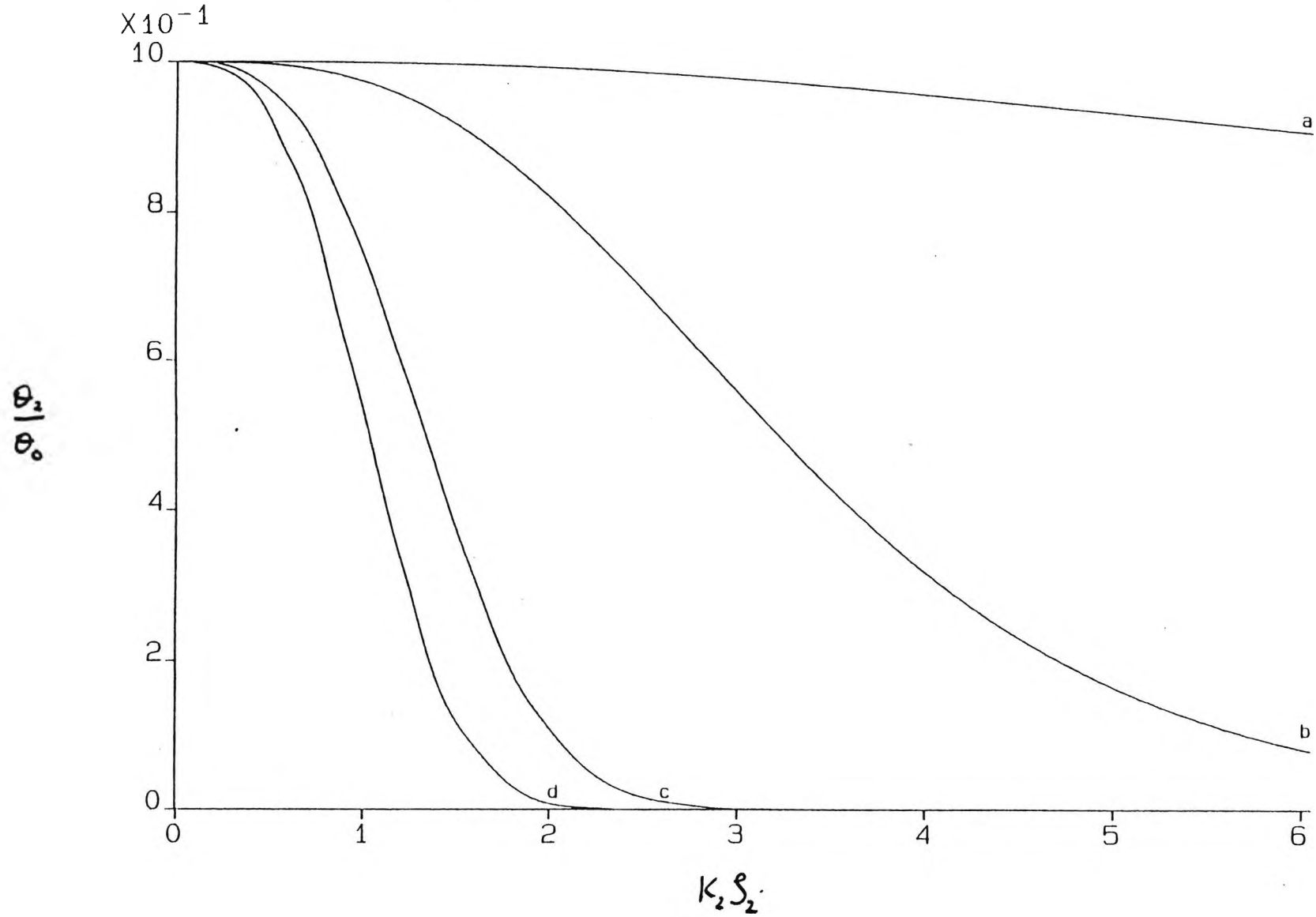
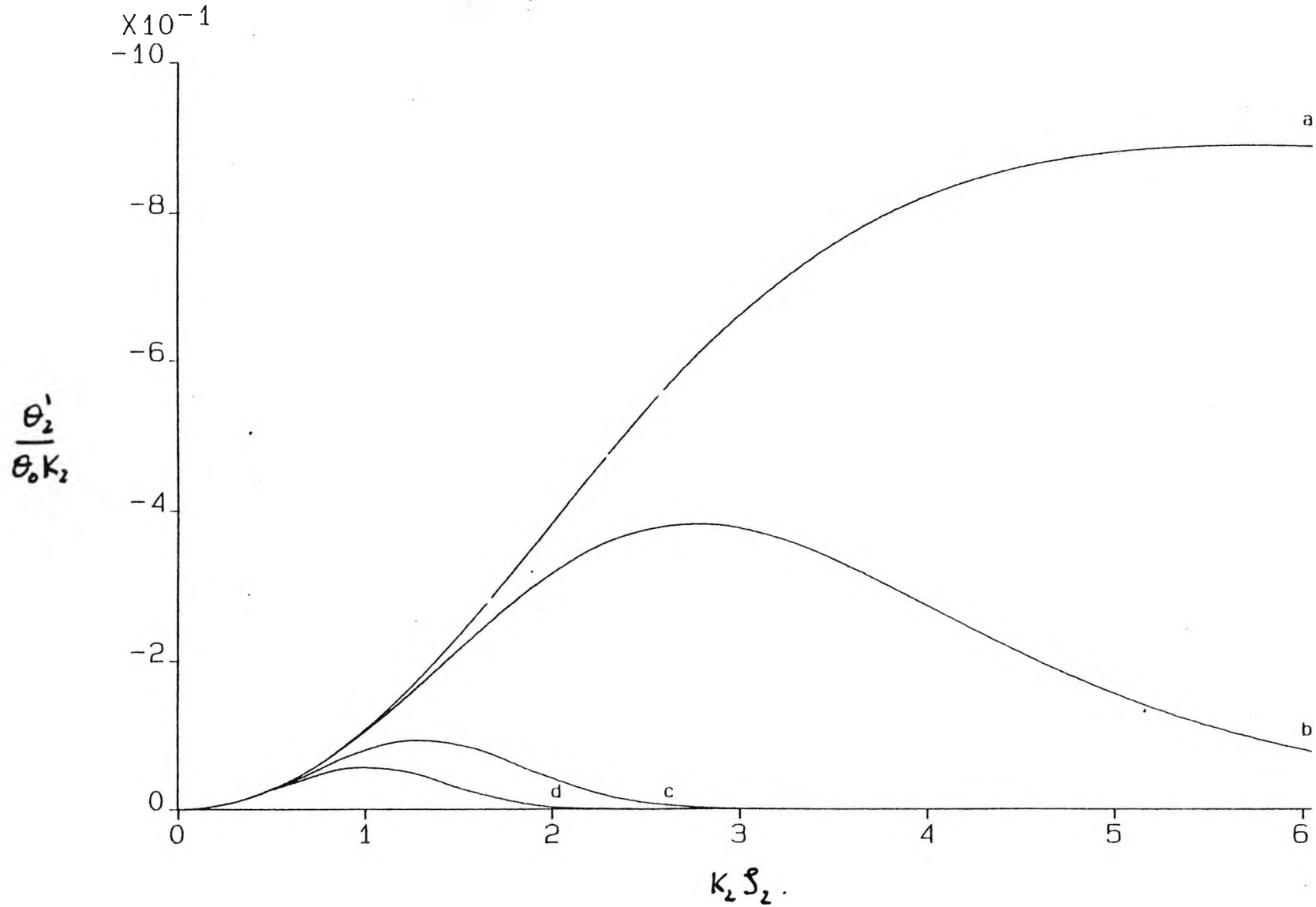


Figure 4.8 Graph of $\theta'_2/\theta_0 K_2$ against $K_2 \zeta_2$ for Prandtl numbers a) 0.028, b) 0.1, c) 0.72 and d) 8.1.



81

CHAPTER 5

The horizontal boundary layer $x = 0(1)$:

numerical solution

5.1 Introduction

This chapter contains a numerical study of the horizontal boundary layer where $x = 0(1)$. The solution is in two parts. In Section 5.2 the solution is found for the region $0 < x < 1$ using a two-region method developed by Smith (1974) but extending it to incorporate the temperature field. The scheme is based on the small x structure outlined in Chapter 4. The solution for $x > 1$ is based on the large x structure outlined in Chapter 4 and is discussed in Section 5.3. The numerical results are summarised and compared with the analytical work of Chapter 4 in Section 5.4.

5.2 Solution for $0 < x < 1$

Following the structure for small x discussed in Section 4.3 of Chapter 4 we consider a two-region solution, similar to that discussed by Smith (1974) consisting, first, of an inner region near the wall where $\eta_2 = \frac{z_2}{x^{1/3}} = 0(1)$ and the stream

function and temperature are written in the form

$$\psi_2 = \xi_2^2 \bar{\psi}_2(\xi_2, \eta_2) \quad (5.2.1)$$

$$T_2 = \xi_2 \bar{T}_2(\xi_2, \eta_2) \quad (5.2.2)$$

$$\text{where } \xi_2 = x^{1/3}, \quad \eta_2 = z_2/x^{1/3}. \quad (5.2.3)$$

Secondly, in the outer region where z_2 is order one the stream function and temperature are written in the form

$$\Psi_2 = \hat{\Psi}_2(\xi_2, z_2) \quad (5.2.4)$$

$$\bar{T}_2 = \hat{\bar{T}}_2(\xi_2, z_2). \quad (5.2.5)$$

The governing equations are the horizontal boundary layer equations (4.2.2) and (4.2.3) with the boundary conditions (4.2.4) and (4.2.5).

(i) Region I (inner region)

Substitution of (5.2.1)-(5.2.3) into (4.2.2) and (4.2.3)

gives

$$\frac{\partial^3 \bar{\Psi}_2}{\partial \eta_2^3} = \frac{1}{3} \left(\frac{\partial \bar{\Psi}_2}{\partial \eta_2} \right)^2 - \frac{2}{3} \bar{\Psi}_2 \frac{\partial^2 \bar{\Psi}_2}{\partial \eta_2^2} + \frac{1}{3} \xi_2 \left[\frac{\partial \bar{\Psi}_2}{\partial \eta_2} \frac{\partial^2 \bar{\Psi}_2}{\partial \xi_2 \partial \eta_2} - \frac{\partial^2 \bar{\Psi}_2}{\partial \eta_2^2} \frac{\partial \bar{\Psi}_2}{\partial \xi_2} \right] \quad (5.2.6)$$

and

$$\frac{1}{\sigma} \frac{\partial^2 \bar{T}_2}{\partial \eta_2^2} = \frac{1}{3} \bar{T}_2 \frac{\partial \bar{\Psi}_2}{\partial \eta_2} - \frac{2}{3} \bar{\Psi}_2 \frac{\partial \bar{T}_2}{\partial \eta_2} + \frac{1}{3} \xi_2 \left[\frac{\partial \bar{\Psi}_2}{\partial \eta_2} \frac{\partial \bar{T}_2}{\partial \xi_2} - \frac{\partial \bar{\Psi}_2}{\partial \xi_2} \frac{\partial \bar{T}_2}{\partial \eta_2} \right] \quad (5.2.7)$$

respectively.

We obtain a system of first order differential equations for discretization by setting

$$\hat{A} = \bar{\Psi}_2, \hat{B} = \frac{\partial \hat{A}}{\partial \eta_2}, \hat{C} = \frac{\partial \hat{B}}{\partial \eta_2}, \hat{D} = \bar{T}_2, \hat{E} = \frac{\partial \hat{D}}{\partial \eta_2} \quad (5.2.8)$$

which when substituted into (5.2.6) and (5.2.7) yield

$$\frac{\partial \hat{C}}{\partial \eta_2} + \frac{2}{3} \hat{A} \hat{C} - \frac{1}{3} \hat{B}^2 = \frac{\xi_2}{3} \left[\hat{B} \frac{\partial \hat{B}}{\partial \xi_2} - \hat{C} \frac{\partial \hat{A}}{\partial \xi_2} \right] \quad (5.2.9)$$

and

$$\frac{1}{\sigma} \frac{\partial \hat{E}}{\partial \eta_2} + \frac{2}{3} \hat{A} \hat{E} - \frac{1}{3} \hat{D} \hat{B} = \frac{\xi_2}{3} \left[\hat{B} \frac{\partial \hat{D}}{\partial \xi_2} - \hat{E} \frac{\partial \hat{A}}{\partial \xi_2} \right]. \quad (5.2.10)$$

The three first order equations in (5.2.8) are approximated by

$$\hat{B}_{j-\frac{1}{2}}^{\wedge} = \frac{\hat{A}_j^{\wedge} - \hat{A}_{j-1}^{\wedge}}{h_j}, \hat{C}_{j-\frac{1}{2}}^{\wedge} = \frac{\hat{B}_j^{\wedge} - \hat{B}_{j-1}^{\wedge}}{h_j}, \hat{E}_{j-\frac{1}{2}}^{\wedge} = \frac{\hat{D}_j^{\wedge} - \hat{D}_{j-1}^{\wedge}}{h_j} \quad (5.2.11)$$

and equations (5.2.9) and (5.2.10) may be written

$$\frac{\hat{C}_j^{\wedge n-1/2} - \hat{C}_{j-1}^{\wedge n-1/2}}{h_j} + \frac{2}{3} (\hat{A}\hat{C})_{j-1/2}^{\wedge n-1/2} - \frac{1}{3} (\hat{B}^2)_{j-1/2}^{\wedge n-1/2} = \frac{\xi_{2n-1/2}}{3} \left[\hat{B}_{j-1/2}^{\wedge n-1/2} \left(\frac{\hat{B}_{j-1/2}^{\wedge n} - \hat{B}_{j-1/2}^{\wedge n-1}}{\Delta_n} \right) - \hat{C}_{j-1/2}^{\wedge n-1/2} \left(\frac{\hat{A}_{j-1/2}^{\wedge n} - \hat{A}_{j-1/2}^{\wedge n-1}}{\Delta_n} \right) \right] \quad (5.2.12)$$

and

$$\frac{\hat{E}_j^{\wedge n-1/2} - \hat{E}_{j-1}^{\wedge n-1/2}}{\sigma h_j} + \frac{2}{3} (\hat{A}\hat{E})_{j-1/2}^{\wedge n-1/2} - \frac{1}{3} (\hat{D}\hat{B})_{j-1/2}^{\wedge n-1/2} = \frac{\xi_{2n-1/2}}{3} \left[\hat{B}_{j-1/2}^{\wedge n-1/2} \left(\frac{\hat{D}_{j-1/2}^{\wedge n} - \hat{D}_{j-1/2}^{\wedge n-1}}{\Delta_n} \right) - \hat{E}_{j-1/2}^{\wedge n-1/2} \left(\frac{\hat{A}_{j-1/2}^{\wedge n} - \hat{A}_{j-1/2}^{\wedge n-1}}{\Delta_n} \right) \right] \quad (5.2.13)$$

where in region I there is a regular network in (ξ_2, η_2) coordinates

$$\xi_{2n} = \xi_{2n-1} + \Delta_n, \quad \eta_{2j} = \eta_{2j-1} + h_j \quad ; \quad n \geq 1, \quad 1 \leq j \leq J. \quad (5.2.14)$$

The wall is denoted by $j = 0 (\eta_2 = 0)$. The outer edge $\eta_2 = \eta_\infty = Jh$

if $h_j = h \forall j$. $n = 0$ denotes the initial station $\xi_2 = 0$ and

$\xi_{2n-1/2} = \xi_{2n} - \frac{1}{2}\Delta_n$. Equations (5.2.11) are centred on

$(\xi_{2n}, \eta_{2j-1/2})$, whilst (5.2.12) and (5.2.13) are centred on

$(\xi_{2n-1/2}, \eta_{2n-1/2})$. The centred averages are defined thus

$$\hat{A}\hat{C} = \frac{1}{4} [\hat{A}_j^{\wedge n} \hat{C}_j^{\wedge n} + \hat{A}_{j-1}^{\wedge n} \hat{C}_{j-1}^{\wedge n} + \hat{A}_j^{\wedge n-1} \hat{C}_j^{\wedge n-1} + \hat{A}_{j-1}^{\wedge n-1} \hat{C}_{j-1}^{\wedge n-1}] \quad (5.2.15)$$

$$\hat{B}^2 = \frac{1}{4} [(\hat{B}_j^{\wedge n})^2 + (\hat{B}_{j-1}^{\wedge n})^2 + (\hat{B}_j^{\wedge n-1})^2 + (\hat{B}_{j-1}^{\wedge n-1})^2] \quad (5.2.16)$$

$$\hat{A}\hat{E} = \frac{1}{4} [\hat{A}_j^{\wedge n} \hat{E}_j^{\wedge n} + \hat{A}_{j-1}^{\wedge n} \hat{E}_{j-1}^{\wedge n} + \hat{A}_j^{\wedge n-1} \hat{E}_j^{\wedge n-1} + \hat{A}_{j-1}^{\wedge n-1} \hat{E}_{j-1}^{\wedge n-1}] \quad (5.2.17)$$

$$\hat{D}\hat{B} = \frac{1}{4} [\hat{D}_j^{\wedge n} \hat{B}_j^{\wedge n} + \hat{D}_{j-1}^{\wedge n} \hat{B}_{j-1}^{\wedge n} + \hat{D}_j^{\wedge n-1} \hat{B}_j^{\wedge n-1} + \hat{D}_{j-1}^{\wedge n-1} \hat{B}_{j-1}^{\wedge n-1}] \quad (5.2.18)$$

$$\hat{C}_j^{\wedge n-1/2} = \frac{1}{2} [\hat{C}_j^{\wedge n} + \hat{C}_j^{\wedge n-1}], \quad \hat{B}_j^{\wedge n-1/2} = \frac{1}{2} [\hat{B}_j^{\wedge n} + \hat{B}_j^{\wedge n-1}], \quad \hat{E}_j^{\wedge n-1/2} = \frac{1}{2} [\hat{E}_j^{\wedge n} + \hat{E}_j^{\wedge n-1}]. \quad (5.2.19)$$

(ii) Region II (outer region)

Substitution of (5.2.4) and (5.2.5) into (4.2.2) and (4.2.3)

gives

$$\frac{d^3 \hat{\Psi}_2}{dz_2^3} = \frac{1}{3\xi_2^2} \left[\frac{d\hat{\Psi}_2}{dz_2} \frac{d^2 \hat{\Psi}_2}{d\xi_2 dz_2} - \frac{d\hat{\Psi}_2}{d\xi_2} \frac{d^2 \hat{\Psi}_2}{dz_2^2} \right] \quad (5.2.20)$$

and

$$\frac{d^2 \hat{T}_2}{dz_2^2} = \frac{\sigma}{3\xi_2^2} \left[\frac{d\hat{\Psi}_2}{dz_2} \frac{d\hat{T}_2}{d\xi_2} - \frac{d\hat{\Psi}_2}{d\xi_2} \frac{d\hat{T}_2}{dz_2} \right] \quad (5.2.21)$$

respectively.

As before we obtain a system of first order equations for discretization by setting

$$\hat{F} = \hat{\Psi}_2, \hat{G} = \frac{d\hat{F}}{dz_2}, \hat{I} = \frac{d\hat{G}}{dz_2}, \hat{J} = \hat{T}_2, \hat{K} = \frac{d\hat{J}}{dz_2} \quad (5.2.22)$$

Substitution into (5.2.20) and (5.2.21) yields

$$\frac{d\hat{I}}{dz_2} = \frac{1}{3\xi_2^2} \left[\hat{G} \frac{d\hat{G}}{d\xi_2} - \hat{I} \frac{d\hat{F}}{d\xi_2} \right] \quad (5.2.23)$$

and

$$\frac{1}{\sigma} \frac{d\hat{K}}{dz_2} = \frac{1}{3\xi_2^2} \left[\hat{G} \frac{d\hat{J}}{d\xi_2} - \hat{K} \frac{d\hat{F}}{d\xi_2} \right] \quad (5.2.24)$$

respectively.

The three first order equations in (5.2.22) are approximated by

$$\hat{G}_{k-\frac{1}{2}}^n = \frac{\hat{F}_k^n - \hat{F}_{k-1}^n}{H_k}, \hat{I}_{k-\frac{1}{2}}^n = \frac{\hat{G}_k^n - \hat{G}_{k-1}^n}{H_k}, \hat{K}_{k-\frac{1}{2}}^n = \frac{\hat{J}_k^n - \hat{J}_{k-1}^n}{H_k}. \quad (5.2.25)$$

Equations (5.2.23) and (5.2.24) may be written as

$$\frac{\hat{I}_{k-\frac{1}{2}}^{n-\frac{1}{2}} - \hat{I}_{k-1}^{n-\frac{1}{2}}}{H_k} = \frac{1}{3\xi_{2n-\frac{1}{2}}^2} \left[\hat{G}_{k-\frac{1}{2}}^{n-\frac{1}{2}} \left(\frac{\hat{G}_{k-\frac{1}{2}}^n - \hat{G}_{k-\frac{1}{2}}^{n-1}}{\Delta_n} \right) - \hat{I}_{k-\frac{1}{2}}^{n-\frac{1}{2}} \left(\frac{\hat{F}_{k-\frac{1}{2}}^n - \hat{F}_{k-\frac{1}{2}}^{n-1}}{\Delta_n} \right) \right] \quad (5.2.26)$$

and

$$\frac{\hat{K}_k^{n-\frac{1}{2}} - \hat{K}_{k-1}^{n-\frac{1}{2}}}{H_k} = \frac{1}{3\xi_{2n-\frac{1}{2}}^2} \left[\hat{G}_{k-\frac{1}{2}}^{n-\frac{1}{2}} \left(\frac{\hat{J}_{k-\frac{1}{2}}^n - \hat{J}_{k-\frac{1}{2}}^{n-1}}{\Delta_n} \right) - \hat{K}_{k-\frac{1}{2}}^{n-\frac{1}{2}} \left(\frac{\hat{F}_{k-\frac{1}{2}}^n - \hat{F}_{k-\frac{1}{2}}^{n-1}}{\Delta_n} \right) \right]. \quad (5.2.27)$$

$k = 0$ corresponds to $z_2 = \eta_\infty \xi_{2n}$, the lower boundary of region

II. The outer edge of region II is given by the maximum value of

$k = K_m$ or $z_2 = K_m H + \eta_\infty \xi_{2n}$ if $H_k = H \forall k$.

(iii) Matching between I and II

The values of ψ_2 , $\frac{\partial \psi_2}{\partial z_2}$, $\frac{\partial^2 \psi_2}{\partial z_2^2}$, T_2 and $\frac{\partial T_2}{\partial z_2}$ must be

equated at the boundary ($\eta_2 = \eta_\infty$ and $z_2 = \eta_\infty \xi_{2n}$), which gives

$$\begin{aligned} \hat{F}_0^\wedge &= \xi_{2n}^2 \hat{A}_J^\wedge, & \hat{G}_0^\wedge &= \xi_{2n} \hat{B}_J^\wedge, & \hat{I}_0^\wedge &= \hat{C}_J^\wedge, \\ \hat{J}_0^\wedge &= \xi_{2n} \hat{D}_J^\wedge, & \hat{K}_0^\wedge &= \hat{E}_J^\wedge & & \text{for } n \geq 0 \end{aligned} \quad (5.2.28)$$

$$(k = 0 \text{ in II} \equiv j = J \text{ in I}). \quad (5.2.29)$$

If a match is achieved for n and $n - 1$, then it is equivalent to a match at $n - 1/2$ and $z_2 = \eta_\infty \xi_{2n-1/2}$.

(iv) Boundary and initial conditions

For region I the wall conditions are, using (4.2.4)

$$\hat{A}_0^\wedge = 0, \hat{B}_0^\wedge = 0, \hat{E}_0^\wedge = 0 \quad (5.2.30)$$

The initial profiles at $\xi_2 = 0$ are, using (4.3.22) and (4.3.49)

with (4.3.51),

$$\hat{A}_j^\circ = \frac{K}{\sigma} \eta_{2j}^2, \hat{B}_j^\circ = \frac{2K}{\sigma} \eta_{2j}, \hat{C}_j^\circ = \frac{2K}{\sigma}, \hat{D}_j^\circ = T_{20}(\eta_{2j}), \hat{E}_j^\circ = T_{20}'(\eta_{2j}); j = 0 \dots J \quad (5.2.31)$$

For region II, the initial profiles at $\xi_2 = 0$ are

$$\hat{F}_k^\circ = f(\eta_{2k}), \hat{G}_k^\circ = f'(\eta_{2k}), \hat{I}_k^\circ = f''(\eta_{2k}), \hat{J}_k^\circ = g(\eta_{2k}), \hat{K}_k^\circ = g'(\eta_{2k}); k = 0 \dots K_m \quad (5.2.32)$$

where f and g are the vertical boundary layer functions determined numerically in Chapter 3.

The conditions at the outer edge are, using (4.2.5)

$$\hat{G}_{K_m}^{\wedge} = 0, \quad \hat{J}_{K_m}^{\wedge} = 1, \quad (5.2.33)$$

(v) Solution procedure

The solution of the parabolic system is computed by stepping downstream in the ξ_2 direction from the initial profiles at $\xi_2 = 0$. When $\hat{F}_k^{n-1}, \hat{G}_k^{n-1}, \dots$ are updated for the next step, allowance must be made for the increase in height at the $k = 0$ point. If we choose a uniform $\Delta_n = \frac{1}{J}$ and let $h_j = H_k \forall j, k$ then updating is simply that the new \hat{F}_k^{n-1} is the old \hat{F}_{k+1}^n . The velocity field is independent of the temperature field and is computed first at each downstream step using a Newton iteration. Full details of the computational procedure are given in Appendix 2.

Once the temperature solution was found, the integral constraints P and Q were computed using Simpsons rule, to monitor the scheme.

In most of the computations the meshwidths used were $h = 0.1, \Delta_n = 0.02$ and the tolerance for which the increments were deemed sufficiently small was 0.0001. J was taken to be 50 and K_m to be 250. The effect of h_j and Δ_n on the solutions $\frac{\partial \psi_2}{\partial z_2}$ and T_2 can be seen in tables 5.1 and 5.2 and on the

integral constraints in table 5.3. Graphs of $\frac{\partial \psi_2}{\partial z_2}$ and T_2

against z_2 were produced for $\sigma = 0.1$ (figures 5.1 and 5.2), $\sigma = 0.72$ (figures 5.3 and 5.4), $\sigma = 8.1$ (figures 5.5 and 5.6) and $\sigma = 17.2$ (figures 5.7 and 5.8) at ξ_2 stations of 0.2, 0.4, 0.6, 0.8 and 1.0. Although σ does not appear explicitly in the momentum equation the initial profiles depend on σ , giving rise to a different velocity field for each Prandtl number. The results show that as σ increases the width z_2 of the jet increases but the width of the thermal boundary layer decreases. As ξ_2 increases the width of the jet increases and its maximum velocity decreases. The integral constraints were confirmed as constant to a reasonable level of accuracy for all ξ_2 (table 5.4).

5.3 Solution for $x > 1$

Following the large x prediction (Chapter 4, Section 4.4) in which the stream function and temperature have the form

$$\psi_2 \sim x^{1/4} \phi_2(\zeta_2), \quad T_2 \sim 1 + x^{-1/4} \theta_2(\zeta_2) \quad \text{as } x \rightarrow \infty \quad \text{where } \zeta_2 = \frac{z_2}{4x^{3/4}},$$

we use the variables

$$\tilde{\xi}_2 = x^{1/4}, \quad \tilde{\eta}_2 = z_2 / \tilde{\xi}_2^3 \quad (5.3.1)$$

in the numerical scheme for $x > 1$ and take

$$\Psi_2 = \tilde{\xi}_2 \hat{\phi}_2(\tilde{\xi}_2, \tilde{\eta}_2), \quad T_2 = 1 - \frac{1}{\tilde{\xi}_2} \hat{\theta}_2(\tilde{\xi}_2, \tilde{\eta}_2). \quad (5.3.2)$$

The overall mesh has the structure shown in figure 5.9. Substitution of (5.3.1) and (5.3.2) into (4.2.2) and (4.2.3) gives

$$\frac{\partial^3 \hat{\phi}_2}{\partial \tilde{\eta}_2^3} = -\frac{1}{4} \left[\hat{\phi}_2 \frac{\partial^2 \hat{\phi}_2}{\partial \tilde{\eta}_2^2} + 2 \left(\frac{\partial \hat{\phi}_2}{\partial \tilde{\eta}_2} \right) \right] + \frac{1}{4} \frac{\tilde{\xi}_2}{\tilde{\eta}_2} \left[\frac{\partial \hat{\phi}_2}{\partial \tilde{\eta}_2} \frac{\partial^2 \hat{\phi}_2}{\partial \tilde{\eta}_2 \partial \tilde{\xi}_2} - \frac{\partial \hat{\phi}_2}{\partial \tilde{\xi}_2} \frac{\partial^2 \hat{\phi}_2}{\partial \tilde{\eta}_2} \right] \quad (5.3.3)$$

and

$$\frac{1}{\sigma} \frac{\partial^2 \hat{\theta}}{\partial \hat{\eta}_2^2} = -\frac{1}{4} \left[\hat{\theta}_2 \frac{\partial \hat{\phi}_2}{\partial \hat{\eta}_2} + \hat{\phi}_2 \frac{\partial \hat{\theta}_2}{\partial \hat{\eta}_2} \right] + \frac{1}{4} \tilde{\xi}_2 \left[\frac{\partial \hat{\phi}_2}{\partial \hat{\eta}_2} \frac{\partial \hat{\theta}_2}{\partial \hat{\xi}_2} - \frac{\partial \hat{\theta}_2}{\partial \hat{\eta}_2} \frac{\partial \hat{\phi}_2}{\partial \hat{\xi}_2} \right] \quad (5.3.4)$$

respectively.

We obtain a system of first order differential equations for discretization by setting

$$\bar{A} = \hat{\phi}_2, \quad \bar{B} = \frac{\partial \bar{A}}{\partial \hat{\eta}_2}, \quad \bar{C} = \frac{\partial \bar{B}}{\partial \hat{\eta}_2}, \quad \bar{D} = \hat{\theta}_2, \quad \bar{E} = \frac{\partial \bar{D}}{\partial \hat{\eta}_2} \quad (5.3.5)$$

which when substituted into (5.3.3) and (5.3.4) give

$$\frac{\partial \bar{C}}{\partial \hat{\eta}_2} + \frac{1}{4} [\bar{A}\bar{C} + 2\bar{B}^2] = \frac{\tilde{\xi}_2}{4} \left[\bar{B} \frac{\partial \bar{B}}{\partial \hat{\xi}_2} - \frac{\partial \bar{A}}{\partial \hat{\xi}_2} \bar{C} \right] \quad (5.3.6)$$

and

$$\frac{1}{\sigma} \frac{\partial \bar{E}}{\partial \hat{\eta}_2} + \frac{1}{4} \frac{\partial}{\partial \hat{\eta}_2} [\bar{D}\bar{A}] = \frac{\tilde{\xi}_2}{4} \left[\frac{\partial}{\partial \hat{\eta}_2} (\bar{A} \frac{\partial \bar{D}}{\partial \hat{\xi}_2}) - \frac{\partial}{\partial \hat{\xi}_2} (\bar{A}\bar{E}) \right] \quad (5.3.7)$$

respectively. The three first order differential equations in (5.3.5) are approximated by

$$\bar{B}_{j-\frac{1}{2}}^n = \frac{\bar{A}_j^n - \bar{A}_{j-1}^n}{h_j}, \quad \bar{C}_{j-\frac{1}{2}}^n = \frac{\bar{B}_j^n - \bar{B}_{j-1}^n}{h_j}, \quad \bar{E}_{j-\frac{1}{2}}^n = \frac{\bar{D}_j^n - \bar{D}_{j-1}^n}{h_j}. \quad (5.3.8)$$

Equations (5.3.6) and (5.3.7) may be written as

$$\frac{\bar{C}_{j-\frac{1}{2}}^{n-\frac{1}{2}} - \bar{C}_{j-1}^{n-\frac{1}{2}}}{h_j} + \frac{1}{4} [\bar{A}\bar{C} + 2\bar{B}^2]_{j-\frac{1}{2}}^{n-\frac{1}{2}} = \quad (5.3.9)$$

$$\frac{1}{4} \tilde{\xi}_2^{n-\frac{1}{2}} \left[\bar{B}_{j-\frac{1}{2}}^{n-\frac{1}{2}} \frac{\bar{B}_j^n - \bar{B}_{j-1}^n}{\Delta_n} - \bar{C}_{j-\frac{1}{2}}^{n-\frac{1}{2}} \frac{(\bar{A}_j^n - \bar{A}_{j-1}^n)}{\Delta_n} \right]$$

and

$$\frac{1}{\sigma h_j} (\bar{E}_j^{n-\frac{1}{2}} - \bar{E}_{j-1}^{n-\frac{1}{2}}) + \frac{1}{4 h_j} [(\bar{D}\bar{A})_j^{n-\frac{1}{2}} - (\bar{D}\bar{A})_{j-1}^{n-\frac{1}{2}}] = \quad (5.3.10)$$

$$\frac{\tilde{\xi}_2^{n-\frac{1}{2}}}{4} \left[\frac{1}{h_j \Delta_n} (\bar{A}_j^{n-\frac{1}{2}} (\bar{D}_j^n - \bar{D}_j^{n-1}) - \bar{A}_{j-1}^{n-\frac{1}{2}} (\bar{D}_{j-1}^n - \bar{D}_{j-1}^{n-1})) - \frac{1}{\Delta_n} ((\bar{A}\bar{E})_{j-\frac{1}{2}}^n - (\bar{A}\bar{E})_{j-\frac{1}{2}}^{n-1}) \right].$$

In this region there is a regular network in $(\tilde{\xi}_2, \tilde{\eta}_2)$ coordinates where $\tilde{\xi}_{2n} = \tilde{\xi}_{2n-1} + \Delta_n$, $\tilde{\eta}_{2j} = \tilde{\eta}_{2j-1} + h_j$; $n \geq 1$, $1 \leq j \leq J$. The wall is denoted by $\tilde{\eta}_2 = 0$; $j = 0$. The outer

edge is at $\bar{\eta}_2 = \bar{\eta}_{2^\infty} = Jh$ if $h_j = h \forall j$. $n = 0$ denotes the initial stations at $\bar{\xi}_2 = 1$ and $\bar{\xi}_{2^{n-1/2}} = \bar{\xi}_{2^n} - \frac{1}{2}\Delta_n$. Equation (5.3.8) is centred at $(\bar{\xi}_{2^n}, \bar{\eta}_{2^{n-1/2}})$ and equations (5.3.9) and (5.3.10) are centred on $(\bar{\xi}_{2^{n-1/2}}, \bar{\eta}_{2^{n-1/2}})$. The centred averages

are defined as

$$\bar{A}\bar{C} = \frac{1}{4} [\bar{A}_j^\wedge \bar{C}_j^\wedge + \bar{A}_{j-1}^\wedge \bar{C}_{j-1}^\wedge + \bar{A}_j^{\wedge-1} \bar{C}_j^{\wedge-1} + \bar{A}_{j-1}^{\wedge-1} \bar{C}_{j-1}^{\wedge-1}] \quad (5.3.11)$$

$$\bar{B}^2 = \frac{1}{4} [(\bar{B}_j^\wedge)^2 + (\bar{B}_{j-1}^\wedge)^2 + (\bar{B}_j^{\wedge-1})^2 + (\bar{B}_{j-1}^{\wedge-1})^2] \quad (5.3.12)$$

$$\bar{A}\bar{D} = \frac{1}{4} [\bar{A}_j^\wedge \bar{D}_j^\wedge + \bar{A}_{j-1}^\wedge \bar{D}_{j-1}^\wedge + \bar{A}_j^{\wedge-1} \bar{D}_j^{\wedge-1} + \bar{A}_{j-1}^{\wedge-1} \bar{D}_{j-1}^{\wedge-1}] \quad (5.3.13)$$

$$\bar{A}\bar{E} = \frac{1}{4} [\bar{A}_j^\wedge \bar{E}_j^\wedge + \bar{A}_{j-1}^\wedge \bar{E}_{j-1}^\wedge + \bar{A}_j^{\wedge-1} \bar{E}_j^{\wedge-1} + \bar{A}_{j-1}^{\wedge-1} \bar{E}_{j-1}^{\wedge-1}] \quad (5.3.14)$$

$$\bar{C}_j^{\wedge-1/2} = \frac{1}{2} [\bar{C}_j^\wedge + \bar{C}_j^{\wedge-1}], \bar{B}_j^{\wedge-1/2} = \frac{1}{2} [\bar{B}_j^\wedge + \bar{B}_j^{\wedge-1}], \bar{E}_j^{\wedge-1/2} = \frac{1}{2} [\bar{E}_j^\wedge + \bar{E}_j^{\wedge-1}]. \quad (5.3.15)$$

The boundary conditions at the wall are, from (4.2.4)

$$\bar{A}_0^\wedge = 0, \bar{B}_0^\wedge = 0, \bar{E}_0^\wedge = 0 \quad (5.3.16)$$

while the conditions at the outer edge are, from (4.2.5),

$$\bar{B}_J^\wedge = 0, \bar{D}_J^\wedge = 0. \quad (5.3.17)$$

The initial profiles for this region are found from the

solution of Section 5.3 at $\xi_2 = 1$:

$$\begin{aligned} \bar{A}_j^0 &= \hat{A}_j^N, \quad 0 \leq j \leq J; \quad \hat{F}_j^N, \quad J+1 \leq j \leq K_M \\ \bar{B}_j^0 &= \hat{B}_j^N, \quad 0 \leq j \leq J; \quad \hat{G}_j^N, \quad J+1 \leq j \leq K_M \\ \bar{C}_j^0 &= \hat{C}_j^N, \quad 0 \leq j \leq J; \quad \hat{I}_j^N, \quad J+1 \leq j \leq K_M \\ \bar{D}_j^0 &= 1 - \hat{D}_j^N, \quad 0 \leq j \leq J; \quad 1 - \hat{J}_j^N, \quad J+1 \leq j \leq K_M \\ \bar{E}_j^0 &= -\hat{E}_j^N, \quad 0 \leq j \leq J; \quad -\hat{K}_j^N, \quad J+1 \leq j \leq K_M. \end{aligned} \quad (5.3.18)$$

Again the solution for the velocity field at step n is computed using a Newton iteration. Full details of the computational procedure are given in Appendix 3. The integral constraints P

and Q were computed at each step using Simpson's rule. In most of the computations the meshwidths used were $h = 0.1$, $\Delta = 0.04$ and the tolerance for which the Newton increments were considered small enough was 0.0001. The value of J was taken as 300. The effect of h on the solution can be seen in tables 5.5 and 5.6 and on the integral constraints in table 5.7.

Graphs for the velocity $\frac{\partial \hat{\phi}_2}{\partial \tilde{\eta}_2}$ and the temperature $\hat{\theta}_2$ were produced for $\sigma = 0.1$ (figures 5.10, 5.11), $\sigma = 0.72$ (figures 5.12, 5.13), $\sigma = 8.1$ (figures 5.14, 5.15) and $\sigma = 17.2$ (figures 5.16, 5.17) at $\tilde{\xi}_2$ stations of 1.2, 1.6, 2.0, 2.4 and 2.8. The results show that the profiles approach a limiting form as expected as $\tilde{\xi}_2 \rightarrow \infty$. In Section 5.4 these results are compared with the large x asymptotic results of Chapter 4, Section 4.4. The integral constraints P and Q remained constant to a good level of accuracy for all $\tilde{\xi}_2$ as expected (see table 5.8).

5.4 Summary and comparisons with analytical results

A graph describing how the results depend on x is presented in figure 5.18 for the case of air ($\sigma = 0.72$): it shows the skin friction $\frac{\partial^2 \psi_2}{\partial \tilde{x}_2^2}(x, 0)$, the stream function at the edge of the jet $\psi_2(x, \infty)$, which gives the entrainment of velocity into the jet, and the wall temperature. As the wall temperature rises from 0 to 1, the isotherms from the vertical boundary layer attach to the lower wall of the cavity. The initial development of the jet is consistent with the small x predictions and as x increases its strength decreases and width increases. The skin friction falls and the stream function at the edge of the jet

risers proportional to $x^{1/4}$, consistent with the large x prediction.

Tables 5.9 - 5.11 contain quantitative information from the computations. We have already seen that the numerical results confirm that the integral constraints P and Q are constant at any x value. Table 5.9 shows the values of P and Q for $\sigma = 0.72$ along the whole boundary layer. As $x \rightarrow \infty$ the stream function and temperature profiles should approach the forms discussed in Chapter 4, Section 4. In particular, the computed values of $\hat{\phi}_2(\infty, \tilde{\xi}_2)$ and $\hat{\theta}_2(0, \tilde{\xi}_2)$ may be compared with the values of K_2 and θ_0 obtained from the integral constraints (4.4.11) and (4.4.22). This is done in table 5.10. The velocity and temperature profiles of the analytical work for large x and of the numerical scheme at $\tilde{\xi}_2 = 4.8$ are compared in table 5.11 and the agreement is excellent.

Finally we discuss the results in the context of the overall flow in the end-zone of the cavity. At large x the external velocity from the recirculating inviscid region above the horizontal boundary layer and the effect of buoyancy come back into play and this leads to the breakdown of the jet structure. It is easily shown that this occurs when $\chi = O(R_1^{2/5})$: firstly, the flow speed in the jet $u = O(R_1^{6/5} \chi^{-1/2})$ becomes comparable with the external inviscid flow speed $O(R_1)$. Secondly the viscous and inertial terms in the jet $O(R_1^3 \chi^{-11/4})$ become comparable with the buoyancy term $O(R_1^{12/5} \chi^{-5/4})$ in the governing equation (3.2.19). This new regime is discussed analytically in Chapter 6 with a full numerical study presented in Chapter 7.

TABLE 5.1

Effect of meshwidth on values of $\frac{\partial \psi_2}{\partial z_2}$ ($\sigma = 0.72$)

z_2	$\xi_2 = 0.2$	$\xi_2 = 0.6$	$\xi_2 = 1.0$
1	a) 0.6111	0.3024	0.1058
	b) 0.6114	0.3020	0.1053
4	0.1568	0.3227	0.3325
	0.1568	0.3233	0.3318
7	0.0109	0.0484	0.2503
	0.0109	0.0483	0.2509
10	0.0006	0.0055	0.0976
	0.0006	0.0054	0.0978

a) $h = 0.1, \Delta = 0.02$

b) $h = 0.2, \Delta = 0.04$

TABLE 5.2

Effect of meshwidth on values of T_2 ($\sigma = 0.72$)

Z_2	$\xi_2 = 0.2$	$\xi_2 = 0.6$	$\xi_2 = 1.0$
1	a) 0.3549	0.3843	0.5385
	b) 0.3550	0.3845	0.5390
4	0.9383	0.8037	0.6116
	0.9383	0.8036	0.6117
7	0.9957	0.9652	0.7819
	0.9957	0.9653	0.7817
10	0.9995	0.9932	0.9054
	0.9995	0.9932	0.9054

a) $h = 0.1, \Delta = 0.02$

b) $h = 0.2, \Delta = 0.04$

TABLE 5.3

Effect of meshwidth on constants P, Q ($\sigma = 0.72$)

ξ_2		(a)	(b)
0.2	P	0.6490	0.6337
	Q	0.7171	0.7112
0.4		0.6489	0.6314
		0.7172	0.6995
0.6		0.6488	0.6339
		0.7171	0.6949
0.8		0.6487	0.6317
		0.7170	0.6978
1.0		0.6485	0.6279
		0.7170	0.7036

a) $h = 0.1, \Delta = 0.02$

b) $h = 0.2, \Delta = 0.04$

TABLE 5.4

The integral constraints P and Q at various ξ_2 stations

ξ_2		$\sigma = 0.1$	$\sigma = 0.72$	$\sigma = 8.1$	$\sigma = 17.2$
0.2	P	39.631	0.64902	4.29247(-3)	9.28222(-4)
	Q	3.85798	0.71711	7.58925(-2)	3.6688 (-2)
0.4		39.630	0.64890	4.29188(-3)	9.28059(-2)
		3.85824	0.71716	7.59031(-2)	3.6695 (-2)
0.6		39.628	0.64886	4.29094(-3)	9.27832(-4)
		3.85797	0.71713	7.59086(-2)	3.6699 (-2)
0.8		39.620	0.64869	4.28994(-3)	9.27565(-4)
		3.85485	0.71705	7.59121(-2)	3.6702 (-2)
1.0		39.608	0.64852	4.28275(-3)	9.24959(-4)
		3.84640	0.71698	7.59147(-2)	3.6713 (-2)

TABLE 5.5

Effect of meshwidth on values of $\frac{\partial \hat{\phi}_2}{\partial \tilde{\eta}_2}$ ($\sigma = 0.72$)

$\tilde{\eta}_2$	$\tilde{\xi}_2 = 1.2$	$\tilde{\xi}_2 = 1.6$	$\tilde{\xi}_2 = 2.0$
2	a) 0.2460	0.2802	0.2910
	b) 0.2456	0.2798	0.2906
6	0.2872	0.2636	0.2550
	0.2875	0.2639	0.2554
10	0.0648	0.0452	0.0403
	0.0649	0.0454	0.0404
14	0.0097	0.0055	0.0046
	0.0097	0.0055	0.0046

a) $h = 0.1, \Delta = 0.04$

b) $h = 0.2, \Delta = 0.04$

TABLE 5.6

Effect of meshwidth on values of $\hat{\theta}_2$ ($\sigma = 0.72$)

$\tilde{\eta}_2$	$\tilde{\xi}_2 = 1.2$	$\tilde{\xi}_2 = 1.6$	$\tilde{\xi}_2 = 2.0$
2	a) 0.4511	0.4502	0.4512
	b) 0.4506	0.4497	0.4507
6	0.2490	0.2324	0.2260
	0.2489	0.2323	0.2259
10	0.0833	0.0663	0.0582
	0.0832	0.0662	0.0581
14	0.0278	0.0162	0.0127
	0.0276	0.0161	0.0126

a) $h = 0.1, \Delta = 0.04$

b) $h = 0.2, \Delta = 0.04$

TABLE 5.7

Effect of meshwidth on constraints P and Q ($\sigma = 0.72$)

ξ		a)	b)
1.2	P	0.6486	0.6481
	Q	0.7170	0.7158
2.0		0.6487	0.6485
		0.7170	0.7158
2.8		0.6488	0.6487
		0.7170	0.7158

a) $h = 0.1, \Delta = 0.04$

b) $h = 0.2, \Delta = 0.04$

TABLE 5.8

The integral constraints P and Q at various $\tilde{\xi}_2$ stations

$\tilde{\xi}_2$		$\sigma = 0.72$	$\sigma = 8.1$	$\sigma = 17.2$
1.2	P	0.6486	4.282(-3)	9.182(-4)
	Q	0.7170	7.592(-2)	3.670(-2)
1.6		0.6487	4.281(-3)	9.107(-4)
		0.7170	7.592(-2)	3.670(-2)
2.0		0.6487	4.281(-3)	9.056(-4)
		0.7170	7.592(-2)	3.670(-2)
2.4		0.6487	4.280(-3)	9.015(-4)
		0.7170	7.592(-2)	3.670(-2)
2.8		0.6488	4.280(-3)	8.982(-4)
		0.7170	7.592(-2)	3.670(-2)

TABLE 5.9

The values of P and Q along the boundary layer ($\sigma = 0.72$)

x	P	Q
0	0.6510	0.7174
$(0.2)^3$	0.6490	0.7171
$(0.6)^3$	0.6489	0.7171
1	0.6485	0.7170
$(1.2)^4$	0.6486	0.7170
$(2.0)^4$	0.6487	0.7170
$(2.8)^4$	0.6488	0.7170

TABLE 5.10

Comparison of K_2 and θ_0 values

σ		a)	b)
0.72	K_2	2.2575	2.2571
	$-\theta_0$	0.4734	0.4749
8.1		0.6430	0.6432
		0.5438	0.5632

a) Values obtained from $\hat{\phi}_2(\infty, \tilde{\xi}_2)$ and $\hat{\theta}_2(0, \tilde{\xi}_2)$ at $\tilde{\xi}_2 = 4.8$.

b) Values of K_2 and θ_0 obtained from integral constraints.

TABLE 5.11

Comparison of velocity $\frac{\partial \hat{\phi}_2}{\partial \tilde{\eta}_2}(\tilde{\eta}_2, \tilde{\xi}_2)$ and temperature $\hat{\theta}_2(\tilde{\eta}_2, \tilde{\xi}_2)$

profiles at $\tilde{\xi}_2 = 4.8$ ($\sigma = 0.72$)

$\tilde{\eta}_2$		Numerical Scheme *	Analysis
0.00	Velocity	0.000	0.000
	Temperature	0.473	0.475
1.61		0.247	0.248
		0.464	0.466
3.38		0.397	0.399
		0.398	0.399
6.48		0.207	0.207
		0.187	0.186

* interpolated values

Figure 5.1 Graph of $\frac{\partial \psi_2}{\partial z_2}$ against z_2 for $\sigma = 0.1$.

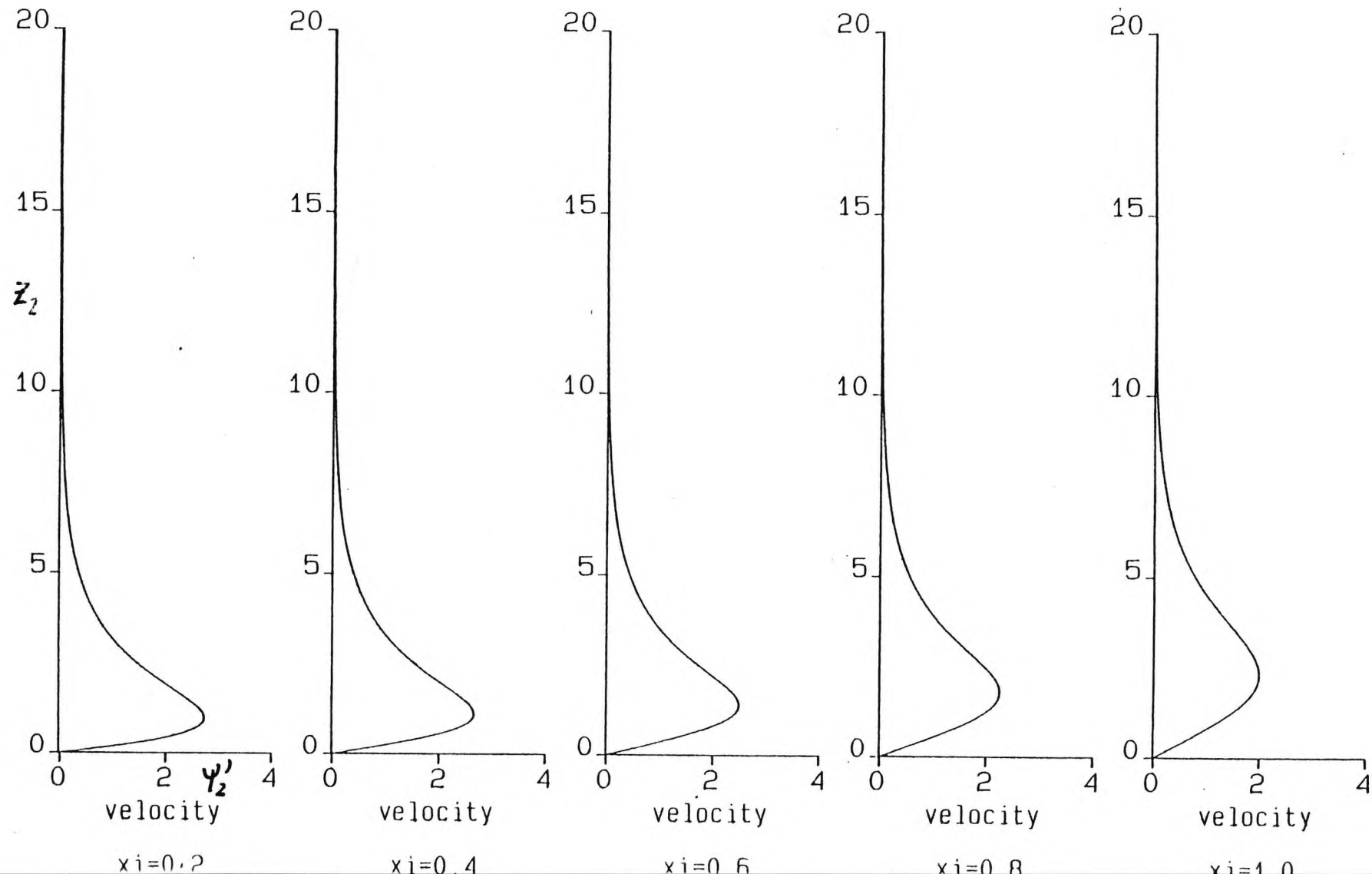


Figure 5.2 Graph of T_2 against z_2 for $\sigma = 0.1$.

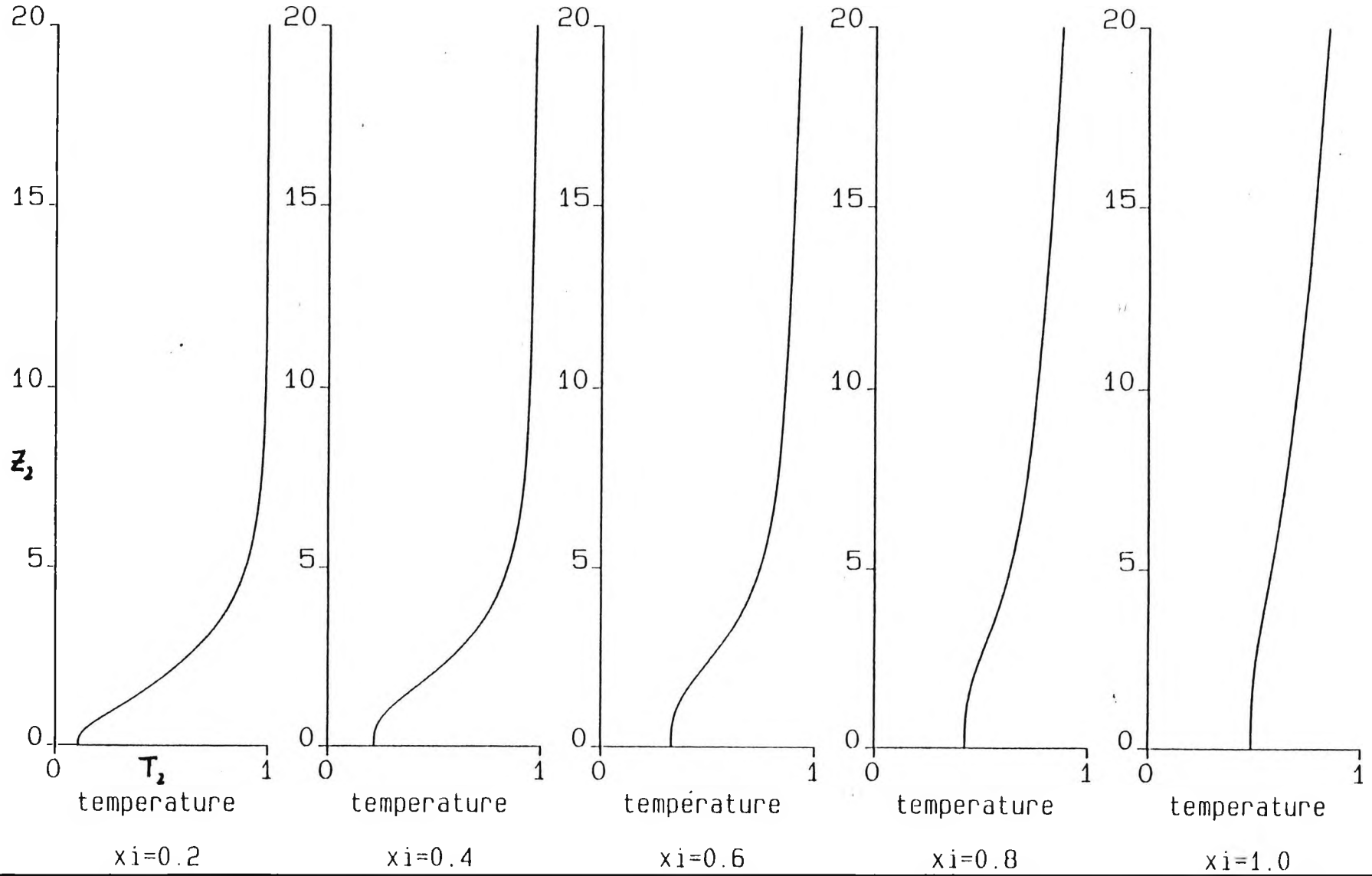


Figure 5.3 Graph of $\frac{\partial \psi_2}{\partial z_2}$ against z_2 for $\sigma = 0.72$.

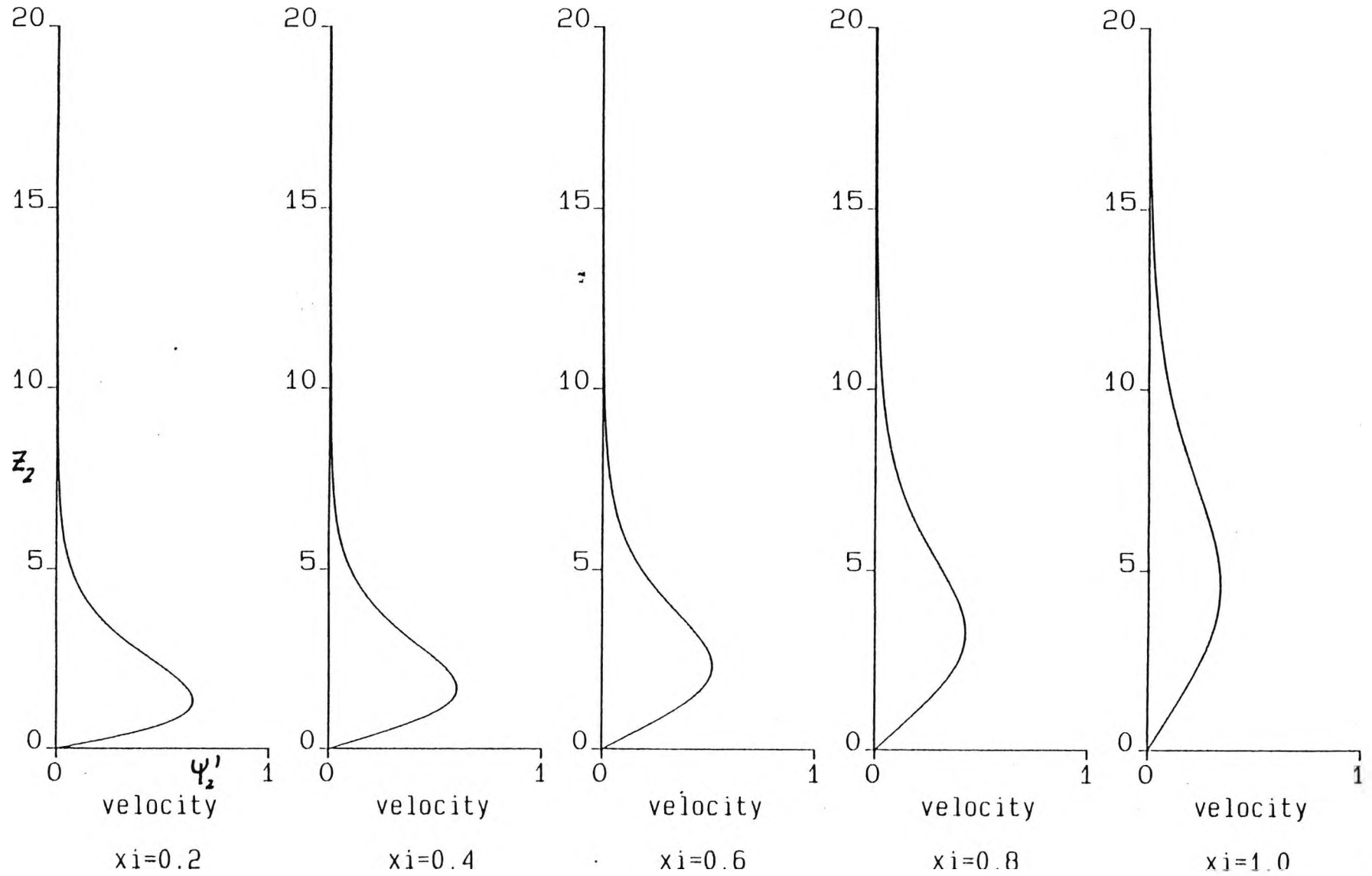


Figure 5.4 Graph of T_2 against z_2 for $\sigma = 0.1$.

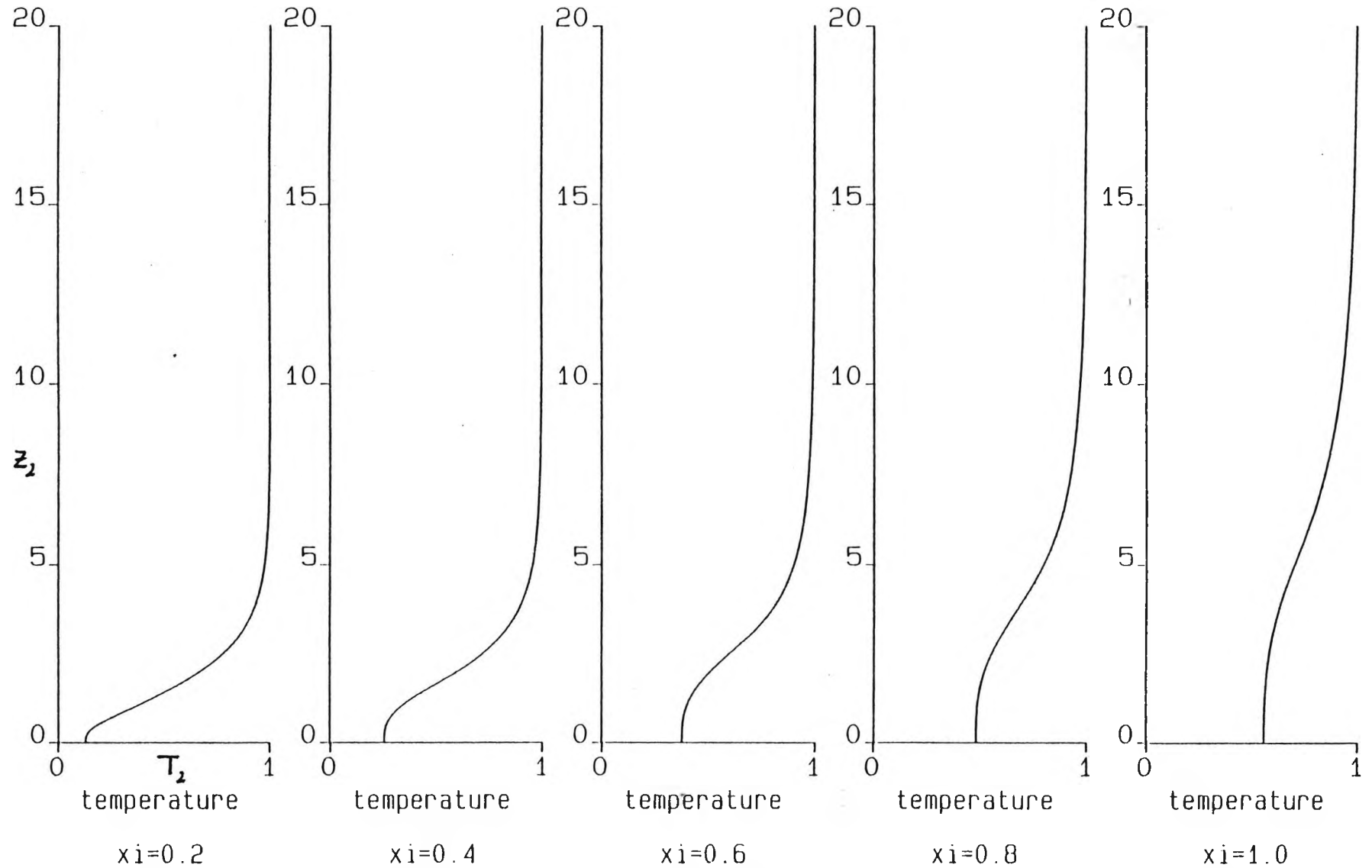


Figure 5.5 Graph of $\frac{\partial \psi_2}{\partial z_2}$ against z_2 for $\sigma = 8.1$.

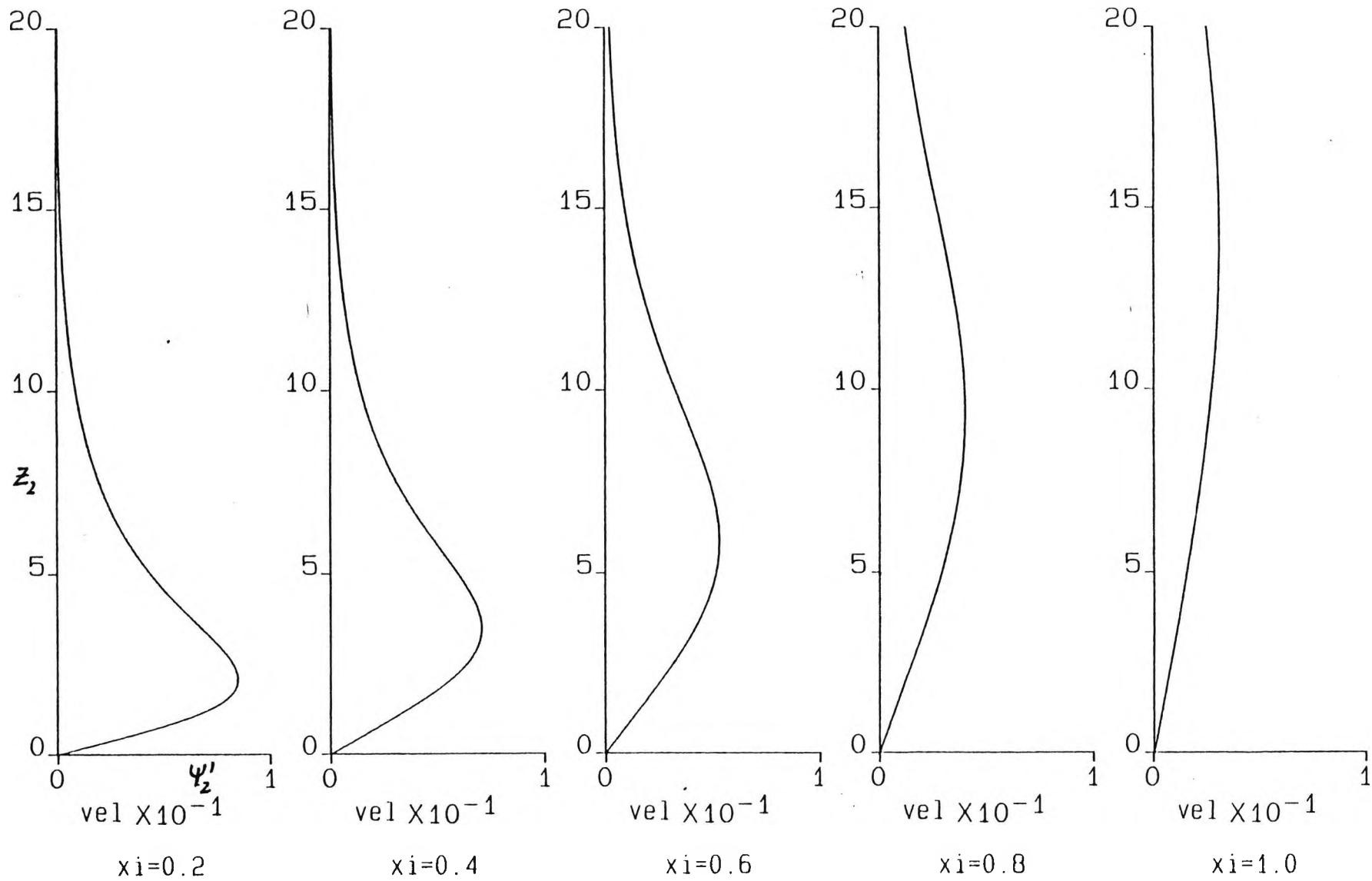


Figure 5.6 Graph of T_2 against z_2 for $\sigma = 8.1$.

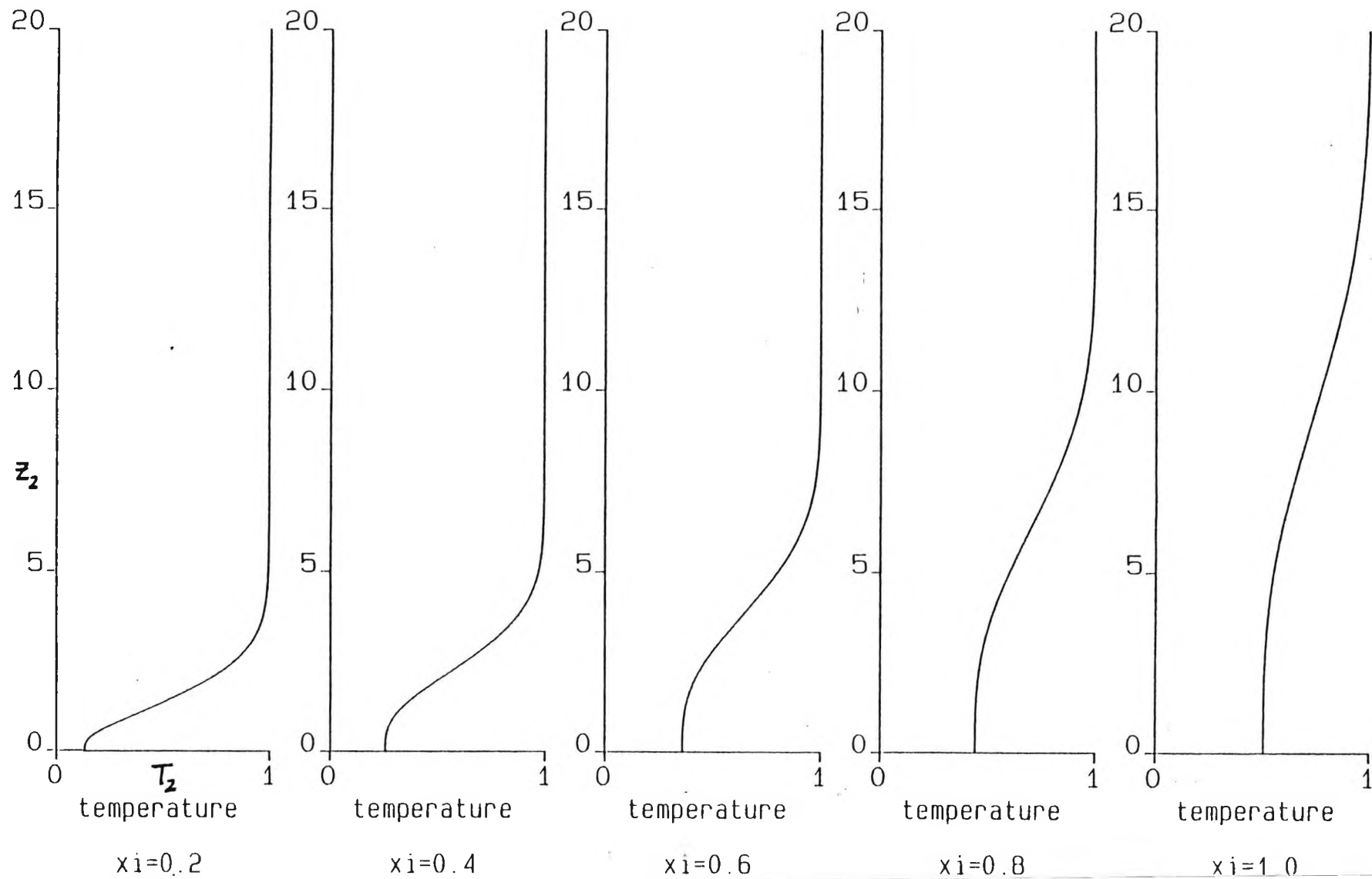


Figure 5.7 Graph of $\frac{\partial \psi_2}{\partial z_2}$ against z_2 for $\sigma = 17.2$.

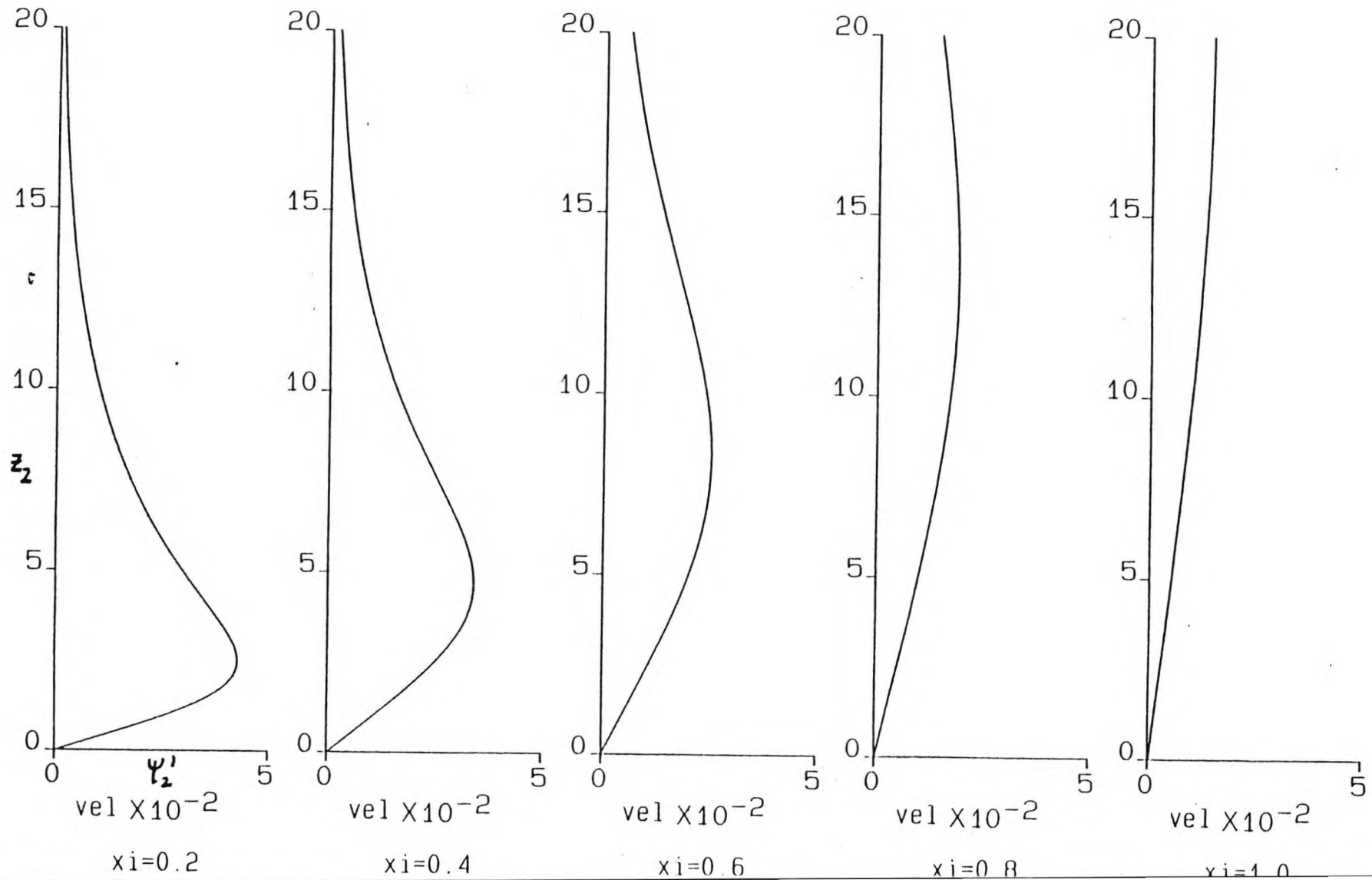
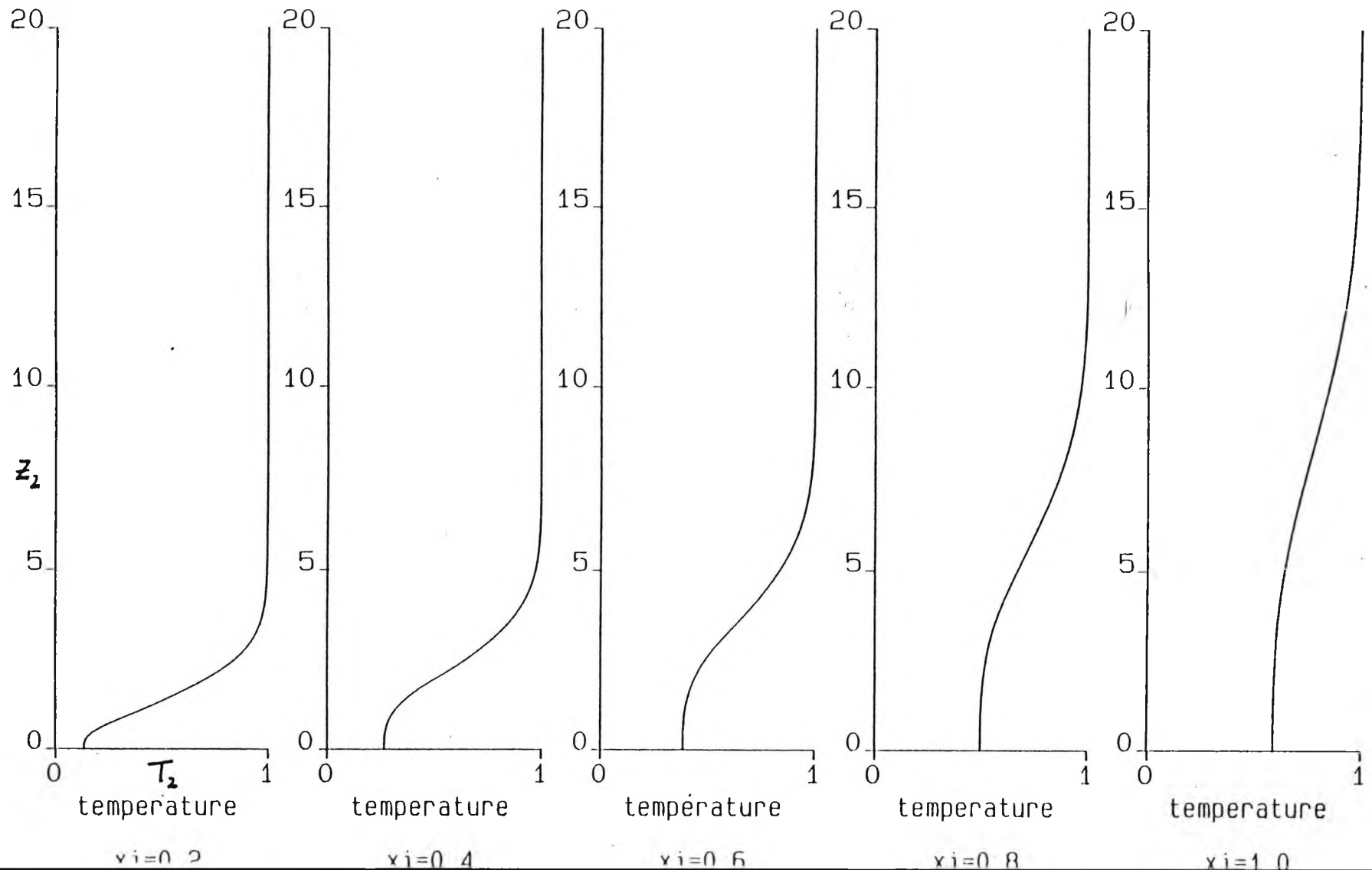


Figure 5.8 Graph of T_2 against z_2 for $\sigma = 17.2$.



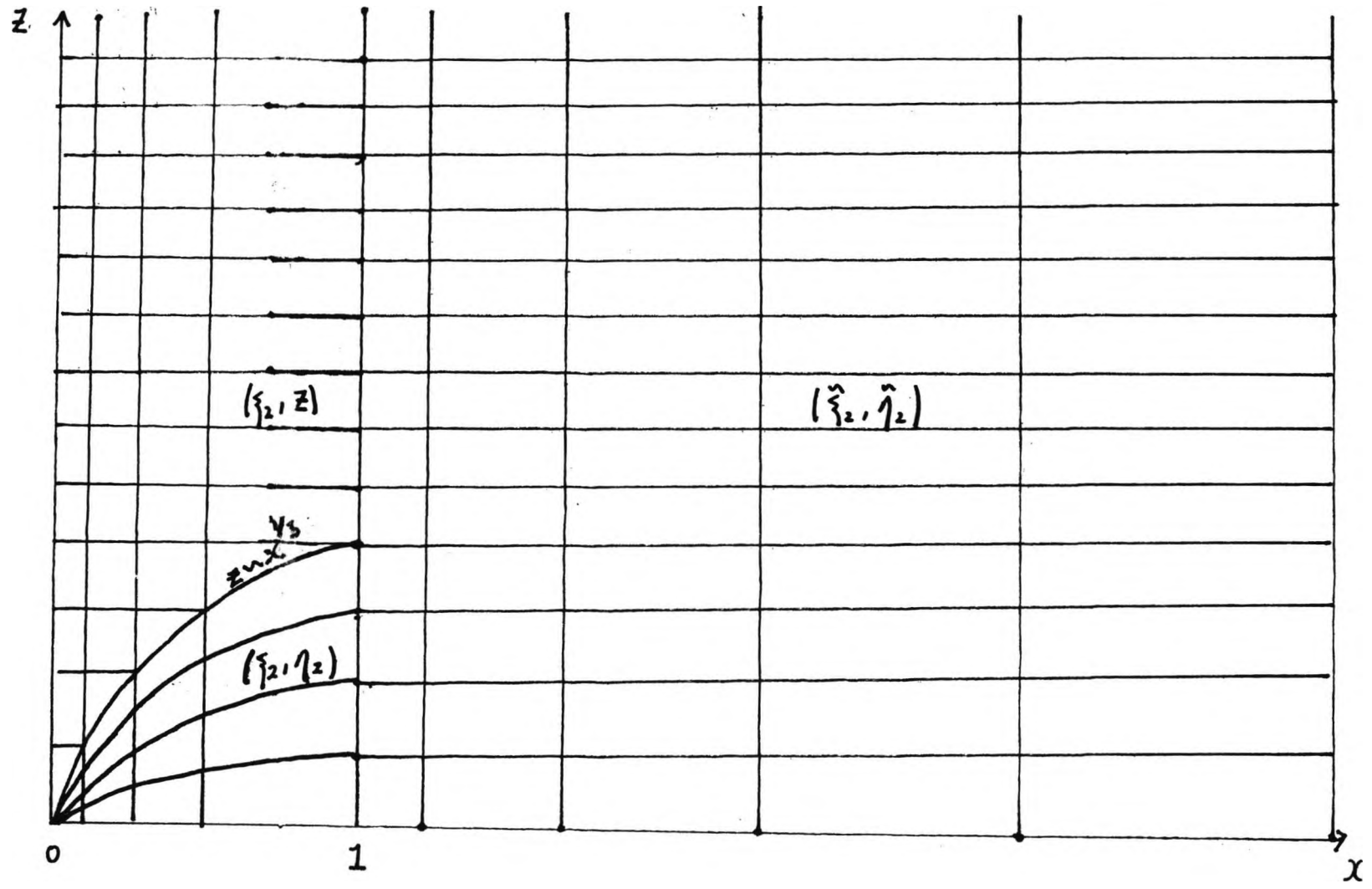


Figure 5.9 Mesh structure.

Figure 5.10 Graph of $\frac{\partial \hat{\phi}_2}{\partial \hat{\eta}_2}$ against $\hat{\eta}_2$ for $\sigma = 0.1$.

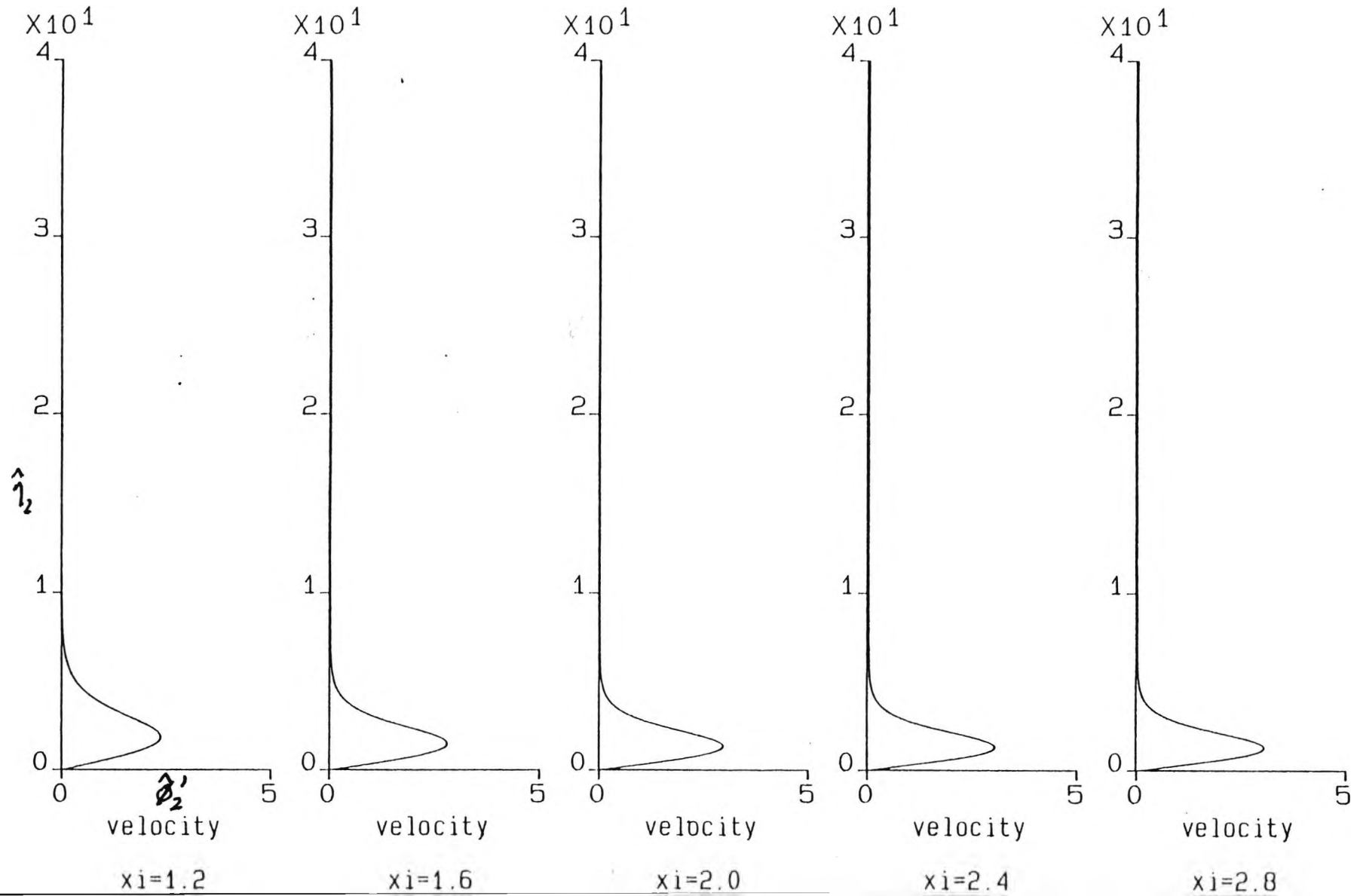


Figure 5.11 Graph of $\hat{\theta}_2$ against $\hat{\eta}_2$ for $\sigma = 0.1$.

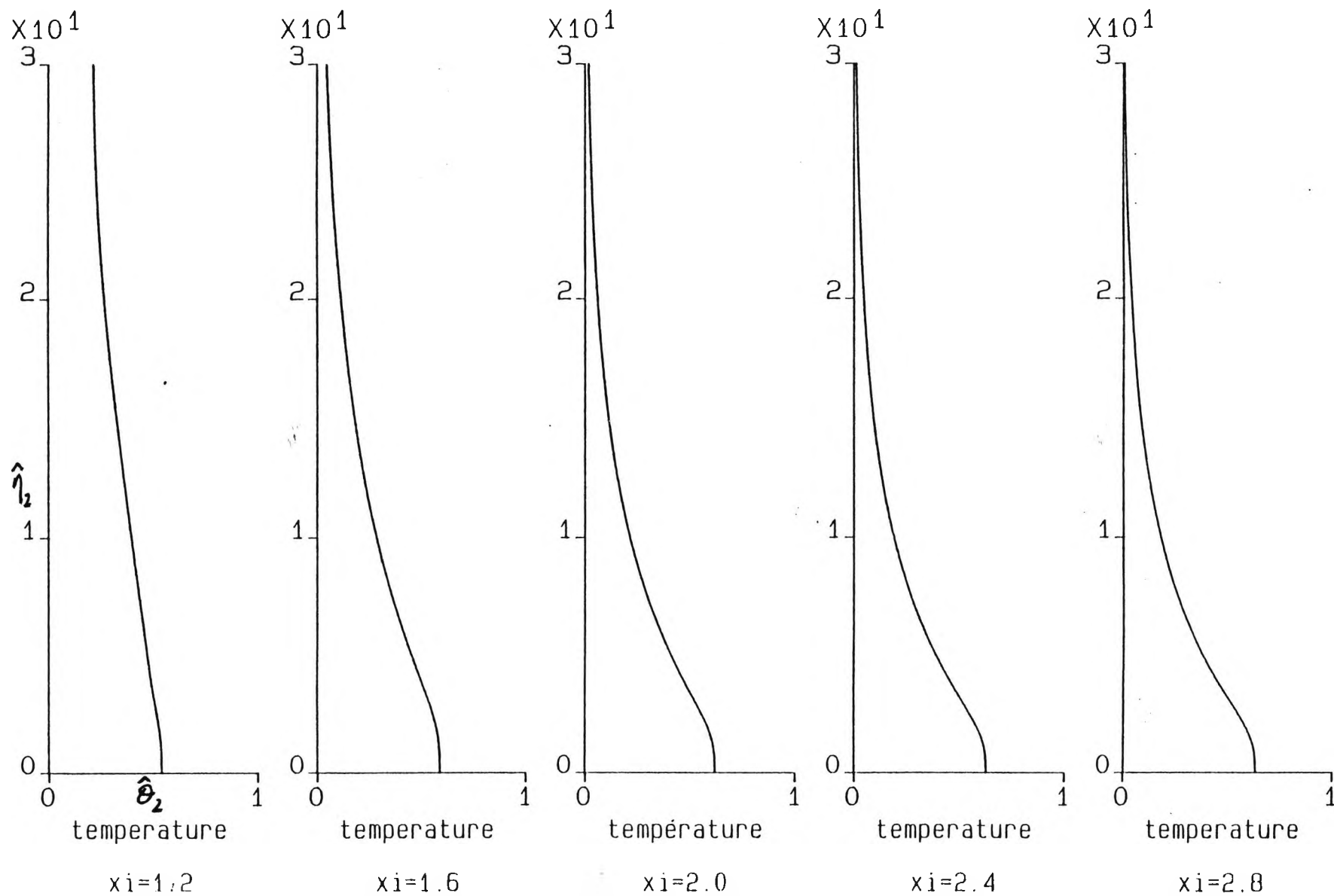


Figure 5.12 Graph of $\frac{\partial \hat{\phi}_2}{\partial \hat{\eta}_2}$ against $\hat{\eta}_2$ for $\sigma = 0.72$.

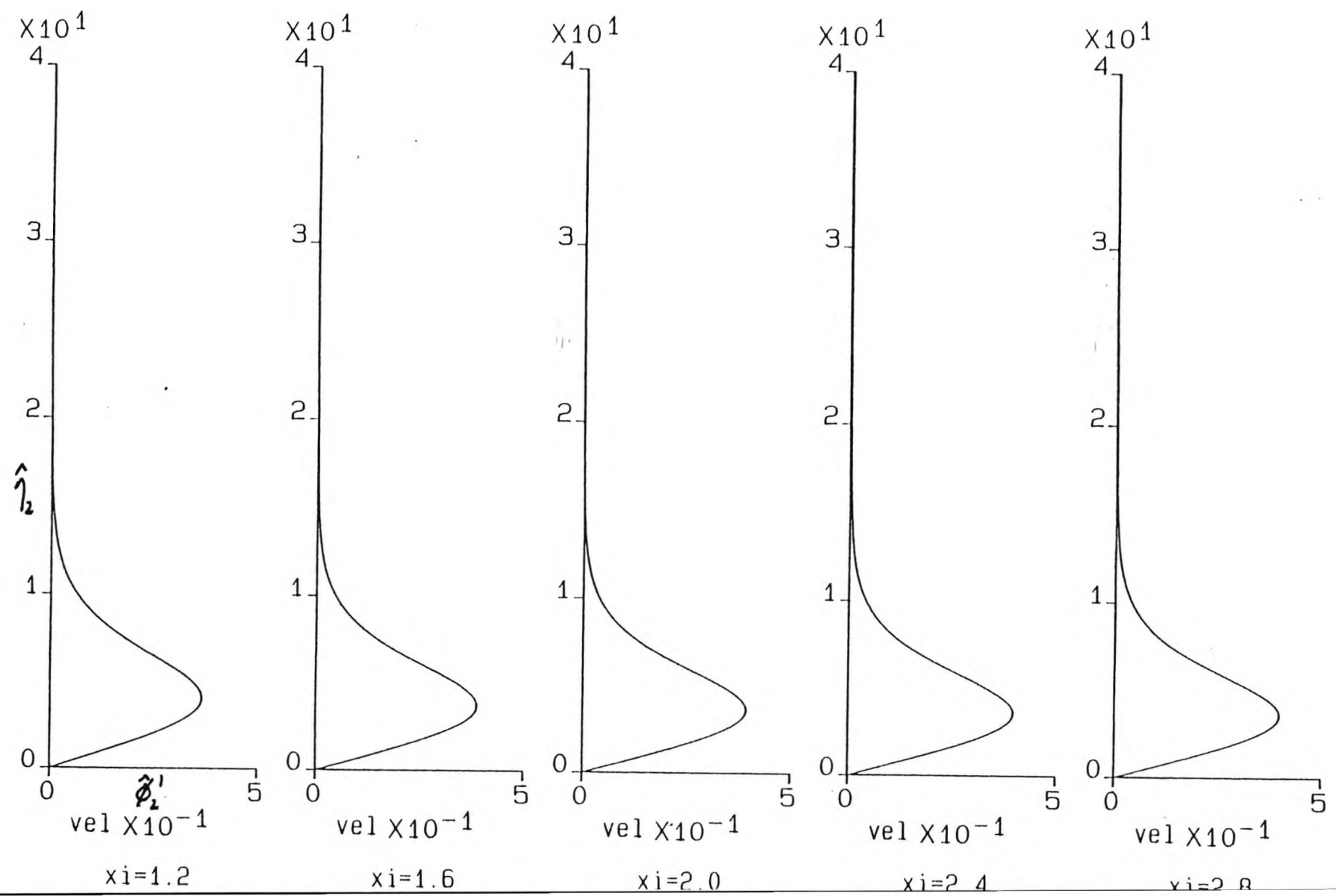


Figure 5.13 Graph of $\hat{\theta}_2$ against $\hat{\eta}_2$ for $\sigma = 0.72$.

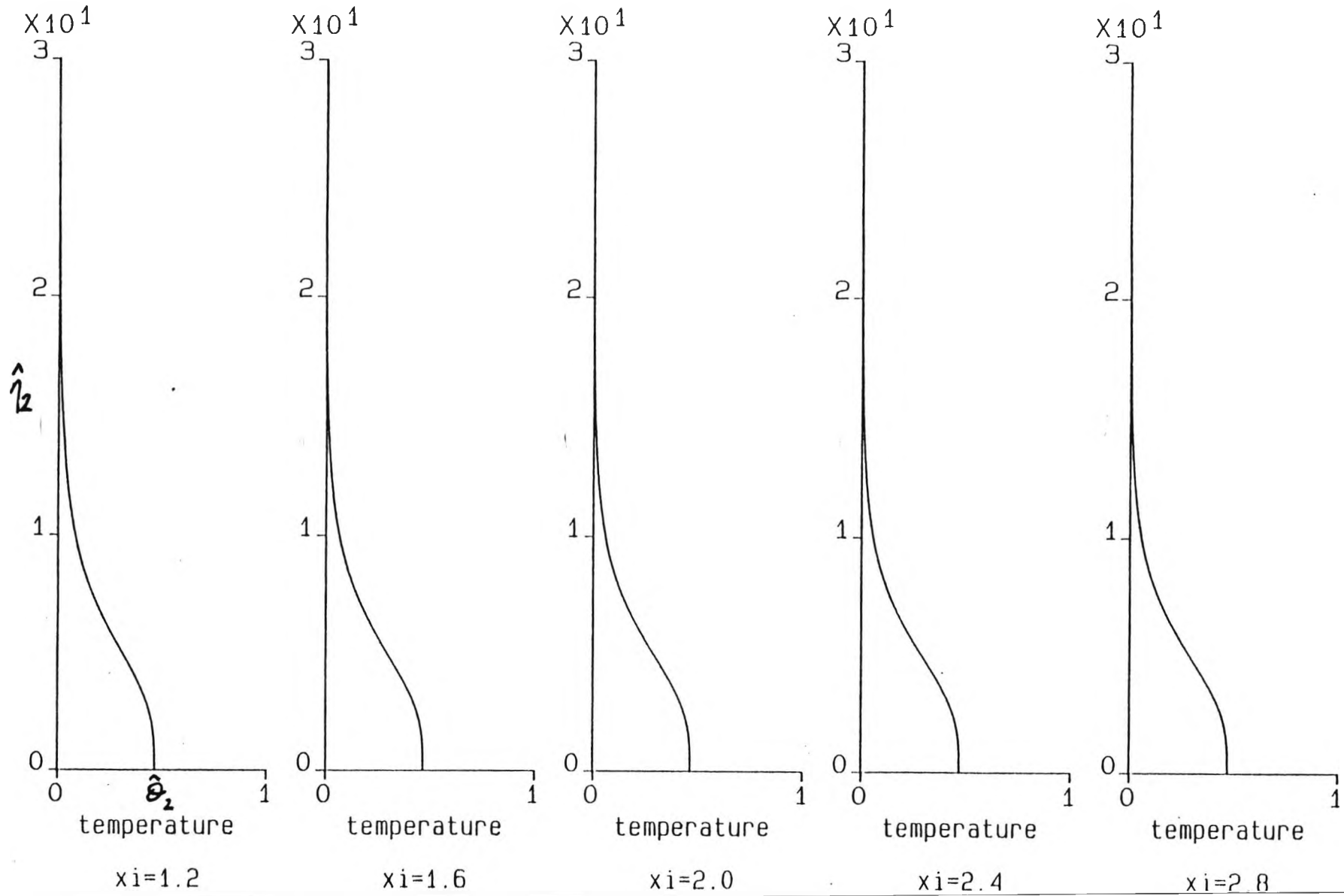


Figure 5.14 Graph of $\frac{\partial \hat{\phi}_2}{\partial \hat{\eta}_2}$ against $\hat{\eta}_2$ for $\sigma = 8.1$.

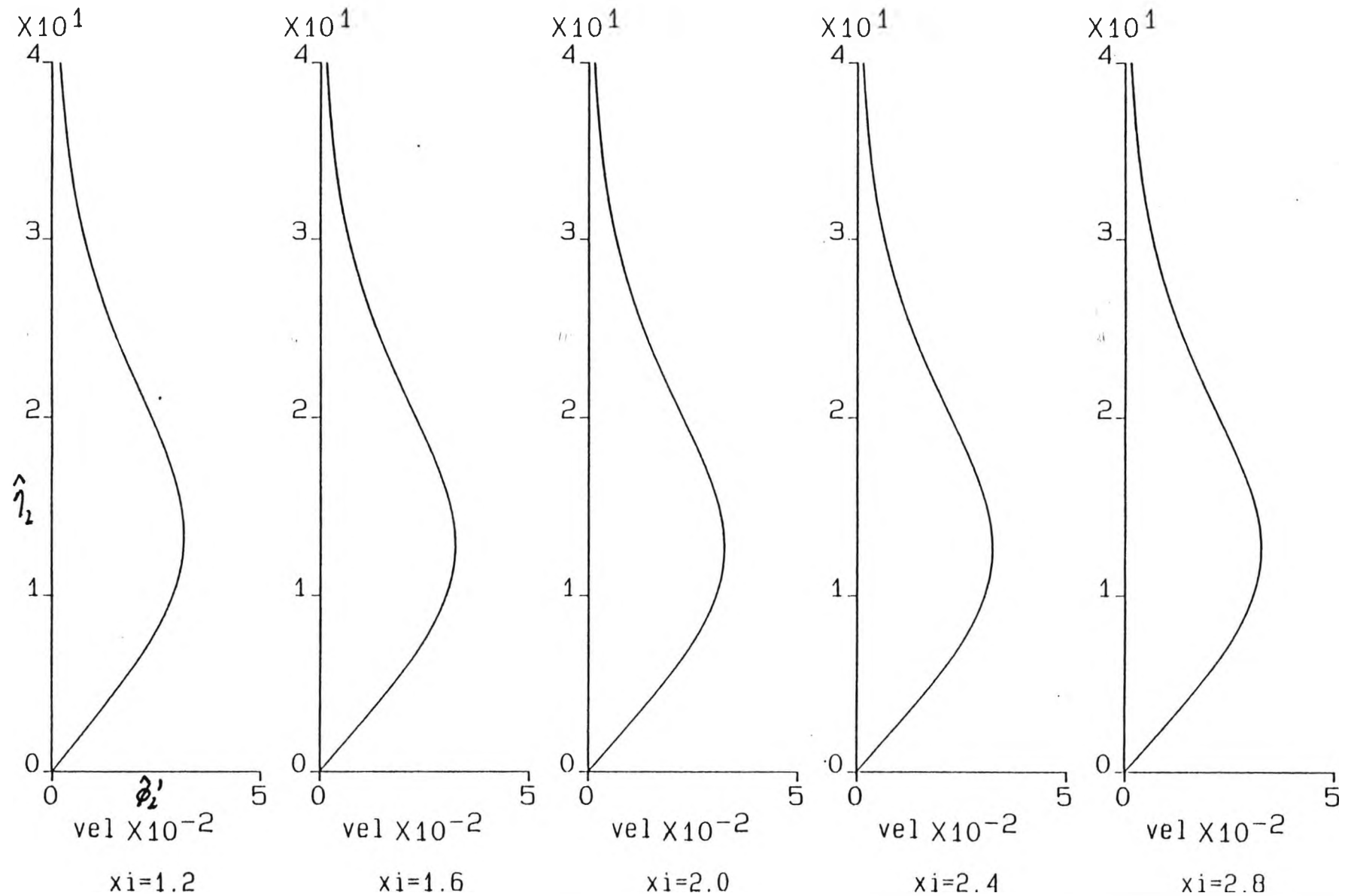


Figure 5.15 Graph of $\hat{\theta}_2$ against $\hat{\eta}_2$ for $\sigma = 8.1$.

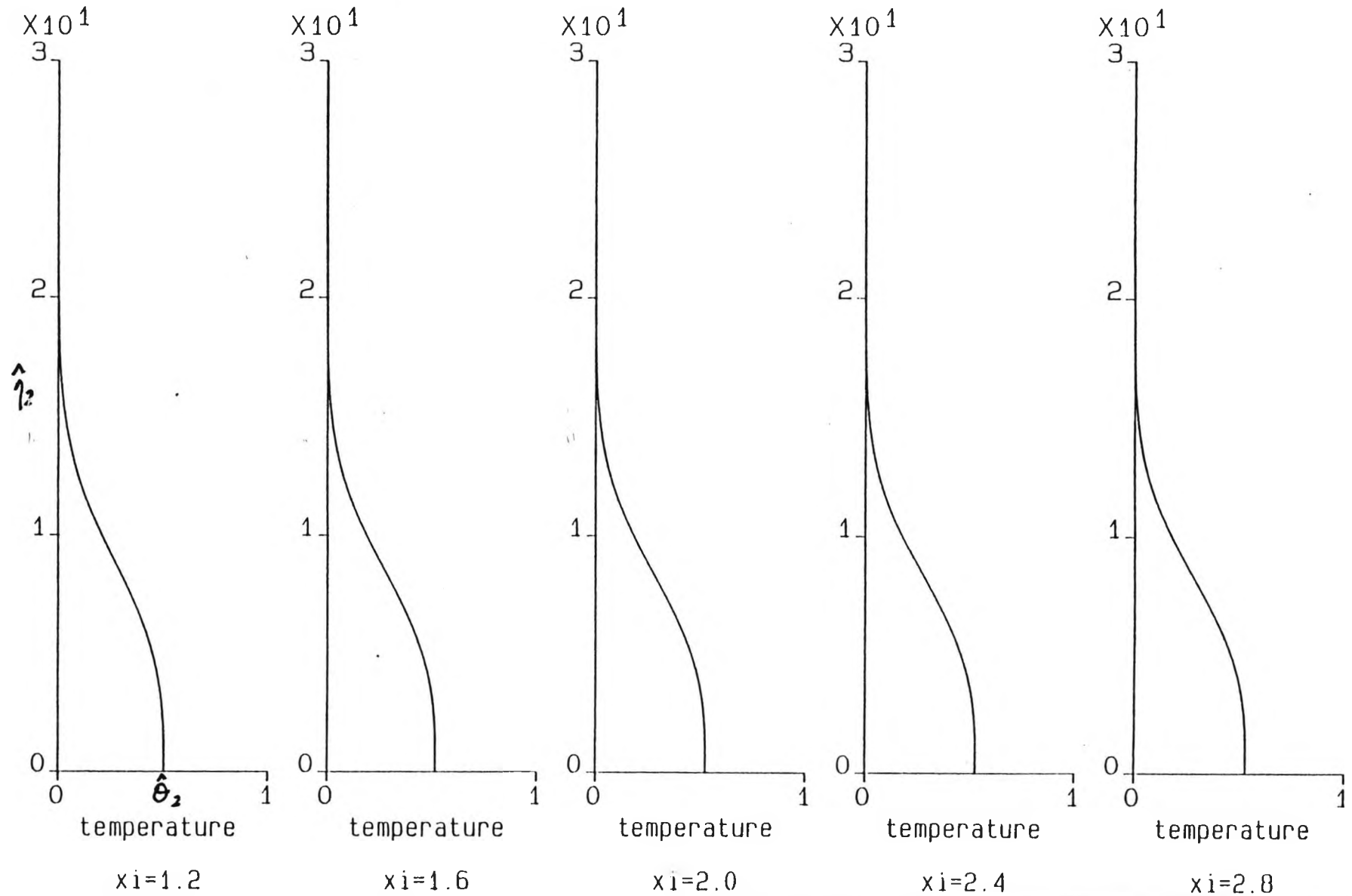


Figure 5.16 Graph of $\frac{\partial \hat{\phi}_2}{\partial \hat{\eta}_2}$ against $\hat{\eta}_2$ for $\sigma = 17.2$.

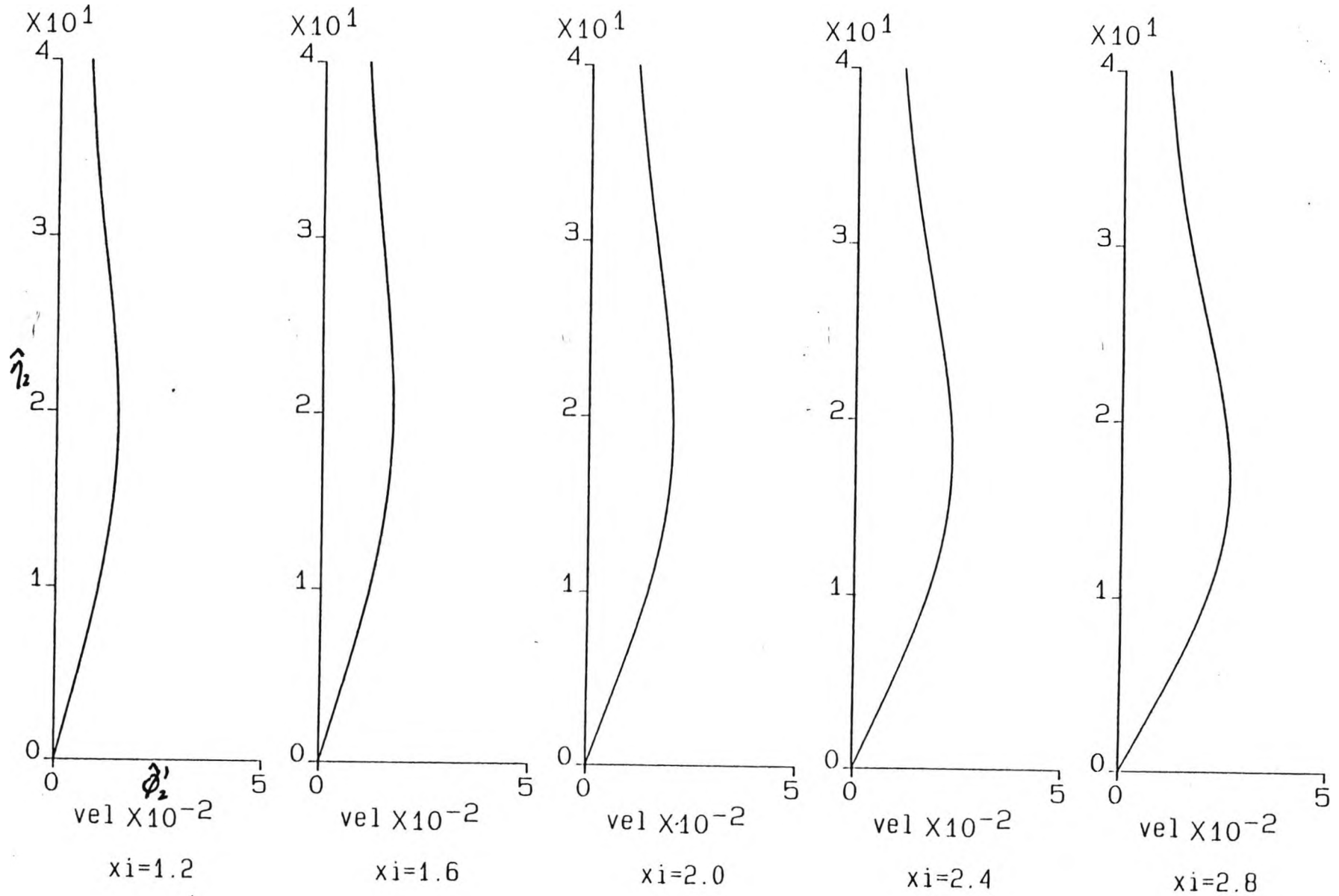
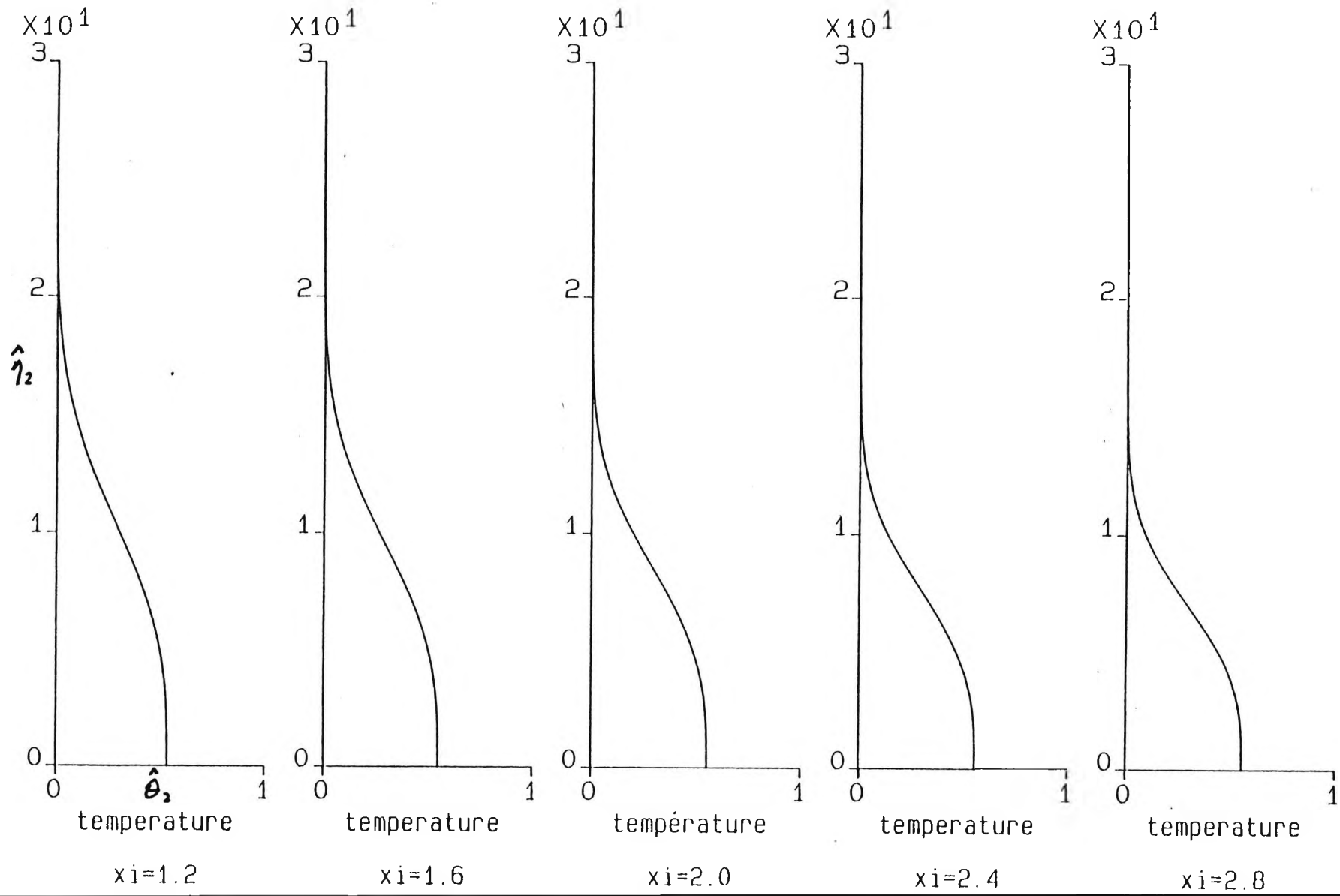


Figure 5.17 Graph of $\hat{\theta}_2$ against $\hat{\eta}_2$ for $\sigma = 17.2$.



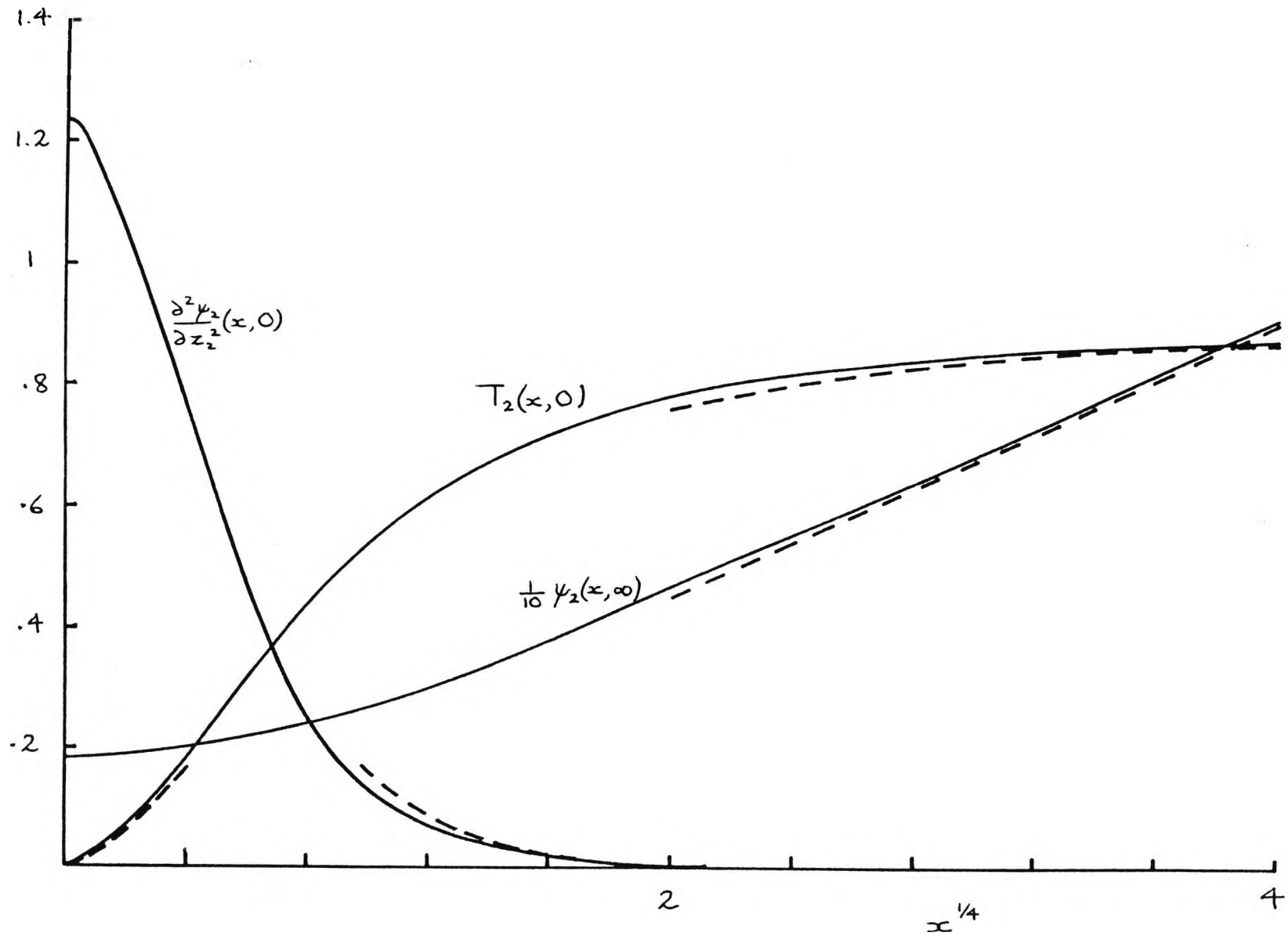


Figure 5.18 Graph of $\psi_2(x_2, \infty)$, $T_2(x_2, 0)$ and $\frac{\partial \psi_2}{\partial z_2}(x_2, 0)$ against $x_2^{1/4}$.

CHAPTER 6

The horizontal buoyancy layer $x = 0(R_1^{2/5})$:

asymptotic solution

6.1 Introduction

As x increases the flow enters a new regime where $x/R_1^{2/5} = 0(1)$ and the buoyancy term reappears in the vorticity equation. This chapter deals with analytical aspects of this horizontal 'buoyancy' layer. In Section 6.2 the governing equations and boundary conditions are derived. A solution for small $x/R_1^{2/5}$ is formulated and found numerically in Section 6.3. An asymptotic form of the solution for large $x/R_1^{2/5}$ is discussed in Section 6.4. The results are summarised in Section 6.5.

6.2 Formulation

The reintroduction of the buoyancy term into the vorticity equation occurs when $x = 0(R_1^{2/5})$. This leads to the following

scalings for a new horizontal boundary layer

$$\begin{aligned} \Psi &= \sigma R_1^{7/10} C_0^{7/24} \hat{\Psi}_3, \quad T = R_1^{7/5} C_0 + R_1^{13/10} C_0^{23/24} \hat{T}_3 \\ x &= R_1^{2/5} C_0^{1/6} \hat{x}_3, \quad z = R_1^{-3/10} C_0^{-1/8} \hat{z}_3. \end{aligned} \quad (6.2.1)$$

Substitution into (3.2.19) and (3.2.20) gives

$$\frac{\partial^4 \hat{\Psi}_3}{\partial \hat{z}_3^4} = \frac{1}{\sigma} \frac{\partial \hat{T}_3}{\partial \hat{x}_3} + \frac{\partial \hat{\Psi}_3}{\partial \hat{z}_3} \frac{\partial^3 \hat{\Psi}_3}{\partial \hat{x}_3 \partial \hat{z}_3^2} - \frac{\partial \hat{\Psi}_3}{\partial \hat{x}_3} \frac{\partial^3 \hat{\Psi}_3}{\partial \hat{z}_3^2} \quad (6.2.2)$$

and

$$\frac{\partial^2 \hat{T}_3}{\partial \hat{z}_3^2} = \sigma \left(\frac{\partial \hat{T}_3}{\partial \hat{x}_3} \frac{\partial \hat{\Psi}_3}{\partial \hat{z}_3} - \frac{\partial \hat{T}_3}{\partial \hat{z}_3} \frac{\partial \hat{\Psi}_3}{\partial \hat{x}_3} \right) \quad (6.2.3)$$

respectively, which are to be solved subject to

$$\hat{\psi}_3 = \frac{d\hat{\psi}_3}{d\hat{z}_3} = \frac{d\hat{T}_3}{d\hat{z}_3} = 0 \quad ; \quad \hat{z}_3 = 0 \quad (6.2.4)$$

and

$$\hat{T}_3 \rightarrow 0, \quad \frac{d\hat{\psi}_3}{d\hat{z}_3} \rightarrow U_3 \quad ; \quad \hat{z}_3 \rightarrow \infty. \quad (6.2.5)$$

The second condition in (6.2.5) arises from the fact that in the boundary layer the velocity term $\frac{\partial \psi}{\partial z}$ is $O(R_1)$. The

recirculating inviscid zone above the horizontal boundary layers also has $O(R_1)$ velocities suggesting that on the scale

$x = O(R_1^{2/5})$ there will now be a constant forcing velocity

$\frac{\partial \psi}{\partial z} = \sigma R_1 c_0^{5/12} U_3$ at the outer edge of the boundary layer.

In Chapter 4 the $x = O(1)$ horizontal boundary layer admitted two integral constraints (4.2.8) and (4.2.11)

$$P = \int_0^\infty \frac{d\hat{\psi}_3}{d\hat{z}_3} \left\{ \int_{\hat{z}_3}^\infty \left(\frac{d\hat{\psi}_3}{d\hat{z}_3} \right)^2 d\hat{z}_3 \right\} d\hat{z}_3, \quad Q = \int_0^\infty \hat{\psi}_3 \frac{d\hat{T}_3}{d\hat{z}_3} d\hat{z}_3$$

with P and Q constant. We may rescale in terms of these two constants

$$\begin{aligned} \hat{\psi}_3 &= P^{1/2} Q^{-1/6} \psi_3 \\ \hat{T}_3 &= P^{-1/2} Q^{7/6} T_3 \\ \hat{x}_3 &= P Q^{-2/3} x_3 \\ \hat{z}_3 &= P^{1/2} Q^{-1/2} z_3 \end{aligned} \quad ((6.2.6)$$

giving

$$\frac{d^4 \psi_3}{dz_3^4} = \frac{1}{\sigma} \frac{dT_3}{dx_3} + \frac{d\psi_3}{dz_3} \frac{d^3 \psi_3}{dx_3 dz_3^2} - \frac{d\psi_3}{dx_3} \frac{d^3 \psi_3}{dz_3^3} \quad (6.2.7)$$

and

$$\frac{d^2 T_3}{dz_3^2} = \sigma \left(\frac{\partial T_3}{\partial x_3} \frac{d\psi_3}{dz_3} - \frac{\partial T_3}{\partial z_3} \frac{d\psi_3}{dx_3} \right) \quad (6.2.8)$$

to be solved subject to

$$\psi_3 = \frac{\partial \Psi_3}{\partial z_3} = \frac{\partial T_3}{\partial z_3} = 0 \quad ; \quad z_3 = 0 \quad (6.2.9)$$

$$\text{and } T_3 \rightarrow 0, \quad \frac{\partial \Psi_3}{\partial z_3} \rightarrow \epsilon \quad \text{as } z_3 \rightarrow \infty \quad (6.2.10)$$

where

$$\epsilon = \frac{u_3}{Q^{1/3}} \quad (6.2.11)$$

The initial profile for ψ_3 is uniquely determined by

$$\int_0^\infty \frac{\partial \Psi_3}{\partial z_3} \left\{ \int_{z_3}^\infty \left(\frac{\partial \Psi_3}{\partial z_3} \right)^2 dz_3 \right\} dz_3 = 1 \quad \text{as } x_3 \rightarrow 0 \quad (6.2.12)$$

and is independent of σ . However due to the reintroduction of the buoyancy term, the integral on the left-hand side of (6.2.12) is not conserved for $x_3 > 0$. The constraint

$$\int_0^\infty \psi_3 \frac{\partial T_3}{\partial z_3} dz_3 = 1 \quad (6.2.13)$$

uniquely determines the initial profile for T_3 although the latter is not independent of σ . Equation (6.2.13) is satisfied for all x_3 , from (6.2.8)-(6.2.10). The initial form of the solution is defined by

$$\psi_3 \sim x_3^{1/4} f_{30}(\eta_3), \quad T_3 \sim x_3^{-1/4} \tau_{30}(\eta_3) \quad ; \quad x_3 \rightarrow 0 \quad (6.2.14)$$

where $\eta_3 = z_3/x_3^{3/4}$ and the functions f_{30} and τ_{30} are scaled forms of ϕ_2 and θ_2 to be defined precisely in Section 6.3 below. The buoyancy layer problem defined by (6.2.7)-(6.2.14) is dependent on just two parameters, ϵ and σ .

6.3 Solution for small x_3

We expand the stream function and temperature as follows

$$\Psi_3 = x_3^{1/4} f_{30}(\eta_3) + x_3^{3/4} f_{31}(\eta_3) + x_3^{5/4} f_{32}(\eta_3) + x_3^{7/4} f_{33}(\eta_3) + \dots \quad (6.3.1)$$

$$T_3 = x_3^{-1/4} \tau_{30}(\eta_3) + x_3^{1/4} \tau_{31}(\eta_3) + x_3^{3/4} \tau_{32}(\eta_3) + x_3^{5/4} \tau_{33}(\eta_3) + \dots \quad (6.3.2)$$

where $\eta_3 = z_3 / x_3^{3/4} = O(1)$. (6.3.3)

Here the leading terms are suggested by the Glauert form and the next terms are generated by ϵ .

(i) Solutions f_{30}, τ_{30}

Substituting (6.3.1), (6.3.2) and (6.3.3) into (6.2.7) we get at $O(x_3^{-11/4})$

$$f_{30}^{iv} = -\frac{5}{4} f_{30}' f_{30}'' - \frac{1}{4} f_{30} f_{30}'''' \quad (6.3.4)$$

with boundary conditions

$$f_{30} = f_{30}' = 0, \eta_3 = 0; f_{30}' \rightarrow 0, \eta_3 \rightarrow \infty. \quad (6.3.5)$$

Equation (6.3.4) can be integrated to give

$$f_{30}''' + \frac{1}{4} f_{30} f_{30}'' + \frac{1}{2} f_{30}'^2 = 0 \quad (6.3.6)$$

and the solution to (6.3.6) satisfying the integral requirement

$$\int_0^\infty f_{30}' \left\{ \int_{\eta_3}^\infty f_{30}'^2 d\eta_3 \right\} d\eta_3 = 1$$

obtained from (6.2.11) is the 'Glauert type' solution

$$f_{30} = K_3 \left\{ g_2 \left(\frac{\eta_3}{4} \right) \right\}^2 \quad \text{where } K_3 = (40)^{\frac{1}{4}} \quad (6.3.7)$$

and

$$\eta_3 = \frac{1}{K_3} \left\{ \log_e \frac{\sqrt{1+g_2+g_2^2}}{1-g_2} + \sqrt{3} \tan^{-1} \left(\frac{\sqrt{3}g_2}{2+g_2} \right) \right\} \quad (6.3.8)$$

as given in (4.4.8).

At $O(x_3^{-7/4})$ in (6.2.8) we obtain

$$\frac{1}{\sigma} \tau_{30}'' = -\frac{1}{4} f_{30}' \tau_{30} - \frac{1}{4} \tau_{30}' f_{30} \quad (6.3.9)$$

with boundary conditions

$$\tau_{30}' = 0, \quad \eta_3 = 0; \quad \tau_{30} \rightarrow 0, \quad \eta_3 \rightarrow \infty. \quad (6.3.10)$$

The solution is

$$\tau_{30} = \theta_{30} \left[1 - \left(g_2 \left(\frac{\eta_3}{4} \right) \right)^3 \right]^\sigma$$

as found in (4.4.20), and the integral constraint

$$\int_0^\infty f_{30} \tau_{30}' d\eta_3 = 1 \quad (6.3.11)$$

obtained from (6.2.13) determines the value of θ_{30} , as given in table 6.1.

(ii) Solutions f_{31}, τ_{31}

At $O(x_3^{-9/4})$ the function f_{31} is found to satisfy

$$f_{31}^{iv} = -\frac{3}{4} f_{30}' f_{31}' - \frac{5}{4} f_{31}' f_{30}'' - \frac{3}{4} f_{30}''' f_{31} - \frac{1}{4} f_{30} f_{31}''' \quad (6.3.12)$$

with boundary conditions

$$f_{31} = f_{31}' = 0, \quad \eta_3 = 0; \quad f_{31}' \rightarrow \epsilon, \quad \eta_3 \rightarrow \infty. \quad (6.3.13)$$

Equation (6.3.11) can be integrated to give

$$f_{31}''' + \frac{3}{4} f_{31} f_{30}'' + \frac{1}{4} f_{30} f_{31}'' + \frac{1}{2} f_{30}' f_{31}' = 0. \quad (6.3.14)$$

At $O(x_3^{-5/4})$ the function τ_{31} is found to satisfy

$$\frac{1}{\sigma} \tau_{31}'' = \frac{1}{4} f_{30}' \tau_{31} - \frac{1}{4} f_{31}' \tau_{30} - \frac{3}{4} \tau_{30}' f_{31} - \frac{1}{4} f_{30} \tau_{31}' \quad (6.3.15)$$

with boundary conditions

$$\tau_{31}' = 0, \eta_3 = 0; \tau_{31} \rightarrow 0, \eta_3 \rightarrow \infty. \quad (6.3.16)$$

Since $f_{30} \rightarrow K_3$ as $\eta_3 \rightarrow \infty$ it is expected that

$$f_{31} \sim \epsilon \eta_3 + a_{31} + O(e^{-1/4 K_3 \eta_3}) \quad (\eta_3 \rightarrow \infty) \quad (6.3.17)$$

$$\tau_{31} \sim 0 + O(e^{-1/4 \sigma K_3 \eta_3}) \quad (\eta_3 \rightarrow \infty). \quad (6.3.18)$$

We can rescale with ϵ such that

$$f_{31} = \epsilon \hat{f}_{31}, \tau_{31} = \epsilon \hat{\tau}_{31} \quad (6.3.19)$$

to obtain

$$\hat{f}_{31}''' = -\frac{3}{4} \hat{f}_{31} f_{30}'' - \frac{1}{4} f_{30} \hat{f}_{31}'' - \frac{1}{2} f_{30}' \hat{f}_{31}' \quad (6.3.20)$$

$$\hat{\tau}_{31}'' = \sigma \left(\frac{1}{4} \hat{\tau}_{31} f_{30}' - \frac{1}{4} \hat{f}_{31}' \tau_{30} - \frac{3}{4} \tau_{30}' \hat{f}_{31} - \frac{1}{4} f_{30} \hat{\tau}_{31}' \right) \quad (6.3.21)$$

to be solved subject to

$$\begin{aligned} \hat{f}_{31} = \hat{f}_{31}' = \hat{\tau}_{31}' = 0, \eta_3 = 0; \\ \hat{\tau}_{31} \rightarrow 0, \hat{f}_{31}' \rightarrow 1, \eta_3 \rightarrow \infty \end{aligned} \quad (6.3.22)$$

and from (6.3.17)

$$a_{31} = \epsilon \hat{a}_{31} \quad (6.3.23)$$

where $\hat{f}_{31} \sim \eta_3 + \hat{a}_{31}; \eta_3 \rightarrow \infty.$

(iii) Solutions f_{32}, τ_{32}

At $O(x_3^{-7/4})$ f_{32} is found to satisfy

$$f_{32}^{iv} = -\frac{1}{4} f_{30}' f_{32}'' - \frac{3}{4} f_{31}' f_{31}'' - \frac{5}{4} f_{32}' f_{30}'' \\ - \frac{1}{4} f_{30} f_{32}''' - \frac{3}{4} f_{31} f_{31}''' - \frac{5}{4} f_{32} f_{30}''' \quad (6.3.24)$$

with boundary conditions

$$f_{32} = f_{32}' = 0, \eta_3 = 0; \quad f_{32} \rightarrow 0, \eta_3 \rightarrow \infty. \quad (6.3.25)$$

Equation (6.3.24) can be integrated to give

$$f_{32}''' = -\frac{1}{4} f_{30} f_{32}'' - \frac{3}{4} f_{31} f_{31}'' - \frac{5}{4} f_{32} f_{30}'' \quad (6.3.26)$$

At $O(x_3^{-3/4})$ τ_{32} is found to satisfy

$$\frac{1}{\sigma} \tau_{32}'' = \frac{3}{4} f_{30}' \tau_{32} + \frac{1}{4} f_{31}' \tau_{31} - \frac{1}{4} \tau_{30} f_{32}' \\ - \frac{5}{4} \tau_{30}' f_{32} - \frac{3}{4} \tau_{31}' f_{31} - \frac{1}{4} f_{30} \tau_{32}' \quad (6.3.27)$$

with boundary conditions

$$\tau_{32}' = 0, \eta_3 = 0; \quad \tau_{32} \rightarrow 0, \eta_3 \rightarrow \infty. \quad (6.3.28)$$

As $\eta_3 \rightarrow \infty$ it is expected that

$$f_{32} \sim O(\eta_3) + a_{32} + O(e^{-(1/4)K_3 \eta_3}) \quad (6.3.29)$$

$$\tau_{32} \sim 0 + O(e^{-\frac{1}{4}K_3 \sigma \eta_3}). \quad (6.3.30)$$

We can rescale with ϵ^2 such that

$$f_{32} = \epsilon^2 \hat{f}_{32}, \quad \tau_{32} = \epsilon^2 \hat{\tau}_{32} \quad (6.3.31)$$

to obtain

$$\hat{f}_{32}''' = -\frac{1}{4} f_{30} \hat{f}_{32}'' - \frac{3}{4} \hat{f}_{31} \hat{f}_{31}'' - \frac{5}{4} \hat{f}_{32} f_{30}''' \quad (6.3.32)$$

$$\begin{aligned} \hat{\tau}_{32}'' = \sigma \left(\frac{3}{4} f_{30}' \hat{\tau}_{32} + \frac{1}{4} \hat{f}_{31}' \hat{\tau}_{31} - \frac{1}{4} \tau_{30} \hat{f}_{32}' \right. \\ \left. - \frac{5}{4} \tau_{30}' \hat{f}_{32} - \frac{3}{4} \hat{\tau}_{31}' \hat{f}_{31} - \frac{1}{4} f_{30} \hat{\tau}_{32}' \right) \end{aligned} \quad (6.3.33)$$

with

$$\begin{aligned} \hat{f}_{32} = \hat{f}_{32}' = \hat{\tau}_{32}' = 0, \quad \eta_3 = 0; \\ \hat{\tau}_{32} \rightarrow 0, \quad \hat{f}_{32}' \rightarrow 0, \quad \eta_3 \rightarrow \infty. \end{aligned} \quad (6.3.34)$$

and from (6.3.29)

$$a_{32} = \epsilon^2 \hat{a}_{32} \quad (6.3.35)$$

where $\hat{a}_{32} = \hat{f}_{32}(0)$.

(iv) Solutions f_{33}, τ_{33}

At $O(x_3^{-5/4})$ f_{33} is found to satisfy

$$\begin{aligned} f_{33}^{IV} = \frac{1}{\sigma} \left(-\frac{1}{4} \tau_{30} - \frac{3}{4} \eta_3 \tau_{30}' \right) + \frac{1}{4} f_{30}' f_{33}'' - \frac{1}{4} f_{31}' f_{32}'' \\ - \frac{3}{4} f_{32}' f_{31}'' - \frac{5}{4} f_{30}'' f_{33}' - \frac{7}{4} f_{30}''' f_{33} - \frac{5}{4} f_{31}'' f_{32}' - \frac{3}{4} f_{32}''' f_{31}' - \frac{1}{4} f_{33}''' f_0 \end{aligned} \quad (6.3.36)$$

with boundary conditions

$$f_{33} = f_{33}' = 0, \quad \eta_3 = 0; \quad f_{33}' \rightarrow 0, \quad \eta_3 \rightarrow \infty. \quad (6.3.37)$$

At $O(x_3^{-1/4})$ τ_{33} is found to satisfy

$$\begin{aligned} \frac{1}{\sigma} \tau_{33}'' = \frac{5}{4} f_{30}' \tau_{33} + \frac{3}{4} f_{31}' \tau_{32} + \frac{1}{4} f_{32}' \tau_{31} - \frac{1}{4} f_{31}' \tau_{30} \\ - \frac{1}{4} \tau_{33}' f_{30} - \frac{3}{4} \tau_{32}' f_{31} - \frac{5}{4} \tau_{31}' f_{32} - \frac{1}{4} \tau_{30}' f_{33} \end{aligned} \quad (6.3.38)$$

with boundary conditions

$$\tau_{33}' = 0, \quad \eta_3 = 0; \quad \tau_{33} \rightarrow 0, \quad \eta_3 \rightarrow \infty. \quad (6.3.39)$$

As $\eta_3 \rightarrow \infty$ it is expected that

$$f_{33} \sim O(\eta_3^2) + O(\eta_3) + a_{33} + O(e^{-\frac{1}{4}K_3 \eta_3}) \quad (6.3.40)$$

$$L_{33} \sim 0 + O(e^{-\frac{1}{4}\sigma K_3 \eta_3}). \quad (6.3.41)$$

We can rescale with ϵ^3 such that

$$f_{33} = \hat{f}_{330} + \epsilon^3 \hat{f}_{331}, \quad L_{33} = \hat{L}_{330} + \epsilon^3 \hat{L}_{331} \quad (6.3.42)$$

to obtain

$$\begin{aligned} \hat{f}_{330}^{iv} = & \frac{1}{\sigma} \left(-\frac{1}{4} L_{30} - \frac{3}{4} \eta_3 L_{30}' \right) + \\ & \frac{1}{4} f_{30}' \hat{f}_{330}'''' - \frac{5}{4} f_{30}'' \hat{f}_{330}' - \frac{7}{4} f_{30}''' \hat{f}_{330} - \frac{1}{4} \hat{f}_{330}''' f_{30}, \end{aligned} \quad (6.3.43)$$

$$\begin{aligned} \hat{f}_{331}^{iv} = & \frac{1}{4} f_{30}' \hat{f}_{331}'' - \frac{1}{4} \hat{f}_{31}' \hat{f}_{32}'' - \frac{3}{4} \hat{f}_{32}' \hat{f}_{31}'' - \frac{5}{4} f_{30}'' \hat{f}_{331}' \\ & - \frac{7}{4} f_{30}''' \hat{f}_{331} - \frac{5}{4} \hat{f}_{31}''' \hat{f}_{32} - \frac{3}{4} \hat{f}_{32}''' \hat{f}_{31} - \frac{1}{4} \hat{f}_{331}' f_{30}, \end{aligned} \quad (6.3.44)$$

$$\hat{L}_{330}'' = \sigma \left(\frac{5}{4} f_{30}' \hat{L}_{330} - \frac{1}{4} \hat{f}_{330}' L_{30} - \frac{1}{4} \hat{L}_{330}' f_{30} - \frac{7}{4} L_{30}' \hat{f}_{330} \right) \quad (6.3.45)$$

and

$$\begin{aligned} \hat{L}_{331}'' = & \sigma \left(\frac{5}{4} f_{30}' \hat{L}_{331} + \frac{3}{4} \hat{f}_{31}' \hat{L}_{32} + \frac{1}{4} \hat{f}_{32}' \hat{L}_{31} - \frac{1}{4} \hat{f}_{331}' L_{30} \right. \\ & \left. - \frac{1}{4} \hat{L}_{331}' f_{30} - \frac{3}{4} \hat{L}_{32}' \hat{f}_{31} - \frac{5}{4} \hat{L}_{31}' \hat{f}_{32} - \frac{7}{4} \hat{f}_{331}' \hat{L}_{30}' \right) \end{aligned} \quad (6.3.46)$$

with

$$\begin{aligned} \hat{f}_{330}' = \hat{f}_{330}'' = \hat{f}_{331}' = \hat{f}_{331}'' = \hat{L}_{330}' = \hat{L}_{331}' = 0, \quad \eta_3 = 0; \\ \hat{f}_{330}', \hat{f}_{331}', \hat{L}_{330}', \hat{L}_{331}' \rightarrow 0, \quad \eta_3 \rightarrow \infty \end{aligned} \quad (6.3.47)$$

It may appear that there is no fourth boundary condition but the conditions on \hat{f}_{330} and \hat{f}_{331} as $\eta_3 \rightarrow \infty$ are in effect two boundary conditions in one as we must eliminate both η_3^2 and η_3

behaviours as $\eta_3 \rightarrow \infty$. Also from (6.3.40)

$$a_{33} = \hat{a}_{330} + \epsilon^3 \hat{a}_{331} \quad (6.3.48)$$

where $\hat{a}_{33i} = \hat{f}_{33i}(\infty)$, $i = 1, 2$.

(v) Numerical Solution

The above systems were solved numerically using a fourth order Runge-Kutta scheme, marching from the origin.

For f_{30} it was necessary to find the value of $f_{30}''(0)$ which gave $f_{30} = (40)^{1/4} \approx 2.52$ as $\eta_3 \rightarrow \infty$. A relation $f_{30}''(0) = \lambda_{30}[f_{30}(\infty)]^{\mu_{30}}$ was assumed and the program run for two different initial values of $f_{30}''(0)$ which enabled the values of λ_{30} and μ_{30} to be fixed. The true value of $f_{30}(\infty) = (40)^{1/4}$ was then put in giving the required value of $f_{30}''(0)$ so that when the program was run for the third time $f_{30} \rightarrow 2.52$ and $f_{30}' \rightarrow 0$ as $\eta_3 \rightarrow \infty$. A graph of f_{30}' against η_3 is presented in figure 6.1. The solution for f_{30} is independent of σ .

The problem for τ_{30} was solved by inserting the value of $\tau_{30}(0)$ as θ_{30} from table 6.1. Figure 6.2 shows a graph of τ_{30} against η_3 for various values of σ .

To obtain the solution for \hat{f}_{31} it was necessary to find the value of $\hat{f}_{31}''(0)$ for which $\hat{f}_{31}' \rightarrow 1$ as $\eta_3 \rightarrow \infty$. As the relationship between $\hat{f}_{31}''(0)$ and $\hat{f}_{31}'(\infty)$ is linear, $\hat{f}_{31}''(0) = \lambda_{31}\hat{f}_{31}'(\infty) + \mu_{31}$ and the program was run twice to fix

λ_{31} and μ_{31} ; then $\hat{f}'_{31}(\infty)$ was set to 1 to give the true value of $\hat{f}''_{31}(0)$. A graph of \hat{f}'_{31} , which is independent of σ , is given in figure 6.3.

A similar method was used to find the value of $\hat{\tau}_{31}(0)$ for which $\hat{\tau}_{31} \rightarrow 0$ as $\eta_3 \rightarrow \infty$ as required. Figure 6.4 shows a graph of $\hat{\tau}_{31}$ against η_3 for various σ . Solutions for \hat{f}_{32} and $\hat{\tau}_{32}$ were found in the same way as those for \hat{f}_{31} and $\hat{\tau}_{31}$. The graph of \hat{f}_{32} is shown in figure 6.5 and graphs of $\hat{\tau}_{32}$ for various σ in figure 6.6.

For \hat{f}_{33i} ($i = 1, 2$) a similar method was adopted but it was necessary to find values of both $\hat{f}''_{33i}(0)$ and $\hat{f}'''_{33i}(0)$ for which $\hat{f}_{33i} \rightarrow 0$ as $\eta_3 \rightarrow \infty$, the two initial conditions being needed in order to eliminate η_3^2 and η_3 behaviours in \hat{f}_{33i} as $\eta_3 \rightarrow \infty$. The solution \hat{f}_{330} is dependent on σ due to the introduction of the buoyancy term in (6.3.43) and graphs of \hat{f}'_{330} for various σ are shown in figure 6.7. The solution for \hat{f}'_{331} is independent of σ (figure 6.8).

The problems for $\hat{\tau}_{330}$ and $\hat{\tau}_{331}$ were solved in the same way as those for $\hat{\tau}_{31}$ and $\hat{\tau}_{32}$. Graphs of $\hat{\tau}_{330}$ and $\hat{\tau}_{331}$ for various σ are shown in figures 6.9 and 6.10. The various constants \hat{a}_{31} , \hat{a}_{32} , \hat{a}_{330} , \hat{a}_{331} arising in the solutions are displayed in table 6.2.

(iv) Pressure

It is of interest to consider the pressure field associated with the above solutions. This is of the form

$$p = R_1^{\frac{21}{10}} \left\{ \sigma c_0^{7/8} P^{\frac{1}{2}} Q^{-\frac{1}{2}} z_3 \right\} + R_1^2 \left\{ \sigma^2 c_0^{5/6} Q^{2/3} \right\} p_3(x_3, z_3) + \dots \quad (6.3.49)$$

to within a constant where, from equations (3.2.16), (3.2.17) and (6.2.1) p_3 satisfies

$$\frac{\partial \psi_3}{\partial z_3} \frac{\partial^2 \psi_3}{\partial x_3 \partial z_3} - \frac{\partial \psi_3}{\partial x_3} \frac{\partial^2 \psi_3}{\partial z_3^2} = -\frac{\partial p_3}{\partial x_3} + \frac{\partial^3 \psi_3}{\partial z_3^3} \quad (6.3.50)$$

and

$$\frac{\partial p_3}{\partial z_3} = \frac{T_3}{\sigma} \quad (6.3.51)$$

From (6.3.51) and the fact that p_3 may be assumed to be zero at the edge of the layer we see that

$$p_3 = -\frac{1}{\sigma} \int_{z_3}^{\infty} T_3 dz_3 \quad (6.3.52)$$

We may expand p_3 for small x_3 as

$$p_3 = x_3^{1/2} p_{30}(\eta_3) + \dots \quad (6.3.53)$$

where from (6.3.52) and (6.3.2)

$$p_{30} = -\frac{1}{\sigma} \int_{\eta_3}^{\infty} T_{30} d\eta_3 \quad (6.3.54)$$

The horizontal pressure gradient

$$\frac{\partial p_3}{\partial x_3} \sim -\frac{x_3^{-1/2}}{\sigma} \left\{ \frac{1}{2} \int_{\eta_3}^{\infty} T_{30} d\eta_3 + \frac{3}{4} \eta_3 T_{30} \right\}, \quad x_3 \rightarrow 0 \quad (6.3.55)$$

and since $\tau_{30} < 0$ for all η_3 this is adverse throughout the layer. In particular the pressure gradient at the wall is given by

$$\frac{\partial p_3}{\partial x_3} \sim -\frac{x_3^{-1/2}}{2\sigma} \int_0^{\infty} T_{30} d\eta_3, \quad x_3 \rightarrow 0. \quad (6.3.56)$$

(v) Summary

In this section we have found that the initial development of the buoyancy layer takes the form

$$\Psi_3 = x_3^{1/4} \hat{f}_{30}(\eta_3) + x_3^{3/4} \epsilon \hat{f}_{31}(\eta_3) + x_3^{5/4} \epsilon^2 \hat{f}_{32}(\eta_3) + x_3^{7/4} [\hat{f}_{330}(\eta_3) + \epsilon^3 \hat{f}_{331}(\eta_3)] + \dots \text{ as } x_3 \rightarrow 0 \quad (6.3.57)$$

and

$$\tau_3 = x_3^{-1/4} \hat{\tau}_{30}(\eta_3) + x_3^{1/4} \epsilon \hat{\tau}_{31}(\eta_3) + x_3^{3/4} \epsilon^2 \hat{\tau}_{32}(\eta_3) + x_3^{5/4} [\hat{\tau}_{330}(\eta_3) + \epsilon^3 \hat{\tau}_{331}(\eta_3)] + \dots \text{ as } x_3 \rightarrow 0. \quad (6.3.58)$$

As shown in section (vi), the effect of buoyancy is to produce an adverse pressure gradient across the layer. The inertial and viscous terms are $O(x_3^{-2})$ so that any effects of this adverse gradient such as flow reversal within the boundary layer are not expected to materialise until the flow has progressed some distance downstream. In addition, the effect of a non-zero external flow ϵ will be to delay or prohibit flow reversal within the layer.

If we take the case of no external flow $\epsilon = 0$, equation (6.3.57) reduces to

$$\Psi_3 = x_3^{1/4} \hat{f}_{30}(\eta_3) + x_3^{7/4} \hat{f}_{330}(\eta_3) + \dots \text{ as } x_3 \rightarrow 0 \quad (6.3.59)$$

and we can estimate the way in which the velocity field

$$\frac{d\Psi_3}{dx_3} = x_3^{-1/2} \left(\hat{f}_{30}' + x_3^{3/2} \hat{f}_{331}' + \dots \right) \quad (6.3.60)$$

may develop downstream.

As can be seen from figure 6.7, \hat{f}'_{330} is negative both close to the wall and at the outer edge, with a positive part in the centre of the boundary layer. A graph of $f'_{30} + x_3^{3/2} \hat{f}'_{330}$, for $\sigma = 0.72$ and for increasing values of x_3 is plotted against z_3 in figure 6.11. It shows that reverse flow is possible, first appearing in the outer parts of the boundary layer with large negative values appearing later at the wall.

6.4 Solution for large x_3

The presence of the buoyancy term together with the integral constraint (6.2.13) suggests scalings $z_3 \sim x_3^{1/2}$, $\psi_3 \sim x_3^{1/2}$, $T_3 \sim x_3^{-1/2}$ as $x_3 \rightarrow \infty$ and we solve using a similarity variable

$$\eta_3 = z_3 / x_3^{1/2} \quad (6.4.1)$$

with

$$\psi_3 \sim x_3^{1/2} \phi_3(\eta_3), \quad T_3 \sim x_3^{-1/2} \theta_3(\eta_3) \quad \text{as } x_3 \rightarrow \infty. \quad (6.4.2)$$

Substitution of (6.4.2) and (6.4.1) into (6.2.7) and (6.2.8) gives

$$\phi_3^{IV} = \frac{-1}{2\sigma} (\theta_3 + \eta_3 \theta_3') - \frac{1}{2} (\phi_3 \phi_3''' + \phi_3' \phi_3'') \quad (6.4.3)$$

and

$$\theta_3'' + \frac{1}{2}\sigma (\theta_3 \phi_3' + \theta_3' \phi_3) = 0 \quad (6.4.4)$$

respectively. Appropriate boundary conditions from (6.2.9), (6.2.10) are

$$\phi_3 = \phi_3' = \theta_3 = 0, \quad \eta_3 = 0; \quad \phi_3' \rightarrow \epsilon, \quad \theta_3 \rightarrow 0, \quad \eta_3 \rightarrow \infty \quad (6.4.5)$$

Equation (6.4.3) may be integrated to give

$$\phi_3''' = \frac{1}{2\sigma} \int_3 \theta_3 - \frac{1}{2} \phi_3 \phi_3'' \quad (6.4.6)$$

and equation (6.4.4) can be integrated twice to give

$$\theta_3 = -\mu_3 \exp\left(-\frac{1}{2}\sigma \int_0^{\int_3} \phi_3 d\phi_3\right) \quad (6.4.7)$$

where μ_3 is assumed positive and can be scaled out of the equation for ϕ_3 using the transformation

$$\phi_3 = \mu_3^{1/5} \hat{\phi}_3(\hat{\int}_3), \quad \int_3 = \mu_3^{-1/5} \hat{\int}_3. \quad (6.4.8)$$

This gives

$$\hat{\phi}_3''' + \frac{1}{2} \hat{\phi}_3 \hat{\phi}_3'' = \frac{1}{2\sigma} \hat{\int}_3 \exp\left(-\frac{1}{2}\sigma \int_0^{\hat{\int}_3} \hat{\phi}_3 d\hat{\int}_3\right) \quad (6.4.9)$$

with

$$\hat{\phi}_3 = \hat{\phi}_3' = 0, \quad \hat{\int}_3 = 0; \quad \hat{\phi}_3' \rightarrow \hat{\epsilon}, \quad \hat{\int}_3 \rightarrow \infty \quad (6.4.10)$$

where

$$\hat{\epsilon} = \mu_3^{-2/5} \epsilon. \quad (6.4.11)$$

The integral constraint (6.2.13) requires that

$$\int_0^\infty \phi_3 \theta_3' d\int_3 = 1 \quad (6.4.12)$$

and gives

$$\mu_3^{6/5} I = 1 \quad (6.4.13)$$

where

$$I = \frac{1}{2}\sigma \int_0^\infty \hat{\phi}_3^2 \exp\left(-\frac{1}{2}\sigma \int_0^{\hat{\int}_3} \hat{\phi}_3 d\hat{\int}_3\right) d\hat{\int}_3. \quad (6.4.14)$$

Solutions of (6.4.9) were computed by specifying $\alpha_3 = \hat{\phi}_3''(0)$ and integrating outwards by a fourth-order Runge-Kutta scheme to

obtain $\hat{\epsilon} = \hat{\phi}'_3(\infty)$. Then ϵ may be calculated retroactively from (6.4.11) and (6.4.13) as

$$\epsilon = \left(\frac{1}{\mathbf{I}}\right)^{1/3} \hat{\epsilon}. \quad (6.4.15)$$

Computations of ϵ as a function of α_3 for $\sigma = 0.1, 0.72, 8.1$ and 17.2 are shown in figure 6.12. This shows that the external flow speed ϵ is restricted to the range $\epsilon > \epsilon_c(\sigma)$, and that for a given ϵ in this range there are dual solutions for ϕ_3 . Some of these contain reverse flow near the wall. Profiles of θ_3 and ϕ'_3 for $\alpha_3 = -0.5, 4.5, 0.4, 0.7, 1.1$ and for $\sigma = 0.72$ are shown in figures 6.13 and 6.14. Table 6.3 gives values of μ_3 for various values of α_3 . The pressure is as found from (6.3.52) using (6.4.1) and (6.4.2)

$$p_3 \sim -\frac{1}{\sigma} \int_{f_3}^{\infty} \theta_3 d\mathcal{S}_3, \quad x_3 \rightarrow \infty \quad (6.4.16)$$

and the horizontal pressure gradient is

$$\frac{dp_3}{dx_3} \sim -\frac{1}{2\sigma} \int_3 \theta_3, \quad x_3 \rightarrow \infty. \quad (6.4.17)$$

Since $\theta_3 < 0$ this is adverse throughout the layer although it vanishes both on the wall and at the outer edge of the layer.

6.5 Summary

In this chapter we have discussed a new regime where $x = 0(R_1^{2/5})$. Here, buoyancy becomes important and couples the momentum and heat equations. In addition we see the development of the jet in the $x = 0(1)$ region into a boundary layer with a forcing velocity at the outer edge of the layer. The problem now

depends on two parameters, the Prandtl number σ and the effective forcing velocity ϵ .

It has been seen that buoyancy produces an adverse pressure gradient whose effect may eventually become apparent downstream as the inertial and viscous terms weaken. The possibility of the emergence of reverse flow has been discussed and consequently we may expect that a full numerical solution based on marching in the x_3 direction and to be discussed in Chapter 7, may break down for some ϵ and σ . This idea is further confirmed by the large x_3 study which suggests that for sufficiently low ϵ there is no simple asymptotic form as $x_3 \rightarrow \infty$.

TABLE 6.1

Values of θ_{30} for various σ

σ	θ_{30}
0.1	-0.42714
0.72	-0.59430
8.1	-1.89486
17.2	-3.03025

TABLE 6.2

Values of	\hat{a}_{31}	\hat{a}_{32}	\hat{a}_{330}	\hat{a}_{331}
	\hat{a}_{31}		-6.91982	
	\hat{a}_{32}		14.93763	
	\hat{a}_{330}		-23.4	($\sigma = 0.72$)
			-0.01	($\sigma = 8.1$)
	\hat{a}_{331}		-138.6	

TABLE 6.3

Values of μ_3 for various α_3 ($\sigma=0.72$)

α_3	μ_3
0.0	0.3817
0.5	0.4092
1.0	0.3910
1.5	0.3688
2.0	0.3493
2.5	0.3330
3.0	0.3193

Figure 6.1 Graph of f'_{30} against η_3 .

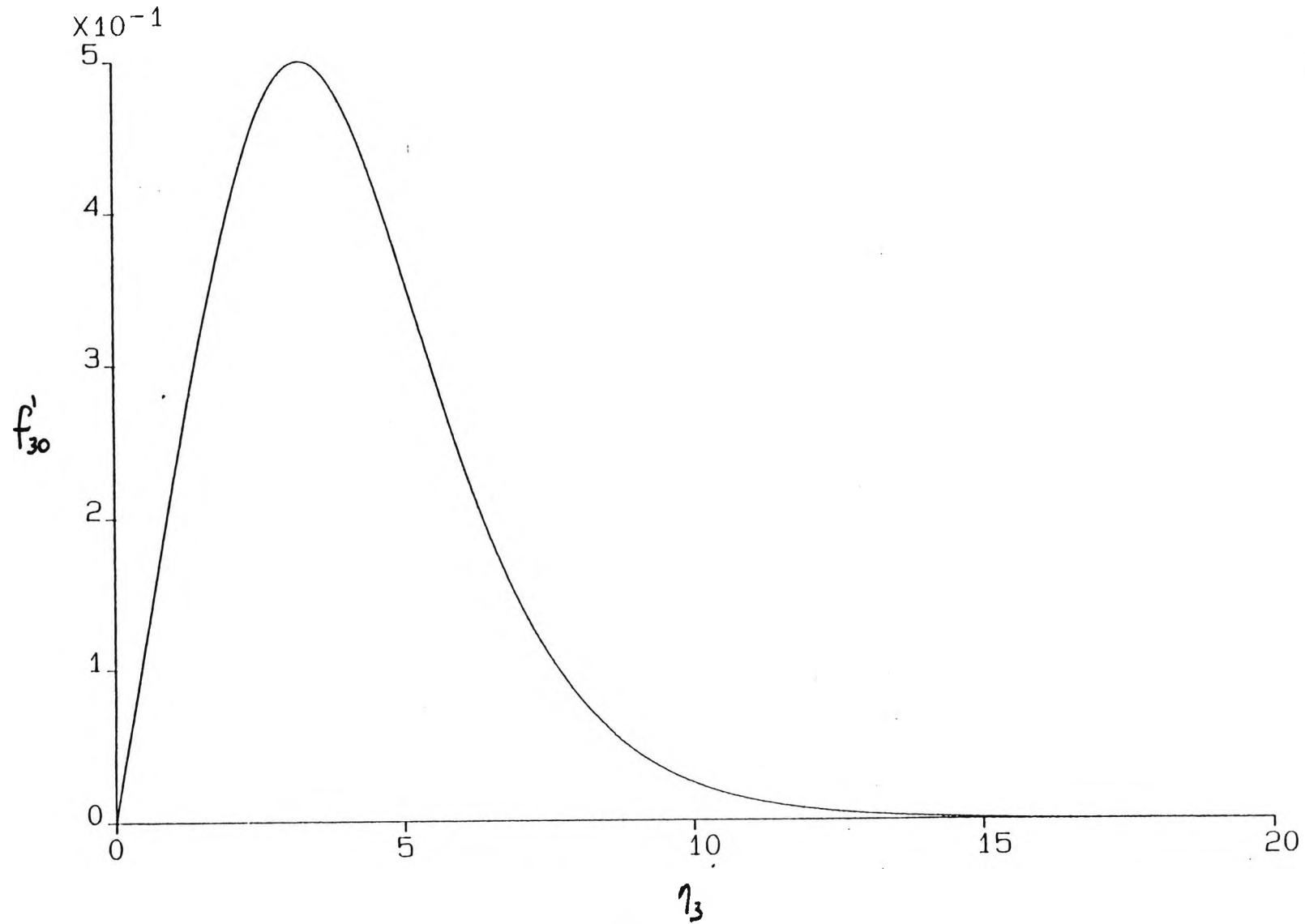


Figure 6.2 Graph of τ_{30} against η_3 for Prandtl numbers
a) 0.1, b) 0.72, c) 8.1 and d) 17.2.

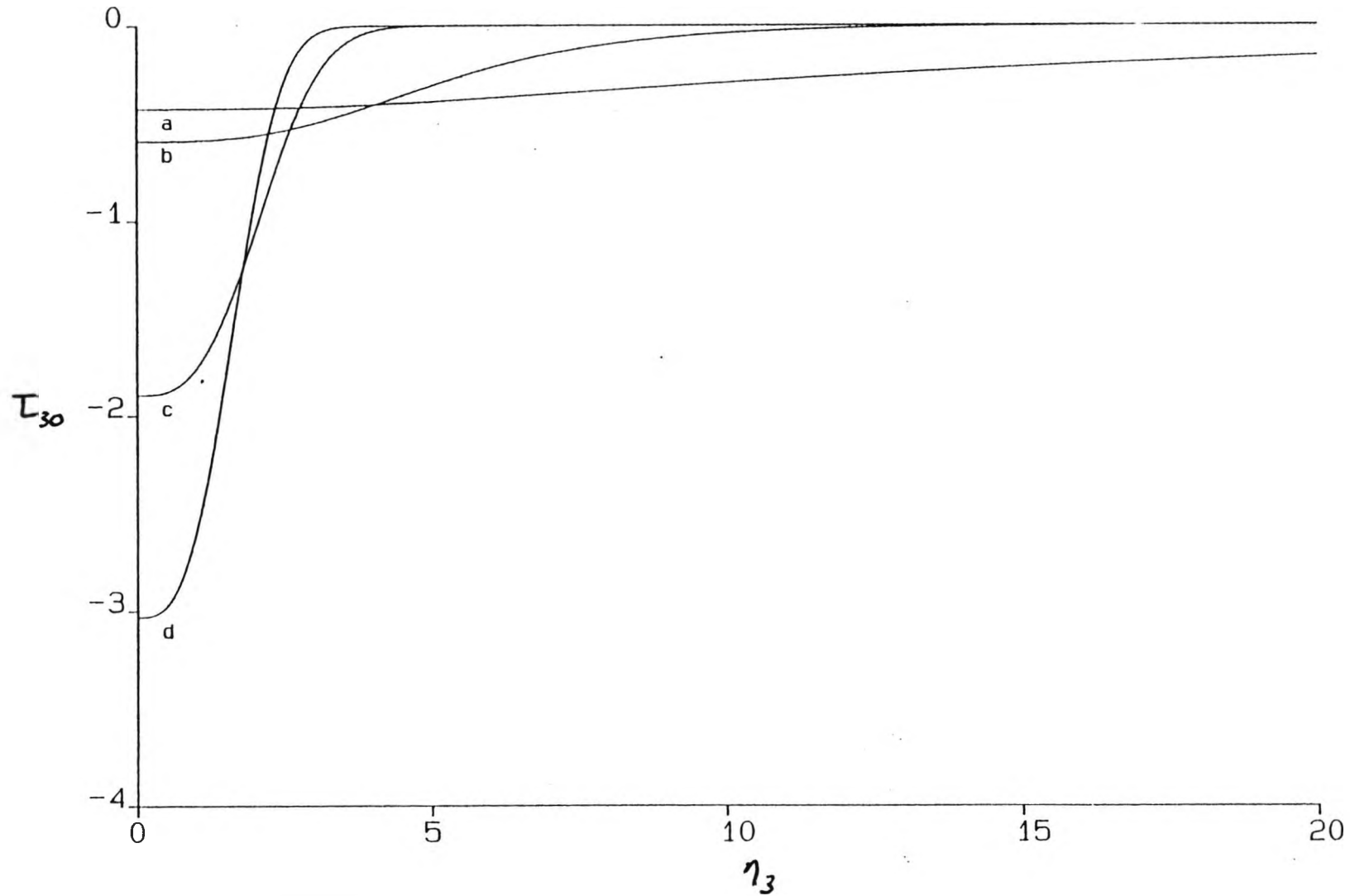


Figure 6.3 Graph of \hat{f}'_{31} against η_3 .

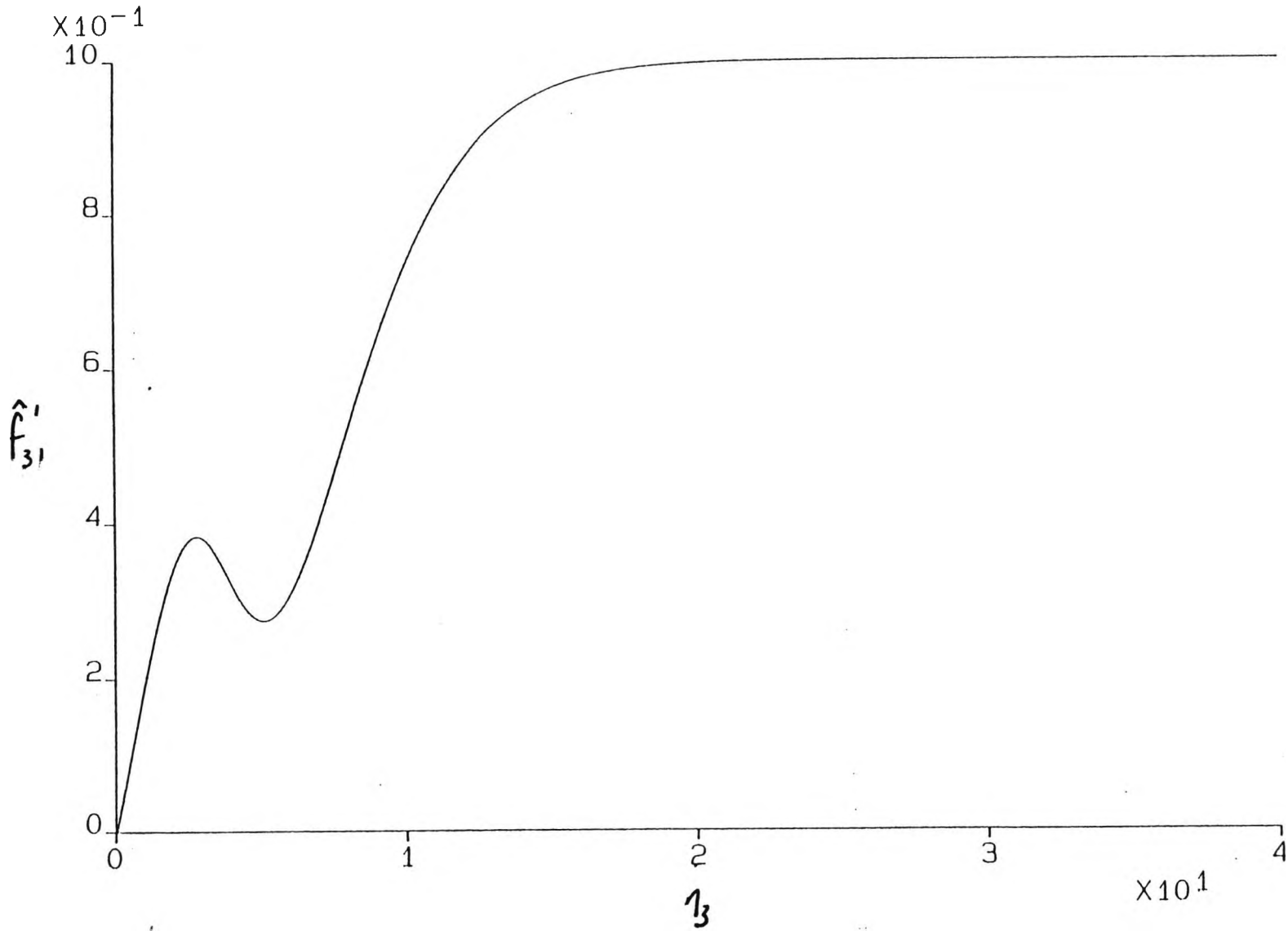


Figure 6.4 Graph of $\hat{\tau}_{31}$ against η_3 for Prandtl numbers
a) 0.1, b) 0.72, c) 8.1 and d) 17.2.

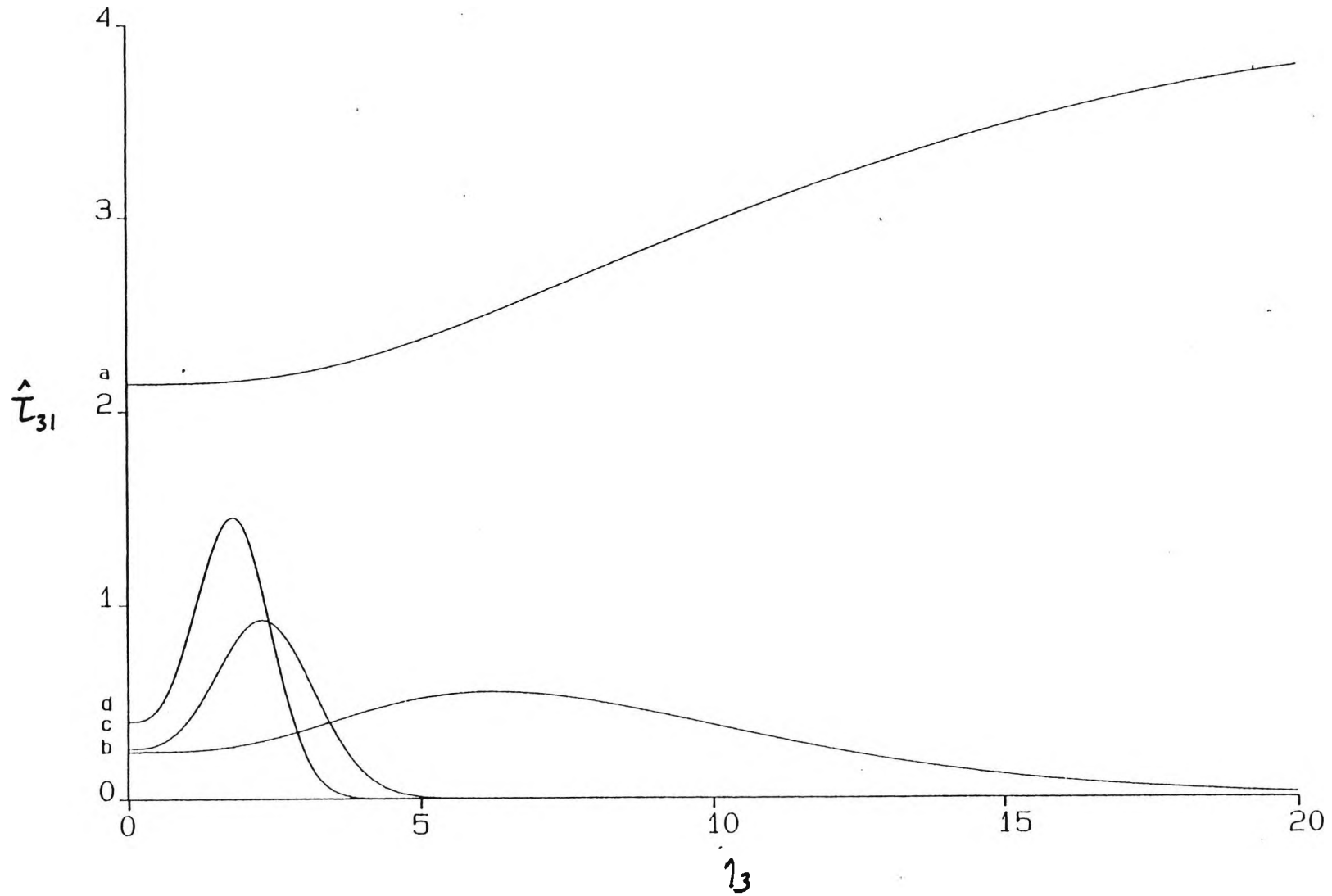


Figure 6.5 Graph of \hat{f}'_{32} against η_3 .

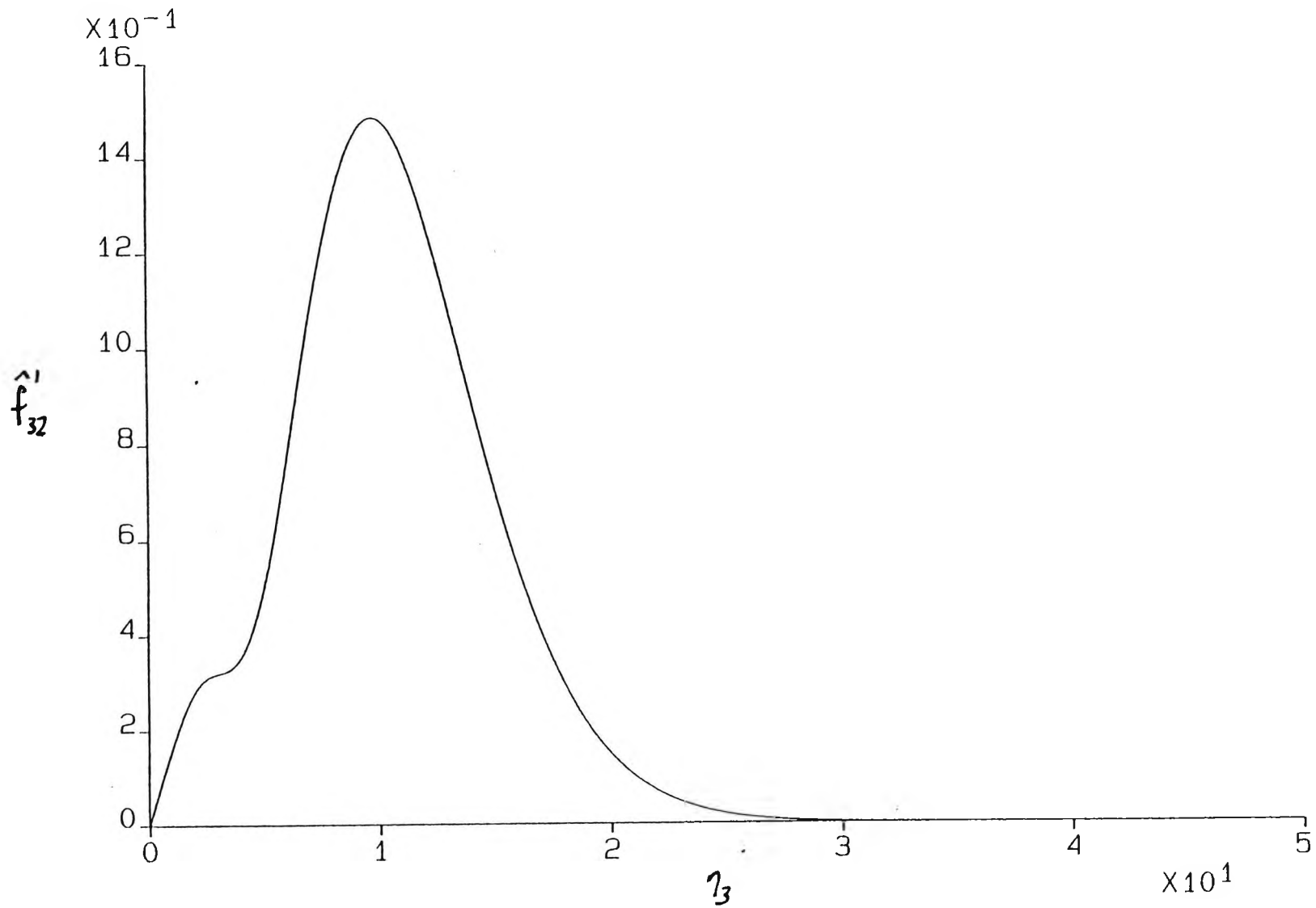


Figure 6.6 Graph of $\hat{\tau}_{32}$ against η_3 for Prandtl numbers
b) 0.72, c) 8.1, d) 17.2.

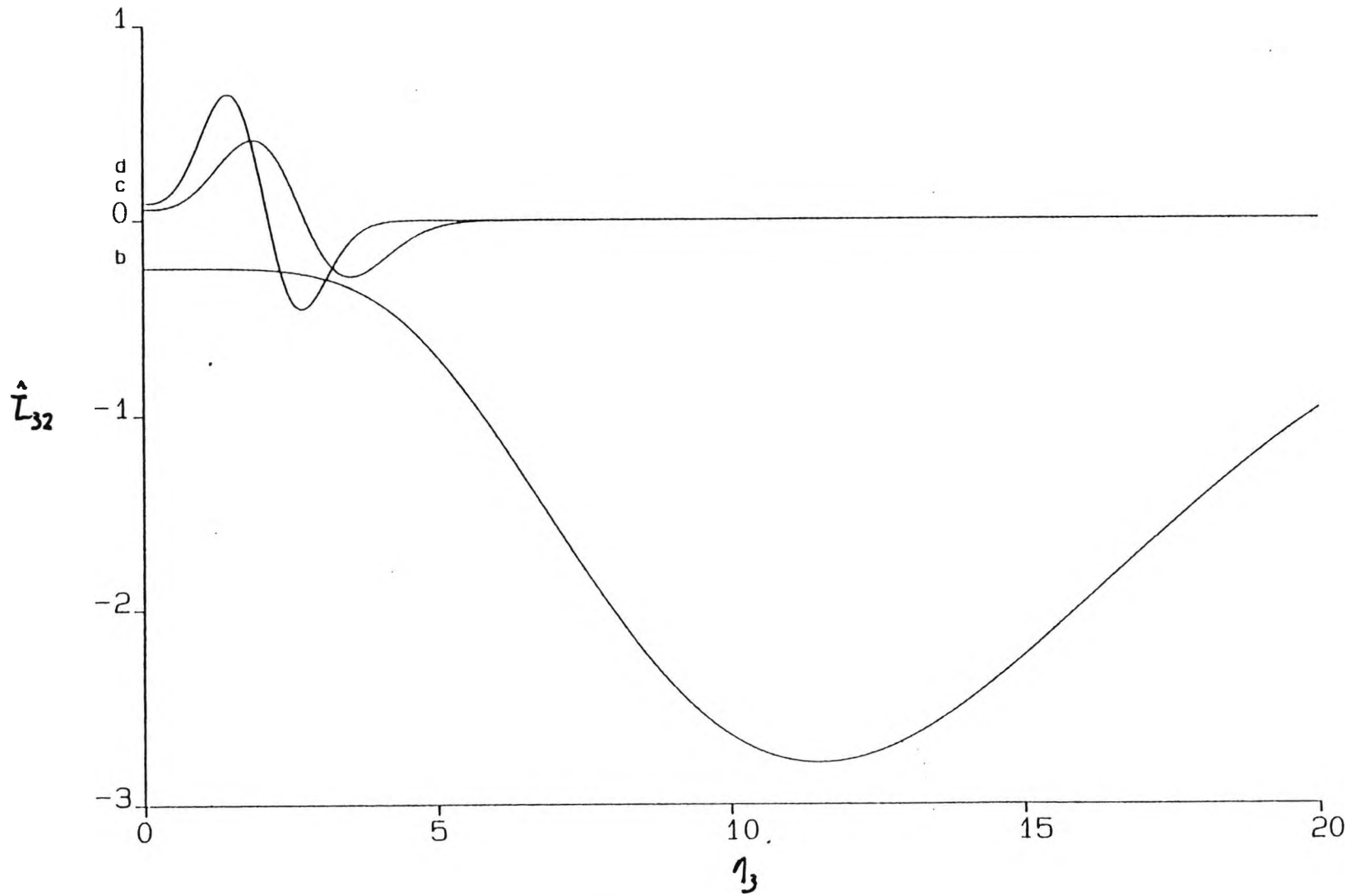


Figure 6.7 Graph of \hat{f}'_{330} against η_3 for Prandtl numbers
a) 0.72 and b) 8.1.

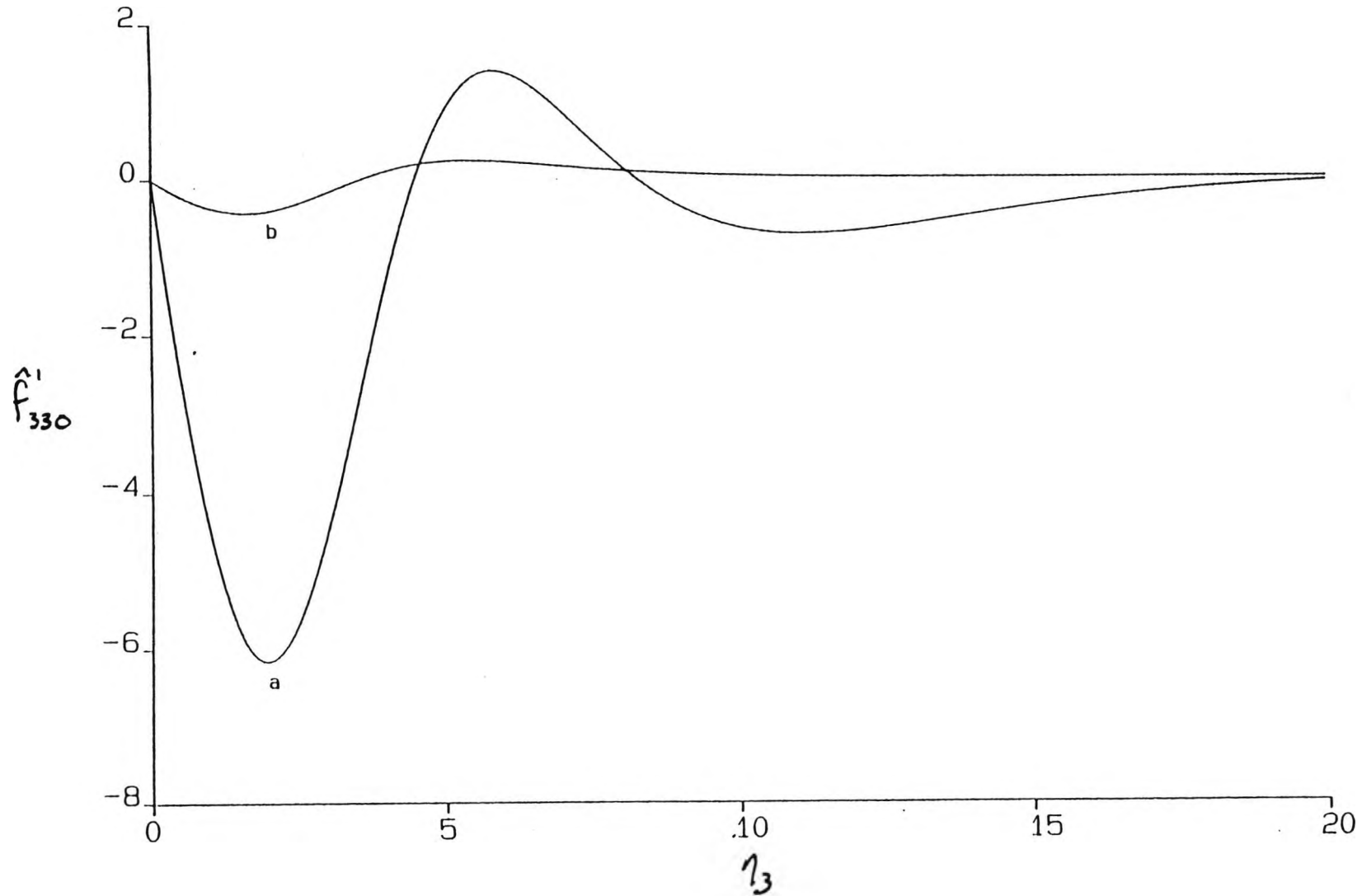


Figure 6.8 Graph of \hat{f}'_{331} against η_3 .

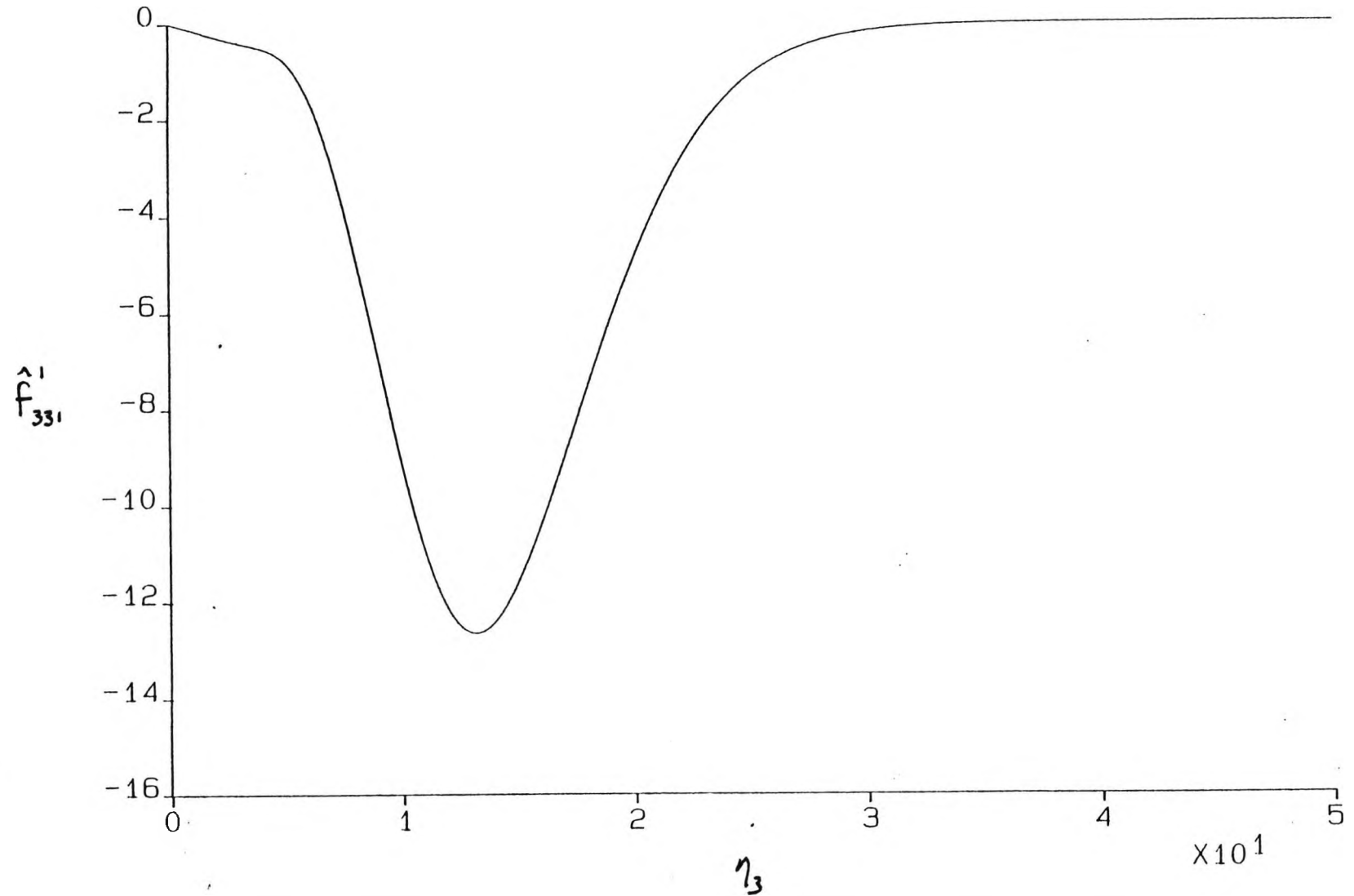
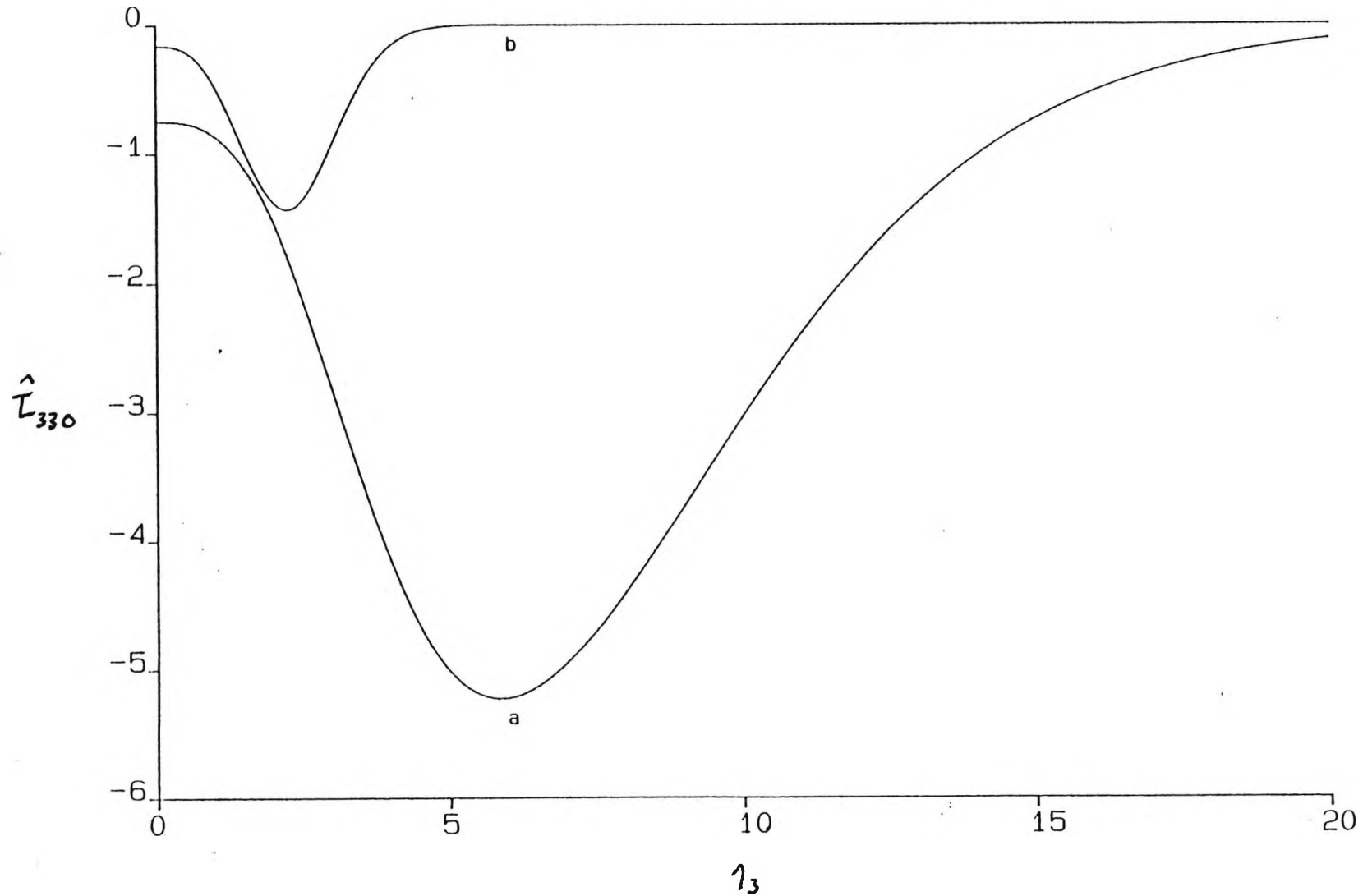


Figure 6.9 Graph of $\hat{\tau}_{330}$ against η_3 for Prandtl numbers
a) 0.1 and b) 0.72.



150

Figure 6.10 Graph of $\hat{\tau}_{331}$ against η_3 for Prandtl numbers
b) 0.72, c) 8.1 and d) 17.2.

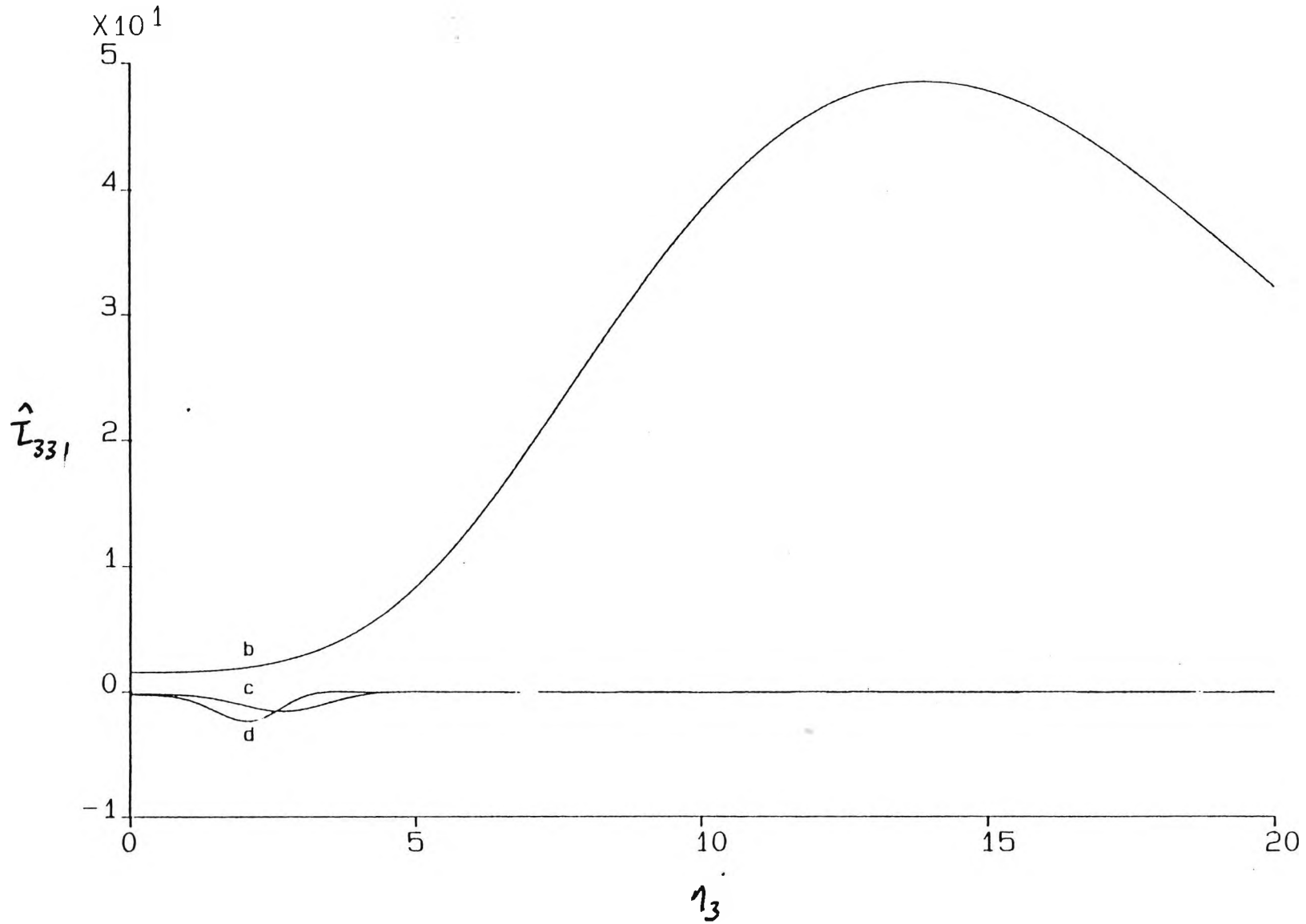


Figure 6.11 Graph of $f'_{30} + x_3^{3/2} f'_{330}$ against z_3 for increasing x_3 at $\sigma = 0.72$.

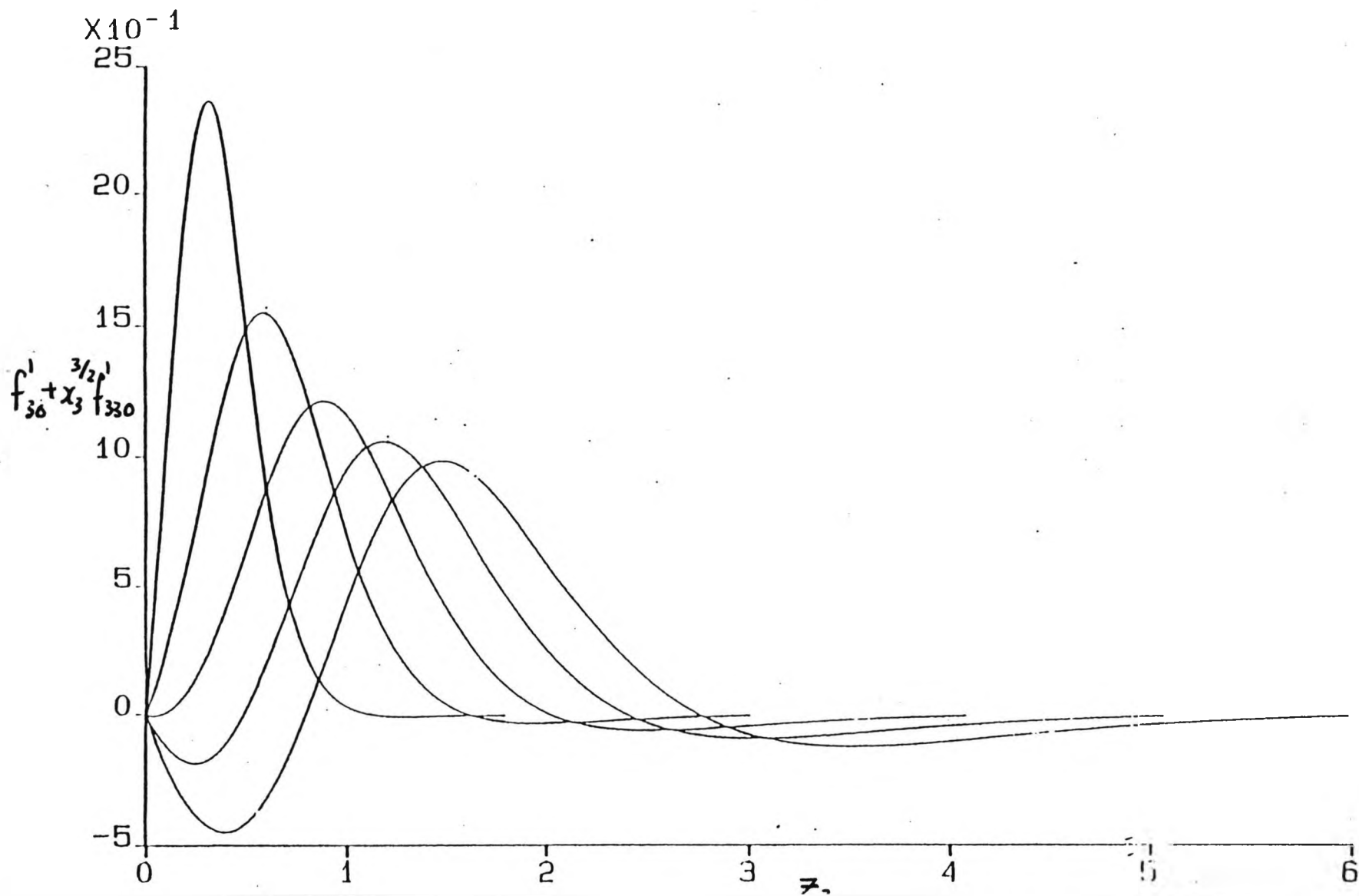


Figure 6.12 Graph of ϵ against α for various σ .

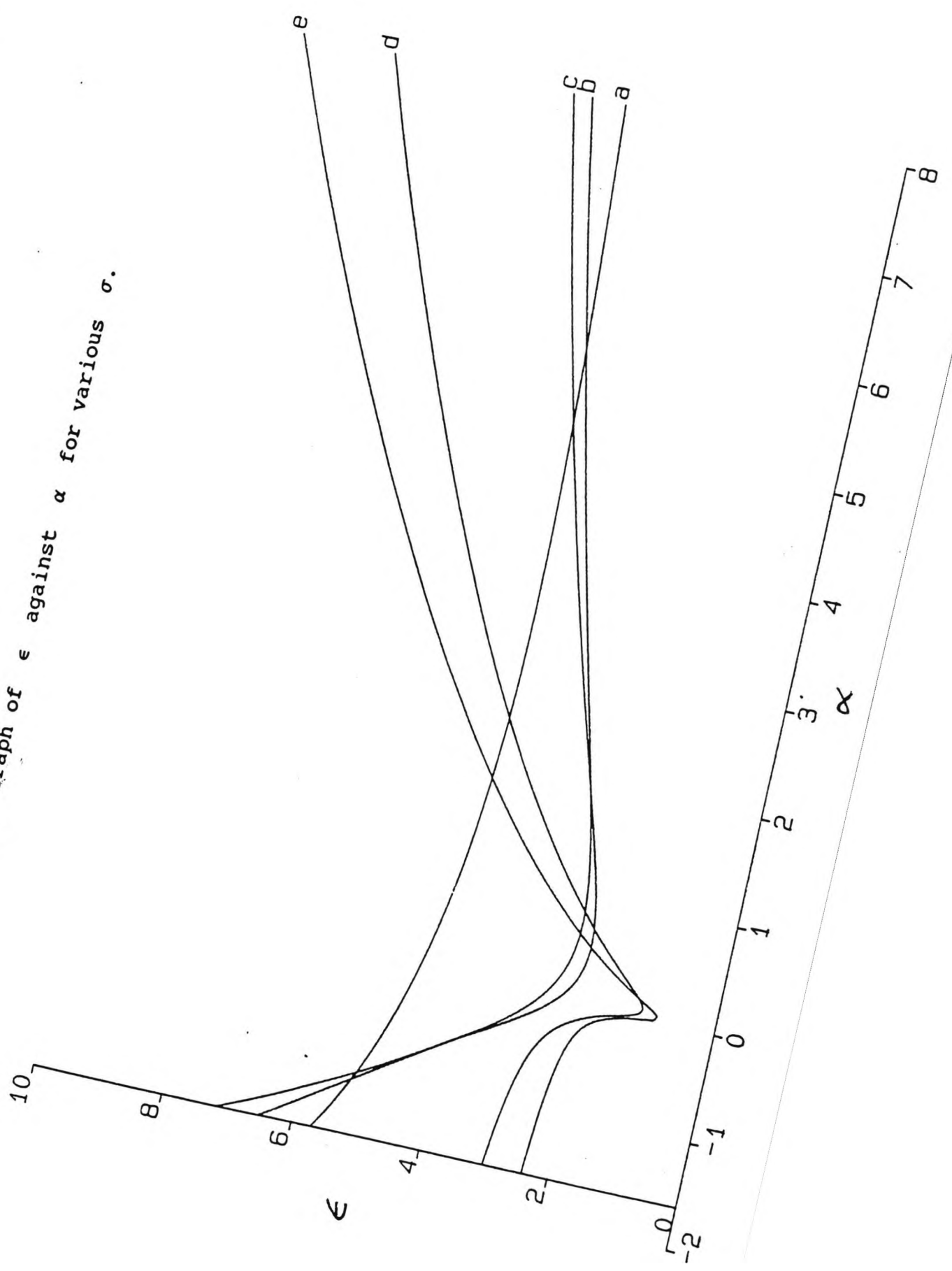


Figure 6.13 ϕ_2 Profiles for $\alpha_3 = -0.5, 4.5, 0.4, 0.7, 1.1$ at $\sigma = 0.72$.

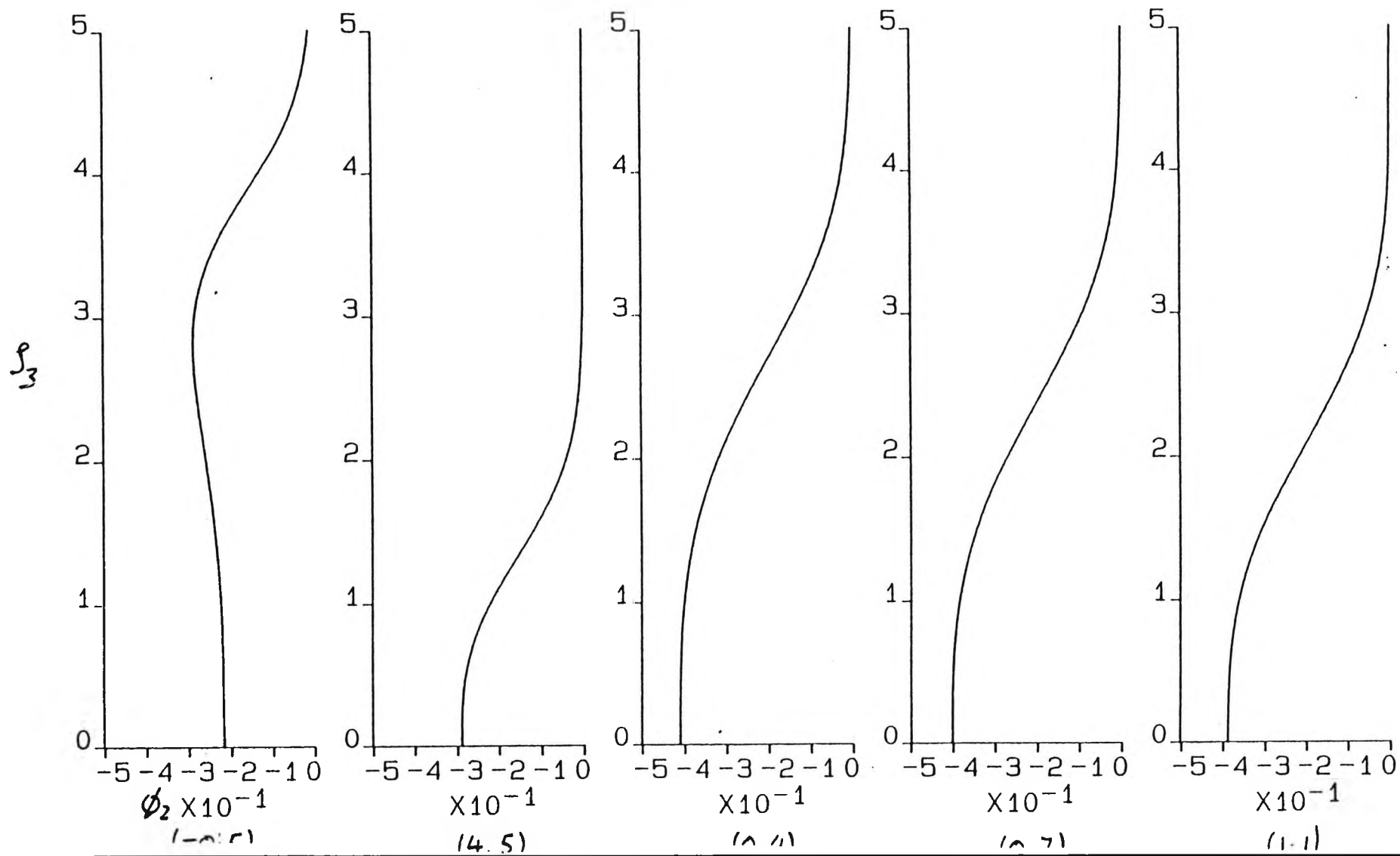
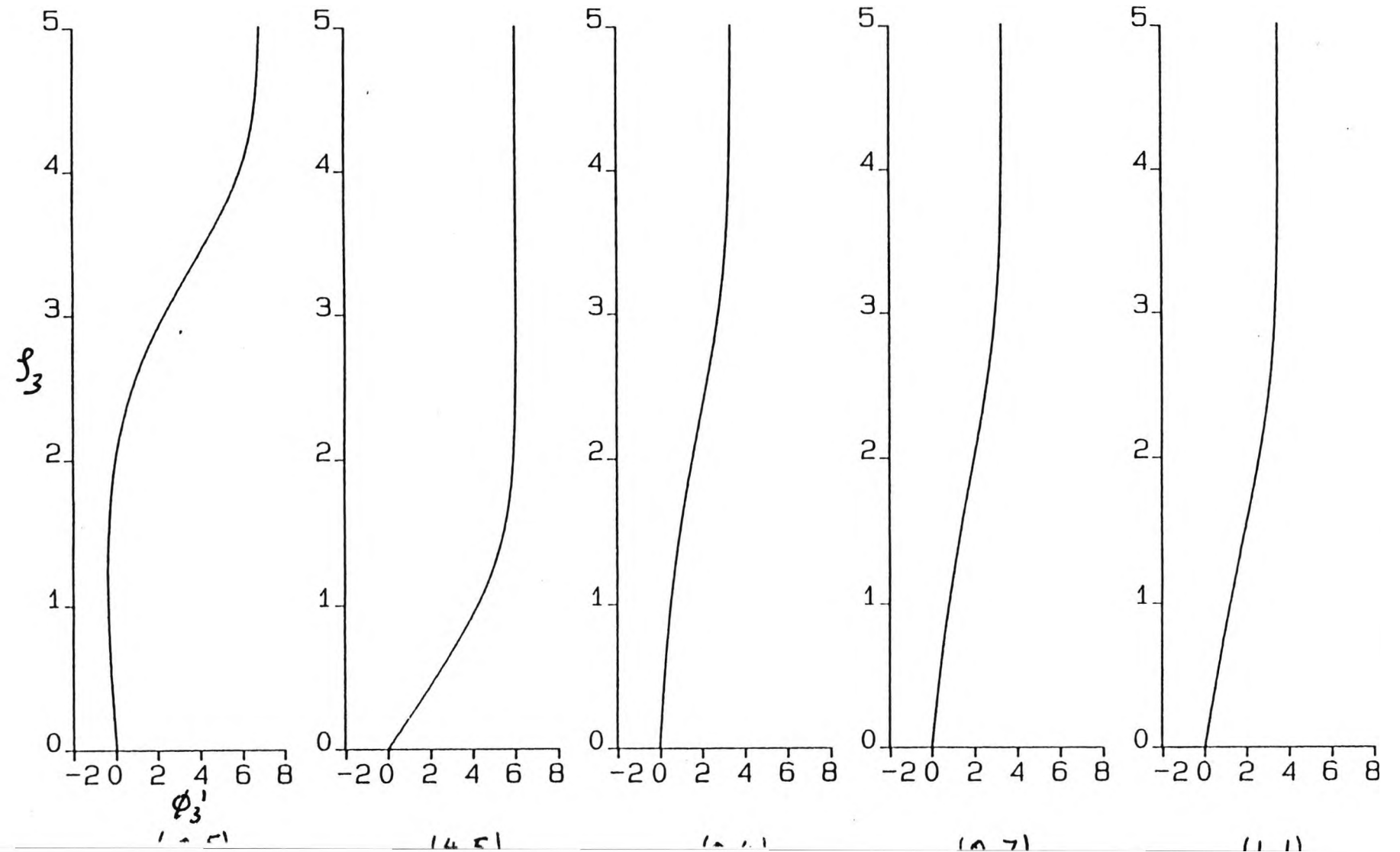


Figure 6.14 ϕ_3' Profiles for $\alpha_3 = -0.5, 4.5, 0.4, 0.7, 1.1$ at $\sigma = 0.72$.



CHAPTER 7

The horizontal buoyancy layer $x = 0(R_1^{2/5})$:

numerical solution

7.1 Introduction

This chapter contains a numerical study of the horizontal boundary layer where $x = 0(R_1^{2/5})$. In this region T_3 and ψ_3 are coupled in contrast to the the situation where $x = 0(1)$ where the stream function could be solved independently of the temperature. The numerical scheme is constructed to take account of the different asymptotic structures for small and large values of x_3 discussed in Chapter 6. The scheme for $x_3 < 1$ is described in Section 7.2 and that for $x_3 > 1$ in Section 7.3. The numerical results are presented in Section 7.4. Section 7.5 considers the implication of the results for the overall structure in the cavity.

7.2 Solution for $0 < x_3 < 1$

In order to accommodate the initial forms of the stream function and temperature $\psi_3 \sim x_3^{1/4} f_{30}$, $T_3 \sim x_3^{-1/4} \tau_{30}$ we use the variables

$$\xi_3 = x_3^{1/4}, \quad \eta_3 = z_3 / \xi_3^3 \quad (7.2.1)$$

in the numerical scheme and take

$$\psi_3 = \xi_3 \hat{\psi}_3(\xi_3, \eta_3), \quad T_3 = \xi_3^{-1} \hat{T}_3(\xi_3, \eta_3), \quad p_3 = \xi_3^2 \hat{p}_3(\xi_3, \eta_3). \quad (7.2.2)$$

Substitution into the momentum and heat equations gives

$$\frac{d^3 \hat{\psi}_3}{d\eta_3^3} = -\frac{1}{\sigma} \left[\xi_3^6 \left(\frac{1}{2} \hat{p}_3 + \frac{1}{4} \xi_3 \frac{d\hat{p}_3}{d\xi_3} - \frac{3}{4} \eta_3 \frac{d\hat{p}_3}{d\eta_3} \right) \right. \\ \left. - \frac{1}{2} \left(\frac{d\hat{\psi}_3}{d\eta_3} \right)^2 - \frac{1}{4} \hat{\psi}_3 \frac{d^2 \hat{\psi}_3}{d\eta_3^2} + \xi_3 \left[\frac{d\hat{\psi}_3}{d\eta_3} \frac{d^2 \hat{\psi}_3}{d\eta_3 d\xi_3} - \frac{d\hat{\psi}_3}{d\eta_3} \frac{d^2 \hat{\psi}_3}{d\eta_3^2} \right] \right] \quad (7.2.3)$$

and

$$\frac{1}{\sigma} \frac{d^2 \hat{T}_3}{d\eta_3^2} = -\frac{1}{4} \hat{T}_3 \frac{d\hat{\psi}_3}{d\eta_3} - \frac{1}{4} \hat{\psi}_3 \frac{d\hat{T}_3}{d\eta_3} + \frac{1}{4} \xi_3 \left[\frac{d\hat{\psi}_3}{d\eta_3} \frac{d\hat{T}_3}{d\xi_3} - \frac{d\hat{T}_3}{d\eta_3} \frac{d\hat{\psi}_3}{d\xi_3} \right] \quad (7.2.4)$$

with

$$\hat{p}_3 = -\frac{1}{\sigma} \int_{\eta_3}^{\infty} \hat{T}_3 d\eta_3. \quad (7.2.5)$$

We obtain a system of first order differential equations for discretization by setting

$$A = \hat{\psi}_3, \quad B = \frac{dA}{d\eta_3}, \quad C = \frac{dB}{d\eta_3}, \quad D = -\int_{\eta_3}^{\infty} \hat{T}_3 d\eta_3, \quad E = \frac{dD}{d\eta_3}, \quad F = \frac{dE}{d\eta_3} \quad (7.2.6)$$

which when substituted into (7.2.3) and (7.2.4) give

$$\frac{dC}{d\eta_3} = -\frac{1}{\sigma} \left[-\frac{1}{2} \xi_3^6 D - \frac{1}{4} \xi_3^7 \frac{dD}{d\xi_3} + \frac{3}{4} \eta_3 \xi_3^6 E \right] \\ - \frac{1}{2} B^2 - \frac{1}{4} AC + \frac{1}{4} \xi_3 \left[B \frac{dE}{d\xi_3} - \frac{dA}{d\xi_3} C \right] \quad (7.2.7)$$

and

$$\frac{dF}{d\eta_3} = \sigma \left[-\frac{1}{4} EB - \frac{1}{4} AF + \frac{1}{4} \xi_3 \left(B \frac{dE}{d\xi_3} - F \frac{dA}{d\xi_3} \right) \right] \quad (7.2.8)$$

respectively.

The four first order differential equations in (7.2.6) are approximated by

$$B_{j+\frac{1}{2}}^{\wedge} = \frac{A_j^{\wedge} - A_{j-1}^{\wedge}}{h_j}, \quad C_{j-\frac{1}{2}}^{\wedge} = \frac{B_j^{\wedge} - B_{j-1}^{\wedge}}{h_j}, \quad E_{j-\frac{1}{2}}^{\wedge} = \frac{D_j^{\wedge} - D_{j-1}^{\wedge}}{h_j}, \\ F_{j-\frac{1}{2}}^{\wedge} = \frac{E_j^{\wedge} - E_{j-1}^{\wedge}}{h_j} \quad (7.2.9)$$

Equations (7.2.7) and (7.2.8) may be written as

$$\begin{aligned} \frac{G_j^{\alpha-\frac{1}{2}} - G_{j-1}^{\alpha-\frac{1}{2}}}{h_j} &= \frac{1}{\sigma} \left[-\frac{1}{2} \xi_3^{\alpha-\frac{1}{2}} D_{j-\frac{1}{2}}^{\alpha-\frac{1}{2}} - \frac{1}{4} \xi_3^{\alpha-\frac{1}{2}} \frac{1}{\Delta_n} (D_{j-\frac{1}{2}}^{\alpha} - D_{j-\frac{1}{2}}^{\alpha-1}) \right. \\ &\quad \left. + \frac{3}{4} \eta_{3j-\frac{1}{2}} \xi_3^{\alpha-\frac{1}{2}} E_{j-\frac{1}{2}}^{\alpha-1} \right] - \frac{1}{2} (B_{j-\frac{1}{2}}^{\alpha-\frac{1}{2}})^2 - \frac{1}{4} (AC)_{j-\frac{1}{2}}^{\alpha-\frac{1}{2}} \\ &\quad + \frac{1}{4} \frac{\xi_3^{\alpha-\frac{1}{2}}}{\Delta_n} \left[B_{j-\frac{1}{2}}^{\alpha-\frac{1}{2}} (B_{j-\frac{1}{2}}^{\alpha} - B_{j-\frac{1}{2}}^{\alpha-1}) - G_{j-\frac{1}{2}}^{\alpha-\frac{1}{2}} (A_{j-\frac{1}{2}}^{\alpha} - A_{j-\frac{1}{2}}^{\alpha-1}) \right] \end{aligned} \quad (7.2.10)$$

and

$$\begin{aligned} \frac{F_j^{\alpha-\frac{1}{2}} - F_{j-1}^{\alpha-\frac{1}{2}}}{\sigma h_j} &= -\frac{1}{4} (EB)_{j-\frac{1}{2}}^{\alpha-\frac{1}{2}} - \frac{1}{4} (AF)_{j-\frac{1}{2}}^{\alpha-\frac{1}{2}} \\ &\quad + \frac{1}{4} \frac{\xi_3^{\alpha-\frac{1}{2}}}{\Delta_n} \left[B_{j-\frac{1}{2}}^{\alpha-\frac{1}{2}} (E_{j-\frac{1}{2}}^{\alpha} - E_{j-\frac{1}{2}}^{\alpha-1}) - F_{j-\frac{1}{2}}^{\alpha-\frac{1}{2}} (A_{j-\frac{1}{2}}^{\alpha} - A_{j-\frac{1}{2}}^{\alpha-1}) \right] \end{aligned} \quad (7.2.11)$$

respectively.

In this region there is a regular network in (ξ_3, η_3)

coordinates where $\xi_{3n} = \xi_{3n-1} + \Delta_n$, $\eta_{3j} = \eta_{3j-1} + h_j$; $n \geq 1$,

$1 \leq j \leq J$. The wall is denoted by $\eta_3 = 0$; $j = 0$. The outer edge is at $\eta_3 = \eta_{3\infty} = Jh$ if $h_j = h \forall j$. $n = 0$ denotes the initial

station at $\xi_3 = 0$ and $\xi_{3n-1/2} = \xi_{3n} - \frac{1}{2} \Delta_n$, $\eta_{3j-1/2} = \eta_{3j} - \frac{1}{2} h_j$.

Equations (7.2.9) are centred on $(\xi_{3n}, \eta_{3j-1/2})$ and equations

(7.2.10) and (7.2.11) are centred on $(\xi_{3n-1/2}, \eta_{3j-1/2})$. The

centred averages are defined as

$$(B^2)_{j-\frac{1}{2}}^{\alpha-\frac{1}{2}} = \frac{1}{4} \left\{ (B_j^{\alpha})^2 + (B_{j-1}^{\alpha})^2 + (B_j^{\alpha-1})^2 + (B_{j-1}^{\alpha-1})^2 \right\} \quad (7.2.12)$$

$$(AC)_{j-\frac{1}{2}}^{\alpha-\frac{1}{2}} = \frac{1}{4} \left\{ (AC)_j^{\alpha} + (AC)_{j-1}^{\alpha} + (AC)_j^{\alpha-1} + (AC)_{j-1}^{\alpha-1} \right\} \quad (7.2.13)$$

$$(BE)_{j-\frac{1}{2}}^{\alpha-\frac{1}{2}} = \frac{1}{4} \left\{ (BE)_j^{\alpha} + (BE)_{j-1}^{\alpha} + (BE)_j^{\alpha-1} + (BE)_{j-1}^{\alpha-1} \right\} \quad (7.2.14)$$

$$(AF)_{j-\frac{1}{2}}^{\alpha-\frac{1}{2}} = \frac{1}{4} \left\{ (AF)_j^{\alpha} + (AF)_{j-1}^{\alpha} + (AF)_j^{\alpha-1} + (AF)_{j-1}^{\alpha-1} \right\} \quad (7.2.15)$$

$$G_j^{\alpha-\frac{1}{2}} = \frac{1}{2} [G_j^{\alpha} + G_j^{\alpha-1}], \quad F_j^{\alpha-\frac{1}{2}} = \frac{1}{2} [F_j^{\alpha} + F_j^{\alpha-1}]. \quad (7.2.16)$$

The wall conditions derived from (6.2.9) are

$$A_0^\wedge = 0, B_0^\wedge = 0, F_0^\wedge = 0 \quad (7.2.17)$$

and the outer edge conditions derived from (6.2.10) are

$$D_J^\wedge = 0, B_J^\wedge = \epsilon \xi_{Jn}^2, E_J^\wedge = 0. \quad (7.2.18)$$

The initial profiles using the small x_3 form discussed in

Chapter 6 are

$$\begin{aligned} A_j^\circ &= f_{30}(\eta_{3j}) \\ B_j^\circ &= f'_{30}(\eta_{3j}) \\ C_j^\circ &= f''_{30}(\eta_{3j}) \end{aligned} \quad (7.2.19)$$

$$D_j^\circ = - \int_{\eta_{1j}}^{\infty} T_{30}(\eta) d\eta$$

$$E_j^\circ = T_{30}(\eta_{3j}) \quad (7.2.20)$$

$$F_j^\circ = T'_{30}(\eta_{3j})$$

The solution is computed by stepping forward from the initial profile in the ξ_3 direction, using Newton iteration at each downstream step (see Appendix 4)

In most of the computations the meshwidths used were $h = 0.1$, $\Delta_n = 0.02$ with the outer boundary J set to 500. The tolerance for which the Newton increments were considered small enough was 0.0001. The effect of h on the solution can be seen in tables 7.1, 7.2 and 7.3 and on the integral constraint in table 7.4. Solutions were found for a range of values of ϵ and σ and are discussed in Section 7.4.

7.3 Solution for $x_3 > 1$

Following the large x_3 prediction (Chapter 6, Section 6.4) in which the stream function and temperature behave as $\psi_3 \sim x_3^{1/2} \phi_3$, $T_3 \sim x_3^{-1/2} \theta_3$ the numerical scheme for $x_3 > 1$ is based on the use of the variables

$$\hat{\xi}_3 = x_3^{1/2}, \quad \hat{\eta}_3 = z_3 / \hat{\xi}_3 \quad (7.3.1)$$

with

$$\psi_3 = \hat{\xi}_3 \hat{\phi}_3(\hat{\xi}_3, \hat{\eta}_3), \quad T_3 = \hat{\xi}_3^{-1} \hat{\theta}_3(\hat{\xi}_3, \hat{\eta}_3), \quad p_3 = \hat{\pi}_3(\hat{\xi}_3, \hat{\eta}_3). \quad (7.3.2)$$

Substitution into the momentum and heat equations gives

$$\begin{aligned} \frac{d^3 \hat{\phi}_3}{d\hat{\eta}_3^3} &= \frac{1}{2} \left(\hat{\xi}_3 \frac{d\hat{\pi}_3}{d\hat{\xi}_3} - \hat{\eta}_3 \frac{d\hat{\pi}_3}{d\hat{\eta}_3} \right) - \frac{1}{2} \hat{\phi}_3 \frac{d^2 \hat{\phi}_3}{d\hat{\eta}_3^2} \\ &+ \frac{1}{2} \hat{\xi}_3 \left[\frac{d\hat{\phi}_3}{d\hat{\eta}_3} \frac{d^2 \hat{\theta}_3}{d\hat{\eta}_3 d\hat{\xi}_3} - \frac{d^2 \hat{\phi}_3}{d\hat{\eta}_3^2} \frac{d\hat{\theta}_3}{d\hat{\xi}_3} \right] \end{aligned} \quad (7.3.3)$$

and

$$\frac{d^2 \hat{\theta}_3}{d\hat{\eta}_3^2} = \frac{1}{2} \sigma \left[- \left(\frac{d\hat{\phi}_3}{d\hat{\eta}_3} \hat{\theta}_3 + \frac{d\hat{\theta}_3}{d\hat{\eta}_3} \hat{\phi}_3 \right) + \left(\frac{d\hat{\phi}_3}{d\hat{\eta}_3} \frac{d\hat{\theta}_3}{d\hat{\xi}_3} - \frac{d\hat{\theta}_3}{d\hat{\eta}_3} \frac{d\hat{\phi}_3}{d\hat{\xi}_3} \right) \right] \quad (7.3.4)$$

with

$$\hat{\pi}_3 = -\frac{1}{\sigma} \int_{\hat{\eta}_3}^{\infty} \hat{\theta}_3 d\hat{\eta}_3 \quad (7.3.5)$$

We obtain a system of first order differential equations for discretization by setting

$$\hat{A} = \hat{\phi}_3, \quad \hat{B} = \frac{d\hat{A}}{d\hat{\eta}_3}, \quad \hat{C} = \frac{d\hat{B}}{d\hat{\eta}_3}, \quad \hat{D} = - \int_{\hat{\eta}_3}^{\infty} \hat{\theta}_3 d\hat{\eta}_3, \quad \hat{E} = \frac{d\hat{D}}{d\hat{\eta}_3}, \quad \hat{F} = \frac{d\hat{E}}{d\hat{\eta}_3} \quad (7.3.6)$$

which when substituted into (7.3.3) and (7.3.4) give

$$\frac{d\hat{C}}{d\hat{\eta}_3} = \frac{\hat{\xi}_3}{2\sigma} \frac{d\hat{D}}{d\hat{\xi}_3} - \frac{\hat{\eta}_3}{2\sigma} \hat{E} - \frac{1}{2} \hat{A} \hat{C} + \frac{1}{2} \frac{\hat{\xi}_3}{\hat{\eta}_3} \left[\hat{B} \frac{d\hat{B}}{d\hat{\xi}_3} - \hat{C} \frac{d\hat{A}}{d\hat{\xi}_3} \right] \quad (7.3.7)$$

and

$$\frac{\partial \hat{F}}{\partial \hat{\xi}_3} = \frac{1}{2} \sigma \left[-\hat{B}\hat{E} - \hat{F}\hat{A} + \hat{\xi}_3 \left(\hat{B} \frac{\partial \hat{E}}{\partial \hat{\xi}_3} - \hat{F} \frac{\partial \hat{A}}{\partial \hat{\xi}_3} \right) \right] \quad (7.3.8)$$

respectively.

The four first order differential equations in (7.3.6) are approximated by

$$\hat{B}_{j-\frac{1}{2}}^{\wedge} = \frac{\hat{A}_j^{\wedge} - \hat{A}_{j-1}^{\wedge}}{h_j}, \quad \hat{C}_{j-\frac{1}{2}}^{\wedge} = \frac{\hat{B}_j^{\wedge} - \hat{B}_{j-1}^{\wedge}}{h_j}, \quad \hat{E}_{j-\frac{1}{2}}^{\wedge} = \frac{\hat{D}_j^{\wedge} - \hat{D}_{j-1}^{\wedge}}{h_j}, \quad \hat{F}_{j-\frac{1}{2}}^{\wedge} = \frac{\hat{E}_j^{\wedge} - \hat{E}_{j-1}^{\wedge}}{h_j}. \quad (7.3.9)$$

Equations (7.3.7) and (7.3.8) may be written as

$$\begin{aligned} \frac{\hat{C}_{j-\frac{1}{2}}^{\wedge \frac{n-1}{2}} - \hat{C}_{j-1}^{\wedge \frac{n-1}{2}}}{h_j} &= -\frac{1}{\sigma} \left[-\frac{\hat{\xi}_3^{n-1/2}}{2\Delta_n} (\hat{D}_{j-\frac{1}{2}}^{\wedge} - \hat{D}_{j-\frac{1}{2}}^{\wedge n-1}) + \frac{\hat{\xi}_3^{n-1/2}}{2} \hat{E}_{j-\frac{1}{2}}^{\wedge \frac{n-1}{2}} \right] - \frac{1}{2} (\hat{A}\hat{C})_{j-\frac{1}{2}}^{\wedge \frac{n-1}{2}} \\ &+ \frac{\hat{\xi}_3^{n-1/2}}{2\Delta_n} \left[\hat{B}_{j-\frac{1}{2}}^{\wedge \frac{n-1}{2}} (\hat{B}_{j-\frac{1}{2}}^{\wedge} - \hat{B}_{j-\frac{1}{2}}^{\wedge n-1}) - \hat{C}_{j-\frac{1}{2}}^{\wedge \frac{n-1}{2}} (\hat{A}_{j-\frac{1}{2}}^{\wedge} - \hat{A}_{j-\frac{1}{2}}^{\wedge n-1}) \right] \end{aligned} \quad (7.3.10)$$

and

$$\begin{aligned} \frac{\hat{F}_{j-\frac{1}{2}}^{\wedge \frac{n-1}{2}} - \hat{F}_{j-1}^{\wedge \frac{n-1}{2}}}{\sigma h_j} &= -\frac{1}{2} (\hat{B}\hat{E})_{j-\frac{1}{2}}^{\wedge \frac{n-1}{2}} - \frac{1}{2} (\hat{A}\hat{F})_{j-\frac{1}{2}}^{\wedge \frac{n-1}{2}} \\ &+ \frac{\hat{\xi}_3^{n-1/2}}{2\Delta_n} \left[\hat{B}_{j-\frac{1}{2}}^{\wedge \frac{n-1}{2}} (\hat{E}_{j-\frac{1}{2}}^{\wedge} - \hat{E}_{j-\frac{1}{2}}^{\wedge n-1}) - \hat{F}_{j-\frac{1}{2}}^{\wedge \frac{n-1}{2}} (\hat{A}_{j-\frac{1}{2}}^{\wedge} - \hat{A}_{j-\frac{1}{2}}^{\wedge n-1}) \right] \end{aligned} \quad (7.3.11)$$

respectively.

In this region there is a regular network in $(\hat{\xi}_3, \hat{\eta}_3)$ coordinates where $\hat{\xi}_3^n = \hat{\xi}_3^{n-1} + \Delta_n$, $\hat{\eta}_3^j = \hat{\eta}_3^{j-1} + h_j$; $n \geq 1$, $1 \leq j \leq J$. The wall is denoted by $\eta = 0$; $j = 0$. The outer edge is at $\hat{\eta}_3 = \hat{\eta}_3^\infty = Jh$ if $h_j = h \forall j$. $n = 0$ denotes the initial station at $\hat{\xi}_3 = 0$ and $\hat{\xi}_3^{n-1/2} = \hat{\xi}_3^n - \frac{1}{2}\Delta_n$, $\hat{\eta}_3^{j-1/2} = \hat{\eta}_3^j - \frac{1}{2}h_j$.

Equations (7.3.9) are centred on $(\hat{\xi}_3^n, \hat{\eta}_3^{j-1/2})$ and equations

(7.3.10) and (7.3.11) are centred on $(\hat{\xi}_3^{n-1/2}, \hat{\eta}_3^{j-1/2})$. The

centred averages are defined as

$$(\hat{A}\hat{C})_{j-\frac{1}{2}}^{n-\frac{1}{2}} = \frac{1}{4} \{ (\hat{A}\hat{C})_j^n + (\hat{A}\hat{C})_j^{n-1} + (\hat{A}\hat{C})_{j-1}^n + (\hat{A}\hat{C})_{j-1}^{n-1} \} \quad (7.3.12)$$

$$(\hat{B}\hat{E})_{j-\frac{1}{2}}^{n-\frac{1}{2}} = \frac{1}{4} \{ (\hat{B}\hat{E})_j^n + (\hat{B}\hat{E})_j^{n-1} + (\hat{B}\hat{E})_{j-1}^n + (\hat{B}\hat{E})_{j-1}^{n-1} \} \quad (7.3.13)$$

$$(\hat{A}\hat{F})_{j-\frac{1}{2}}^{n-\frac{1}{2}} = \frac{1}{4} \{ (\hat{A}\hat{F})_j^n + (\hat{A}\hat{F})_j^{n-1} + (\hat{A}\hat{F})_{j-1}^n + (\hat{A}\hat{F})_{j-1}^{n-1} \} \quad (7.3.14)$$

$$\hat{\zeta}_j^{n-\frac{1}{2}} = \frac{1}{2} [\hat{\zeta}_j^n + \hat{\zeta}_j^{n-1}], \quad \hat{F}_j^{n-\frac{1}{2}} = \frac{1}{2} [\hat{F}_j^n + \hat{F}_j^{n-1}]. \quad (7.3.15)$$

The wall conditions (derived from (6.2.9)) are

$$A_0^\wedge = B_0^\wedge = F_0^\wedge = 0 \quad (7.3.16)$$

while the outer edge conditions derived from (6.2.10) are

$$D_J^\wedge = 0, \quad B_J^\wedge = \epsilon, \quad E_J^\wedge = 0. \quad (7.3.17)$$

At the changeover point $x_3 = 1$, the stream function \hat{A} , velocity \hat{B} , velocity gradient \hat{C} , pressure \hat{D} , temperature \hat{E} , and temperature gradient \hat{F} are the values A, B, C, D, E, F at $x_3 = 1$ for the $0 < x_3 < 1$ region. Further details of the computational scheme are given in Appendix 5.

In most of the computations the meshwidths used were $h = 0.1$, $\Delta_n = 0.02$ with the outer boundary J set to 500. The tolerance for which the Newton increments were considered small enough was 0.0001. The effect of h on the solution can be seen in tables 7.5, 7.6 and 7.7 and on the integral constraint in table 7.8. Solutions were obtained for a range of ϵ and σ values and are discussed in Section 7.4.

7.4 Numerical Results

The range of ϵ considered was from 0 to 10 and most results were obtained for $\sigma = 0.72$ (air) and 8.1 (water). As discussed in Chapter 6 the flow did break down at finite x_3 for some values of ϵ and σ , although there appeared to be two types of breakdown, one in which reverse flow developed and another in which the solution terminated in a singularity.

Reverse-flow breakdown occurred for the case $\sigma = 0.72$, $\epsilon = 0$. As mentioned in Chapter 6 the reverse flow prediction for $\epsilon = 0$ suggested that negative velocities might first occur towards the edge of the boundary layer and this was indeed the case. Graphs of the scaled velocity (figure 7.1), scaled temperature (figure 7.2) and scaled pressure (figure 7.3) for $\hat{\xi}_3 = 0.08, 0.16, 0.24$ and 0.32 have been plotted.

A singularity breakdown was observed for higher values of ϵ . The case investigated in detail was $\epsilon = 1, \sigma = 0.72$. Graphs of the scaled velocity (figure 7.4), scaled temperature (figure 7.5) and scaled pressure (figure 7.6) show that the flow appeared to be developing in a regular manner. However this broke down quickly as the singularity was approached. Near to the singularity the skin friction increased rapidly (figure 7.7). Plots of the scaled velocity, scaled temperature and scaled pressure close to the breakdown point at $\hat{\xi}_3 \approx 0.5336$ are presented in figures 7.8, 7.9 and 7.10 respectively.

For higher values of ϵ the flow was able to develop all the way along the boundary layer as was expected from the large x_3 study of Chapter 6. For $\sigma = 0.72, \epsilon = 3.5$ the flow broke down in the manner described for $\sigma = 0.72, \epsilon = 1$ at a point

between $\xi_3 = 1.78$ and $\xi_3 = 1.80$; the scaled graphs for this case for the velocity, temperature and pressure are shown in figures 7.11 - 7.13. Graphs of the actual velocity $\frac{\partial \psi_3}{\partial z_3}$, temperature T_3 and pressure p_3 plotted against z_3 are shown in figures 7.14 - 7.16. When the value of ϵ was raised to 4 the flow was able to develop fully downstream. Results for this case are presented in figures 7.17 - 7.19 (scaled velocity, scaled temperature and scaled pressure) and figures 7.20 - 7.22 (actual velocity, temperature and pressure). The figures show that the solution has settled down to some final form.

The value of ϵ for which the flow breaks down is dependent on σ . This is demonstrated by the case of $\epsilon = 3$, $\sigma = 8.1$ for which the flow is able to develop all the way along the boundary layer, and for $\epsilon = 3$, $\sigma = 0.72$ for which the flow breaks down. Scaled graphs of the velocity, temperature and pressure for $\xi_3 = 0.2, 0.4, 0.6, 0.8$ and 1.0 are presented in figures 7.23 - 7.25 and show well the change from the jet structure to the new structure of the flow driven by buoyancy and the forcing external velocity. Scaled graphs of the further development of the flow for this case are shown in figures 7.26 - 7.28 and again demonstrate that the flow settles down to a final form. Graphs of the actual velocity, temperature and pressure are shown in figures 7.29 - 7.31. The downstream development of the buoyancy layer for the case of air ($\sigma = 0.72$) is summarised in figures 7.32 - 7.35. Figure 7.32 shows the wall pressure plotted against ξ_3 for various ϵ . The results confirm the small x_3 and large x_3 asymptotic results:

$$P_3(x_3, 0) \sim -x_3^{\frac{1}{2}} \frac{1}{\sigma} \int_0^{\infty} T_{30} d\eta_3 \quad (x_3 \rightarrow 0) \quad (7.4.1)$$

$$P_3(x_3, 0) \sim -\frac{1}{\sigma} \int_0^{\infty} \theta_3 d\zeta_3 \quad (x_3 \rightarrow \infty) \quad (7.4.2)$$

The cases $\epsilon = 4$ and 10 that develop all the way along the boundary layer seem to approach their asymptotic values and even those cases which break down but for which $\epsilon > \epsilon_c$ actually appear to be approaching their large x_3 asymptotes prior to termination. The cases $\epsilon = 1$ and 2 which were studied in detail close to the singularity see a rapid decrease in wall pressure near to the breakdown point and this is consistent with the skin friction rising sharply (see figure 7.33). The wall temperature (figure 7.34), however, is little affected by the rapid rise in skin friction and decrease in pressure.

Asymptotic forms for the skin friction and wall temperature at small and large values of x_3 are:

$$u_{z_3}(x_3, 0) \sim x_3^{-5/4} (f_{30}''(0) + x_3^{3/2} f_{31}''(0)) \quad (x_3 \rightarrow 0) \quad (7.4.3)$$

$$T_3(x_3, 0) \sim x_3^{-1/4} (T_{30}(0) + x_3^{1/2} T_{31}(0)) \quad (x_3 \rightarrow 0) \quad (7.4.4)$$

$$u_{z_3}(x_3, 0) \sim x_3^{-1/2} \phi_3''(0) \quad (x_3 \rightarrow \infty) \quad (7.4.5)$$

$$T_3(x_3, 0) \sim x_3^{-1/2} \theta_3(0) \quad (x_3 \rightarrow \infty) \quad (7.4.6)$$

and these are included in figures 7.33 and 7.34.

The ^{negative} displacement $D_3(x_3)$ is defined by the outer behaviour

$$\psi_3 \sim \epsilon Z_3 + D_3(x_3) \quad \text{as } Z_3 \rightarrow \infty \quad (7.4.7)$$

and follows its asymptotes

$$D_3 \sim x_3^{\frac{1}{4}} f_{30}(\infty) = x_3^{\frac{1}{4}} K_3 \quad (x_3 \rightarrow 0) \quad (7.4.8)$$

$$D_3 \sim x_3^{\frac{1}{2}} \lim_{\xi_3 \rightarrow \infty} (\phi_3 - \epsilon \xi_3) \quad (x_3 \rightarrow \infty) \quad (7.4.9)$$

well (see figure 7.35). Near to the singularity breakdown point it turns up sharply indicating that fluid is being brought back down into the boundary layer.

More comprehensive comparisons with the small x_3 asymptotes have also been made. From the asymptotic study the velocity is

$$\frac{d\psi_3}{dz_3} = x_3^{-\frac{1}{2}} \left(f'_{30} + x_3^{\frac{1}{2}} \epsilon \hat{f}'_{31} + x_3 \epsilon^2 \hat{f}'_{32} + x_3^{\frac{3}{2}} (\hat{f}'_{330} + \epsilon^3 \hat{f}'_{331}) + \dots \right) \quad (7.4.10)$$

using the scaled function introduced in Chapter 6 and from the numerical study of Section 7.2 the velocity is

$$\frac{d\psi_3}{dz_3} = x_3^{-\frac{1}{2}} \frac{d\hat{\psi}_3}{d\eta_3} \quad (7.4.11)$$

In tables 7.9 and 7.10 the values of $\frac{\partial \hat{\psi}_3}{\partial \eta_3}$ are compared with

$f'_{30} + x_3^{3/2} \hat{f}'_{330}$, which is the reduced form for $\epsilon = 0$, for the cases $\sigma = 0.72$ and 8.1. Similarly, the asymptotic expression for the temperature is

$$T_3 = x_3^{-1/4} \left(T_{30} + x_3^{\frac{1}{4}} \epsilon \hat{T}_{31} + x_3 \epsilon^2 \hat{T}_{32} + x_3^{\frac{3}{2}} (\hat{T}_{330} + \epsilon^3 \hat{T}_{331}) + \dots \right) \quad (7.4.12)$$

using the scaled functions introduced in Chapter 6 and from the numerical study of Section 7.2 the temperature is

$$T_3 = x_3^{-1/4} \hat{T}_3 \quad (7.4.13)$$

In tables 7.11 and 7.12 the values of \hat{T}_3 are compared with

$\tau_{30} + x_3^{3/2} \hat{\tau}_{330}$, the reduced form for $\epsilon = 0$, for the cases $\sigma = 0.72$ and 8.1 .

Tables 7.9 - 7.12 show good agreement between the numerical and asymptotic solutions. However this is not the case for larger values of ϵ . We may write equation (7.4.10) as

$$\xi_3^2 \frac{d\psi}{dz_3} = f_{30}' + (\xi_3^2 \epsilon) \hat{f}_{31}' + (\xi_3^2 \epsilon)^2 \hat{f}_{32}' + \xi_3^6 \hat{f}_{330}' + (\xi_3^2 \epsilon)^3 \hat{f}_{331}' + \dots \quad (7.4.14)$$

where $\xi_3 = x_3^{1/4}$ and the next term in the expansion involves $(\xi_3^2 \epsilon)^4$ and ξ_3^8 . Thus for equation (7.4.14) to be accurate to within about 10^{-4} we require

$$(\xi_3^2 \epsilon)^4 \leq 10^{-4} \quad \text{and} \quad \xi_3^8 \leq 10^{-4} \quad (7.4.15)$$

or

$$\xi_3^2 \epsilon \leq 0.10 \quad \text{and} \quad \xi_3 \leq 0.32. \quad (7.4.16)$$

Table 7.13 shows the effect of these restrictions for different ϵ . Confirmation of the trend of a smaller range of validity for higher ϵ is shown in tables 7.14 - 7.16. For $\epsilon = 10$ conditions (7.4.16) require $\xi_3 \leq 0.1$, so the expansion rapidly breaks down near $x_3 = 0$.

Results of the full computations for $\epsilon = 10$ are shown in figures 7.36 - 7.59 for $\sigma = 0.72$ and 8.1 . The development of the velocity for $\sigma = 0.72$ along the horizontal boundary layer can be seen in figures 7.36, 7.37 (scaled form) and 7.38, 7.39 (actual form), the temperature in figures 7.40, 7.41 (scaled forms) and 7.42, 7.43 (actual forms) and the pressure in figures 7.44, 7.45 (scaled forms) and 7.46, 7.47 (actual forms). Corresponding results for the case $\sigma = 8.1$ are shown in figures 7.48 - 7.59.

7.5 Discussion

In this section the implications of the present theory for the structure of the high Rayleigh number flow in the end zone of a shallow laterally heated cavity are considered. The basis of the theory is the model proposed in Chapter 3 in which a vertical boundary layer of width $O(R_1^{-3/5})$ lies along the cold end wall. At the base of this boundary layer the streamlines and isotherms are assumed to be carried around the corner into a horizontal boundary layer of width $O(R_1^{-3/5})$ and length $x = O(1)$. In this region buoyancy does not influence the flow to a first approximation and as a result the stream function and temperature fields uncouple giving a wall jet of the type first analysed by Glauert (1956). As x increases, and the jet diffuses, buoyancy reappears on the scale $x = O(R_1^{2/5})$ and the jet evolves into a new boundary layer, partially driven by an external forcing velocity. This external velocity is associated with an inviscid recirculating zone above the horizontal boundary layers.

The horizontal boundary layers effect the transition to the main outer part of the end zone where $x = O(R_1)$. The results of Chapter 7 suggest that for only a restricted range of ϵ is a straightforward development possible, and this range appears to be even more restrictive than that suggested by the asymptotic prediction $\epsilon > \epsilon_c(\sigma)$.

Further work is needed to describe the analytical form of the singularity that develops in the buoyancy layer at low values of ϵ , and to find the actual value of ϵ . The latter task is a particularly difficult one as it involves finding the recirculating flow in the main outer and inviscid zones above the horizontal boundary layers. These are formidable nonlinear

problems involving, among other things, a solution of the horizontal boundary-layer equations with substantial reverse flow.

TABLE 7.1

Effect of meshwidths on values of $\frac{\partial \hat{\psi}_3}{\partial \eta_3}$ ($\sigma = 0.72, \epsilon = 10$)

η_3	$\xi_3 = 0.2$	$\xi_3 = 0.6$	$\xi_3 = 1.0$
2	a) 0.6649	4.1594	10.0613
	b) 0.6648	4.1598	10.0618
4	0.7184	3.6130	10.0243
	0.7185	3.6132	10.0252
6	0.5470	3.6365	10.0184
	0.5470	3.6364	10.0188
8	0.5097	3.6009	10.0127
	0.5098	3.6010	10.0131

a) $h = 0.1, \Delta = 0.02$

b) $h = 0.2, \Delta = 0.02$

TABLE 7.2

Effect of meshwidths on values of \hat{T}_3 ($\sigma = 0.72, \epsilon = 10$)

η_3	$\xi_3 = 0.2$	$\xi_3 = 0.6$	$\xi_3 = 1.0$
0	a) -0.4916	-0.2490	-0.1609
	b) -0.4917	-0.2486	-0.1602
2	-0.4376	-0.0662	-0.0022
	-0.4376	-0.0661	-0.0022

a) $h = 0.1, \Delta = 0.02$

b) $h = 0.2, \Delta = 0.02$

TABLE 7.3

Effect of meshwidths on values of $\hat{\sigma}p_3(\xi_3, 0)$ ($\sigma = 0.72, \epsilon = 10$)

$\xi_3 = 0.2$	$\xi_3 = 0.6$	$\xi_3 = 1.0$
a) 1.8917	0.4042	0.1676
b) 1.8919	0.4028	0.1663

a) $h = 0.1, \Delta = 0.02$ b) $h = 0.2, \Delta = 0.02$

TABLE 7.4

Effect of meshwidths on integral constraint (6.2.13) ($\sigma = 0.72, \epsilon = 10$)

ξ_3	$h = 0.1, \Delta = 0.02$	$h = 0.2, \Delta = 0.02$
0.2	1.001738	1.001668
0.4	1.001434	1.000535
0.6	1.001049	0.999143
0.8	1.000578	0.997453
1.0	0.999848	0.994754

TABLE 7.5

Effect of meshwidths on values of $\frac{\partial \hat{\phi}_3}{\partial \hat{\eta}_3}$ ($\sigma = 0.72, \epsilon = 10$)

$\hat{\eta}_3$	$\hat{\xi}_3 = 1.2$	$\hat{\xi}_3 = 1.6$	$\hat{\xi}_3 = 2.0$
1	a) 8.8343	8.7904	8.7669
	b) 8.8087	8.7513	8.7224
2	10.0405	10.0316	10.0258
	10.0410	10.0324	10.0266
3	10.0282	10.0224	10.0186
	10.0282	10.0225	10.0187

a) $h = 0.1, \Delta = 0.02$

b) $h = 0.2, \Delta = 0.02$

TABLE 7.6

Effect of meshwidths on values of $\hat{\theta}_3$ ($\sigma = 0.72, \epsilon = 10$)

$\hat{\eta}_3$	$\hat{\xi}_3 = 1.2$	$\hat{\xi}_3 = 1.6$	$\hat{\xi}_3 = 2.0$
0	a) -0.1704	-0.1709	-0.1712
	b) -0.1705	-0.1702	-0.1702
1	-0.0928	-0.0934	-0.0937
	-0.0933	-0.0941	-0.0945
2	-0.0029	-0.0029	-0.0030
	-0.0030	-0.0031	-0.0032

a) $h = 0.1, \Delta = 0.02$

b) $h = 0.2, \Delta = 0.02$

TABLE 7.7

Effect of meshwidths on values of $\sigma \hat{\Pi}(\hat{\xi}_3, 0)$ ($\sigma = 0.72, \epsilon = 10$)

$$\hat{\xi}_3 = 1.2$$

$$\hat{\xi}_3 = 1.6$$

$$\hat{\xi}_3 = 2.0$$

a) 0.1820

0.1828

0.1833

b) 0.1823

0.1831

0.1835

a) $h = 0.1, \Delta = 0.02$

b) $h = 0.2, \Delta = 0.02$

TABLE 7.8

Effect of meshwidths on integral constraint (6.2.13) ($\sigma = 0.72$, $\epsilon = 10$)

$\hat{\xi}_3$	$h = 0.1, \Delta = 0.02$	$h = 0.2, \Delta = 0.02$
1.2	0.999701	0.997848
1.4	0.999637	0.997848
1.6	0.999576	0.997818
1.8	0.999516	0.997778
2.0	0.999457	0.997732

TABLE 7.9

Comparison of a) numerical and b) small x_3 asymptotic velocity solutions for $\sigma = 0.72, \epsilon = 0$

η_3	ξ_3			
	0.08	0.16	0.24	0.32
1.0	a) 0.2197	0.2197	0.2189	0.2147
	b) 0.2197	0.2196	0.2183	0.2119
2.0	0.4059	0.4058	0.4048	0.3992
	0.4059	0.4058	0.4041	0.3992
4.0	0.4658	0.4658	0.4656	0.4645
	0.4657	0.4656	0.4654	0.4645
8.0	0.0813	0.0813	0.0813	0.0813
	0.0812	0.0813	0.0814	0.0821

TABLE 7.10

Comparison of a) numerical and b) small x_3 asymptotic velocity solutions for $\sigma = 8.1, \epsilon = 0$

η_3	ξ_3		
	0.2	0.4	0.6
1.0	a) 0.2197	0.2183	0.1997
	b) 0.2197	0.2176	0.1958
4.0	0.4658	0.4663	0.4717
	0.4657	0.4663	0.4731
16.0	0.0006	0.0006	0.0006
	0.0006	0.0006	0.0006

TABLE 7.11

Comparison of a) numerical and b) small x_3 asymptotic temperature solutions for $\sigma = 0.72, \epsilon = 0$

η_3	ξ_3			
	0.08	0.16	0.24	0.32
0.0	a) -0.5942	-0.5941	-0.5943	-0.5949
	b) -0.5943	-0.5943	-0.5943	-0.5954
1.0	-0.5902	-0.5902	-0.5903	-0.5911
	-0.5904	-0.5904	-0.5906	-0.5916
4.0	-0.4086	-0.4086	-0.4093	-0.4131
	-0.4086	-0.4087	-0.4098	-0.4151
8.0	-0.0955	-0.0955	-0.0963	-0.1005
	-0.0955	-0.0956	-0.0966	-0.1016

TABLE 7.12

Comparison of a) numerical and b) small x_3 asymptotic temperature solutions for $\sigma = 8.1$, $\epsilon = 0$

η_3	ξ_3		
	0.2	0.4	0.6
0.0	-1.8922	-1.8928	-1.9006
	-1.8949	-1.8958	-1.9052
1.0	-1.7553	-1.7572	-1.7808
	-1.7583	-1.7610	-1.7894
4.0	-0.0281	-0.0287	-0.0379
	-0.0280	-0.0289	-0.0376

TABLE 7.13

Approximate range of validity ξ_{3c} for given ϵ

ϵ	ξ_{3c}
0	0.32
1	0.32
3	0.18
10	0.10

TABLE 7.14

Comparison of wall temperatures for numerical and small x_3 asymptotic solutions for $\sigma = 0.72$, $\epsilon = 1$

ξ_3	$\hat{T}_3(\xi_3, 0)_{\text{num}}$	$\hat{T}_3(\xi_3, 0)_{\text{asy}}$
0.12	-0.5903	-0.5908
0.24	-0.5802	-0.5809
0.36	-0.5655	-0.5654
0.48	-0.5492	-0.5440

TABLE 7.15

Comparison of wall temperatures for numerical and small x_3 asymptotic solution for $\sigma = 8.1$, $\epsilon = 3$

ζ_3	$\hat{T}_3(\zeta_3, 0)_{\text{num}}$	$\hat{T}_3(\zeta_3, 0)_{\text{asy}}$
0.2	-1.8554	-1.8625
0.4	-1.7529	-1.7725
0.6	-1.5946	-1.7478

TABLE 7.16

Comparison of wall temperatures for numerical and small x_3 asymptotic solutions for $\sigma = 0.72$, $\epsilon = 10$

ξ_3	$\hat{T}_3(\xi_3, 0)_{\text{num}}$	$\hat{T}_3(\xi_3, 0)_{\text{asy}}$
0.2	-0.5070	-0.4349
0.4	-0.2719	-5.5956

Figure 7.1 Graph of scaled velocity at $\xi_3 = 0.08, 0.16, 0.24$ and 0.32 ($\epsilon = 0, \sigma = 0.72$).

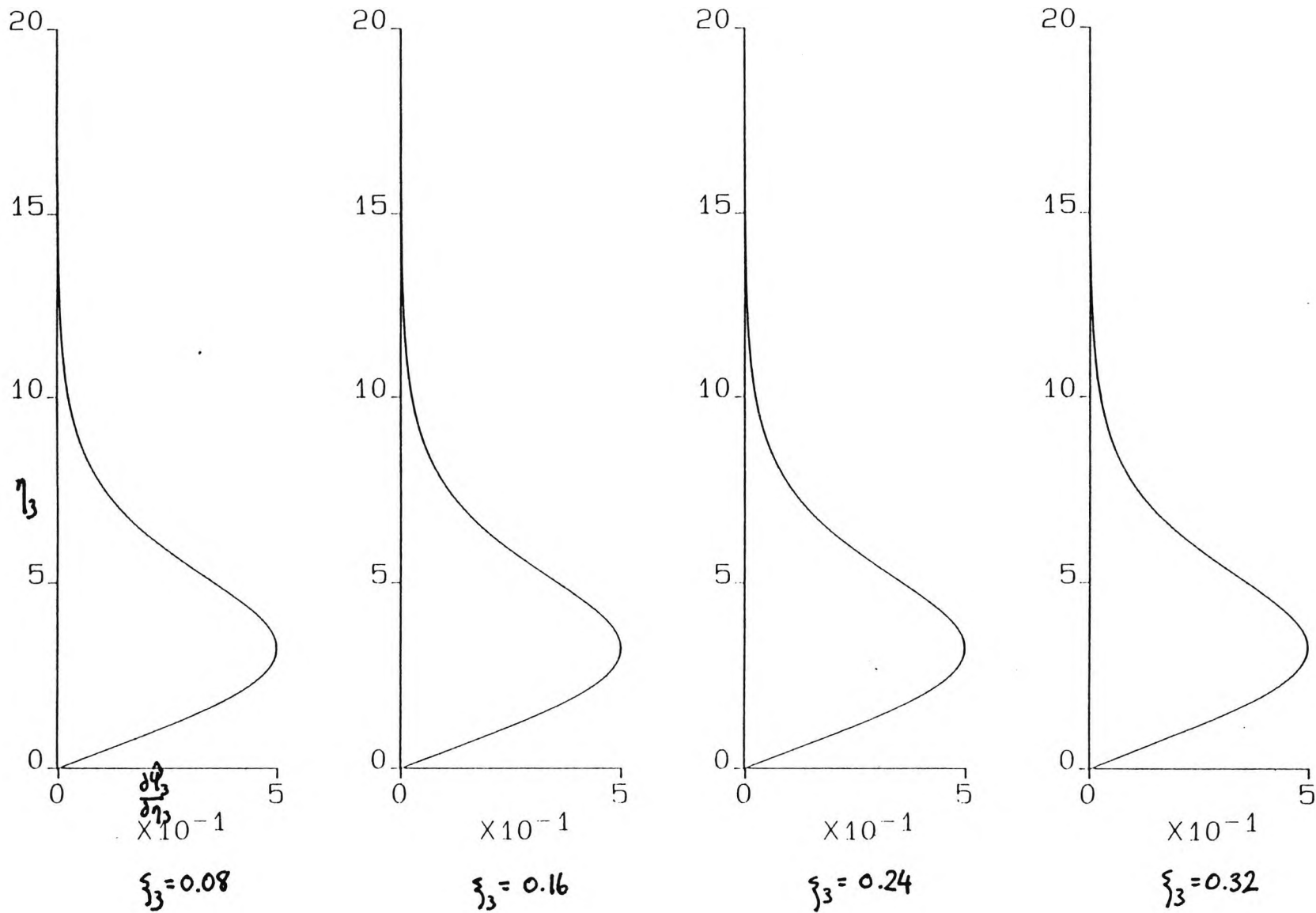


Figure 7.2 Graph of scaled temperature at $\xi_3 = 0.08, 0.16, 0.24$ and 0.32 ($\epsilon = 0, \sigma = 0.72$).

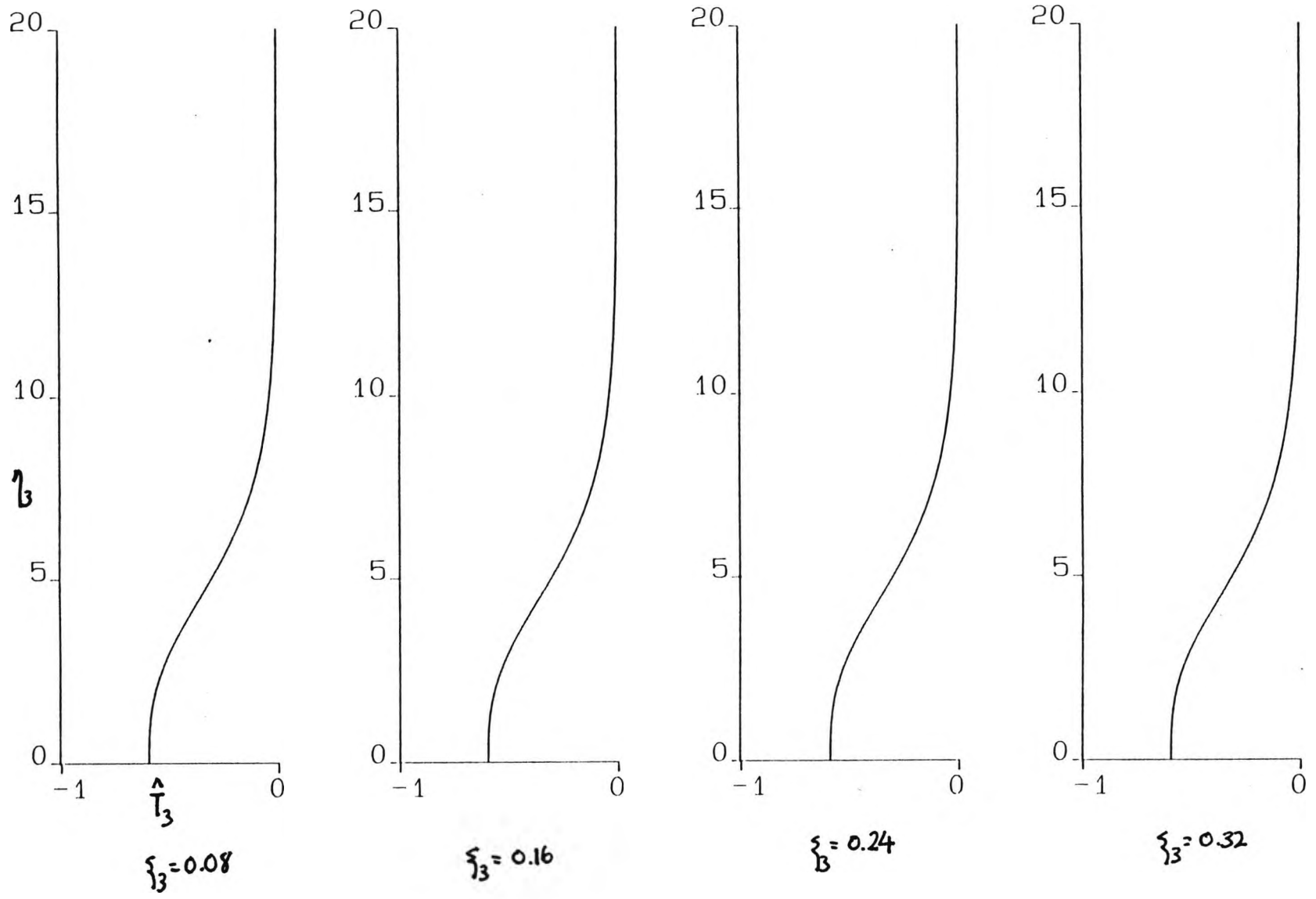
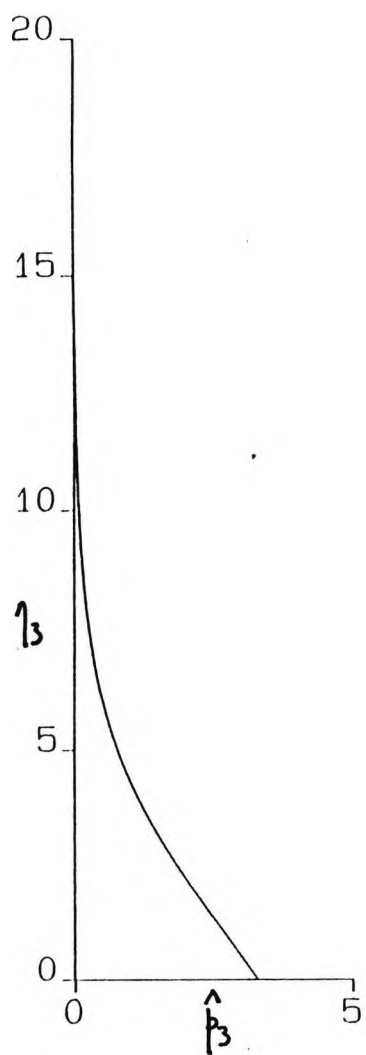
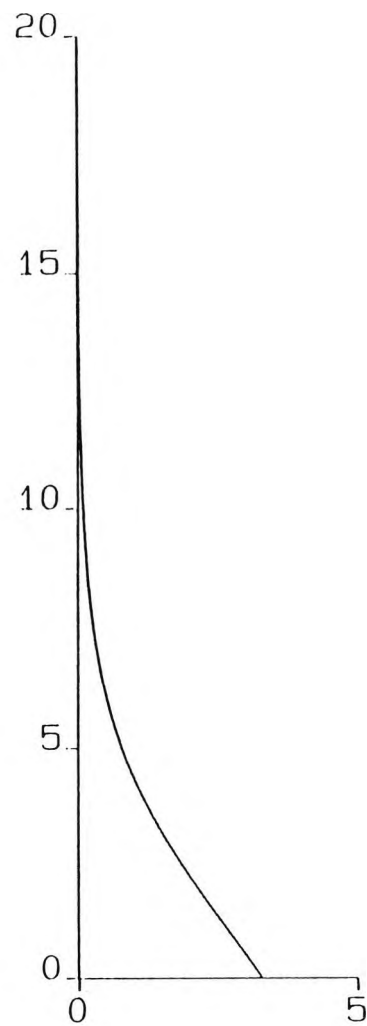


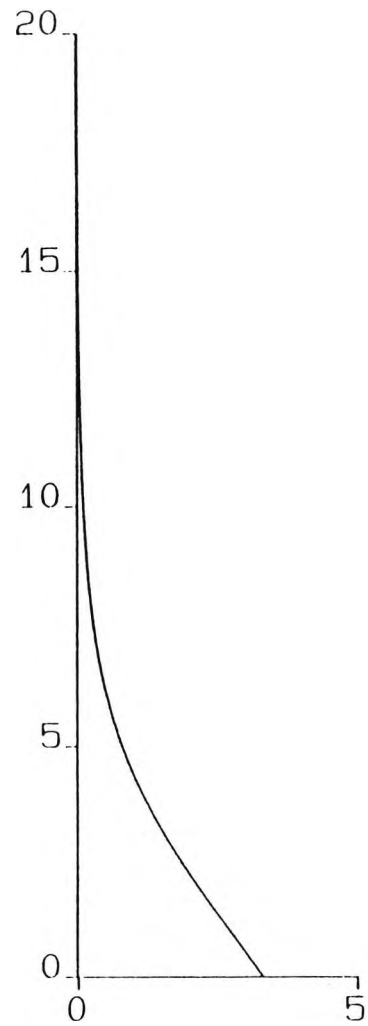
Figure 7.3 Graph of scaled pressure at $\xi_3 = 0.08, 0.16, 0.24$ and 0.32 ($\epsilon = 0, \sigma = 0.72$).



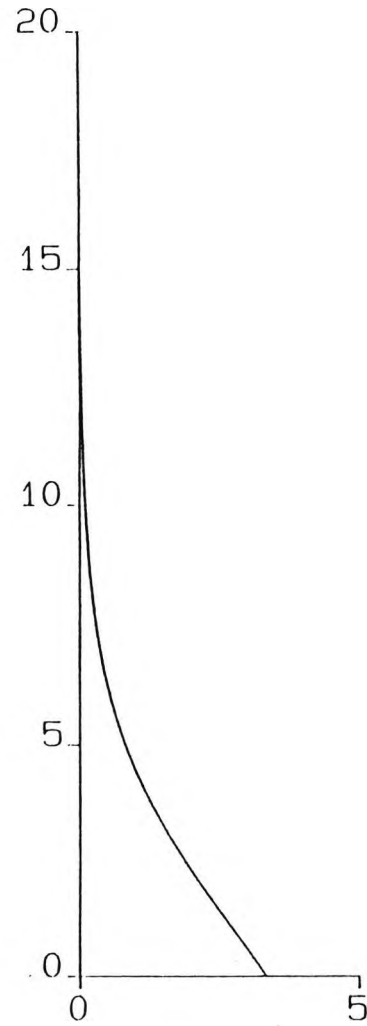
$\xi_3 = 0.08$



$\xi_3 = 0.16$



$\xi_3 = 0.24$



$\xi_3 = 0.32$

Figure 7.4 Graph of scaled velocity at $\xi_3 = 0.08, 0.16, 0.24$ and 0.32 ($\epsilon = 1, \sigma = 0.72$).

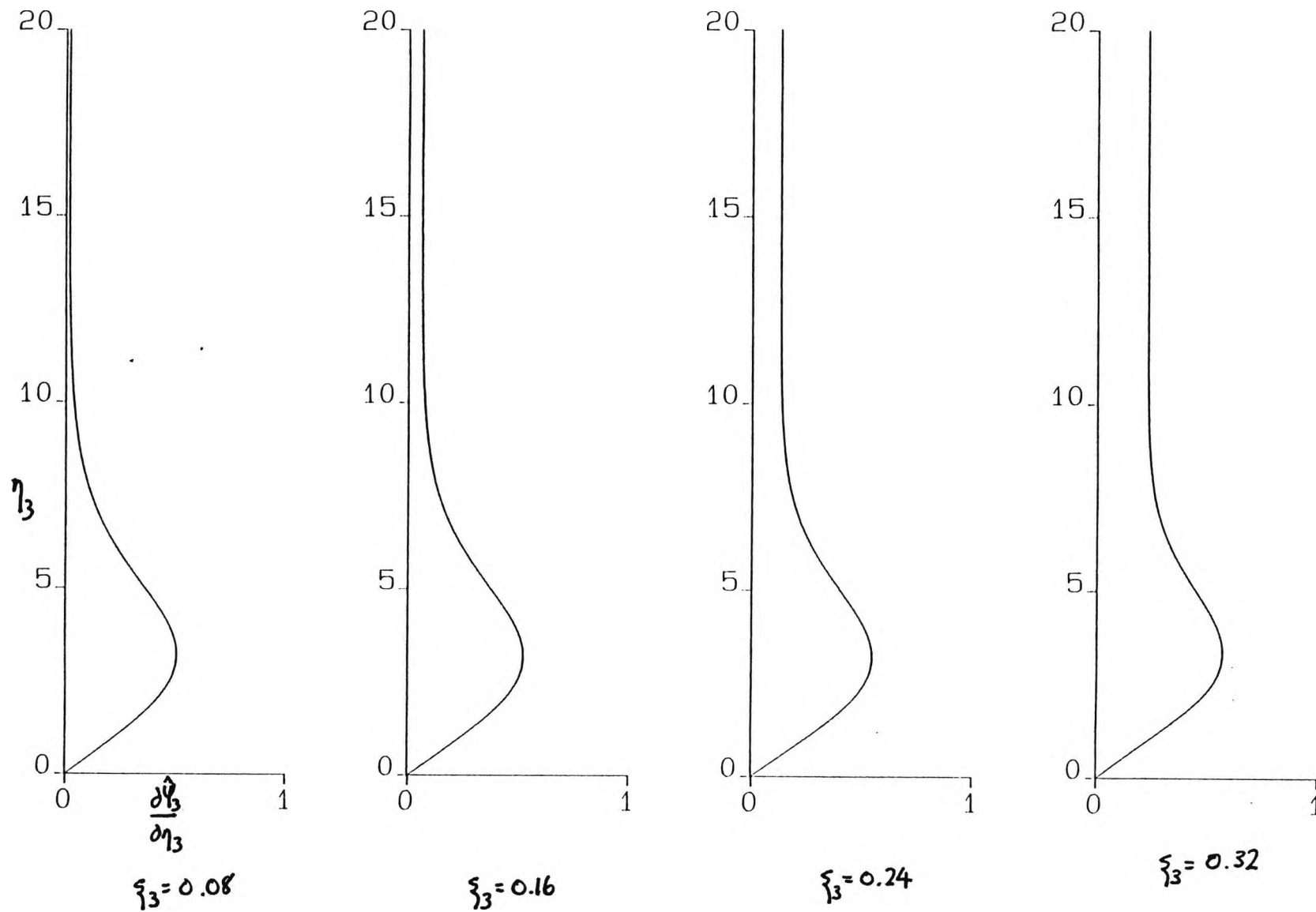


Figure 7.5 Graph of scaled temperature at $\xi_3 = 0.08, 0.16, 0.24$ and 0.32 ($\epsilon = 1, \sigma = 0.72$).

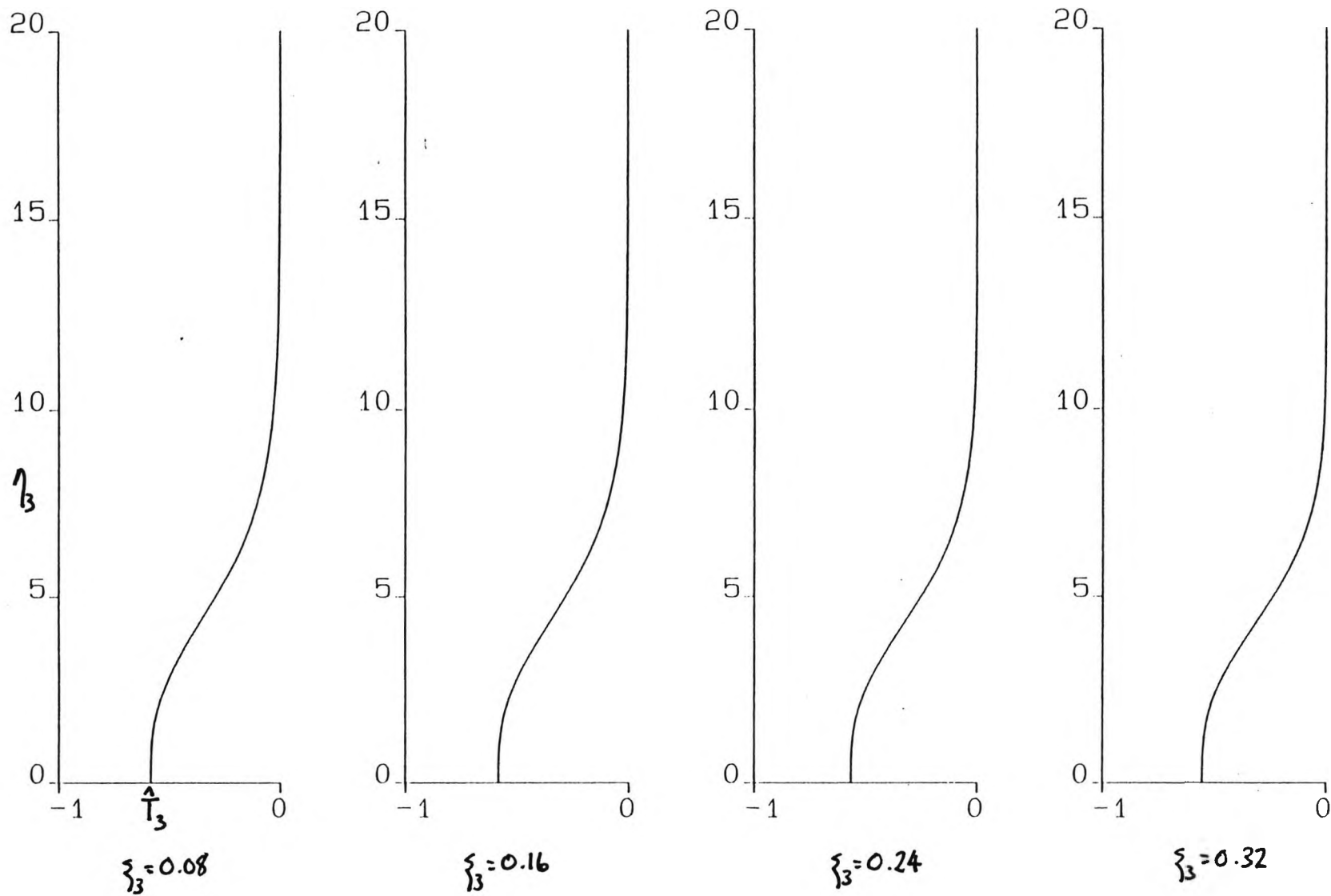


Figure 7.6 Graph of scaled pressure at $\xi_3 = 0.08, 0.16, 0.24$ and 0.32 ($\epsilon = 1, \sigma = 0.72$).

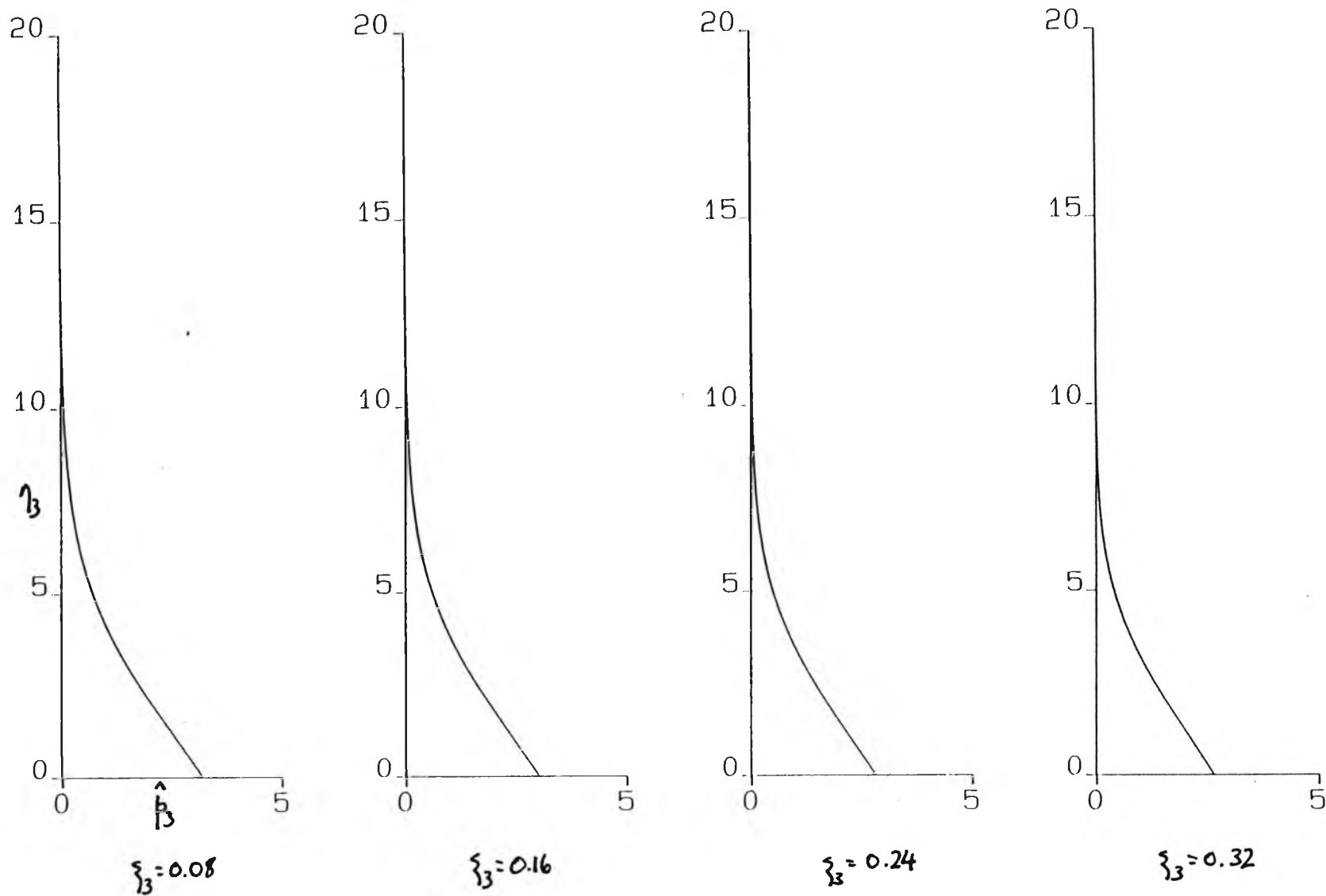


Figure 7.7 Graph of scaled shear stress $\xi_3 = 0.5331, 0.5332, 0.5333, 0.5334, 0.5335$ ($\epsilon = 1, \sigma = 0.72$).

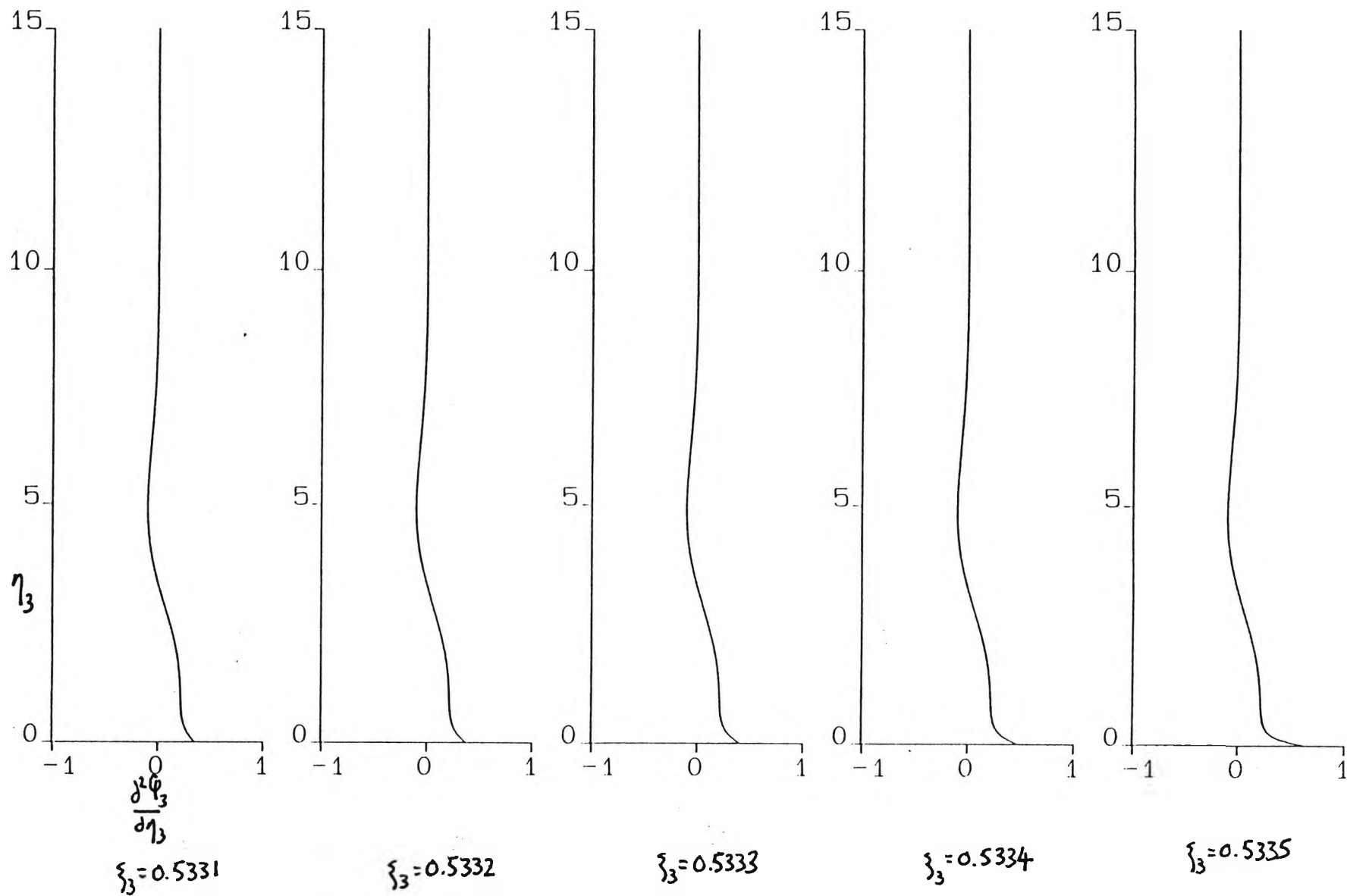


Figure 7.8 Graph of scaled velocity at $\xi_3 = 0.5331, 0.5332, 0.5333, 0.5334, 0.5335$ ($\epsilon = 1, \sigma = 0.72$).

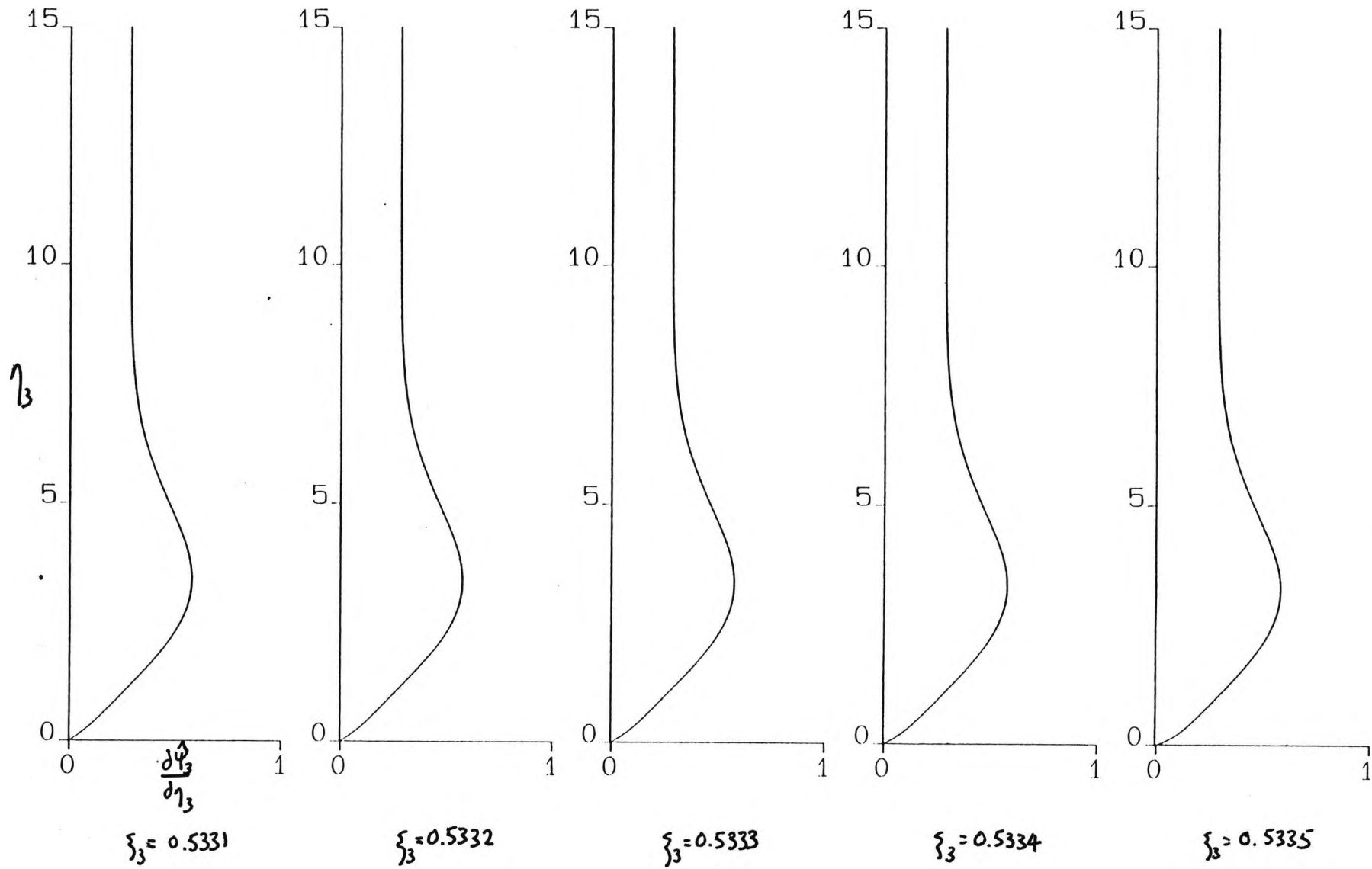


Figure 7.9 Graph of scaled temperature at $\xi_3 = 0.5331, 0.5332, 0.5333, 0.5334, 0.5335$ ($\epsilon = 1, \sigma = 0.72$).

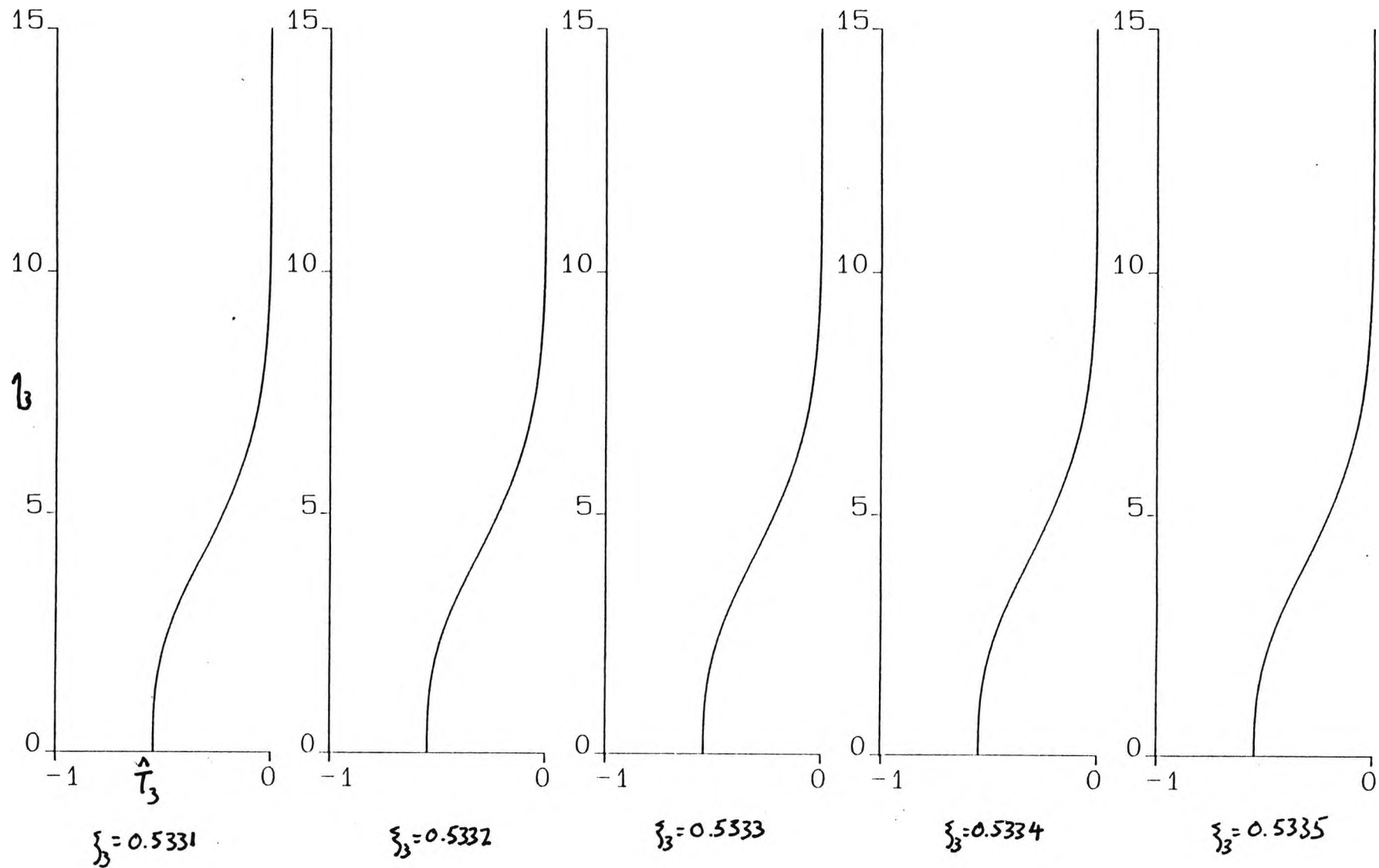


Figure 7.10 Graph of scaled pressure at $\xi_3 = 0.5331, 0.5332, 0.5333, 0.5334, 0.5335$ ($\epsilon = 1, \sigma = 0.72$).

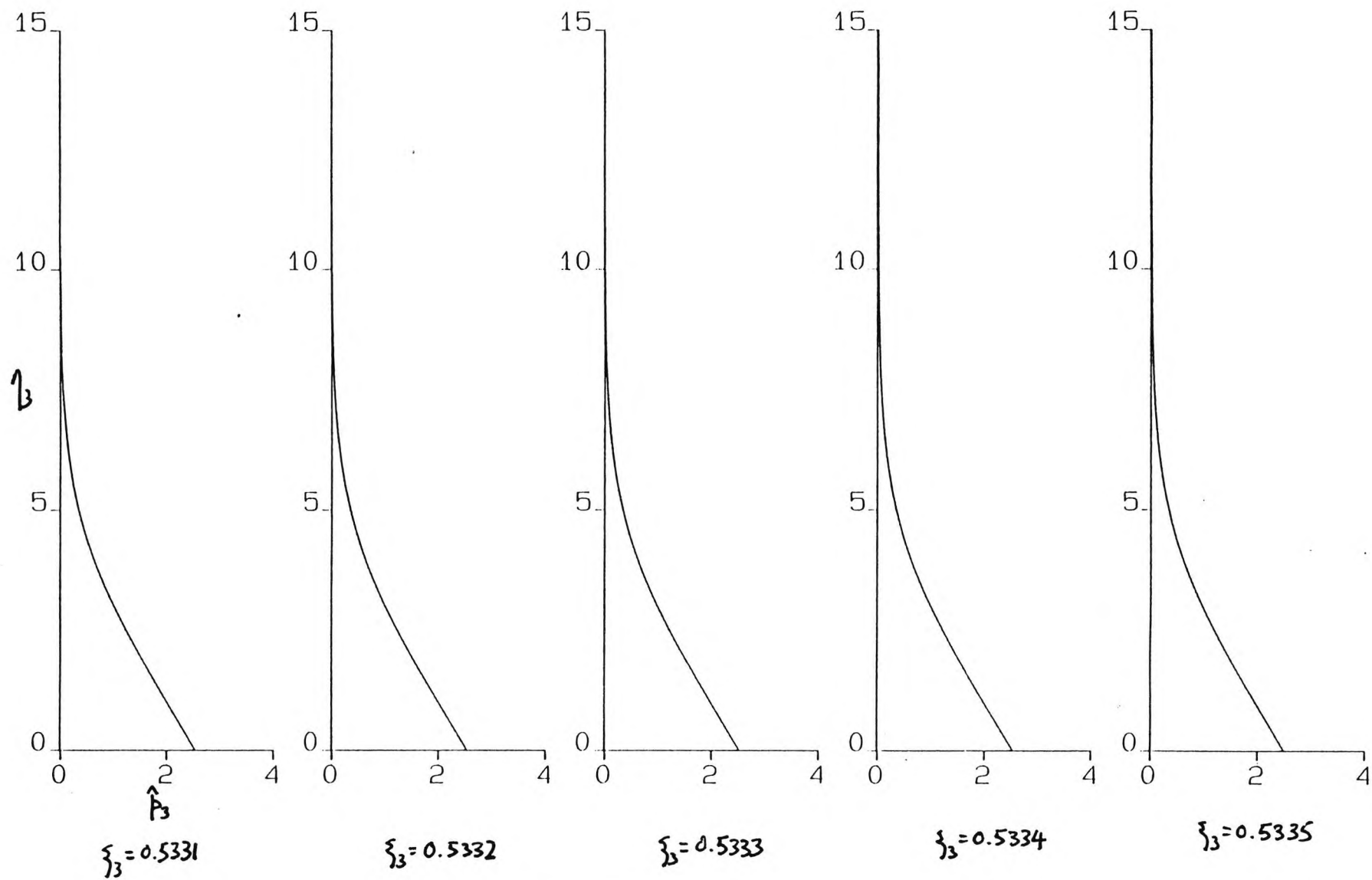


Figure 7.11 Graph of scaled velocity at $\xi_3 = 0.2, 0.4, 0.6, 0.8, 1.0$ ($\epsilon = 3.50, \sigma = 0.72$).

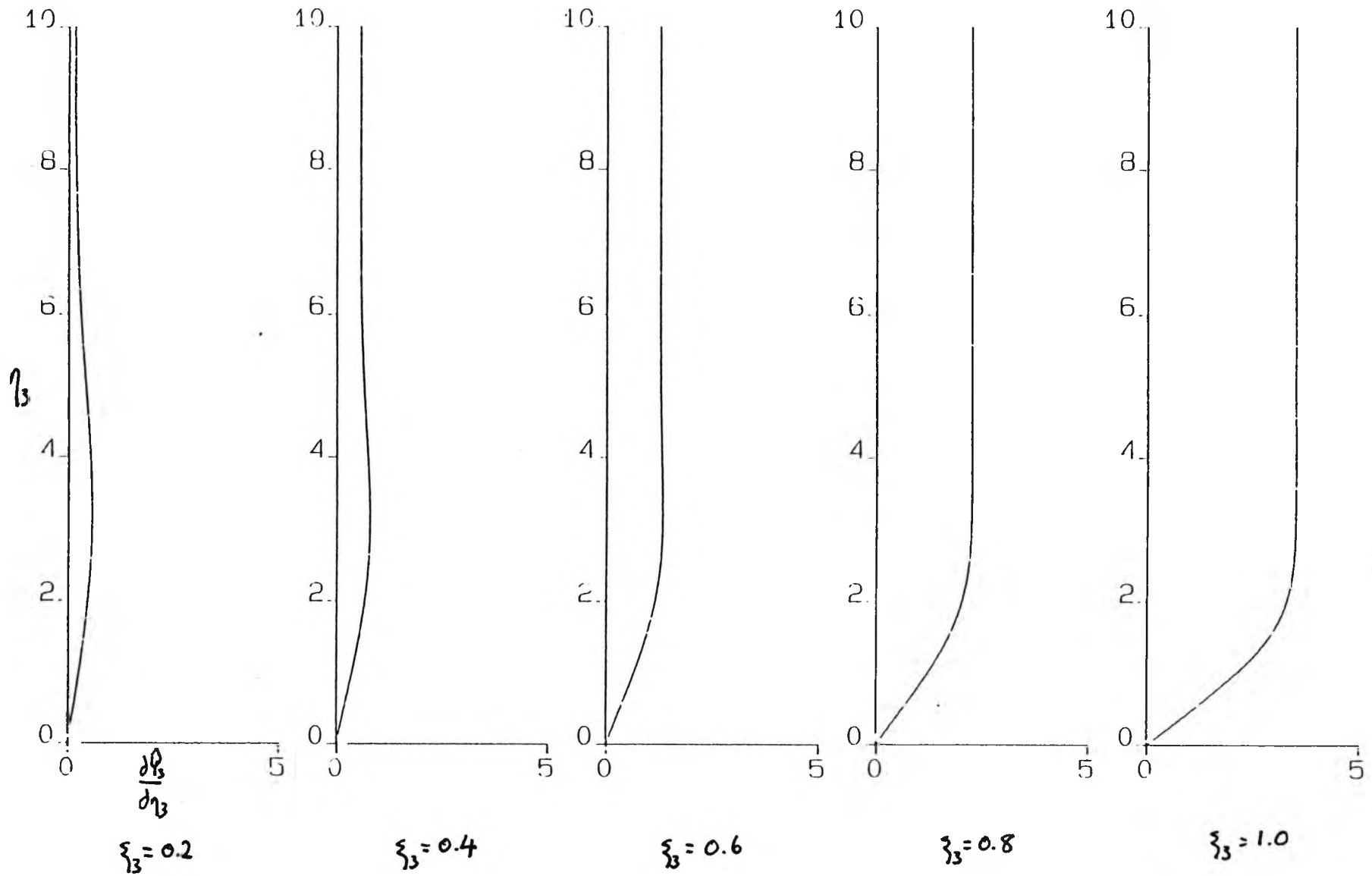


Figure 7.12 Graph of scaled temperature at $\xi_3 = 0.2, 0.4, 0.6, 0.8, 1.0$ ($\epsilon = 3.50, \sigma = 0.72$).

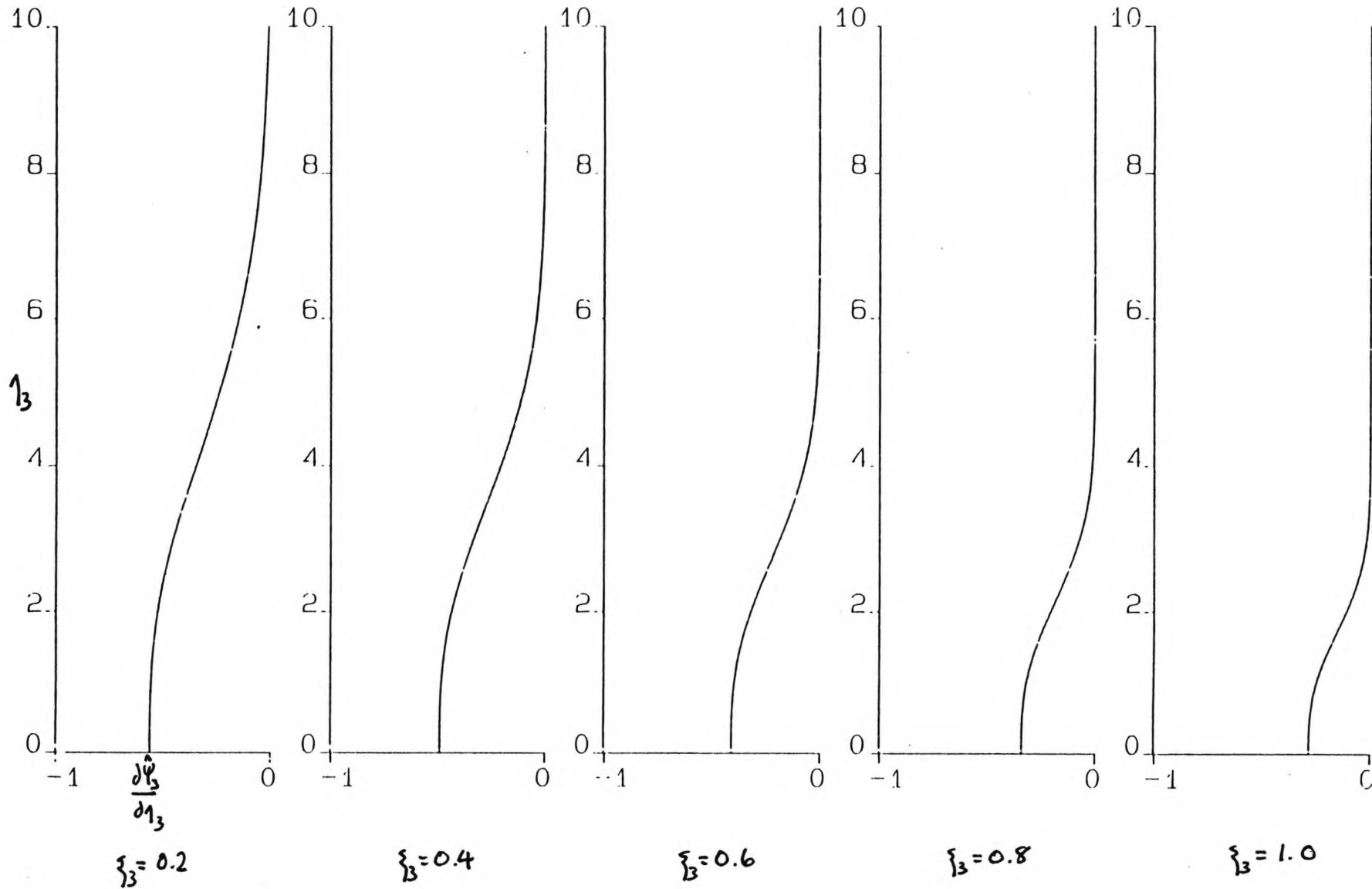


Figure 7.13 Graph of scaled pressure at $\xi_3 = 0.2, 0.4, 0.6, 0.8, 1.0$ ($\epsilon = 3.50, \sigma = 0.72$).

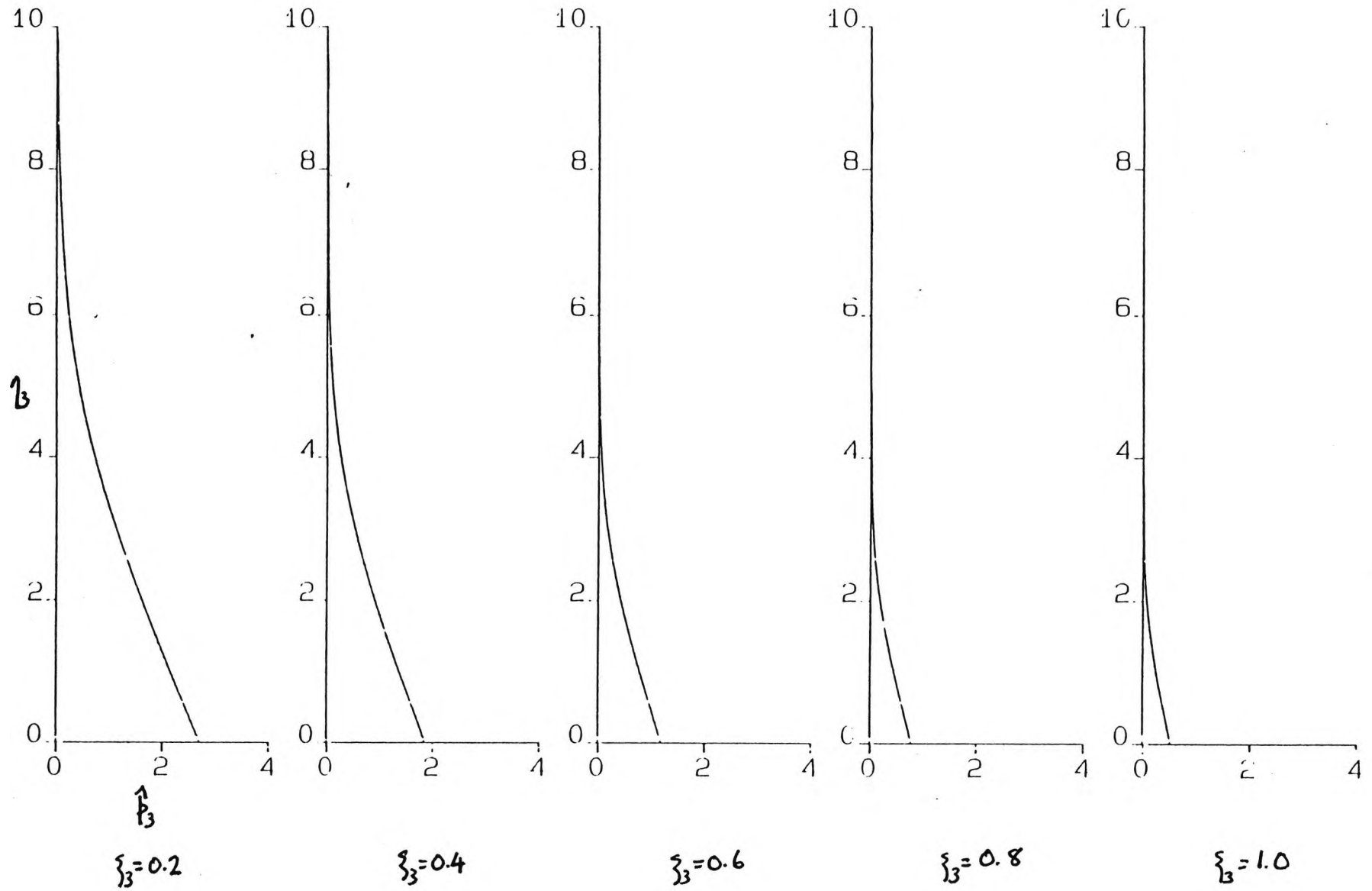


Figure 7.14 Graph of actual velocity at $\xi_3 = 0.2, 0.4, 0.6, 0.8, 1.0$ ($\epsilon = 3.50, \sigma = 0.72$).

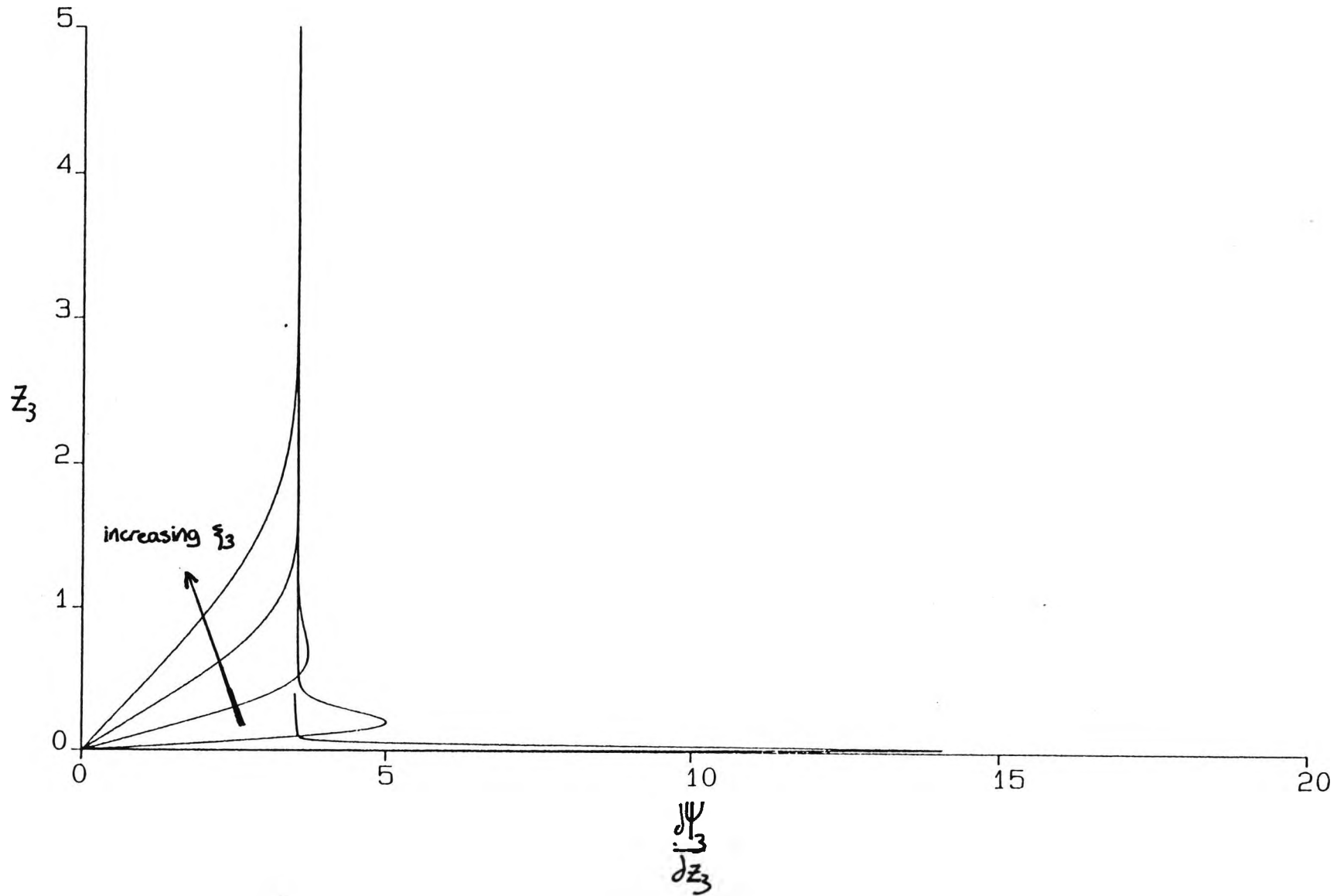


Figure 7.15 Graph of actual temperature at $\xi_3 = 0.2, 0.4, 0.6, 0.8, 1.0$ ($\epsilon = 3.50, \sigma = 0.72$).

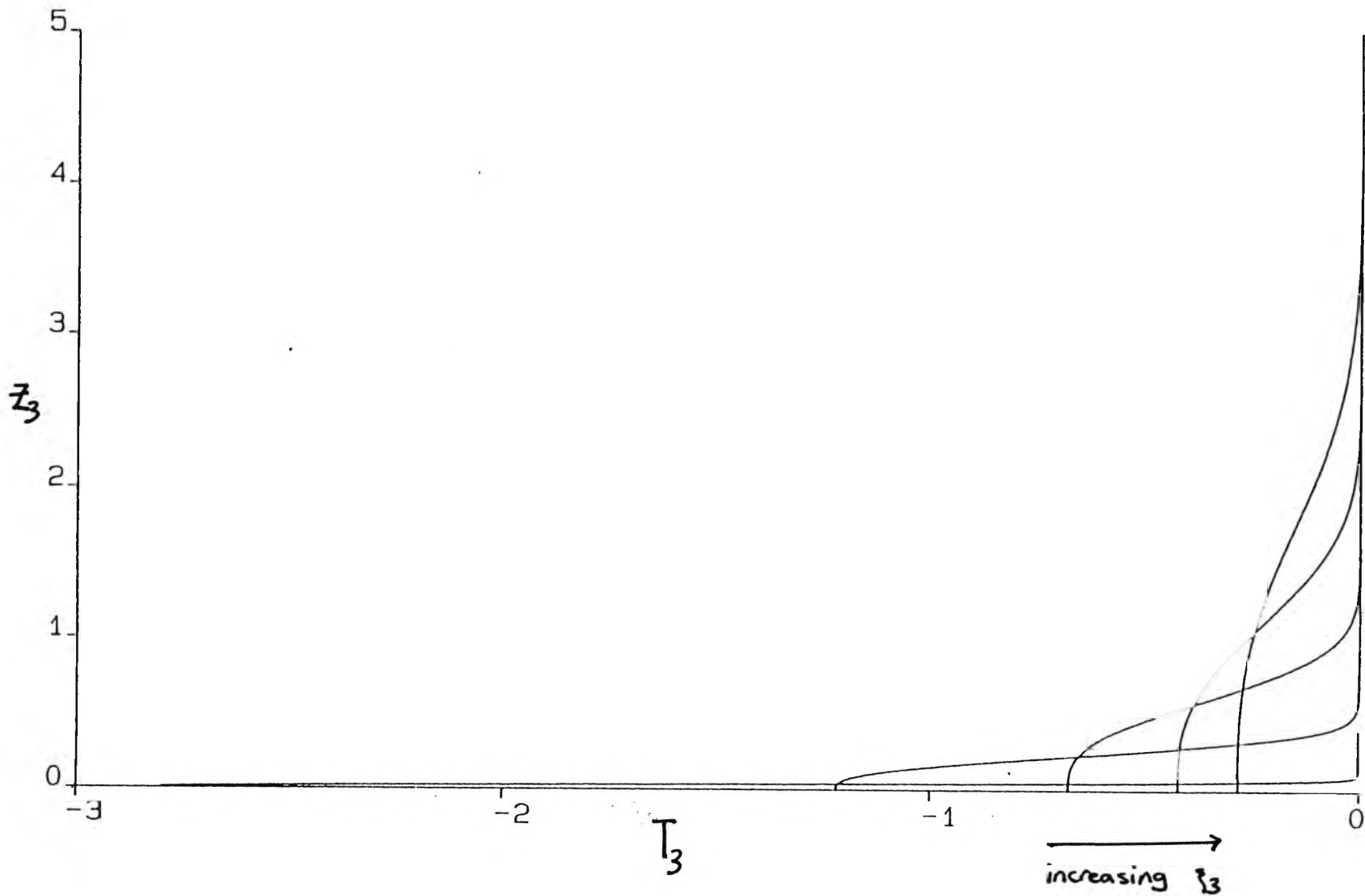


Figure 7.16 Graph of actual pressure at $\xi_3 = 0.2, 0.4, 0.6, 0.8, 1.0$ ($\epsilon = 3.50, \sigma = 0.72$).

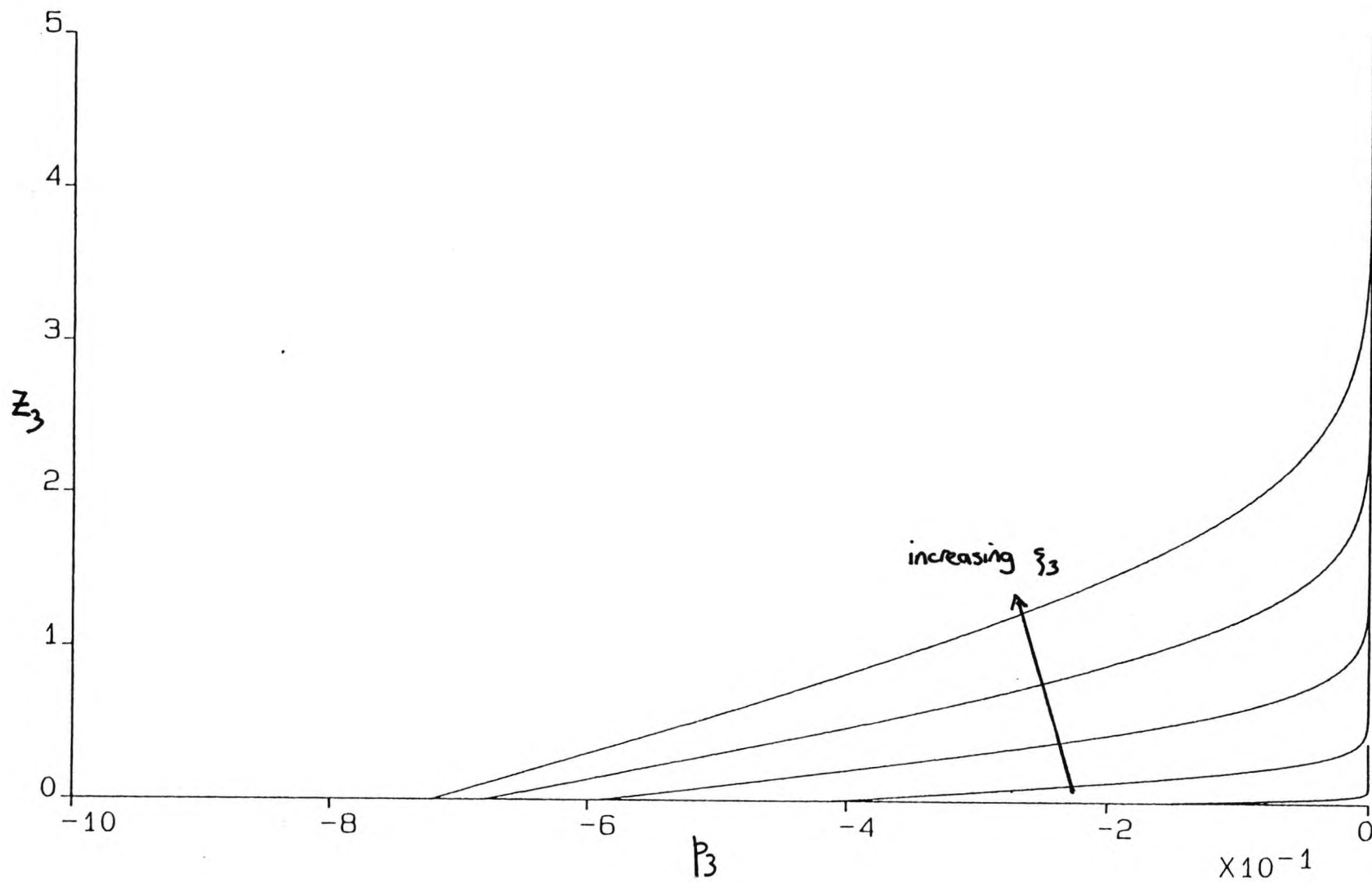


Figure 7.17 Graph of scaled velocity at $\hat{\xi}_3 = 1.2, 1.4, 1.6, 1.8, 2.0$ ($\epsilon = 4, \sigma = 0.72$).

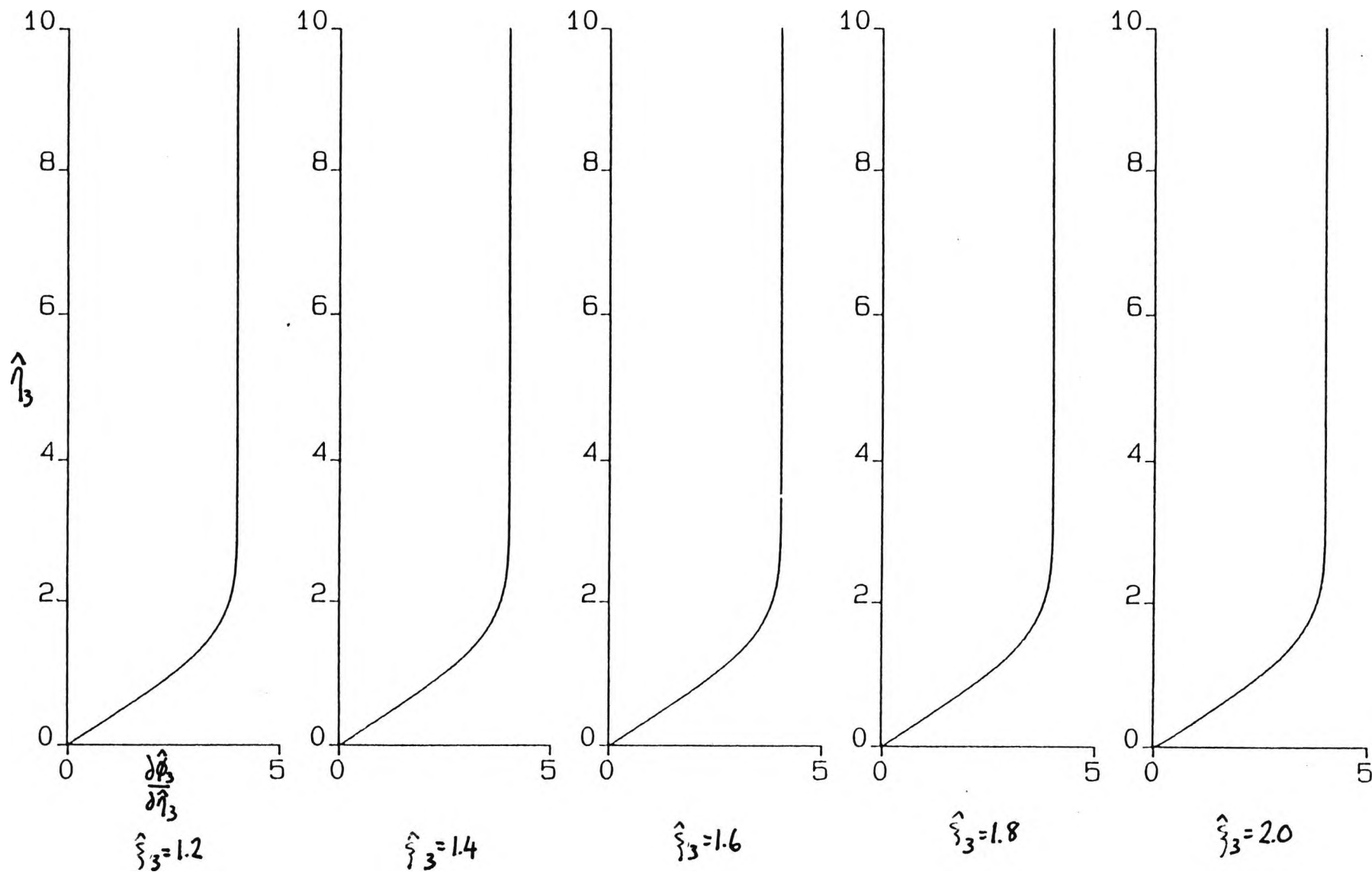


Figure 7.18 Graph of scaled temperature at $\hat{\xi}_3 = 1.2, 1.4, 1.6, 1.8, 2.0$ ($\epsilon = 4, \sigma = 0.72$).

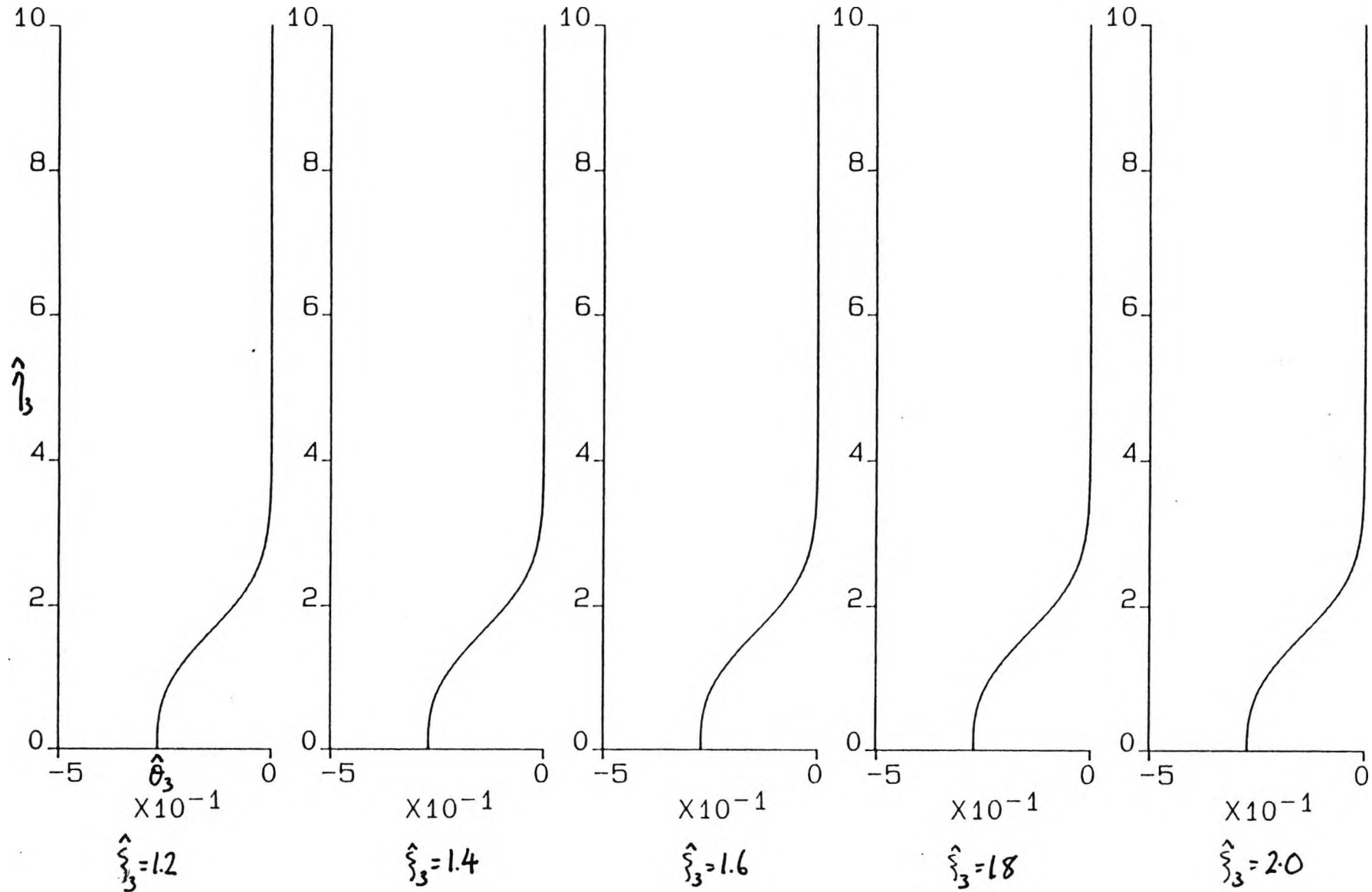


Figure 7.19 Graph of scaled pressure at $\hat{\xi}_3 = 1.2, 1.4, 1.6, 1.8, 2.0$ ($\epsilon = 4, \sigma = 0.72$).

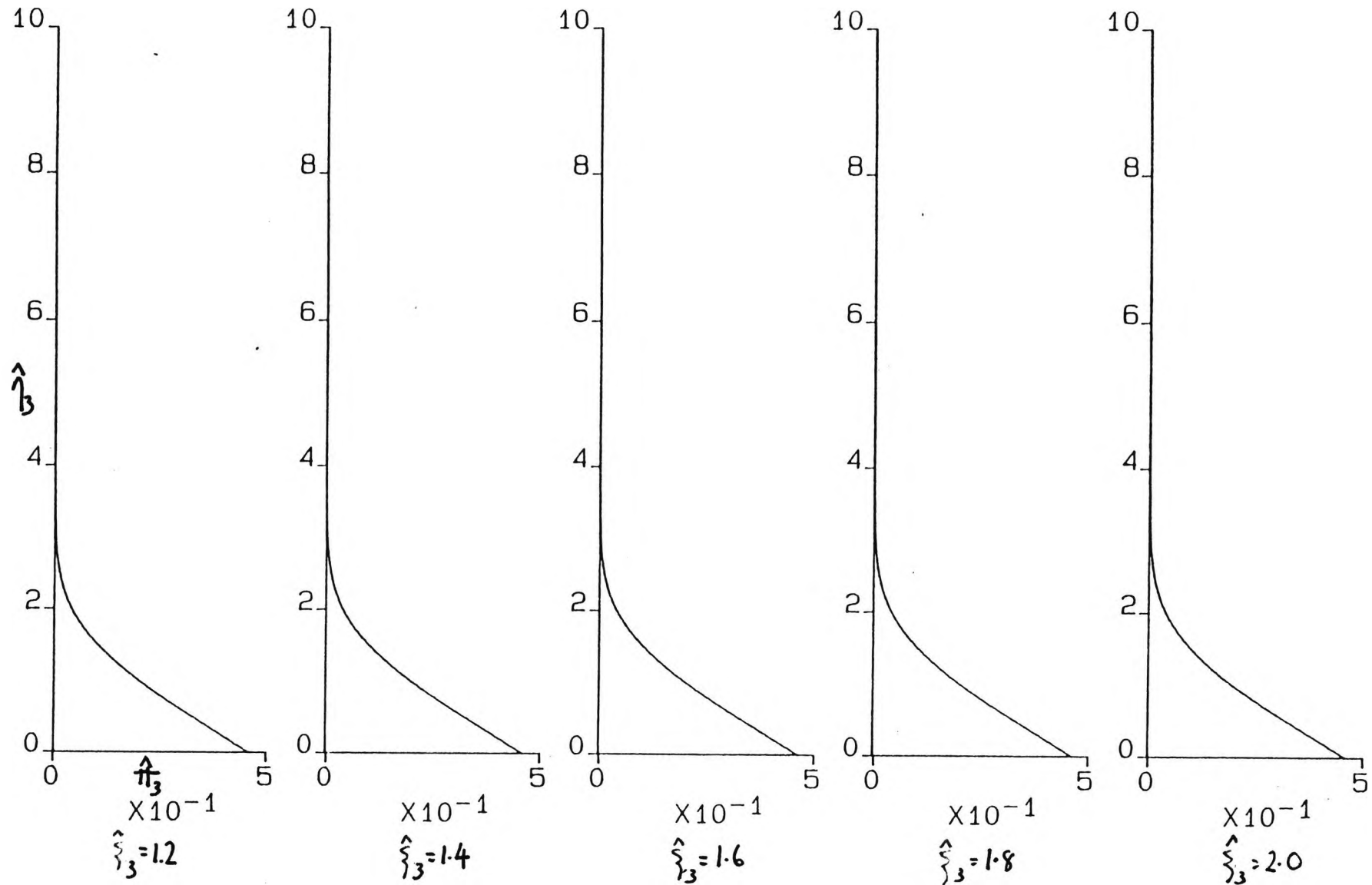


Figure 7.20 Graph of actual velocity at $\hat{\xi}_3 = 1.2, 1.4, 1.6, 1.8, 2.0$ ($\epsilon = 4, \sigma = 0.72$).

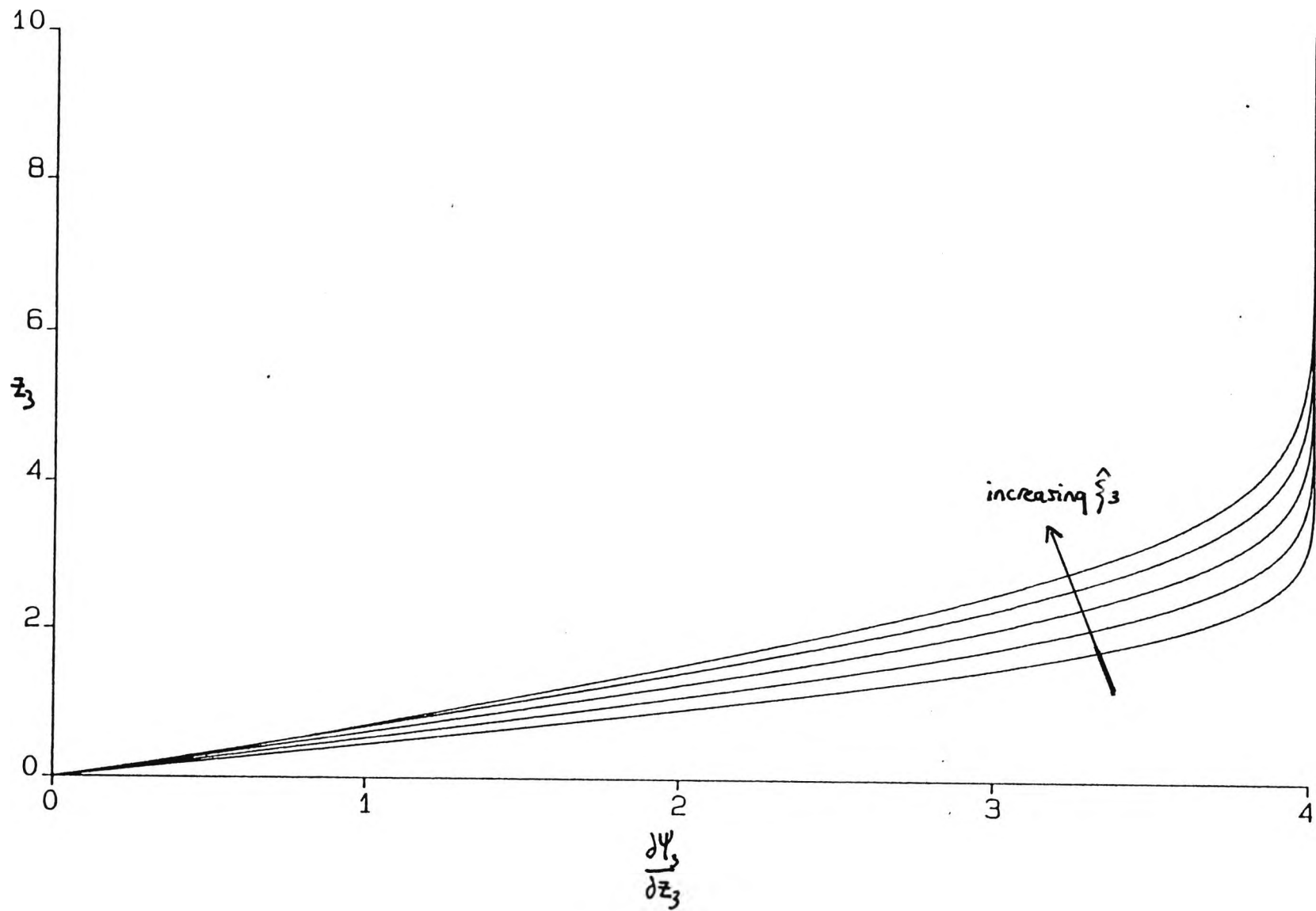


Figure 7.21 Graph of actual temperature at $\hat{\xi}_3 = 1.2, 1.4, 1.6, 1.8, 2.0$ ($\epsilon = 4, \sigma = 0.72$).

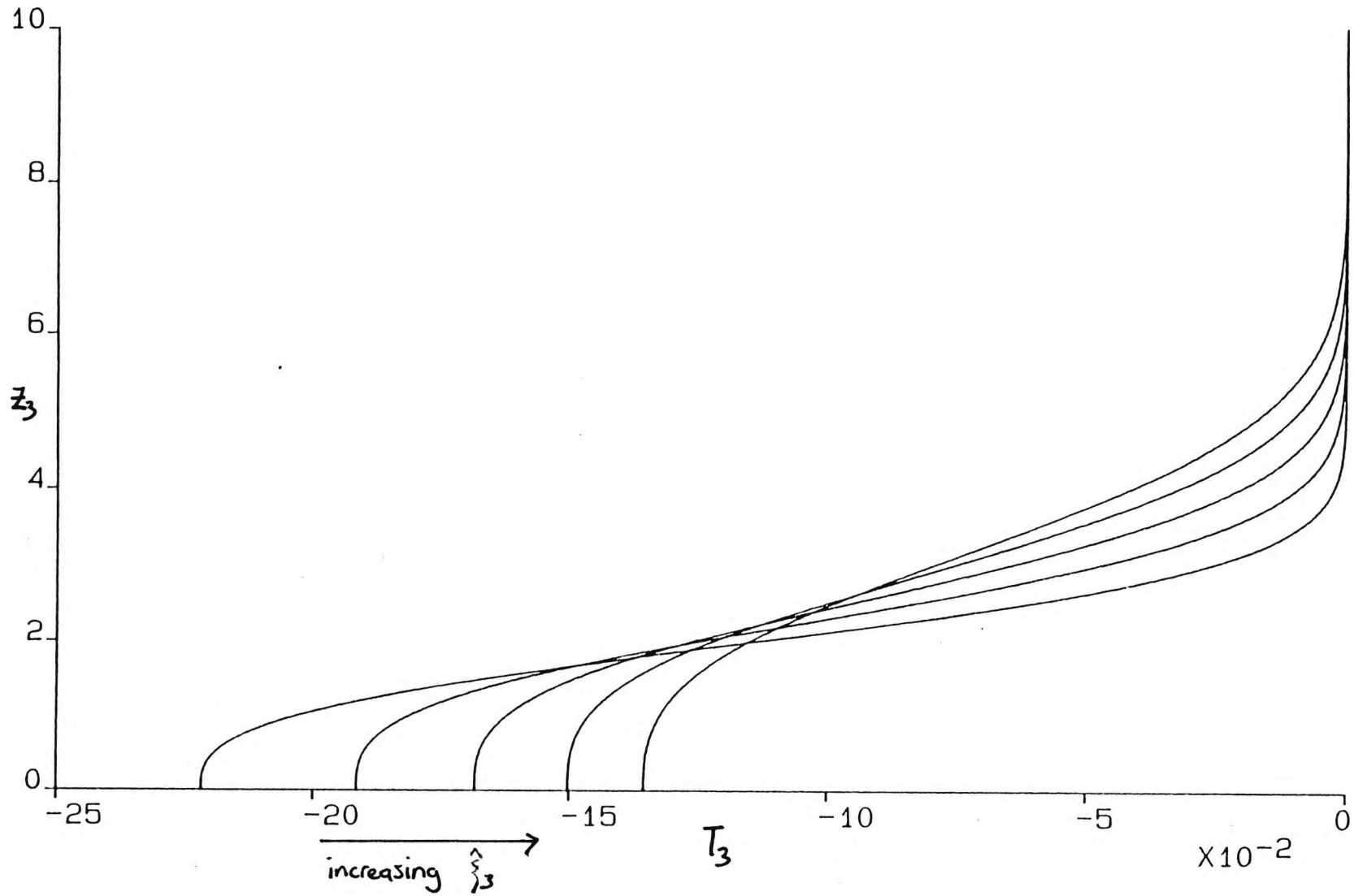


Figure 7.22 Graph of actual pressure at $\hat{\xi}_3 = 1.2, 1.4, 1.6, 1.8, 2.0$ ($\epsilon = 4, \sigma = 0.72$).

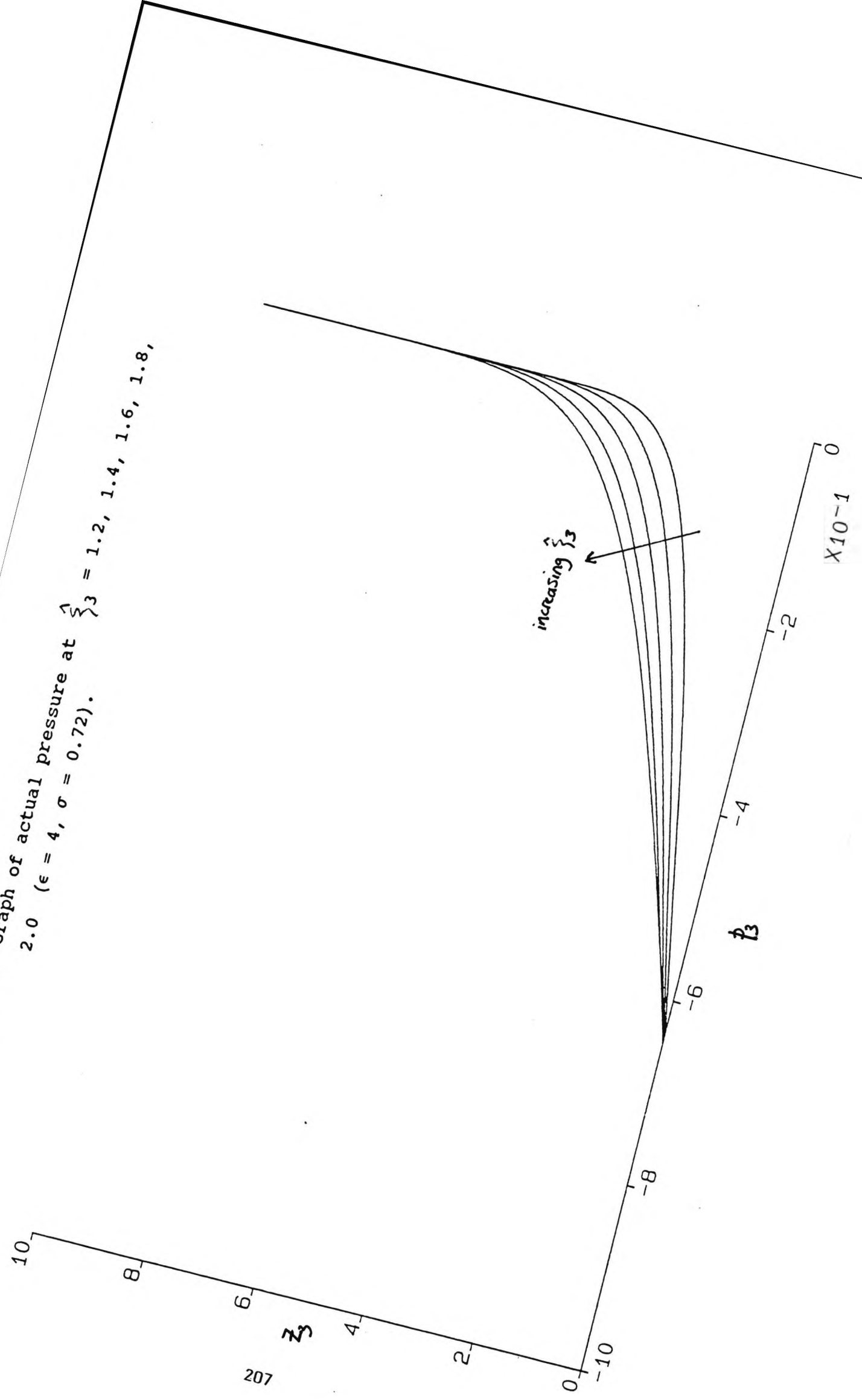


Figure 7.23 Graph of scaled velocity at $\xi_3 = 0.2, 0.4, 0.6, 0.8, 1.0$ ($\epsilon = 3, \sigma = 8.1$).

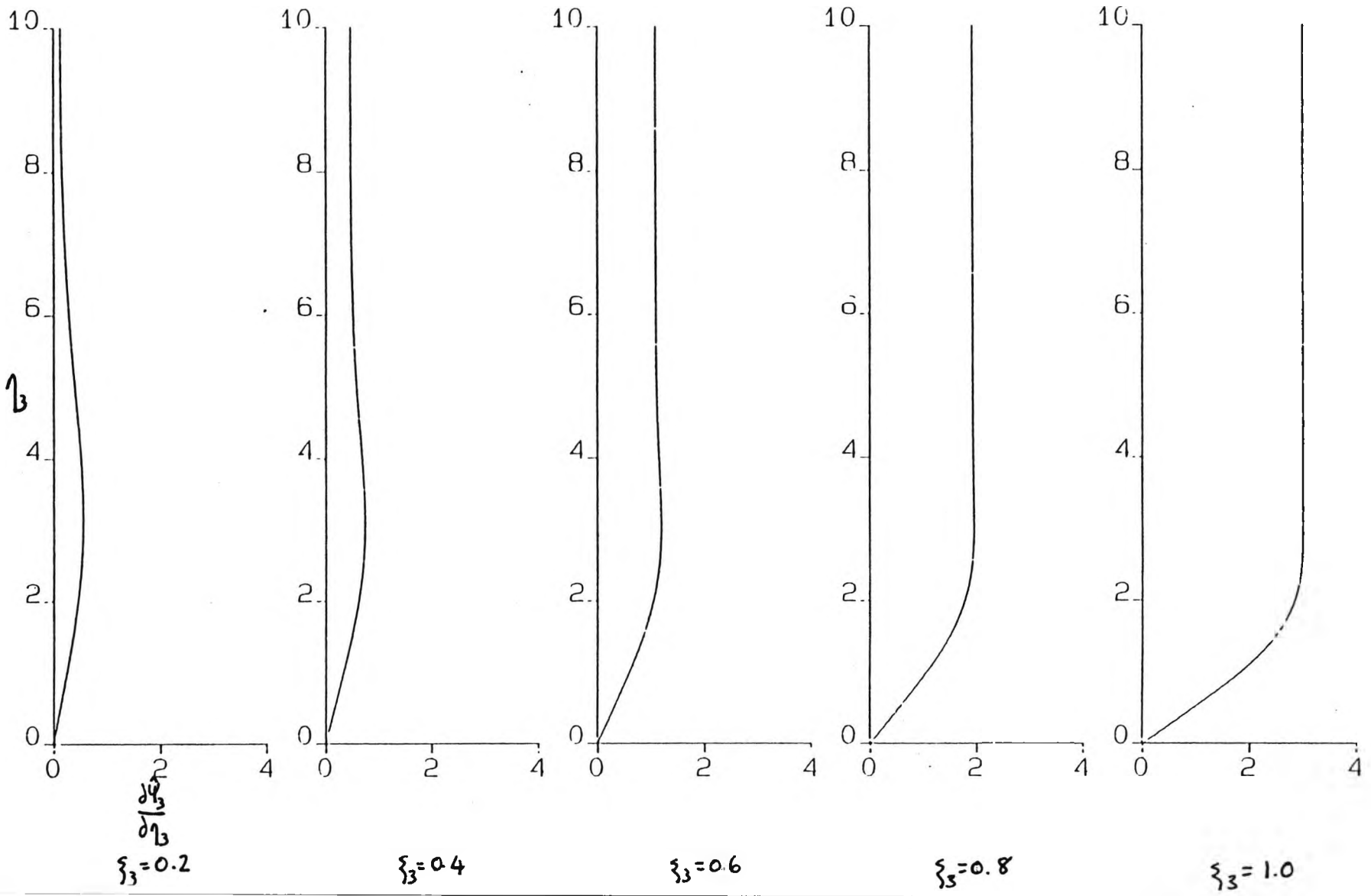


Figure 7.24 Graph of scaled temperature at $\xi_3 = 0.2, 0.4, 0.6, 0.8, 1.0$ ($\epsilon = 3, \sigma = 8.1$).

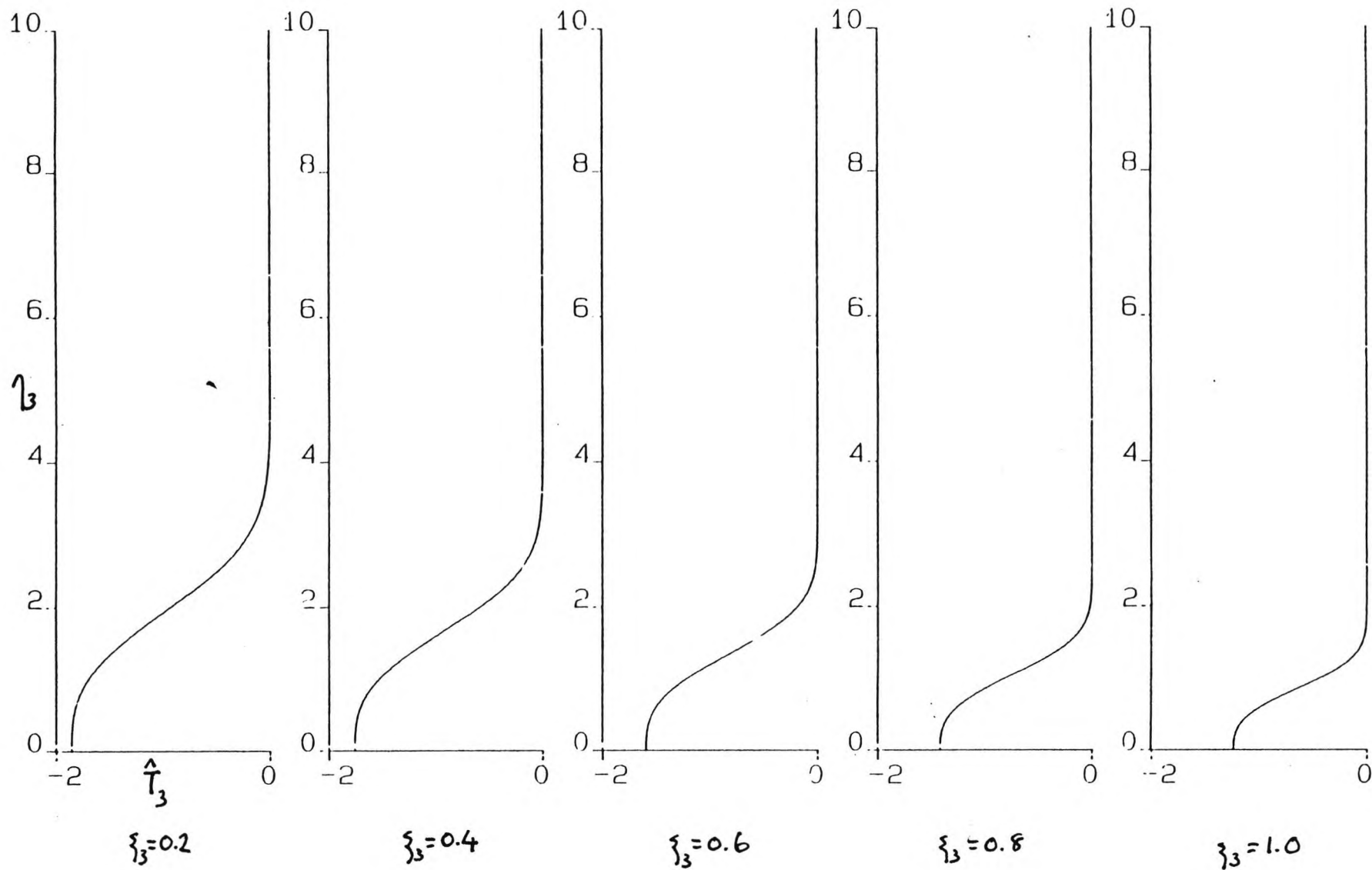


Figure 7.25 Graph of scaled pressure at $\xi_3 = 0.2, 0.4, 0.6, 0.8, 1.0$ ($\epsilon = 3, \sigma = 8.1$).

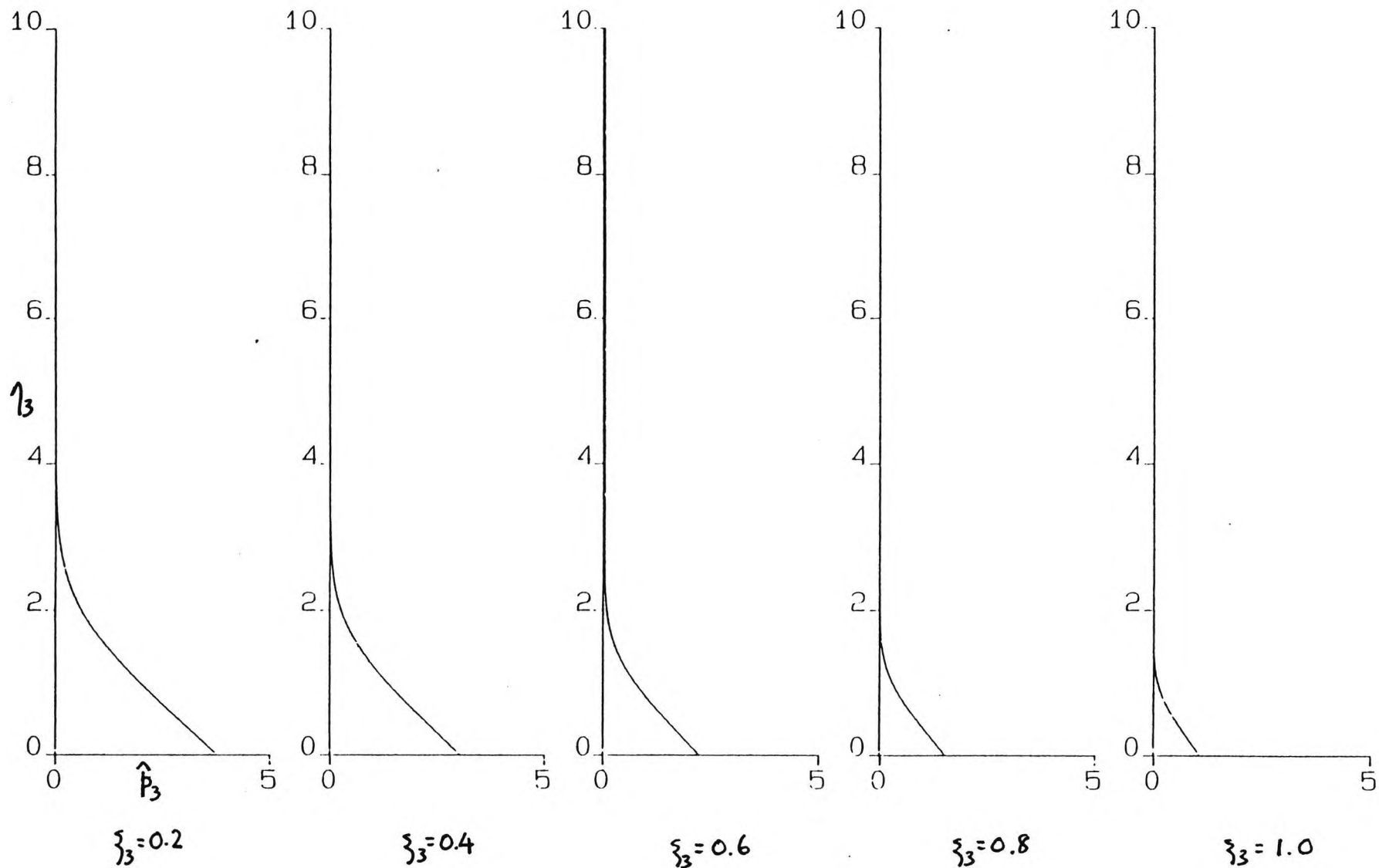


Figure 7.26 Graph of scaled velocity at $\hat{\xi}_3 = 1.2, 1.4, 1.6, 1.8, 2.0$ ($\epsilon = 3, \sigma = 8.1$).

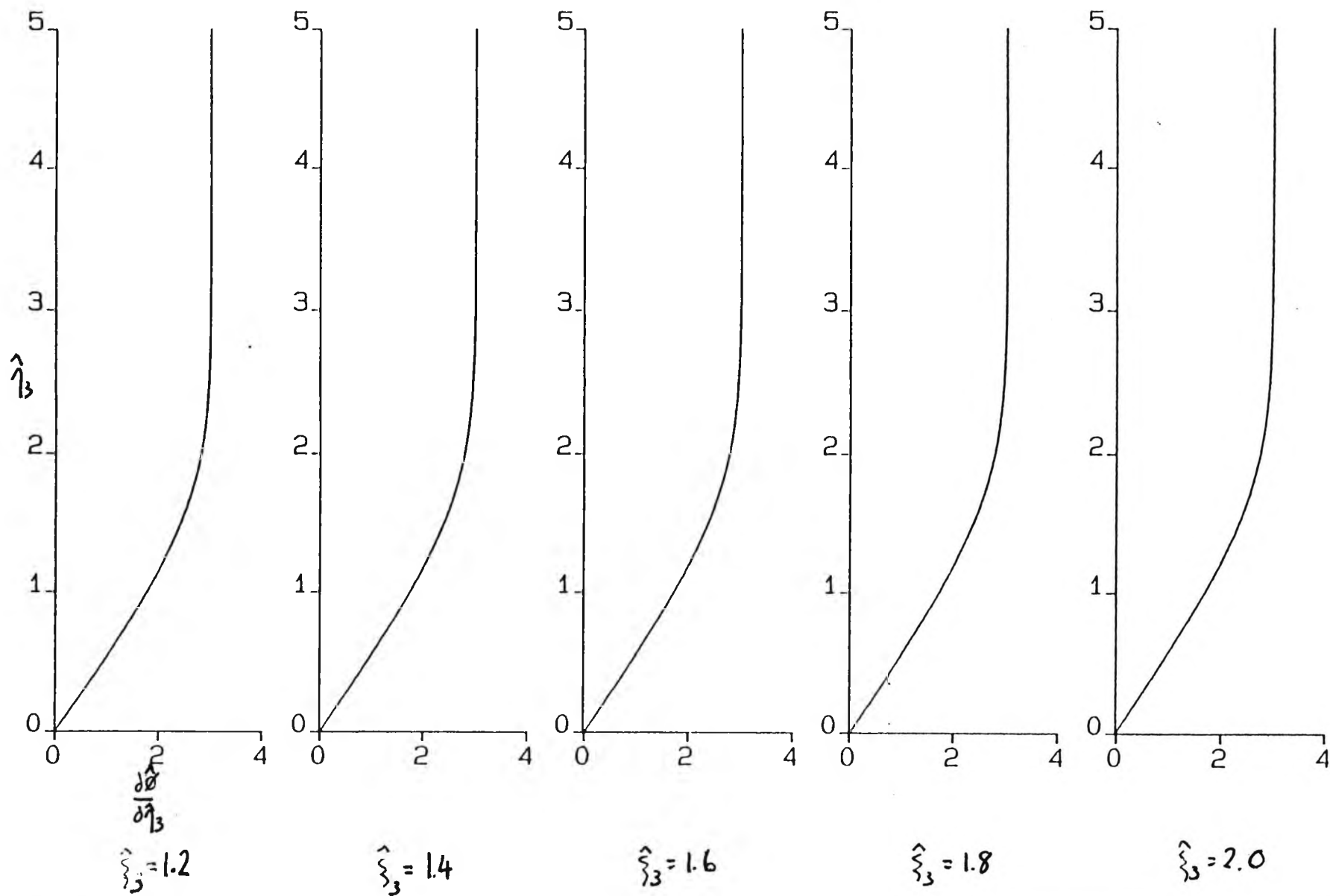


Figure 7.27 Graph of scaled temperature at $\hat{\xi}_3 = 1.2, 1.4, 1.6, 1.8, 2.0$ ($\epsilon = 3, \sigma = 8.1$).

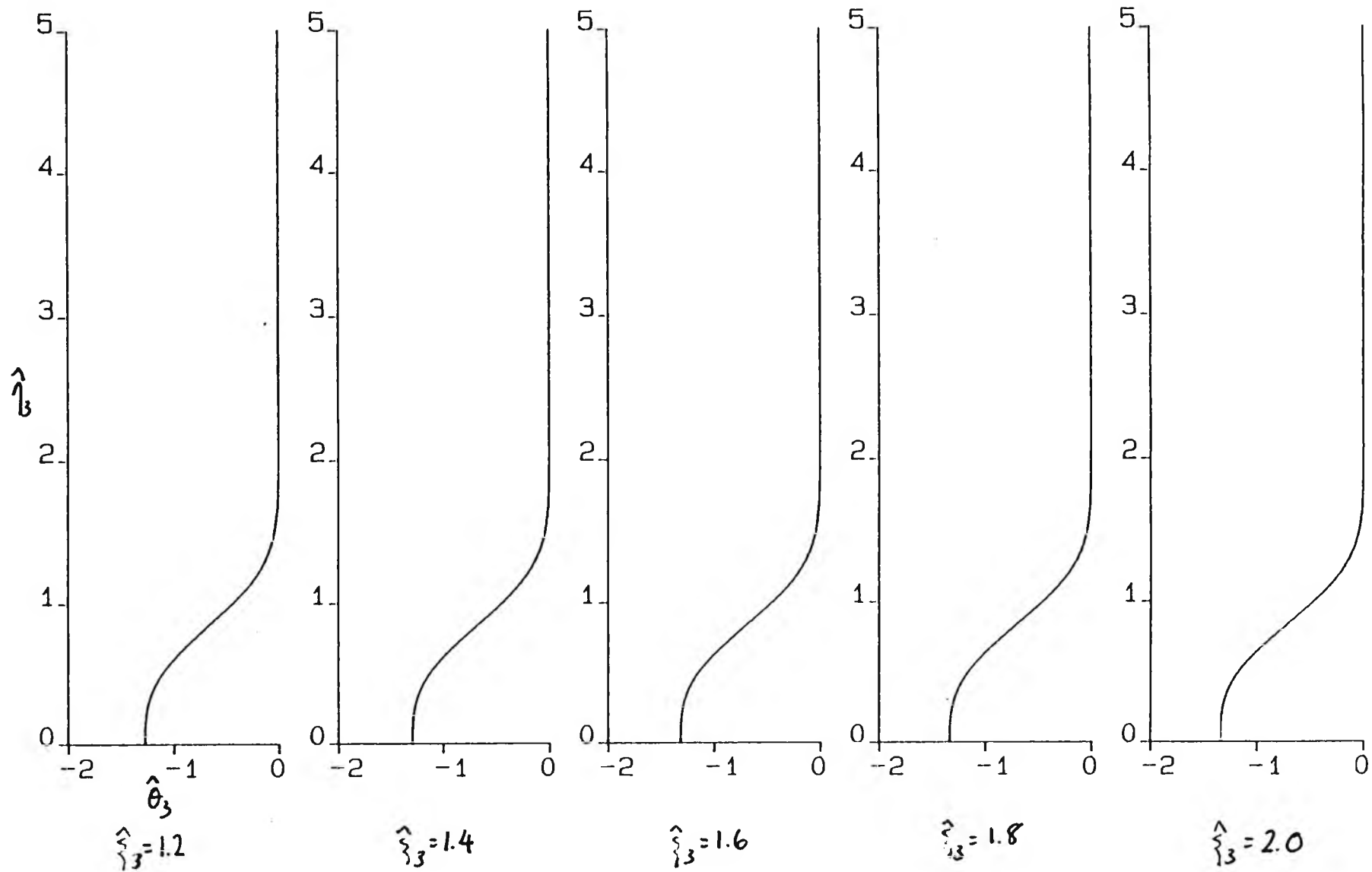


Figure 7.28 Graph of scaled pressure at $\hat{\xi}_3 = 1.2, 1.4, 1.6, 1.8, 2.0$ ($\epsilon = 3, \sigma = 8.1$).

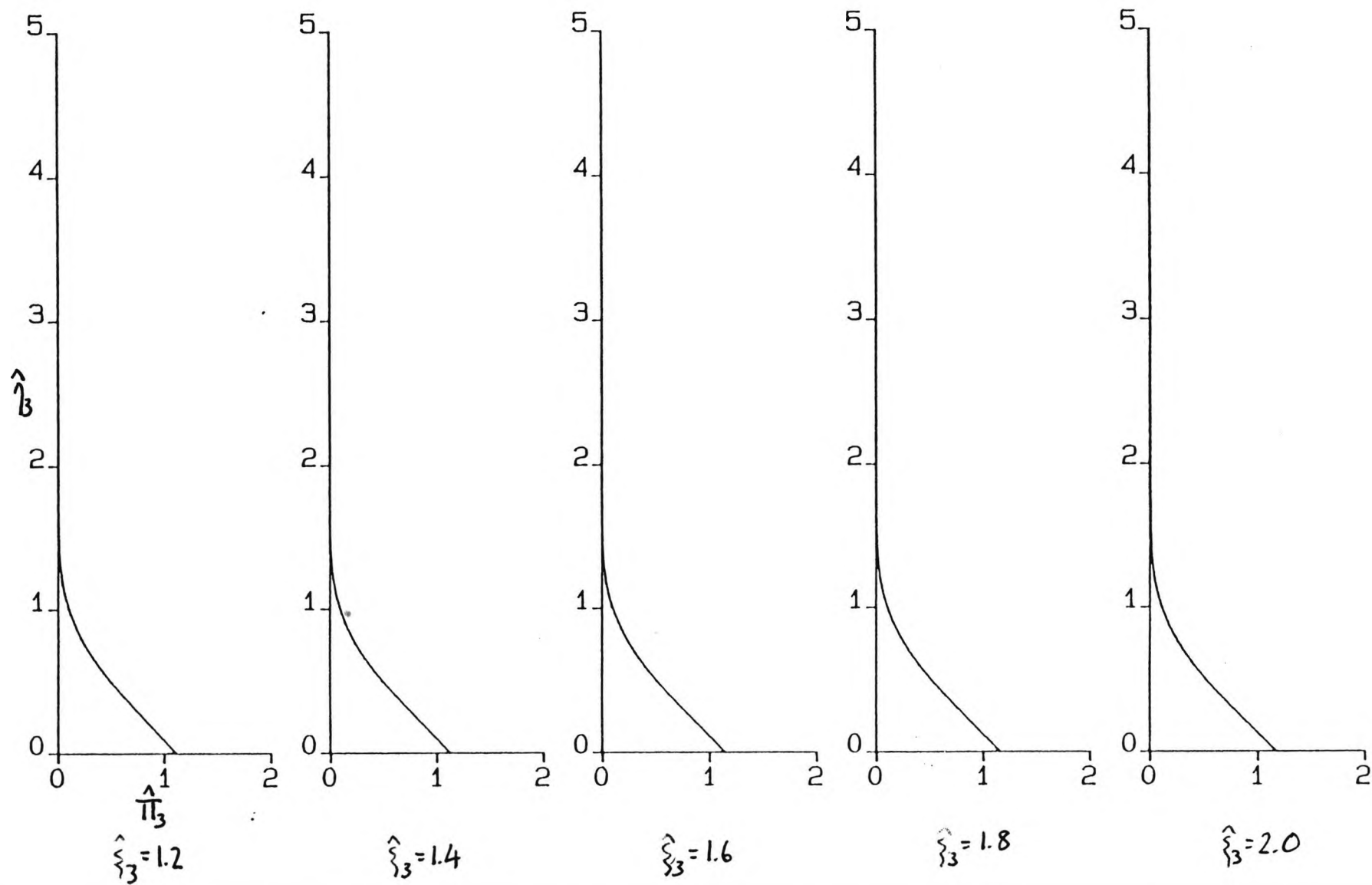


Figure 7.29 Graph of actual velocity at $\hat{\xi}_3 = 1.2, 1.4, 1.6, 1.8, 2.0$ ($\epsilon = 3, \sigma = 8.1$).

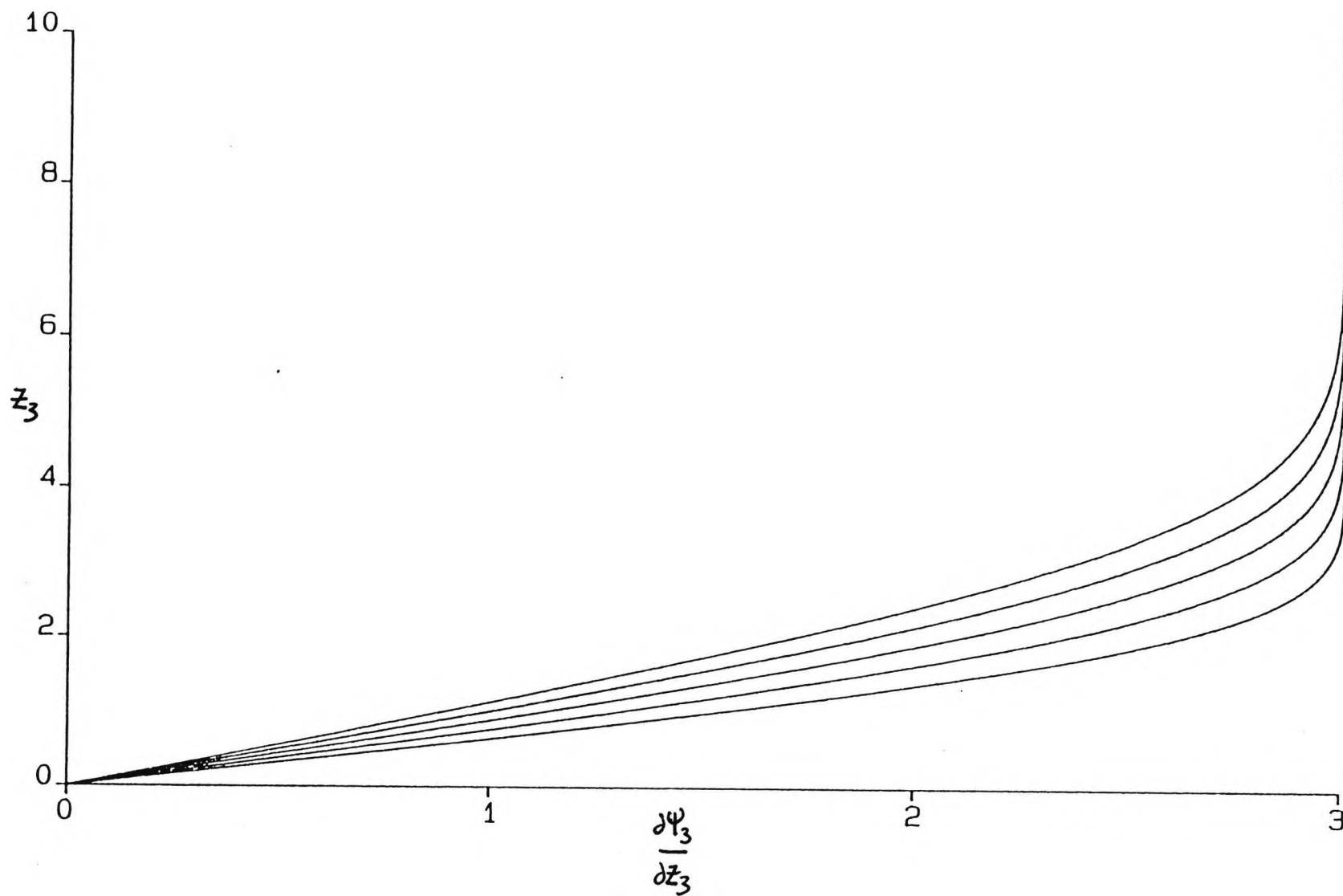


Figure 7.30 Graph of actual temperature at $\hat{\xi}_3 = 1.2, 1.4, 1.6, 1.8, 2.0$ ($\epsilon = 3, \sigma = 8.1$).

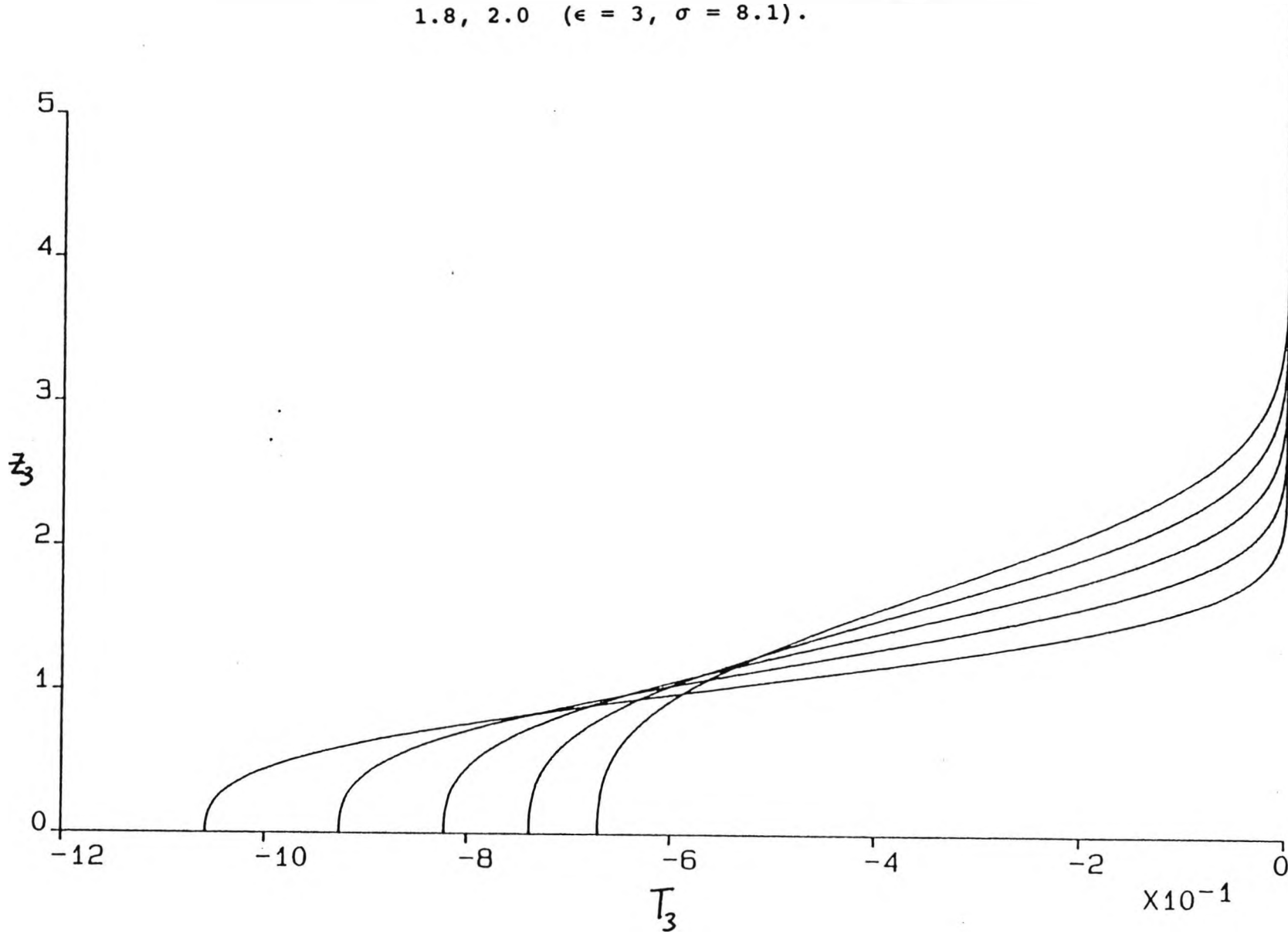
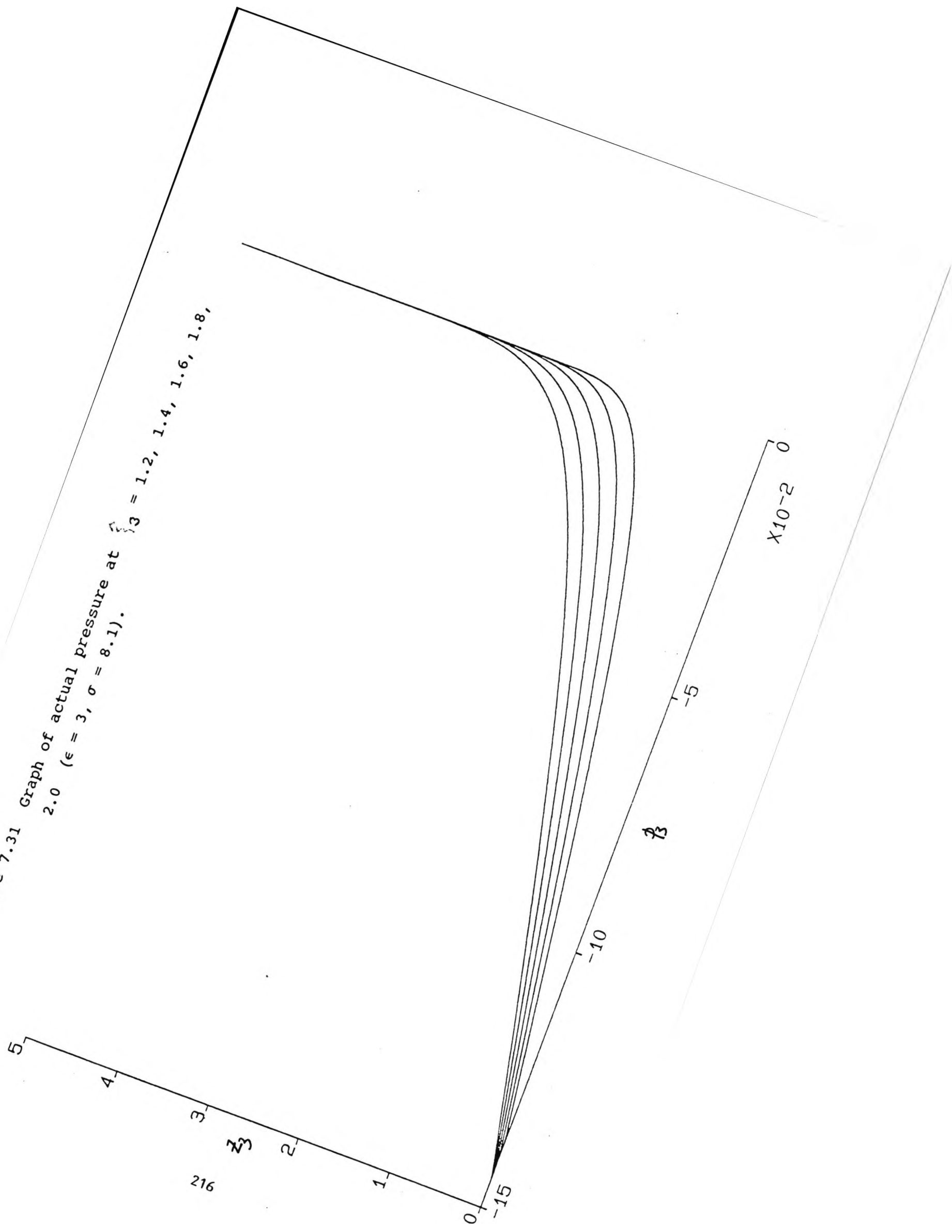


Figure 7.31 Graph of actual pressure at $\beta = 1.2, 1.4, 1.6, 1.8,$
 2.0 ($\epsilon = 3, \sigma = 8.1$).



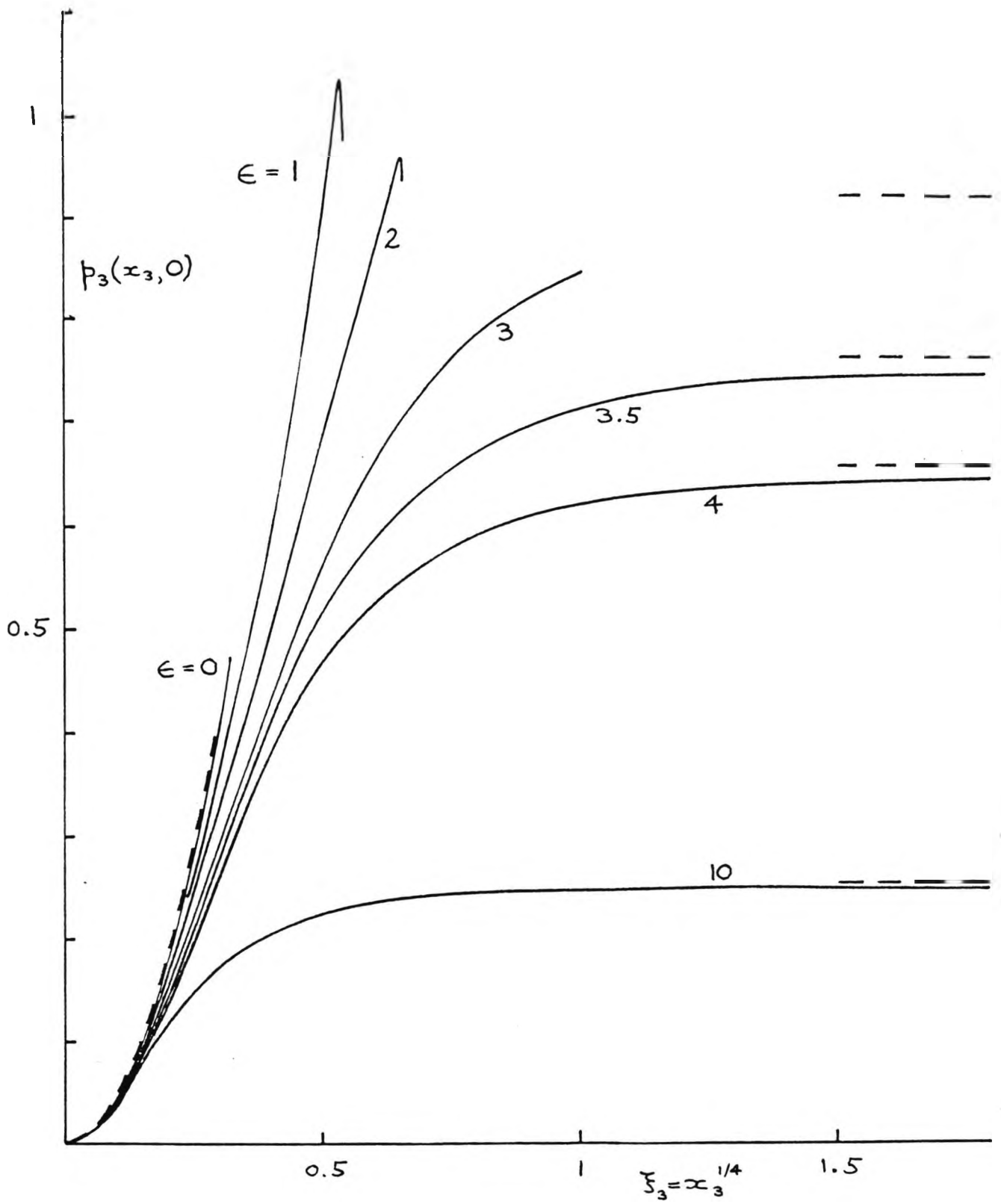


Figure 7.32 Graph of Wall Pressure against ξ_3 for various ϵ .

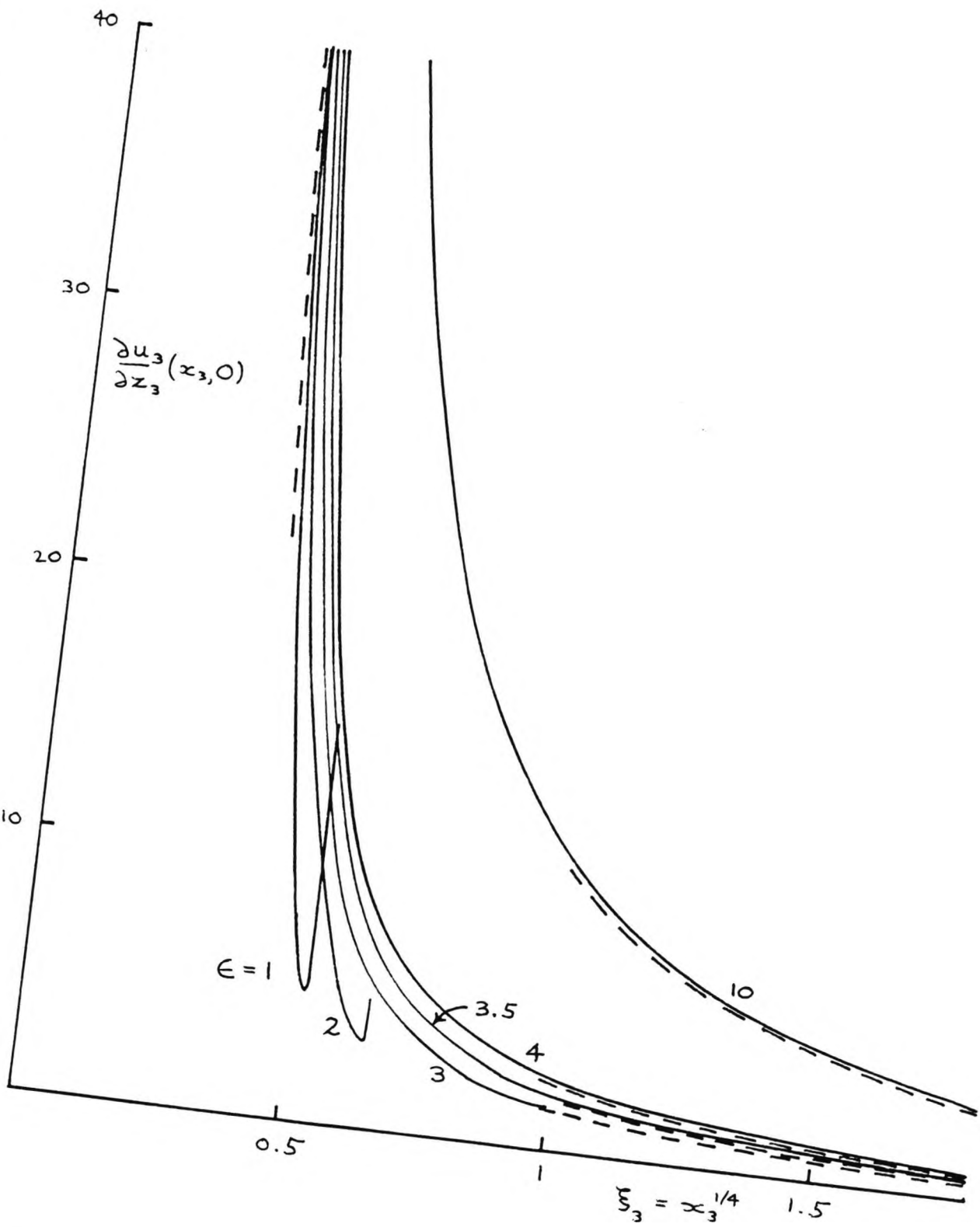


Figure 7.33 Graph of Skin Friction against ξ_3 for various ϵ .

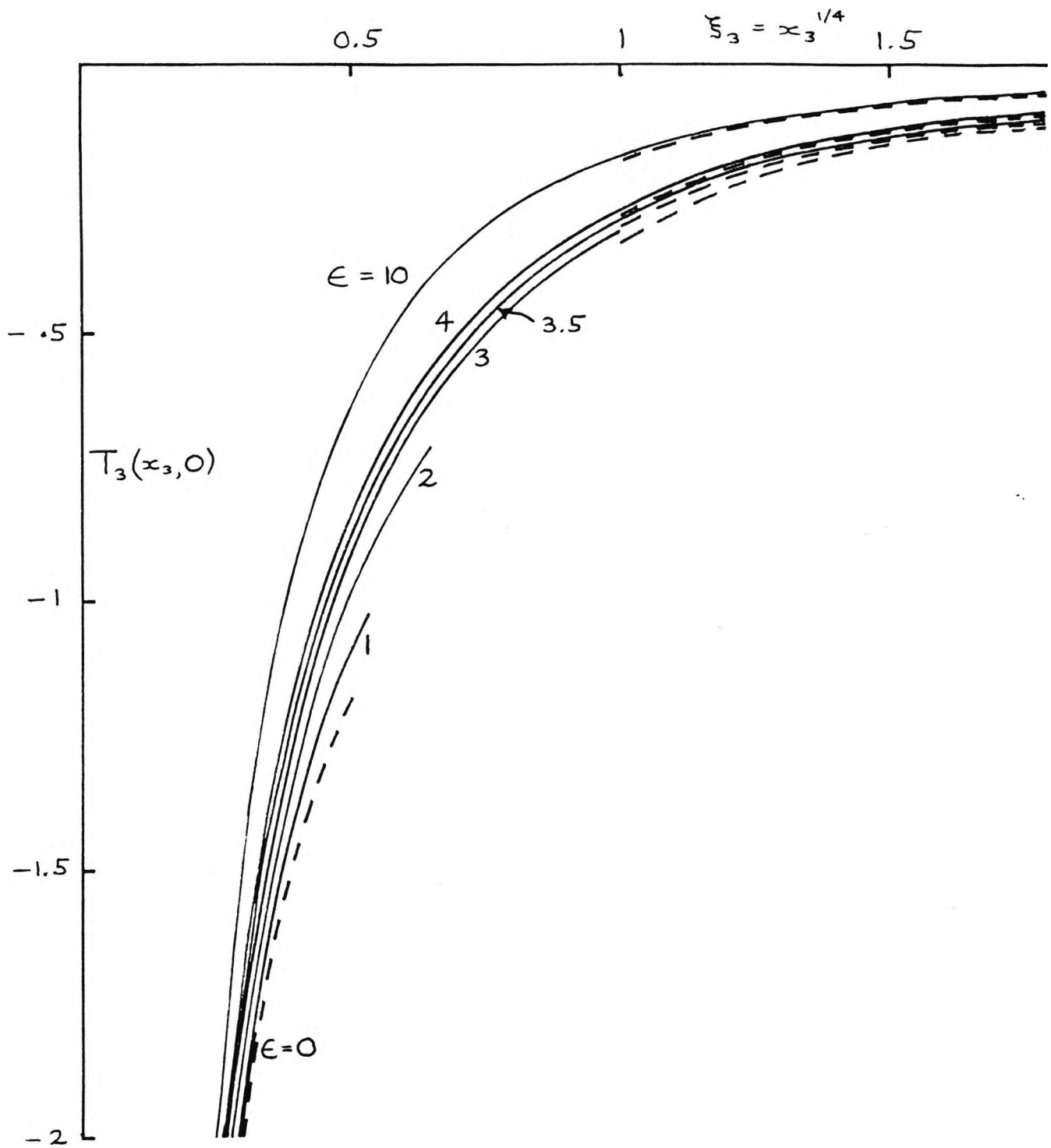


Figure 7.34 Graph of Wall Temperature against ξ_3 for various ϵ .

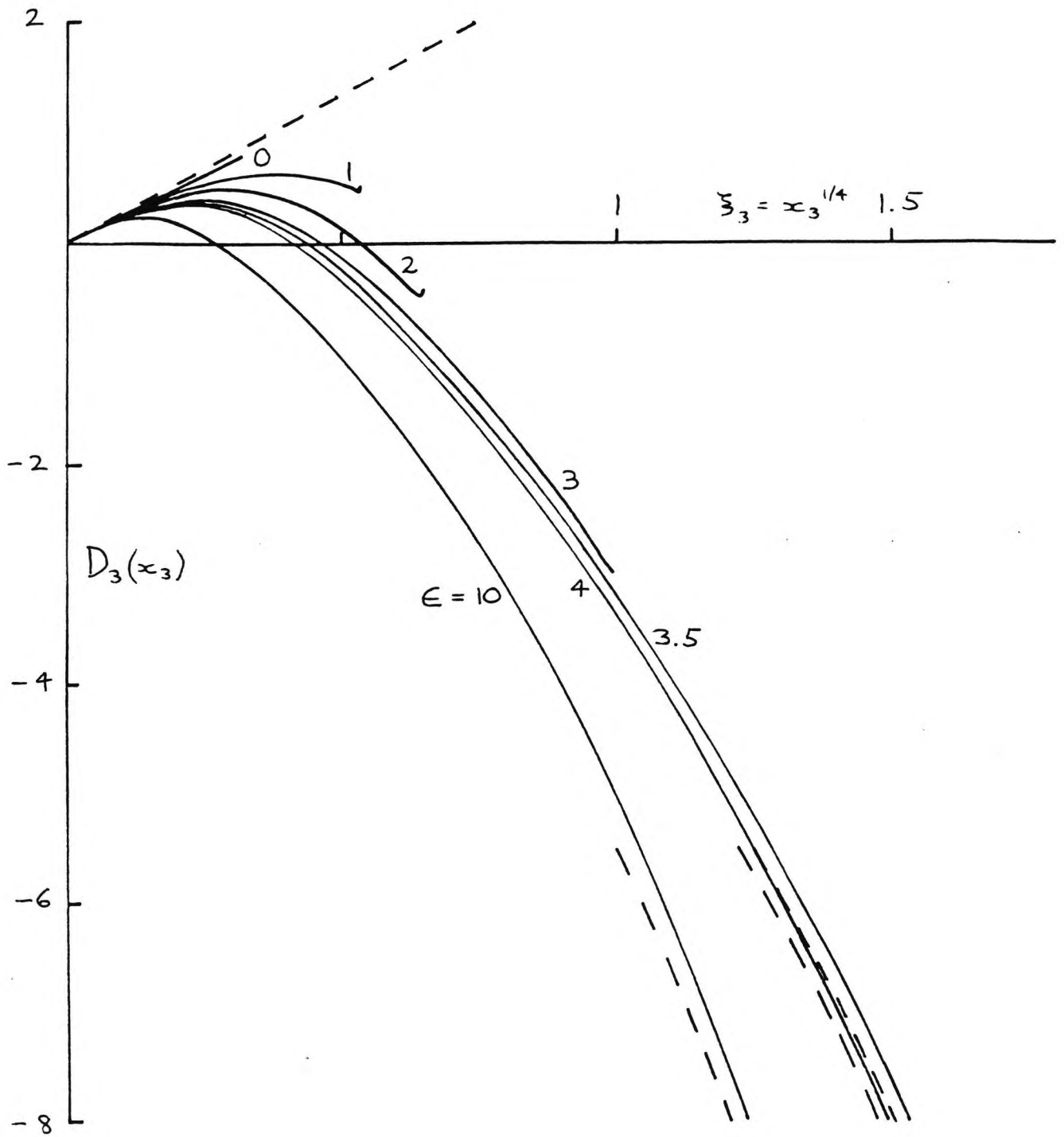


Figure 7.35 Graph of Displacement against ξ_3 for various ϵ .

Figure 7.36 Graph of scaled velocity at $\xi_3 = 0.2, 0.4, 0.6, 0.8, 1.0$ ($\epsilon = 10.0, \sigma = 0.72$).

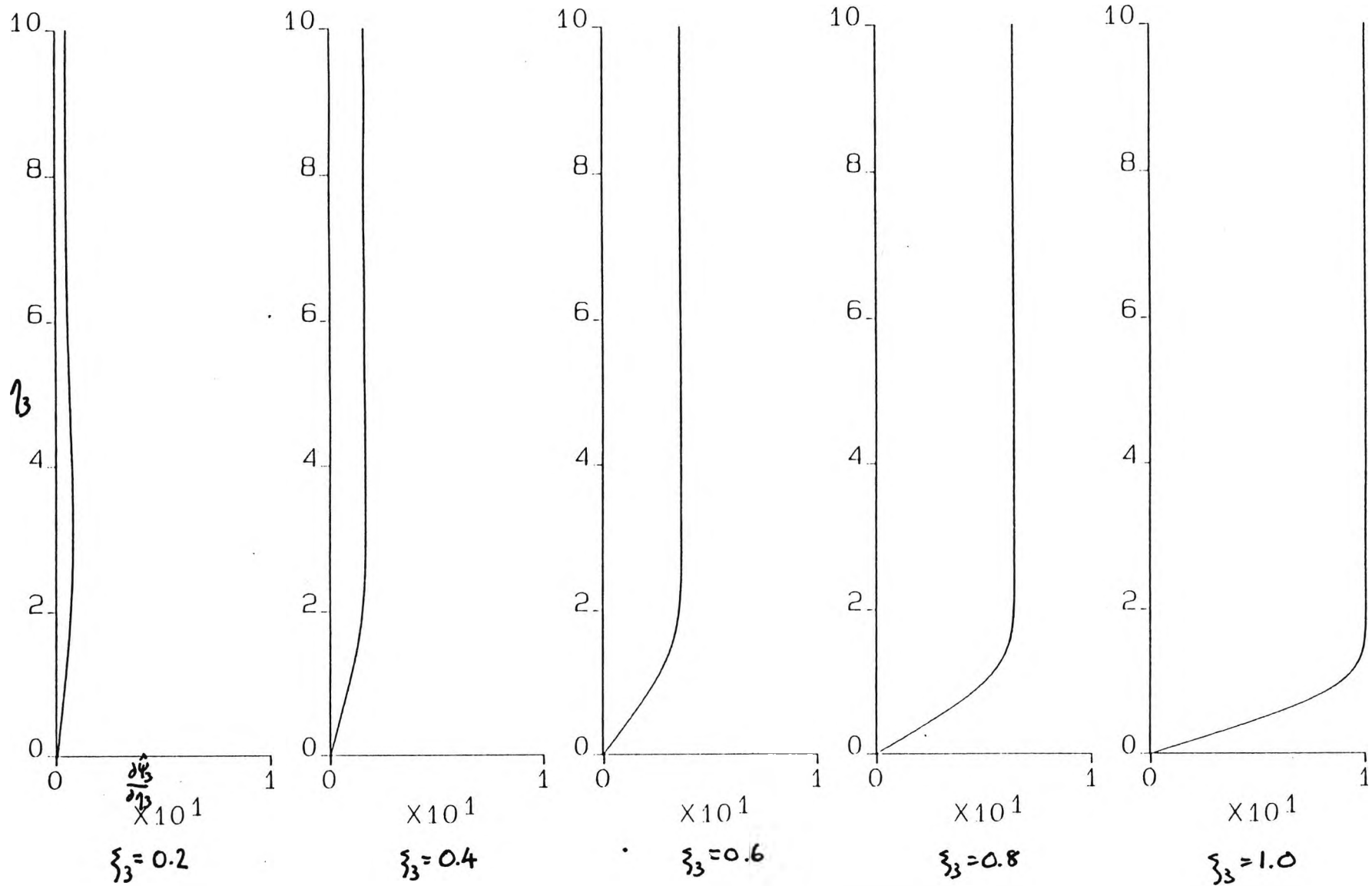


Figure 7.37 Graph of scaled velocity at $\hat{\xi}_3 = 1.2, 1.4, 1.6, 1.8, 2.0$ ($\epsilon = 10.0, \sigma = 0.72$).

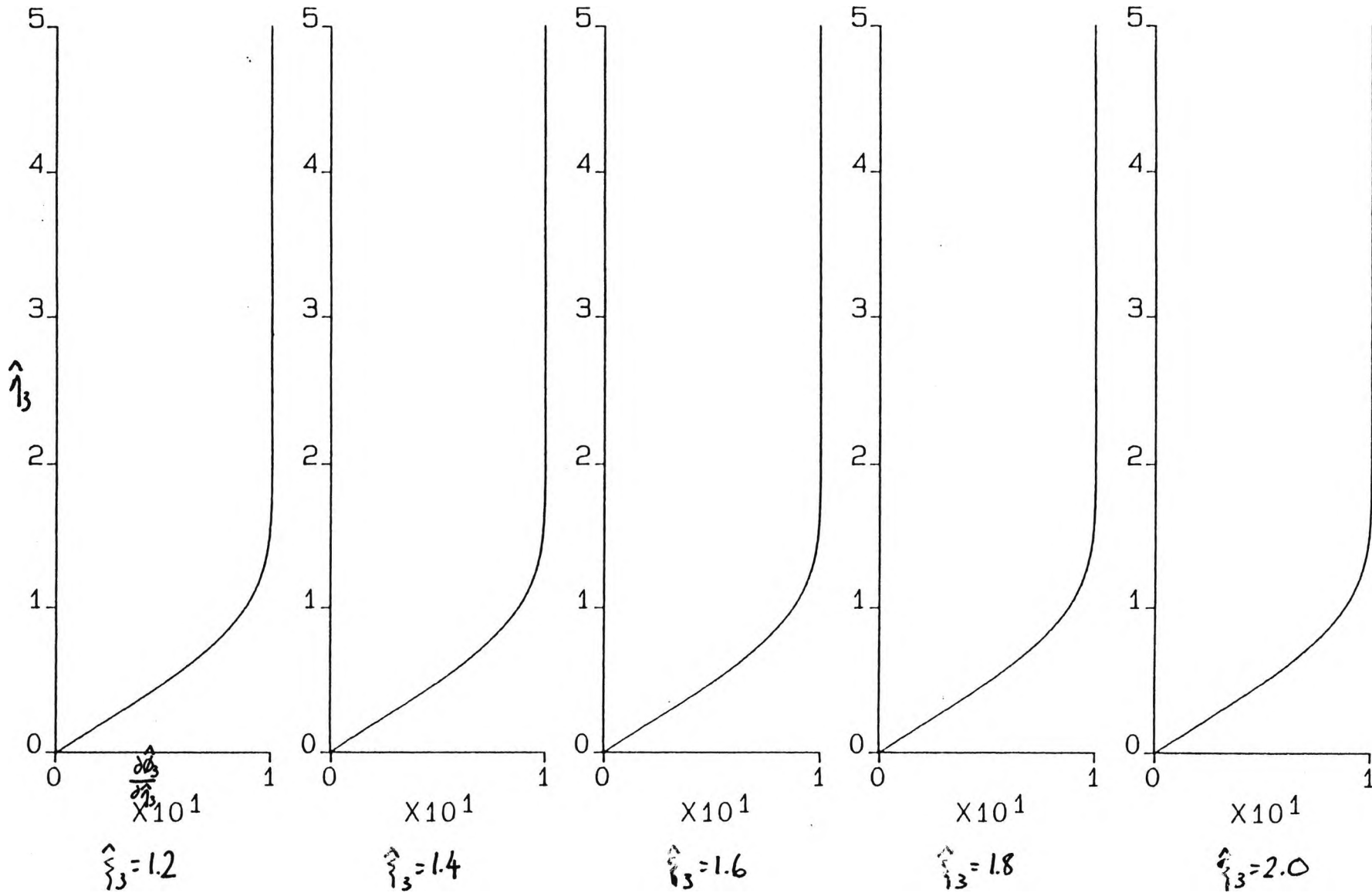


Figure 7.38 Graph of actual velocity at $\xi_3 = 0.2, 0.4, 0.6, 0.8, 1.0$ ($\epsilon = 10.0, \sigma = 0.72$).

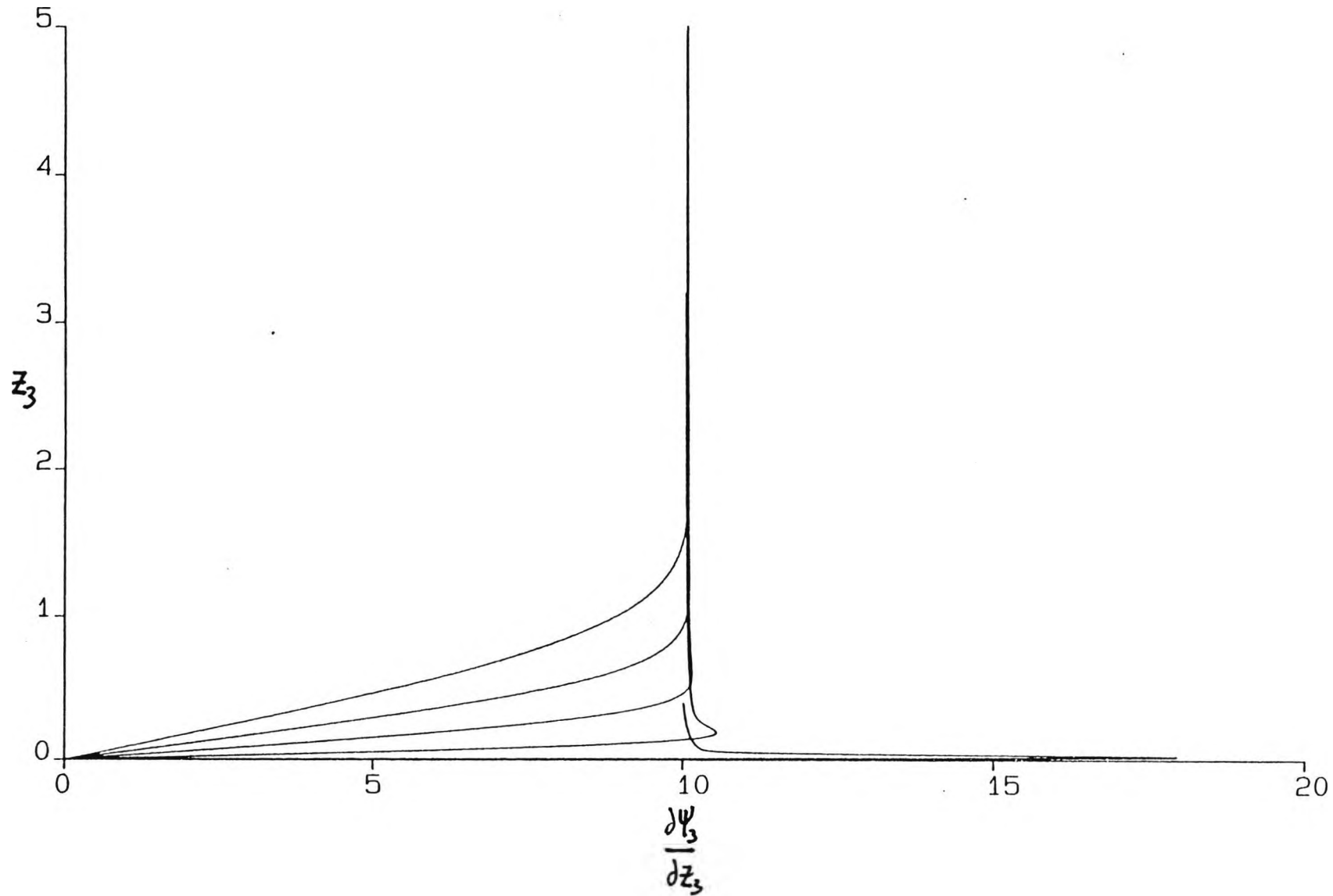


Figure 7.39 Graph of actual velocity at $\lambda_3 = 1.2, 1.4, 1.6, 1.8, 2.0$ ($\epsilon = 10.0, \sigma = 0.72$).

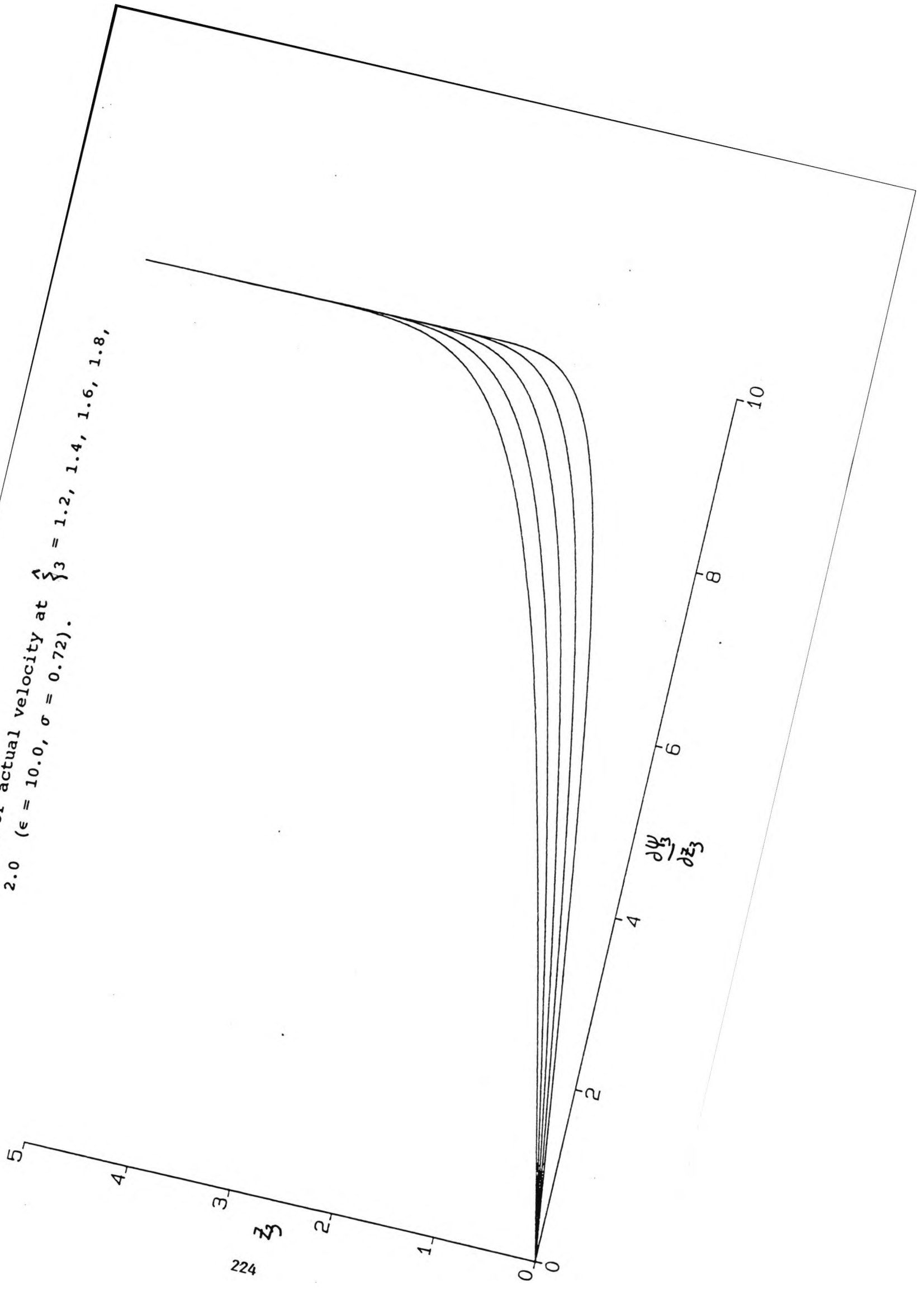


Figure 7.40 Graph of scaled temperature at $\xi_3 = 0.2, 0.4, 0.6, 0.8, 1.0$ ($\epsilon = 10.0, \sigma = 0.72$).

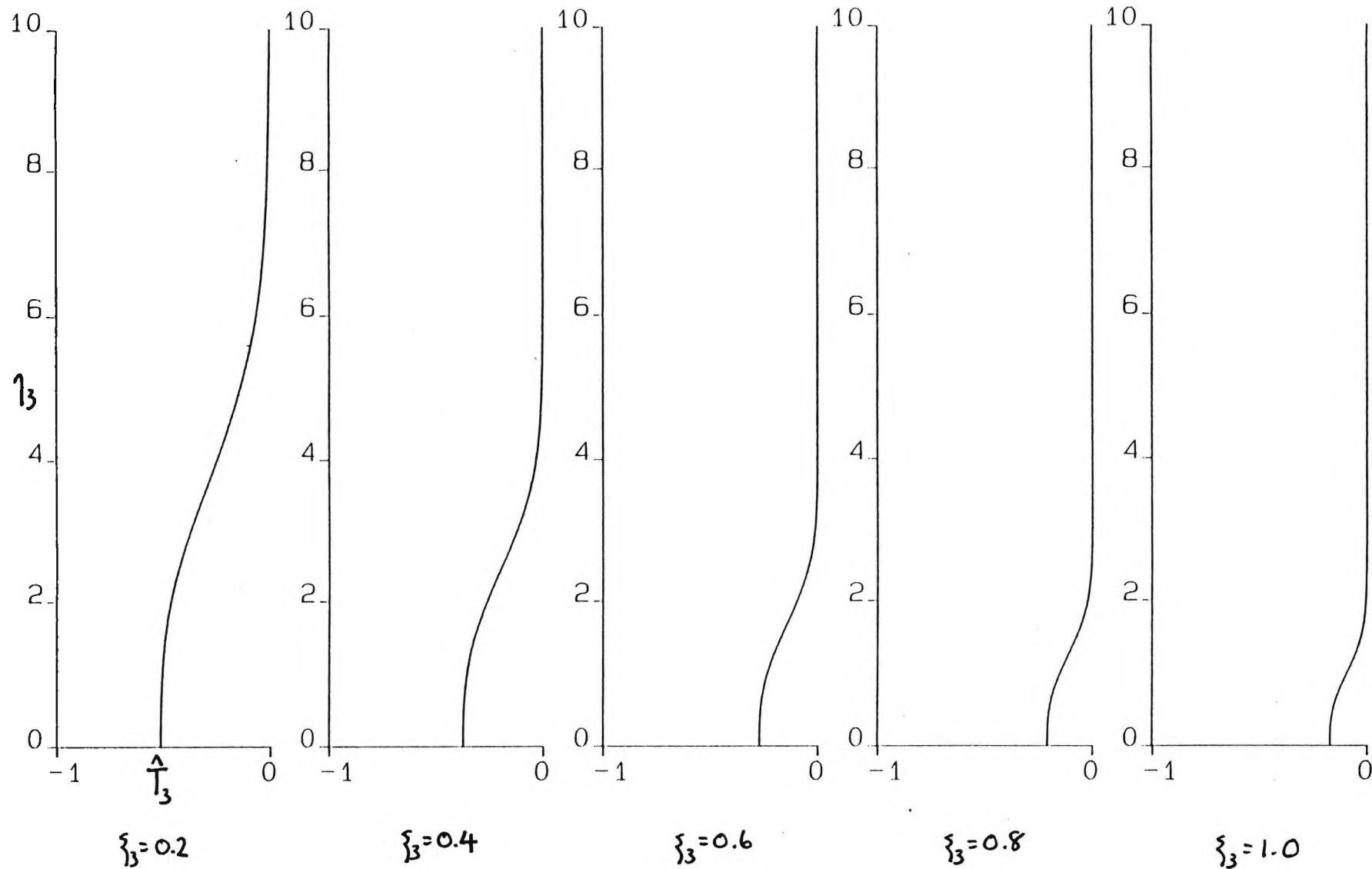


Figure 7.41 Graph of scaled temperature at $\hat{\xi}_3 = 1.2, 1.4, 1.6, 1.8, 2.0$ ($\epsilon = 10.0, \sigma = 0.72$).

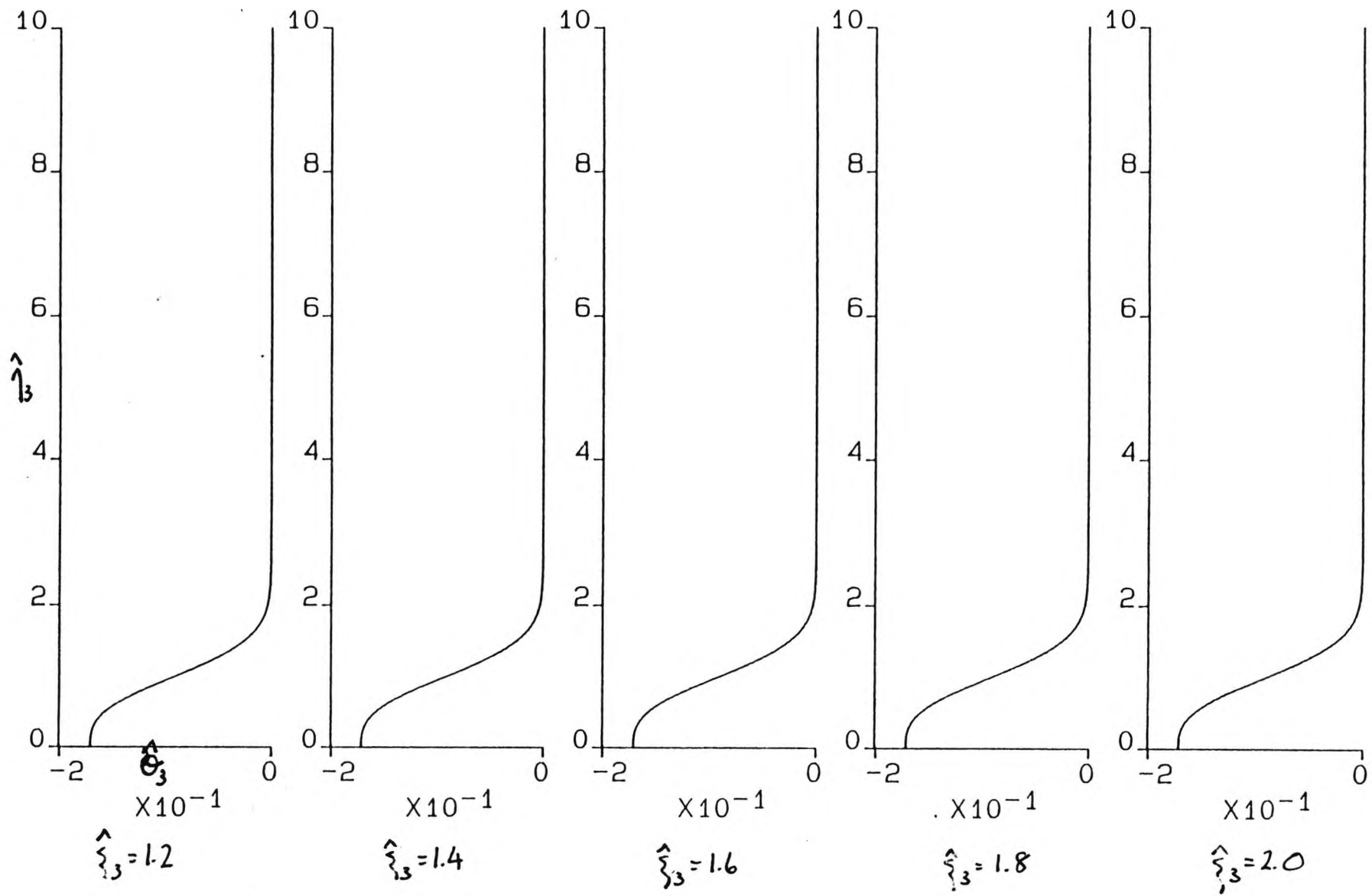


Figure 7.42 Graph of actual temperature at $\xi_3 = 0.2, 0.4, 0.6, 0.8, 1.0$ ($\epsilon = 10.0, \sigma = 0.72$).

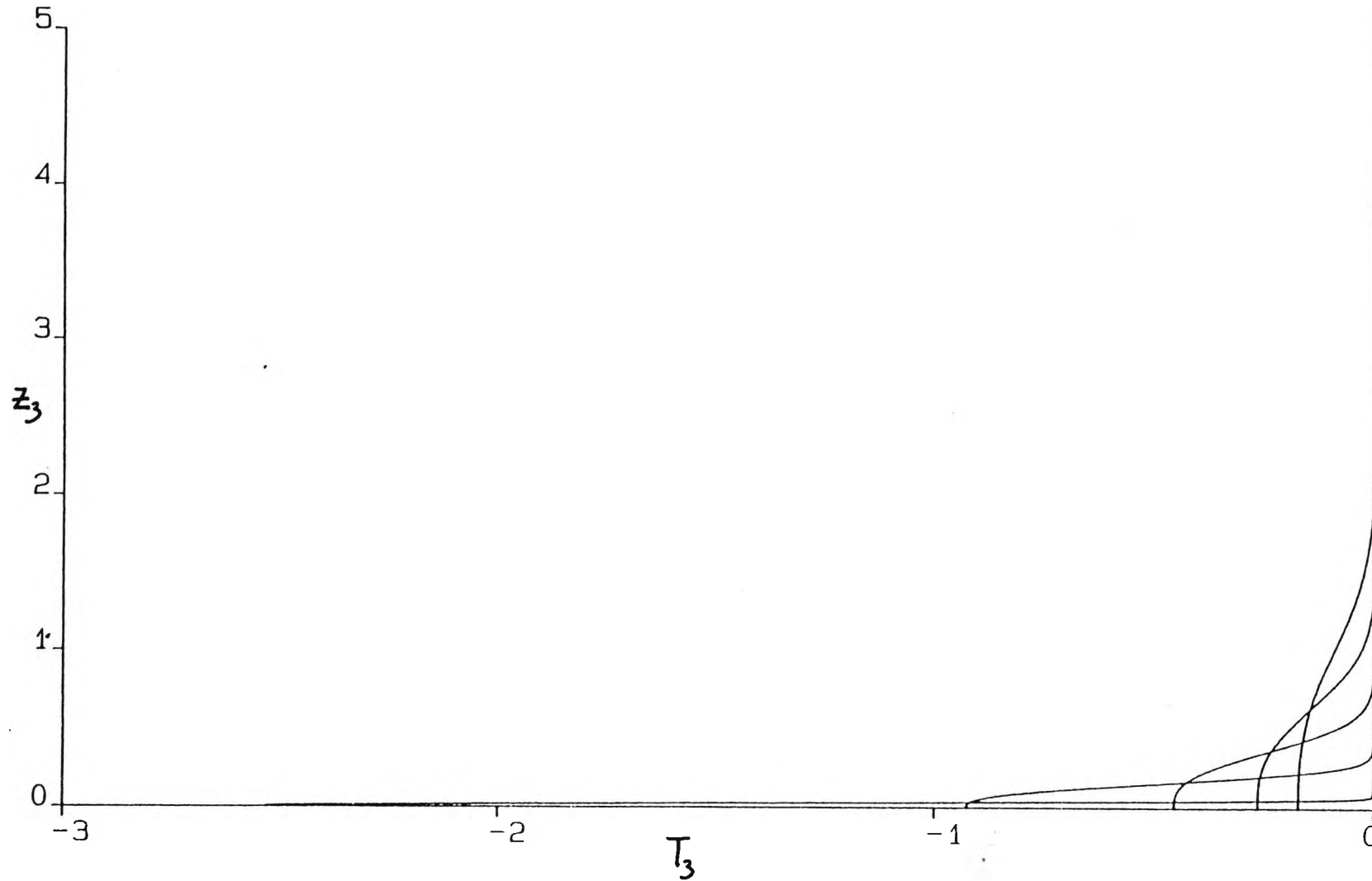


Figure 7.43 Graph of actual temperature at $\hat{\tau}_3 = 1.2, 1.4, 1.6, 1.8, 2.0$ ($\epsilon = 10.0, \sigma = 0.72$).

228

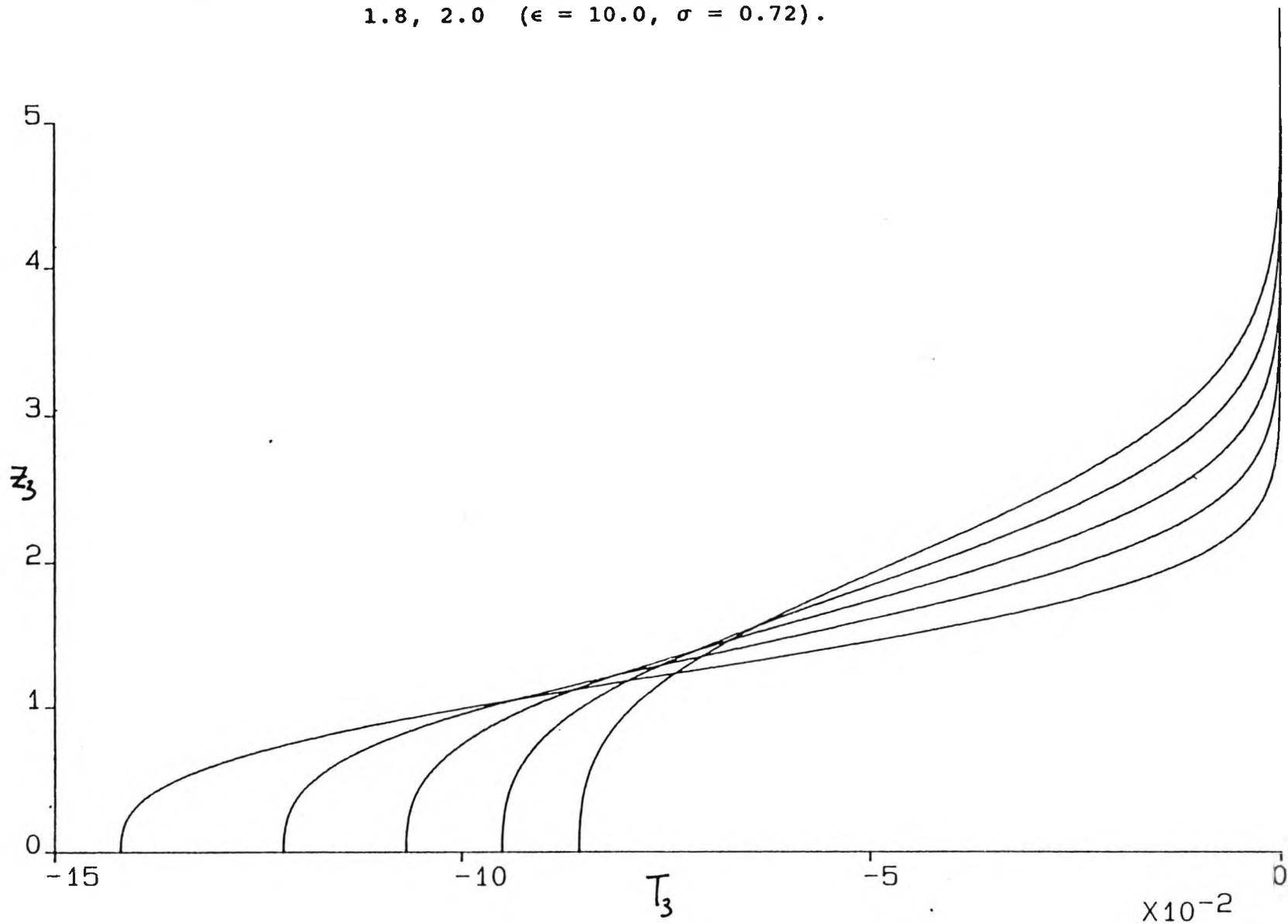


Figure 7.44 Graph of scaled pressure at $\xi_3 = 0.2, 0.4, 0.6, 0.8, 1.0$ ($\epsilon = 10.0, \sigma = 0.72$).

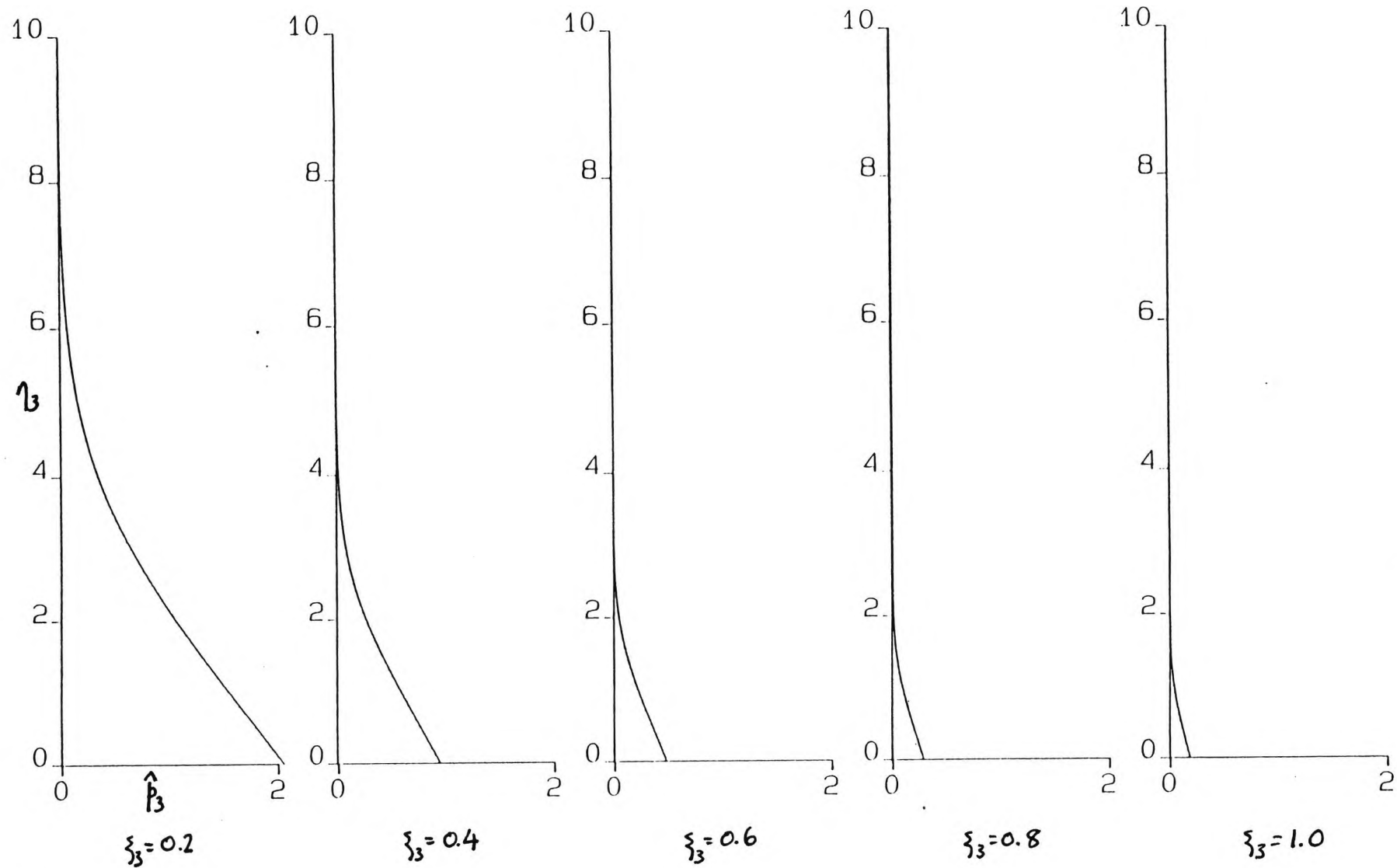


Figure 7.45 Graph of scaled pressure at $\hat{\xi}_3 = 1.2, 1.4, 1.6, 1.8, 2.0$ ($\epsilon = 10.0, \sigma = 0.72$).

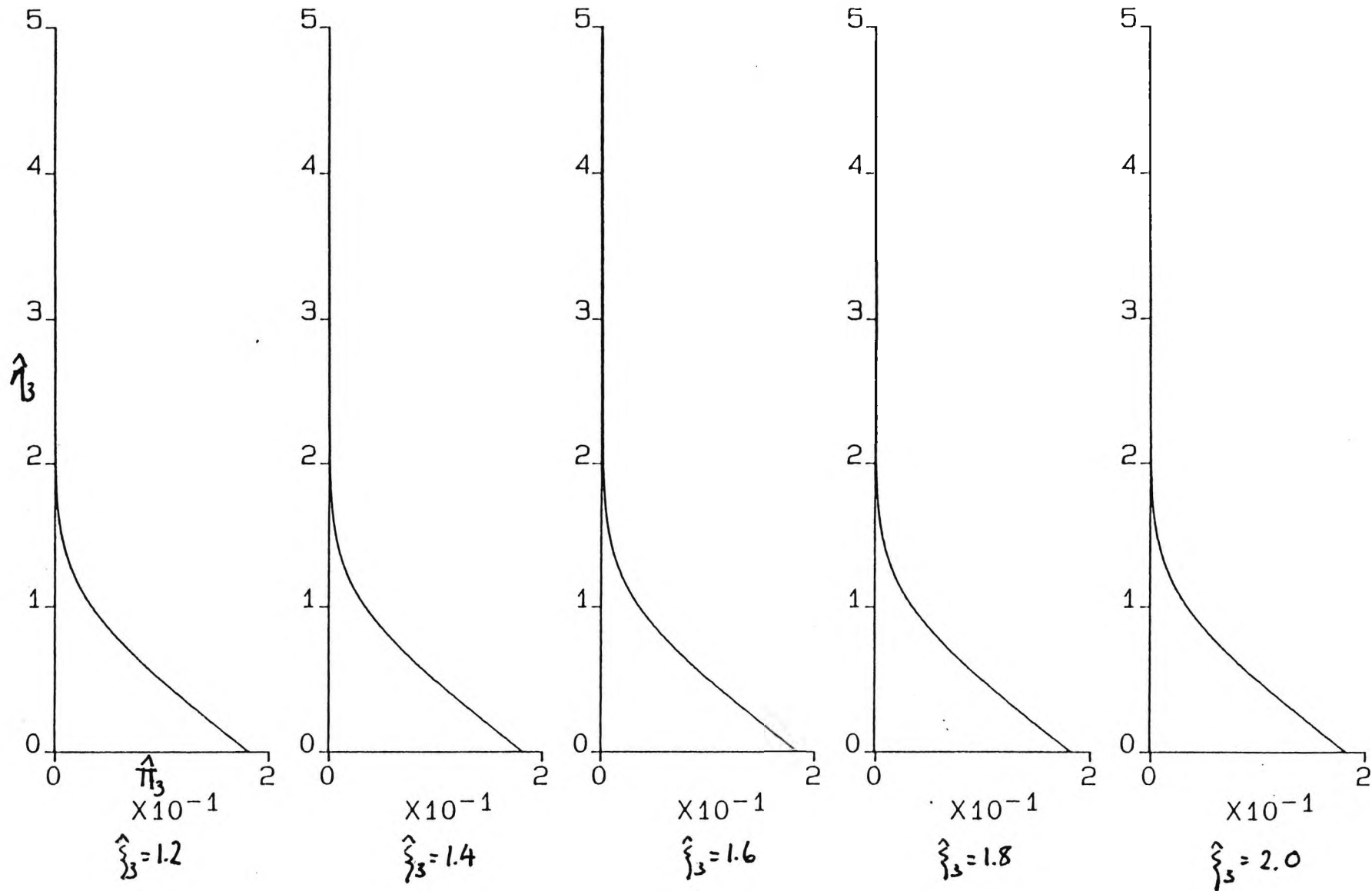


Figure 7.46 Graph of actual pressure at $\xi_3 = 0.2, 0.4, 0.6, 0.8, 1.0$ ($\epsilon = 10.0, \sigma = 0.72$).

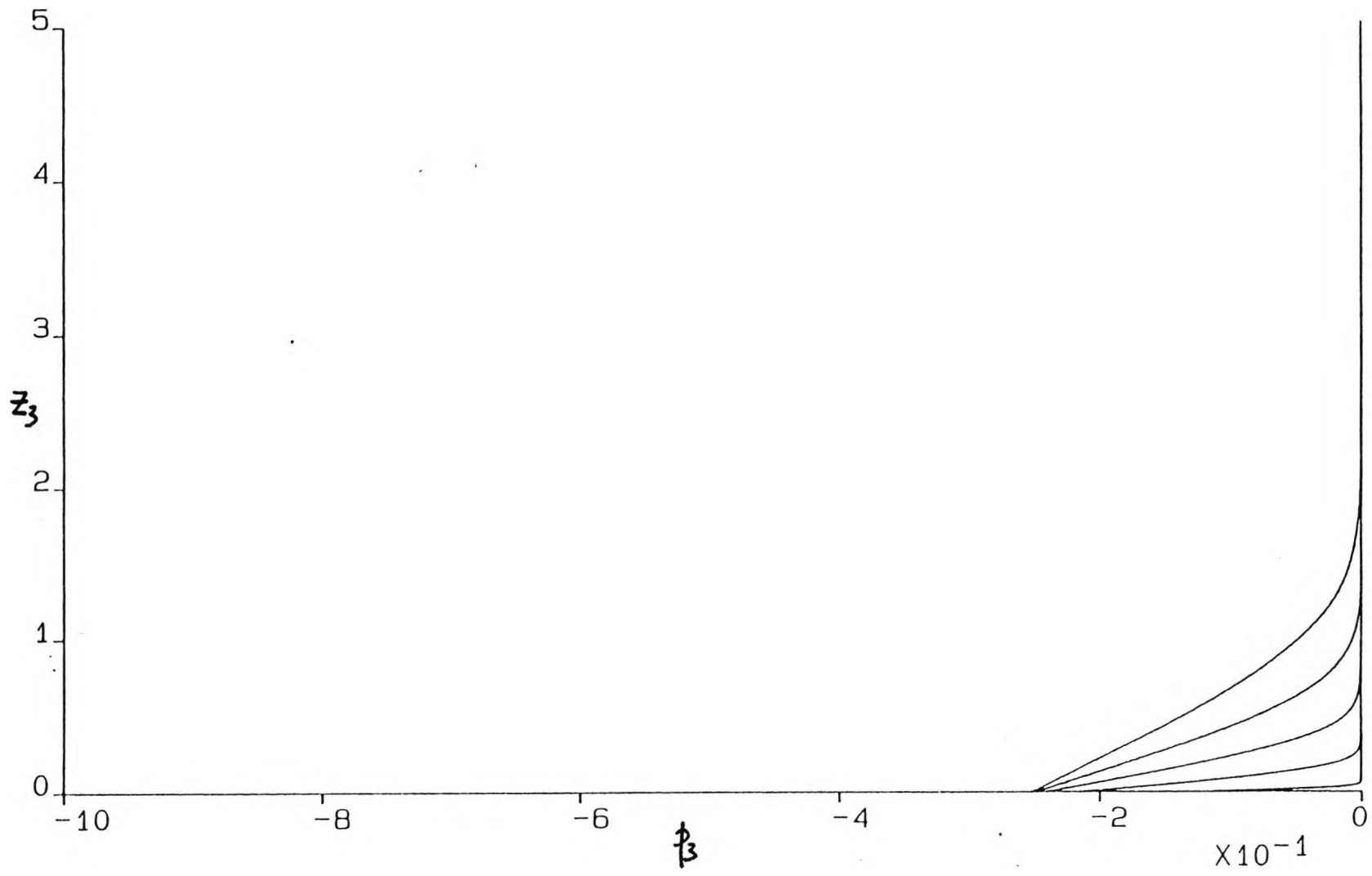


Figure 7.47 Graph of actual pressure at $\hat{\zeta}_3 = 1.2, 1.4, 1.6, 1.8, 2.0$ ($\epsilon = 10.0, \sigma = 0.72$).

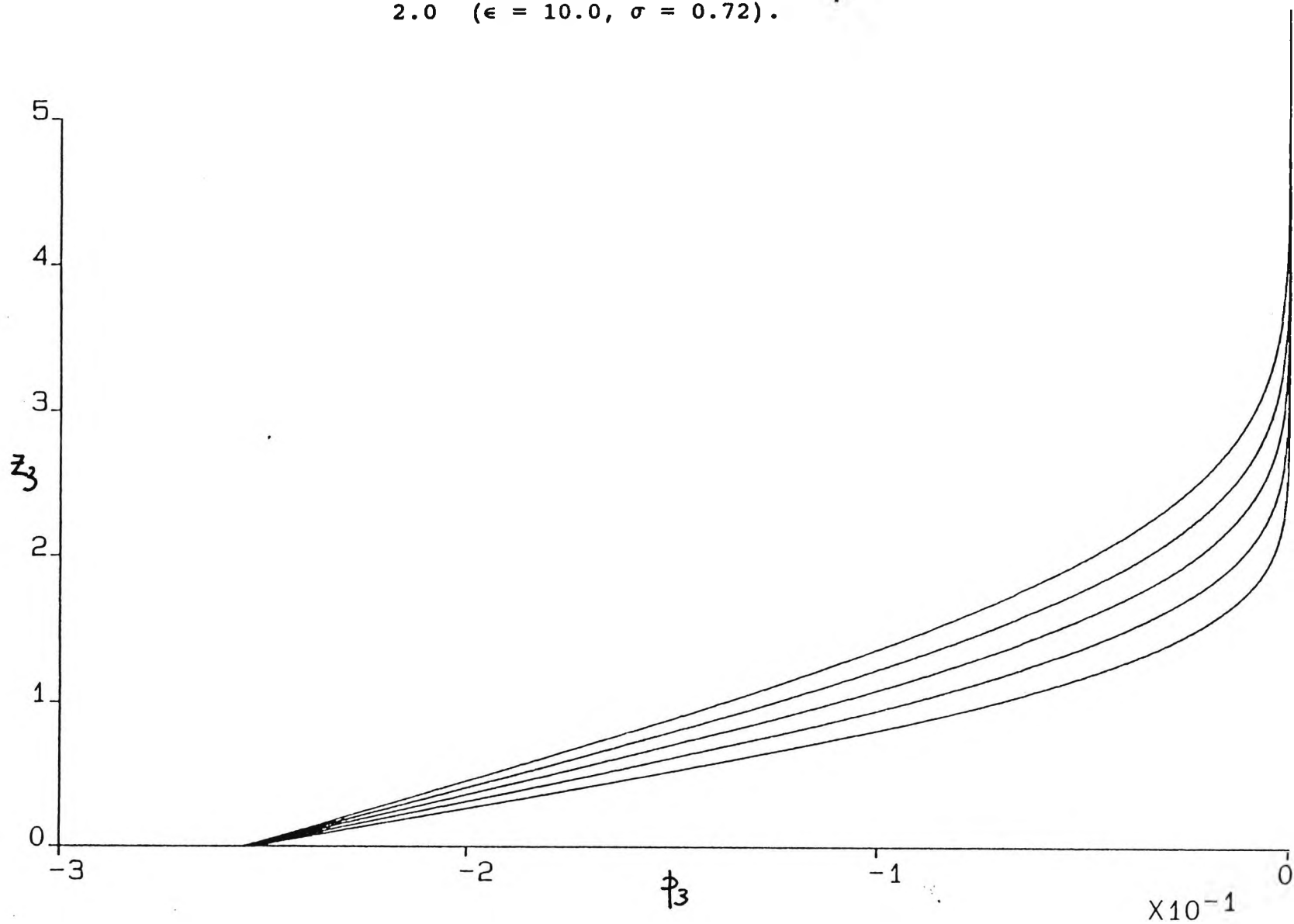


Figure 7.48 Graph of scaled velocity at $\xi_3 = 0.2, 0.4, 0.6, 0.8, 1.0$ ($\epsilon = 10.0, \sigma = 0.72$).

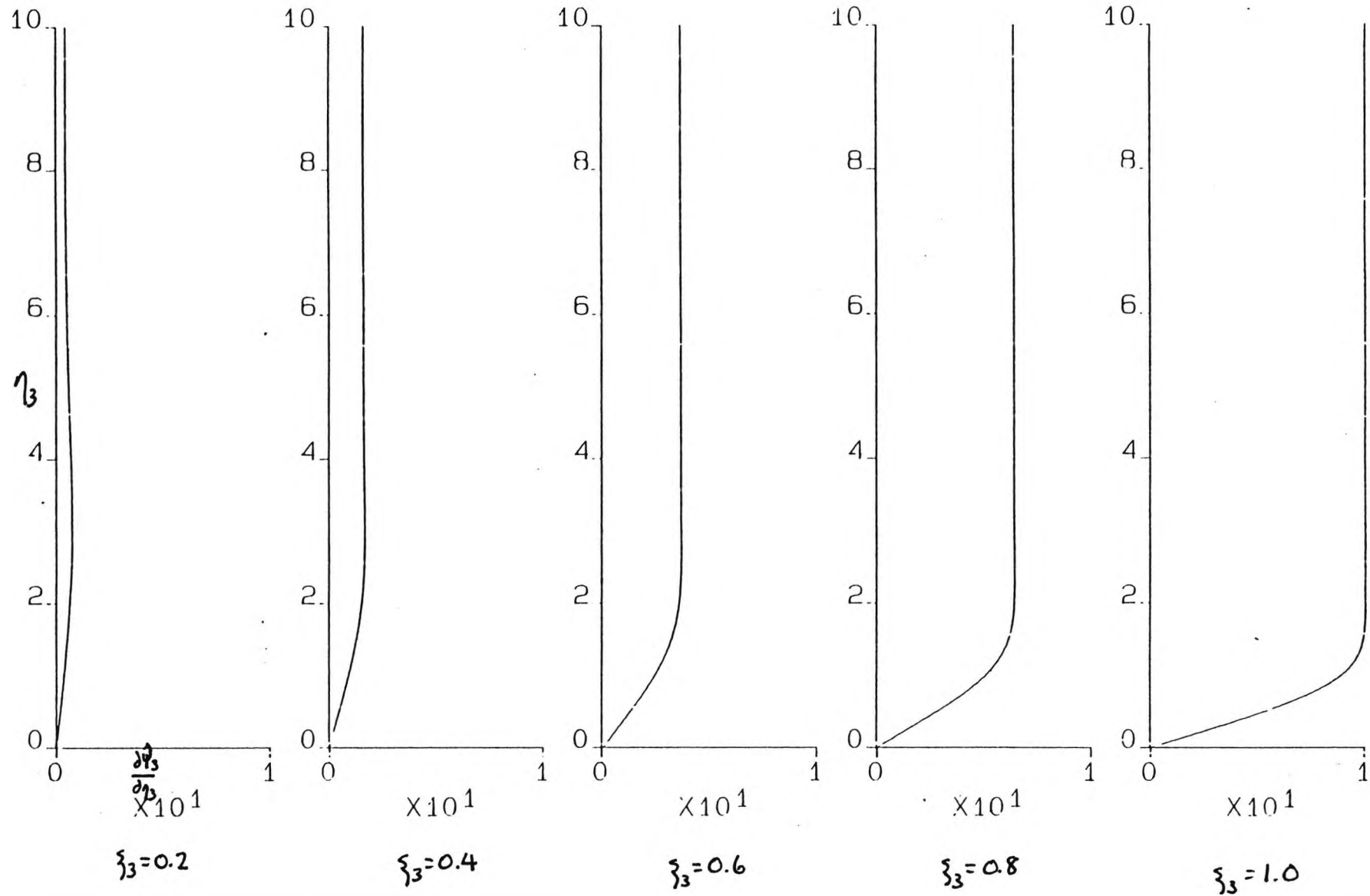


Figure 7.49 Graph of scaled velocity at $\hat{\zeta}_3 = 1.2, 1.4, 1.6, 1.8, 2.0$ ($\epsilon = 10.0, \sigma = 0.72$).

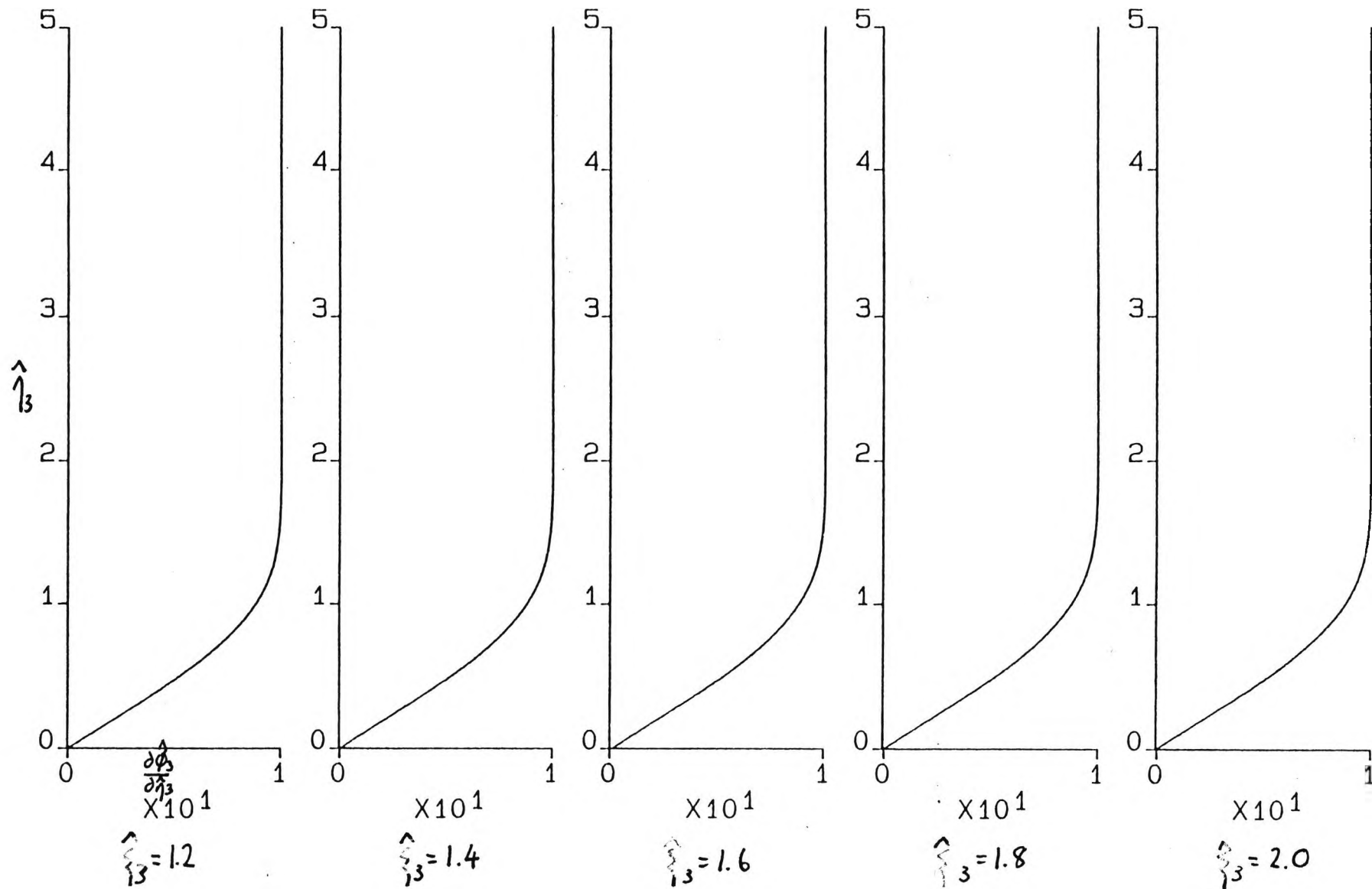


Figure 7.50 Graph of actual velocity at $\xi_3 = 0.2, 0.4, 0.6, 0.8, 1.0$ ($\epsilon = 10.0, \sigma = 8.1$).

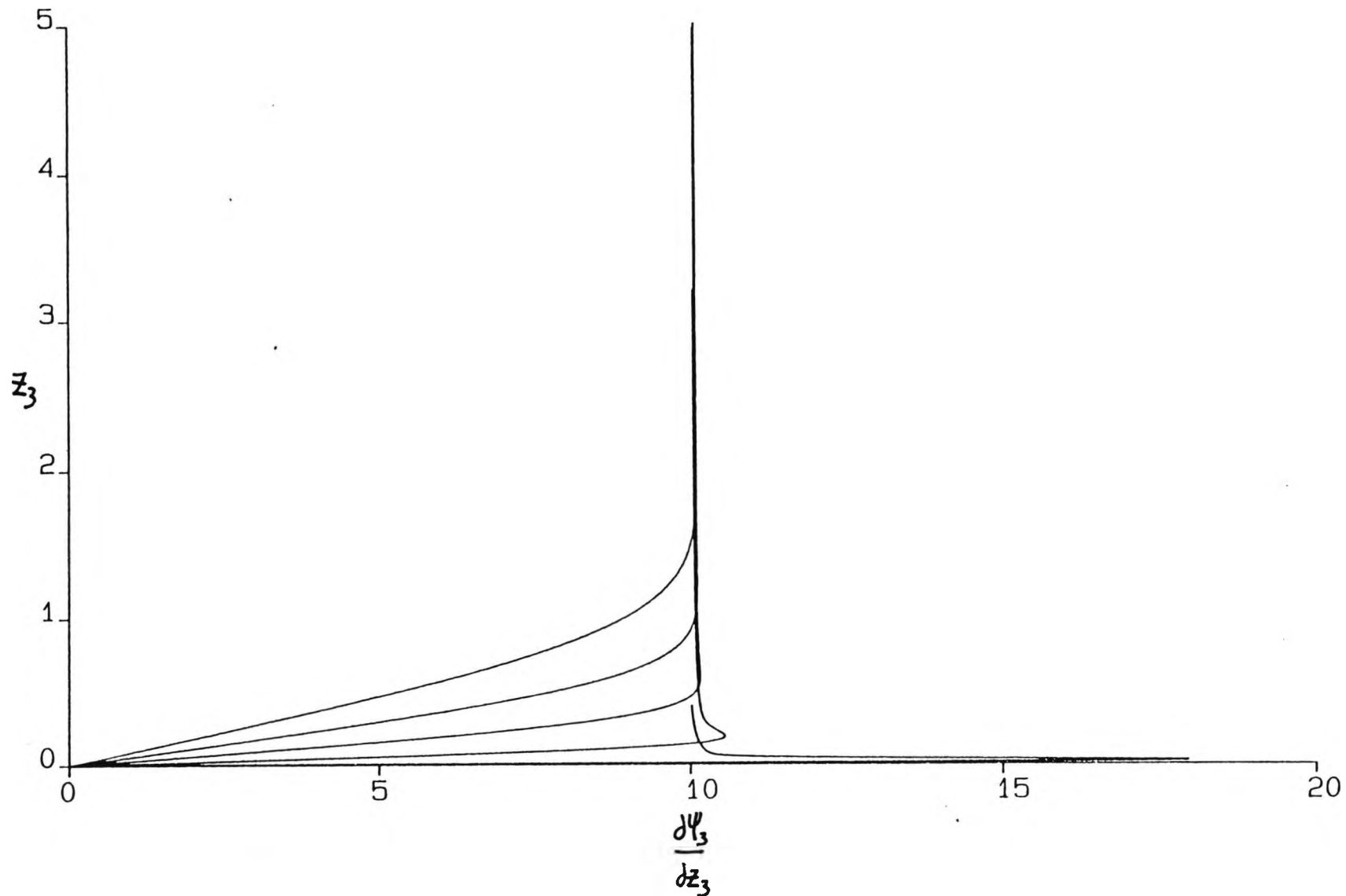


Figure 7.51 Graph of actual velocity $\hat{z}_3 = 1.2, 1.4, 1.6, 1.8, 2.0$ ($\epsilon = 10.0, \sigma = 8.1$).

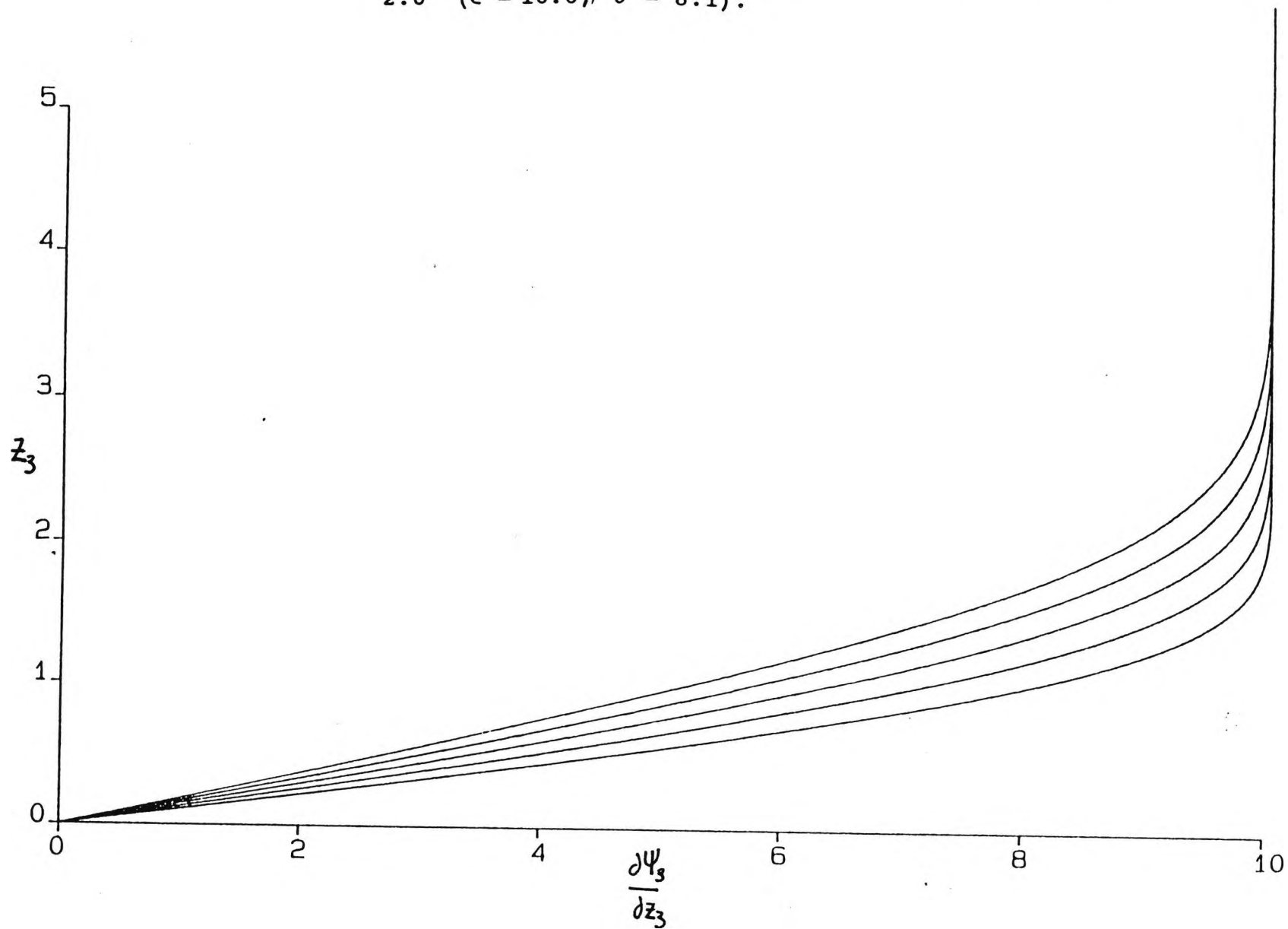


Figure 7.52 Graph of scaled temperature at $\xi_3 = 0.2, 0.4, 0.6, 0.8, 1.0$ ($\epsilon = 10.0, \sigma = 8.1$).

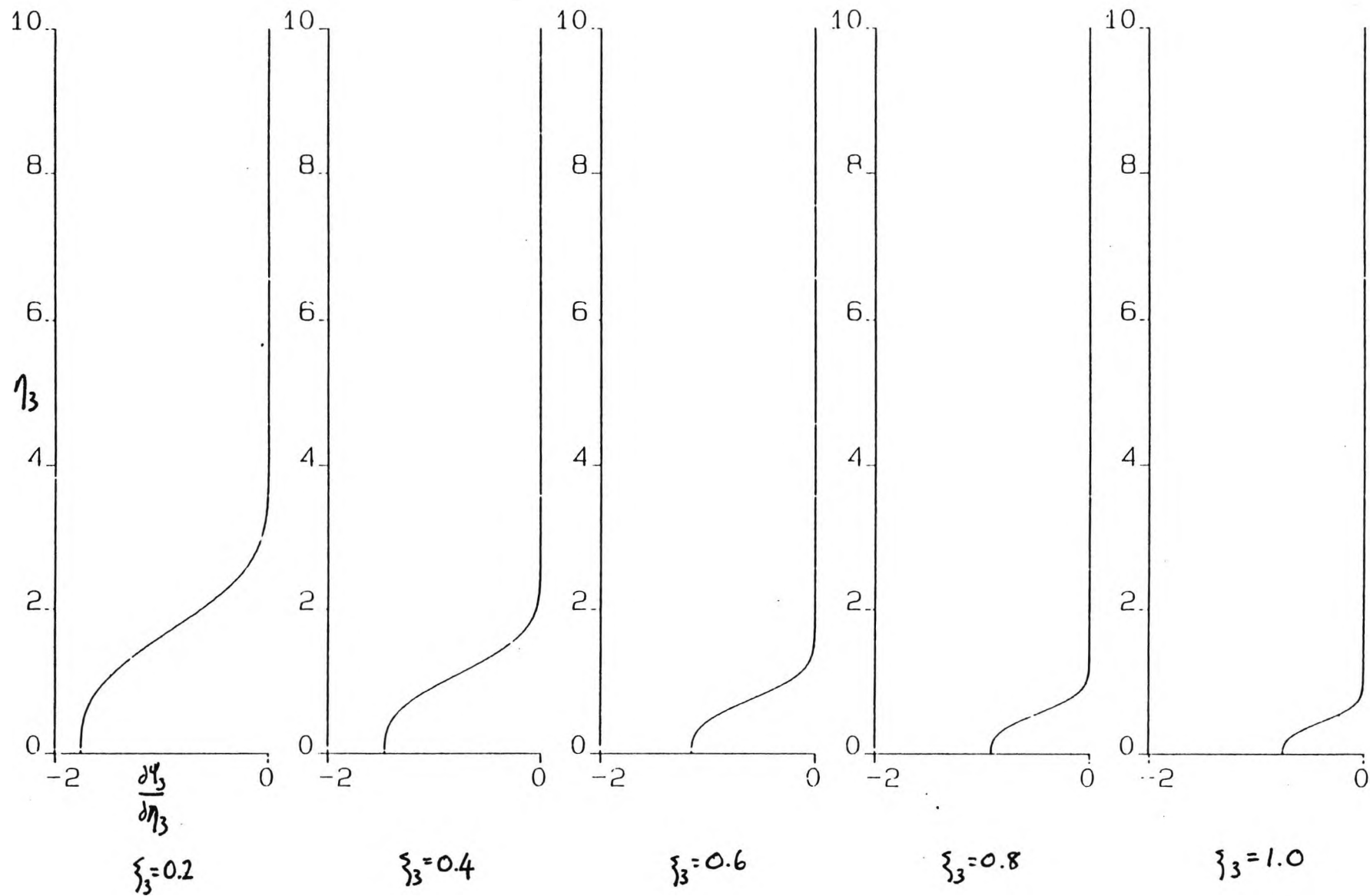


Figure 7.53 Graph of scaled temperature at $\hat{\xi}_3 = 1.2, 1.4, 1.6, 1.8, 2.0$ ($\epsilon = 10.0, \sigma = 8.1$).

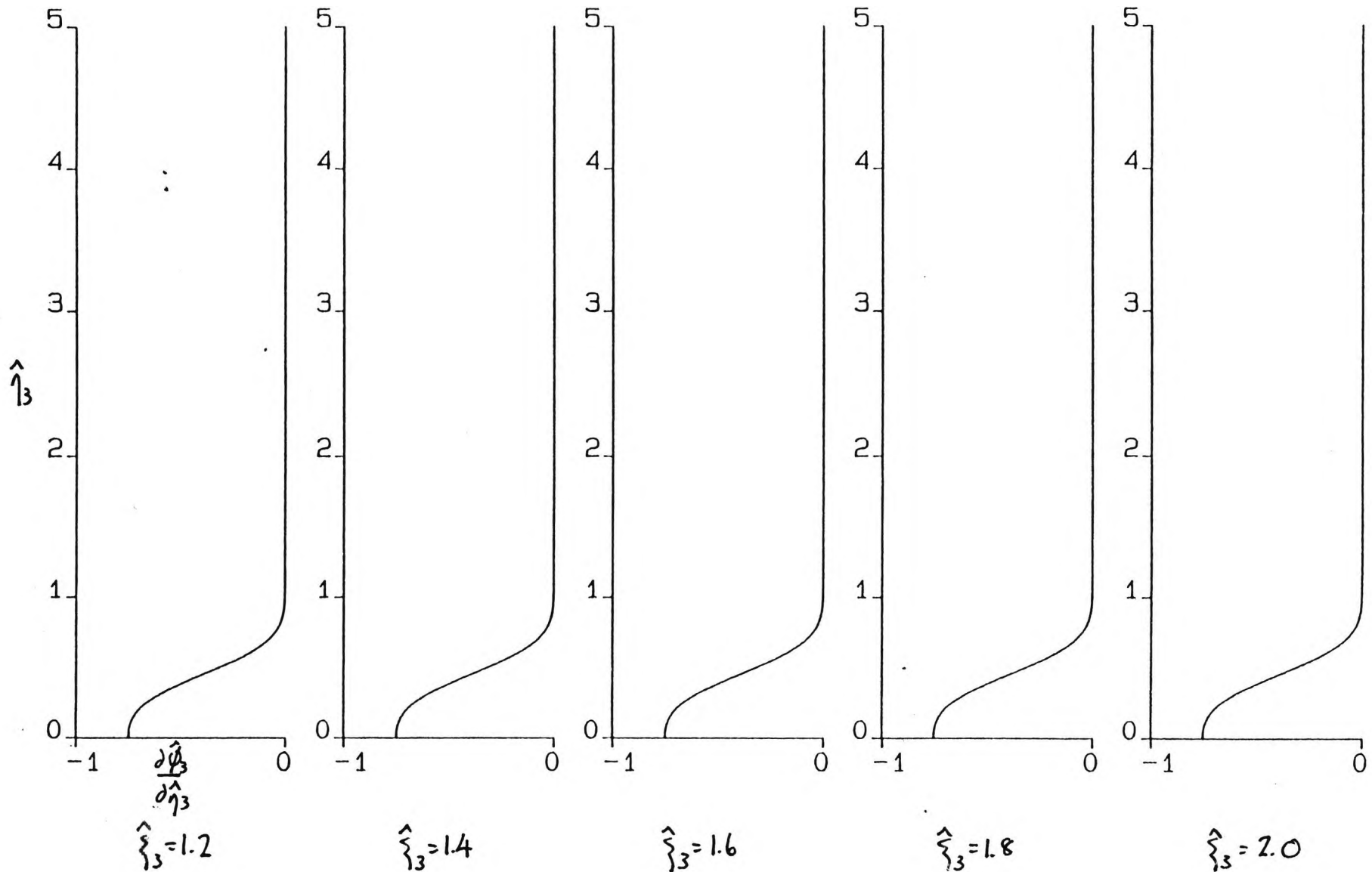


Figure 7.54 Graph of actual temperature at $\xi_3 = 0.2, 0.4, 0.6, 0.8, 1.0$ ($\epsilon = 10.0, \sigma = 8.1$).

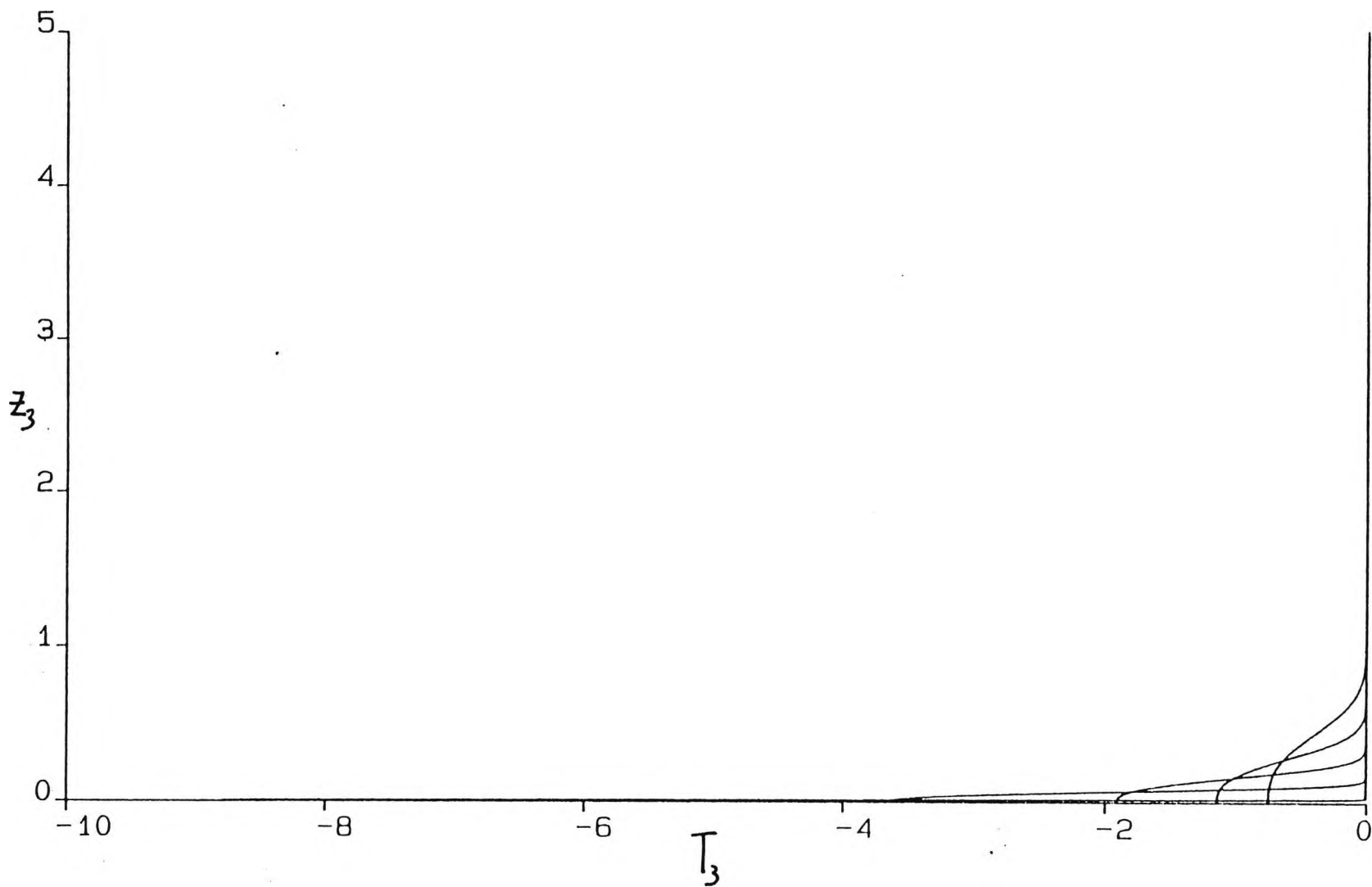


Figure 7.55 Graph of actual temperature at $\hat{\xi}_3 = 1.2, 1.4, 1.6, 1.8, 2.0$ ($\epsilon = 10.0, \sigma = 8.1$).

240

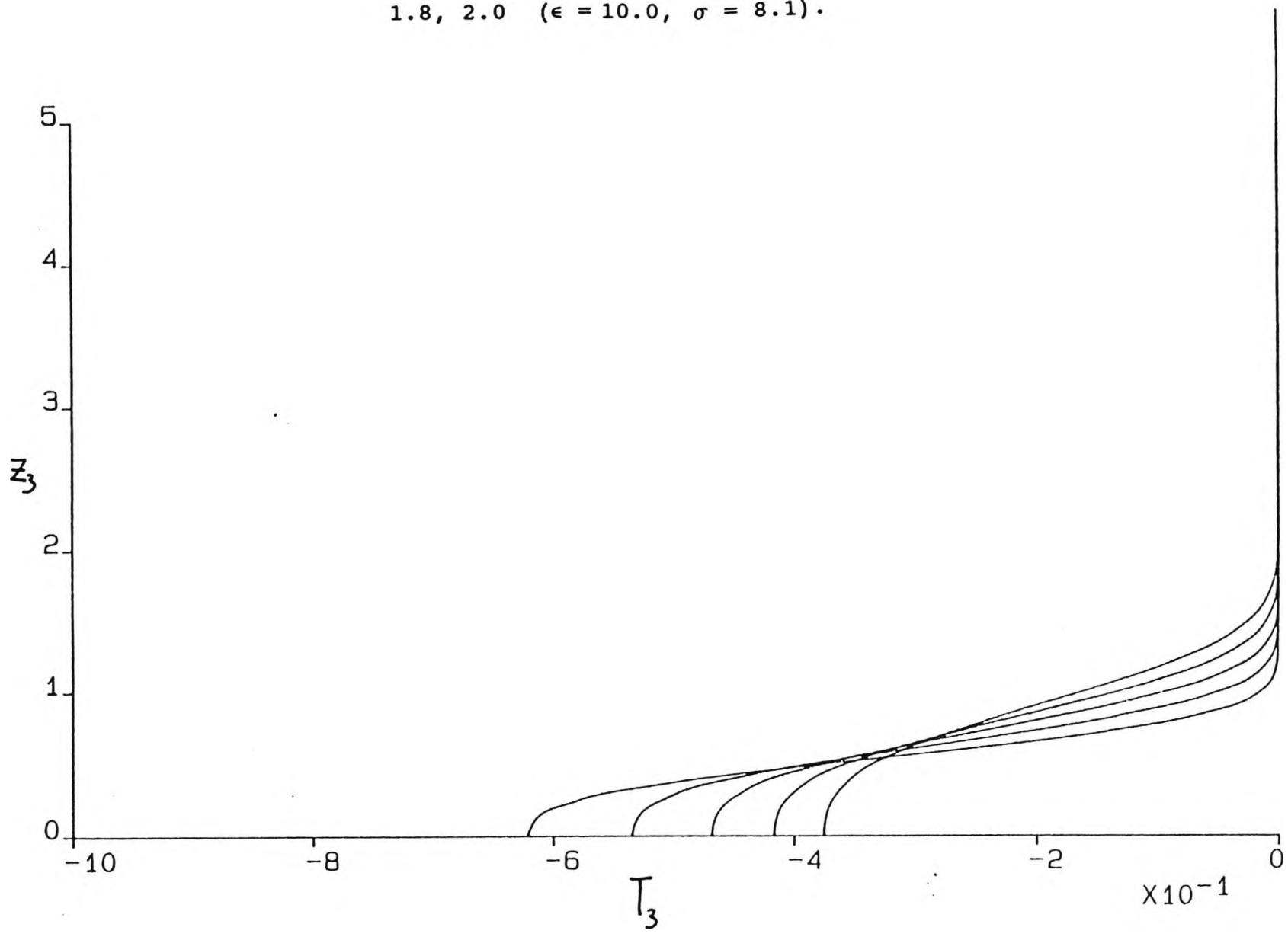


Figure 7.56 Graph of scaled pressure at $\xi_3 = 0.2, 0.4, 0.6, 0.8, 1.0$ ($\epsilon = 10.0$ $\sigma = 8.1$).

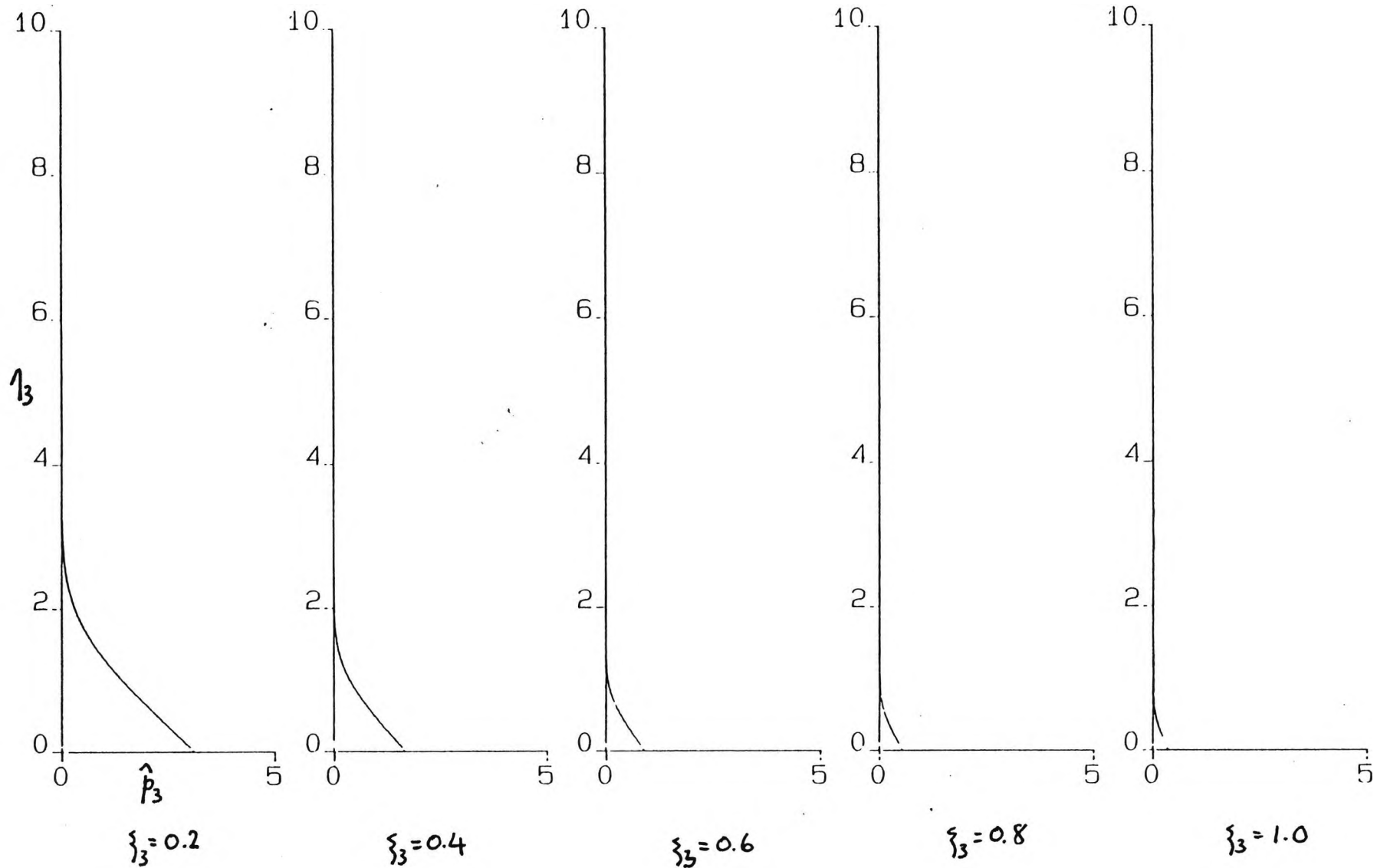


Figure 7.57 Graph of scaled pressure at $\hat{\xi}_3 = 1.2, 1.4, 1.6, 1.8, 2.0$ ($\epsilon = 10.0, \sigma = 8.1$).

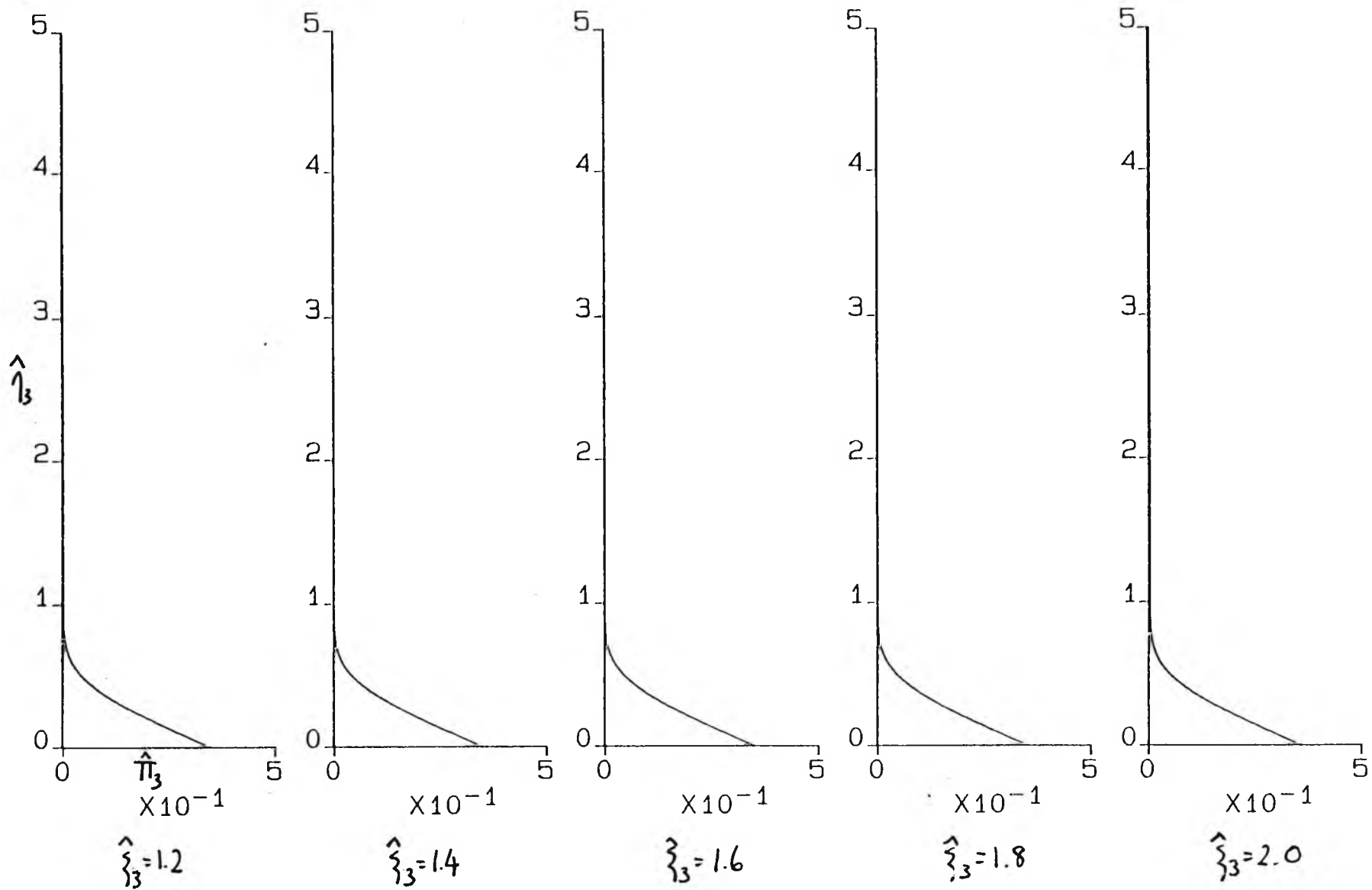


Figure 7.58 Graph of actual velocity at $\xi_3 = 0.2, 0.4, 0.6, 0.8, 1.0$ ($\epsilon = 10.0, \sigma = 8.1$).

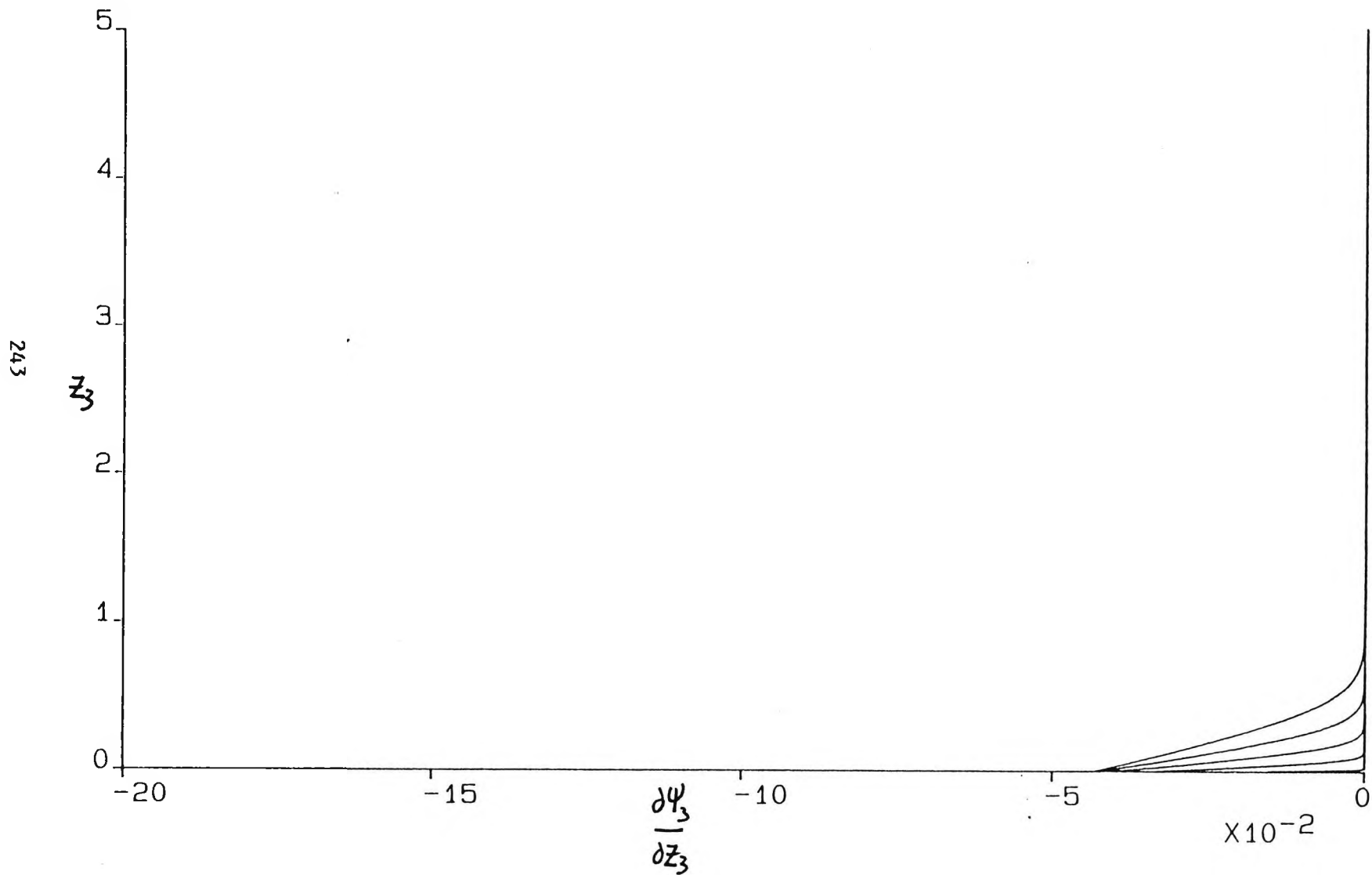
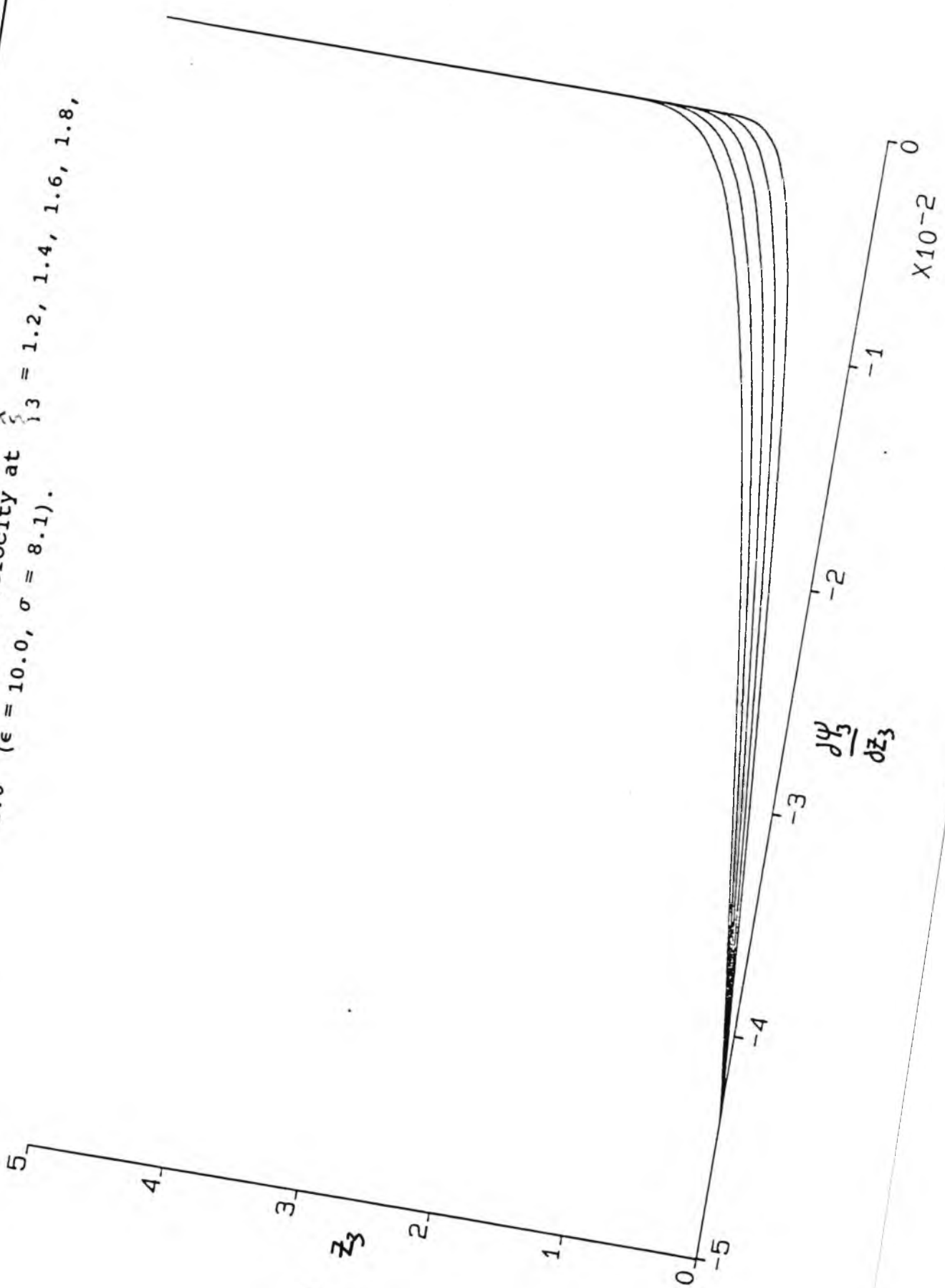


Figure 7.59 Graph of actual velocity at $\hat{\xi}_3 = 1.2, 1.4, 1.6, 1.8, 2.0$ ($\epsilon = 10.0, \sigma = 8.1$).



APPENDIX 1

Numerical Scheme for the vertical boundary-layer equation

Letting $A_j^{(r)}$, $B_j^{(r)}$, $C_j^{(r)}$, $D_j^{(r)}$ and $E_j^{(r)}$ denote the r th approximation to the true solution, we write the $(r+1)$ th approximation as $A_j^{(r+1)} = A_j^{(r)} + \delta A_j^{(r)}$, $B_j^{(r+1)} = B_j^{(r)} + \delta B_j^{(r)}$, and so on, and then linearize by neglecting all the δ^2 terms. Substituting into (3.4.9) and (3.4.10) we find that

$$\begin{aligned} & \alpha_j^{(r)} \delta A_j^{(r)} + \beta_j^{(r)} \delta B_j^{(r)} + \gamma_j^{(r)} \delta C_j^{(r)} + \lambda_j^{(r)} \delta D_j^{(r)} + \\ & \bar{\alpha}_j^{(r)} \delta A_{j-1}^{(r)} + \bar{\beta}_j^{(r)} \delta B_{j-1}^{(r)} + \bar{\gamma}_j^{(r)} \delta C_{j-1}^{(r)} + \bar{\lambda}_j^{(r)} \delta D_{j-1}^{(r)} = \\ & -S_{j-\frac{1}{2}}^{(r)} \end{aligned} \tag{A.1.1}$$

where

$$\begin{aligned} \alpha_j^{(r)} &= \frac{3h_j}{8\sigma} C_j^{(r)}, \quad \bar{\alpha}_j^{(r)} = \frac{3h_j}{8\sigma} C_{j-1}^{(r)}, \quad \beta_j^{(r)} = -\frac{h_j}{2\sigma} B_j^{(r)}, \quad \bar{\beta}_j^{(r)} = -\frac{h_j}{2\sigma} B_{j-1}^{(r)} \\ \gamma_j^{(r)} &= 1 + \frac{3h_j}{8\sigma} A_j^{(r)}, \quad \bar{\gamma}_j^{(r)} = -1 + \frac{3h_j}{8\sigma} A_{j-1}^{(r)}, \quad \lambda_j^{(r)} = -\frac{1}{2} h_j, \quad \bar{\lambda}_j^{(r)} = -\frac{1}{2} h_j \\ S_{j-\frac{1}{2}}^{(r)} &= C_j^{(r)} - C_{j-1}^{(r)} + \frac{h_j}{\sigma} \left\{ \frac{3}{8} (A_j^{(r)} C_j^{(r)} + A_{j-1}^{(r)} C_{j-1}^{(r)}) - \frac{1}{4} (B_j^{(r)})^2 + (B_{j-1}^{(r)})^2 \right\} \\ & \quad - \frac{1}{2} h_j [D_j^{(r)} + D_{j-1}^{(r)}] + h_j \end{aligned} \tag{A.1.2}$$

and

$$a_j^{(r)} A_j^{(r)} + e_j^{(r)} E_j^{(r)} + \bar{a}_j^{(r)} A_{j-1}^{(r)} + \bar{e}_j^{(r)} E_{j-1}^{(r)} = -R_{j-\frac{1}{2}}^{(r)} \tag{A.1.3}$$

where

$$\begin{aligned} a_j^{(r)} &= \frac{3h_j}{8} E_j^{(r)}, \quad \bar{a}_j^{(r)} = \frac{3h_j}{8} E_{j-1}^{(r)}, \quad e_j^{(r)} = 1 + \frac{3h_j}{8} A_j^{(r)}, \quad \bar{e}_j^{(r)} = -1 + \frac{3h_j}{8} A_{j-1}^{(r)} \\ R_{j-\frac{1}{2}}^{(r)} &= E_j^{(r)} - E_{j-1}^{(r)} + \frac{3h_j}{8} [A_j^{(r)} E_j^{(r)} - A_{j-1}^{(r)} E_{j-1}^{(r)}]. \end{aligned} \tag{A.1.4}$$

where

$$[P]_j = \begin{bmatrix} -1 & 0 & -\frac{1}{2}h_j & 0 & 0 & 1 & 0 & -\frac{1}{2}h_j & 0 & 0 \\ 0 & -1 & 0 & -\frac{1}{2}h_j & 0 & 0 & 1 & 0 & -\frac{1}{2}h_j & 0 \\ 0 & 0 & -1 & 0 & -\frac{1}{2}h_j & 0 & 0 & 1 & 0 & -\frac{1}{2}h_j \\ \bar{a}_j & 0 & 0 & \bar{e}_j & 0 & b_j & 0 & 0 & e_j & 0 \\ \bar{r}_j & \bar{\lambda}_j & \bar{\alpha}_j & 0 & \bar{\beta}_j & r_j & \lambda_j & \alpha_j & 0 & \beta_j \end{bmatrix}$$

$$[Q]_j = \begin{bmatrix} k_{j-1/2} \\ m_{j-1/2} \\ L_{j-1/2} \\ -R_{j-1/2} \\ -S_{j-1/2} \end{bmatrix} .$$

There are N blocks of $[P]$, forming a diagonal across a_1 .

To solve this matrix problem, the four elements $\bar{a}_j, \bar{r}_j, \bar{\lambda}_j, \bar{\alpha}_j$ in the bottom left corner and the three $-\frac{1}{2}h_j$ elements in the top right corner in each block $[P]_j$ are reduced to zero by Gaussian elimination. This is made possible because each block may be treated separately. The three elements (all equal to one) on the diagonal at the top left corner of the matrix a_1 are used to reduce to zero the first three columns of $[P]_1$. The elements beneath the diagonal can then be 'stripped off' enabling the increments to be read off in reverse order ($N \rightarrow 1$). The matrices a_1 and b_1 are then recalculated and the procedure continued until all the increments are sufficiently small.

APPENDIX 2

Numerical scheme for the horizontal boundary-layer $x < 1$

For region I, equation (5.2.12) may be written in the form

$$\hat{C}_j^n - \hat{C}_{j-1}^n + \frac{1}{3} h_j [2\hat{A}\hat{C} - \hat{B}^2]_{j-\frac{1}{2}}^n - \frac{h_j \xi_{2n-\frac{1}{2}}}{3\Delta_n} \left[(\hat{B}^2)_{j-\frac{1}{2}}^n - \hat{C}_{j-1}^n (\hat{A}_{j-\frac{1}{2}}^n - \hat{A}_{j-\frac{3}{2}}^{n-1}) - \hat{C}_{j-\frac{1}{2}}^{n-1} \hat{A}_{j-\frac{1}{2}}^n \right] = \hat{S}_{j-\frac{1}{2}}^{n-1} \quad (\text{A.2.1})$$

where

$$\hat{S}_{j-\frac{1}{2}}^{n-1} = -\hat{C}_j^{n-1} + \hat{C}_{j-1}^{n-1} - \frac{1}{3} h_j [2\hat{A}\hat{C} - \hat{B}^2]_{j-\frac{1}{2}}^{n-1} + \frac{h_j \xi_{2n-\frac{1}{2}}}{3\Delta_n} \left[-(\hat{B}^2)_{j-\frac{1}{2}}^{n-1} + \hat{C}_{j-\frac{1}{2}}^{n-1} \hat{A}_{j-\frac{1}{2}}^{n-1} \right]. \quad (\text{A.2.2})$$

This is a nonlinear problem for the solution at step n and we therefore use a Newton iteration scheme by letting $\hat{A}_j^{(r)}$, $\hat{B}_j^{(r)}$, $\hat{C}_j^{(r)}$ denote the r th approximation to the true solution and write the $(r+1)$ th approximation as

$$\hat{A}_j^{(r+1)} = \hat{A}_j^{(r)} + \delta \hat{A}_j^{(r)}, \quad \hat{B}_j^{(r+1)} = \hat{B}_j^{(r)} + \delta \hat{B}_j^{(r)}, \quad \hat{C}_j^{(r+1)} = \hat{C}_j^{(r)} + \delta \hat{C}_j^{(r)}. \quad (\text{A.2.3})$$

Ignoring all the δ^2 terms after substitution into (A.2.1) gives

$$\begin{aligned} \hat{a}_j^{(r)} \delta \hat{A}_j^{(r)} + \hat{b}_j^{(r)} \delta \hat{B}_j^{(r)} + \hat{d}_j^{(r)} \delta \hat{C}_j^{(r)} + \\ \bar{\hat{a}}_j^{(r)} \delta \hat{A}_{j-1}^{(r)} + \bar{\hat{b}}_j^{(r)} \delta \hat{B}_{j-1}^{(r)} + \bar{\hat{d}}_j^{(r)} \delta \hat{C}_{j-1}^{(r)} = \hat{S}_{j-\frac{1}{2}}^{n-1} + \hat{\gamma}_{j-\frac{1}{2}}^{(r)} \end{aligned} \quad (\text{A.2.4})$$

where

$$\hat{\gamma}_{j-\frac{1}{2}}^{(r)} = \hat{C}_{j-1}^{(r)} - \hat{C}_j^{(r)} - \frac{1}{3} h_j [2\hat{A}\hat{C} - \hat{B}^2]_{j-\frac{1}{2}}^{(r)} + \frac{h_j \xi_{2n-\frac{1}{2}}}{3\Delta_n} \left\{ (\hat{B}^2)_{j-\frac{1}{2}}^{(r)} - \hat{C}_{j-1}^{(r)} (\hat{A}_{j-\frac{1}{2}}^{(r)} - \hat{A}_{j-\frac{3}{2}}^{(r-1)}) - \hat{C}_{j-\frac{1}{2}}^{(r-1)} \hat{A}_{j-\frac{1}{2}}^{(r)} \right\} \quad (\text{A.2.5})$$

$$\begin{aligned} \hat{a}_j^{(r)} &= \frac{1}{3} h_j \hat{C}_j^{(r)} + \frac{h_j}{6\Delta_n} \xi_{2n-\frac{1}{2}} (\hat{C}_{j-\frac{1}{2}}^{(r)} + \hat{C}_{j-\frac{3}{2}}^{(r-1)}), \quad \bar{\hat{a}}_j^{(r)} = \frac{1}{3} h_j \hat{C}_{j-1}^{(r)} + \frac{h_j}{6\Delta_n} \xi_{2n-\frac{1}{2}} (\hat{C}_{j-\frac{1}{2}}^{(r)} + \hat{C}_{j-\frac{3}{2}}^{(r-1)}) \\ \hat{b}_j^{(r)} &= -\frac{1}{3} h_j \hat{B}_j^{(r)} - \frac{h_j}{3\Delta_n} \xi_{2n-\frac{1}{2}} \hat{B}_{j-\frac{1}{2}}^{(r)}, \quad \bar{\hat{b}}_j^{(r)} = -\frac{1}{3} h_j \hat{B}_{j-1}^{(r)} - \frac{h_j}{3\Delta_n} \xi_{2n-\frac{1}{2}} \hat{B}_{j-\frac{1}{2}}^{(r)} \\ \hat{d}_j^{(r)} &= 1 + \frac{1}{3} h_j \hat{A}_j^{(r)} + \frac{h_j}{6\Delta_n} \xi_{2n-\frac{1}{2}} (\hat{A}_{j-\frac{1}{2}}^{(r)} - \hat{A}_{j-\frac{3}{2}}^{(r-1)}) \\ \bar{\hat{d}}_j^{(r)} &= -1 + \frac{1}{3} h_j \hat{A}_{j-1}^{(r)} + \frac{h_j}{6\Delta_n} \xi_{2n-\frac{1}{2}} (\hat{A}_{j-\frac{1}{2}}^{(r)} - \hat{A}_{j-\frac{3}{2}}^{(r-1)}). \end{aligned} \quad (\text{A.2.6})$$

Incorporating the Newton scheme into recurrence relations (5.2.11)

gives

$$\delta \hat{A}_j^{(r)} - \delta \hat{A}_{j-1}^{(r)} - \frac{1}{2} h_j (\delta \hat{B}_j^{(r)} + \delta \hat{B}_{j-1}^{(r)}) = \hat{\alpha}_{j-\frac{1}{2}}$$

and

$$\delta \hat{B}_j^{(r)} - \delta \hat{B}_{j-1}^{(r)} - \frac{1}{2} h_j (\delta \hat{C}_j^{(r)} + \delta \hat{C}_{j-1}^{(r)}) = \hat{\beta}_{j-\frac{1}{2}}$$

where

$$\hat{\alpha}_{j-\frac{1}{2}} = \frac{1}{2} h_j (\hat{B}_j^{(r)} + \hat{B}_{j-1}^{(r)}) + \hat{A}_{j-1}^{(r)} - \hat{A}_j^{(r)}$$

$$\hat{\beta}_{j-\frac{1}{2}} = \frac{1}{2} h_j (\hat{C}_j^{(r)} + \hat{C}_{j-1}^{(r)}) + \hat{B}_{j-1}^{(r)} - \hat{B}_j^{(r)}$$

(A.2.7)

For Region II equation (5.2.26) may be written in the form

$$\hat{I}_k^{\hat{n}} - \hat{I}_{k-1}^{\hat{n}} - \frac{H_k}{3\Delta_n \xi_{k-\frac{1}{2}}^2} \left[(\hat{G}^{\hat{n}})_{k-\frac{1}{2}}^{\hat{n}} - \hat{I}_{k-\frac{1}{2}}^{\hat{n}} (\hat{F}_{k-\frac{1}{2}}^{\hat{n}} - \hat{F}_{k-\frac{1}{2}}^{\hat{n}-1}) - \hat{I}_{k-\frac{1}{2}}^{\hat{n}-1} \hat{F}_{k-\frac{1}{2}}^{\hat{n}} \right]$$

(A.2.8)

$$= \hat{R}_{k-\frac{1}{2}}^{\hat{n}-1}$$

where

$$\hat{R}_{k-\frac{1}{2}}^{\hat{n}-1} = \hat{I}_{k-1}^{\hat{n}-1} - \hat{I}_k^{\hat{n}-1} - \frac{H_k}{3\Delta_n \xi_{k-\frac{1}{2}}^2} \left[(\hat{G}^{\hat{n}-1})_{k-\frac{1}{2}}^{\hat{n}-1} - \hat{I}_{k-\frac{1}{2}}^{\hat{n}-1} \hat{F}_{k-\frac{1}{2}}^{\hat{n}-1} \right]$$

(A.2.9)

As in the inner region we use a Newton iteration scheme where we let $\hat{F}_R^{(r)}$, $\hat{G}_R^{(r)}$, $\hat{I}_R^{(r)}$ denote the r th approximation to the true solution and write the $(r+1)$ th approximation as

$$\hat{F}_k^{(r+1)} = \hat{F}_k^{(r)} + \delta \hat{F}_k^{(r)}, \quad \hat{G}_k^{(r+1)} = \hat{G}_k^{(r)} + \delta \hat{G}_k^{(r)}, \quad \hat{I}_k^{(r+1)} = \hat{I}_k^{(r)} + \delta \hat{I}_k^{(r)}$$

(A.2.10)

Substitution into (A.2.8) ignoring all δ^2 terms gives

$$\hat{\lambda}_k^{(r)} \delta \hat{F}_k^{(r)} + \hat{\mu}_k^{(r)} \delta \hat{G}_k^{(r)} + \hat{\nu}_k^{(r)} \delta \hat{I}_k^{(r)} +$$

$$\bar{\lambda}_k^{(r)} \delta \hat{F}_{k-1}^{(r)} + \bar{\mu}_k^{(r)} \delta \hat{G}_{k-1}^{(r)} + \bar{\nu}_k^{(r)} \delta \hat{I}_{k-1}^{(r)} = \hat{R}_{k-\frac{1}{2}}^{\hat{n}-1} + \hat{\Gamma}_{k-\frac{1}{2}}^{(r)}$$

(A.2.11)

where

$$\begin{aligned} \hat{F}_{k-\frac{1}{2}}^{(r)} &= \hat{I}_{k-1}^{(r)} - \hat{I}_k^{(r)} + \frac{H_k}{3\Delta_n \xi_2^{n-\frac{1}{2}}} \left[(\hat{G}^2)_{k-\frac{1}{2}}^{(r)} + \hat{I}_{k-\frac{1}{2}}^{(r)} (\hat{F}_{k-1}^{(r)} - \hat{F}_{k-\frac{1}{2}}^{(r)}) - \hat{I}_{k-\frac{1}{2}}^{(r)} \hat{F}_{k-\frac{1}{2}}^{(r)} \right] \\ \hat{\chi}_k^{(r)} &= \frac{H_k}{6\Delta_n \xi_2^{n-\frac{1}{2}}} \left[\hat{I}_{k-\frac{1}{2}}^{(r)} + \hat{I}_{k-1}^{(r)} \right] = \bar{\chi}_k^{(r)}, \quad \hat{\mu}_k^{(r)} = \frac{-H_k}{3\Delta_n \xi_2^{n-\frac{1}{2}}} \hat{G}_{k-\frac{1}{2}}^{(r)} = \bar{\mu}_k^{(r)}. \end{aligned} \quad (\text{A.2.12})$$

$$\hat{D}_k^{(r)} = 1 + \frac{H_k}{6\Delta_n \xi_2^{n-\frac{1}{2}}} (\hat{F}_{k-\frac{1}{2}}^{(r)} - \hat{F}_{k-1}^{(r)}), \quad \bar{D}_k^{(r)} = -1 + \frac{H_k}{6\Delta_n \xi_2^{n-\frac{1}{2}}} (\hat{F}_{k-\frac{1}{2}}^{(r)} - \hat{F}_{k-1}^{(r)}).$$

Incorporating the Newton scheme into the recurrence relations

(5.2.25) gives

$$\delta \hat{F}_k^{(r)} - \delta \hat{F}_{k-1}^{(r)} - \frac{1}{2} H_k (\delta \hat{G}_k^{(r)} + \delta \hat{G}_{k-1}^{(r)}) = \hat{\rho}_{k-\frac{1}{2}}^{(r)}$$

and

$$\delta \hat{G}_k^{(r)} - \delta \hat{G}_{k-1}^{(r)} - \frac{1}{2} H_k (\delta \hat{I}_k^{(r)} + \delta \hat{I}_{k-1}^{(r)}) = \hat{\omega}_{k-\frac{1}{2}}^{(r)}$$

where

$$\hat{\rho}_{k-\frac{1}{2}}^{(r)} = \hat{F}_{k-1}^{(r)} - \hat{F}_k^{(r)} + \frac{1}{2} H_k (\hat{G}_k^{(r)} + \hat{G}_{k-1}^{(r)})$$

$$\hat{\omega}_{k-\frac{1}{2}}^{(r)} = \hat{G}_{k-1}^{(r)} - \hat{G}_k^{(r)} + \frac{1}{2} H_k (\hat{I}_k^{(r)} + \hat{I}_{k-1}^{(r)}).$$

(A.2.13)

For the boundary and matching conditions we have from

(5.2.30)

$$\delta \hat{A}_0^{(r)} = -\hat{A}_0^{(r)}, \quad \delta \hat{B}_0^{(r)} = -\hat{B}_0^{(r)}, \quad (\text{A.2.14})$$

from (5.2.28)

$$\begin{aligned} \delta \hat{F}_0^{(r)} - \sum_2^n \delta \hat{A}_J^{(r)} &= \sum_2^n \hat{A}_J^{(r)} - \hat{F}_0^{(r)} \\ \delta \hat{G}_0^{(r)} - \sum_2^n \delta \hat{B}_J^{(r)} &= \sum_2^n \hat{B}_J^{(r)} - \hat{G}_0^{(r)} \\ \delta \hat{I}_0^{(r)} - \delta \hat{C}_J^{(r)} &= \hat{C}_J^{(r)} - \hat{I}_0^{(r)} \end{aligned} \quad (\text{A.2.15})$$

and from (5.2.33)

$$\delta \hat{G}_{k_m}^{(r)} = -\hat{G}_{k_m}^{(r)}.$$

(A.2.16)

The linear system represented by (A.2.1) - (A.2.2), (A.2.4) - (A.2.9), (A.2.11) - (A.2.16) consists of $3J + 3K + 6$ equations, and these may be assembled into a single matrix equation

$$\hat{a}_1 x = \hat{b}_1 \quad (\text{A.2.17})$$

which has the structure shown in figure A.2.1. The blocks comprising the matrix \hat{a}_1 can be treated separately; each block is first reduced to the form

$$\begin{pmatrix} * & * & * & * & 0 & 0 \\ 0 & * & * & * & * & 0 \\ 0 & 0 & * & * & * & * \end{pmatrix}$$

by Gaussian elimination, where * represents a non-zero value. Then the last row of the last block (row $3J + 3K + 5$) is interchanged with the bottom row (the outer edge condition) giving this structure at the bottom right corner of \hat{a}_1 :

$$\begin{pmatrix} * & * & * & * & 0 & 0 \\ 0 & * & * & * & * & 0 \\ - & - & - & 0 & 1 & 0 \\ 0 & 0 & * & * & * & * \end{pmatrix} ,$$

This enables a diagonal of elements to be 'stripped off' and thus the increments may be read off in ascending order ($1 \rightarrow 3J + 3K + 6$). The matrices \hat{a}_1 and \hat{b}_1 are then recalculated and the procedure continued until all the increments are sufficiently small.

Once the solution for the velocity has been found at step n we can solve for the temperature.

For Region I equation (5.2.13) may be written in the form

$$\begin{aligned} \hat{E}_j^n - \hat{E}_{j-1}^n + \frac{\sigma h_j}{3} [2(\hat{A}\hat{E})_{j-\frac{1}{2}}^n - (\hat{D}\hat{B})_{j-\frac{1}{2}}^n] - \frac{\sigma h_j}{3\Delta_n} \xi_2^{n-\frac{1}{2}} [\\ \hat{B}_{j-\frac{1}{2}}^n (\hat{D}_{j-\frac{1}{2}}^n - \hat{D}_{j-\frac{1}{2}}^{n-1}) + \hat{B}_{j-\frac{1}{2}}^{n-1} \hat{D}_{j-\frac{1}{2}}^n - \hat{E}_{j-\frac{1}{2}}^n (\hat{A}_{j-\frac{1}{2}}^n - \hat{A}_{j-\frac{1}{2}}^{n-1}) \\ - \hat{E}_{j-\frac{1}{2}}^{n-1} \hat{A}_{j-\frac{1}{2}}^n] = S'_{j-\frac{1}{2}} \end{aligned} \quad (\text{A.2.18})$$

where

$$\begin{aligned} S'_{j-\frac{1}{2}} = -\hat{E}_j^n + \hat{E}_{j-1}^n + \frac{1}{3}\sigma h_j [-2(\hat{A}\hat{E})_{j-\frac{1}{2}}^{n-1} + (\hat{D}\hat{B})_{j-\frac{1}{2}}^{n-1}] \\ + \frac{\sigma h_j}{3\Delta_n} \xi_2^{n-\frac{1}{2}} [-\hat{B}_{j-\frac{1}{2}}^{n-1} \hat{D}_{j-\frac{1}{2}}^{n-1} + \hat{E}_{j-\frac{1}{2}}^{n-1} \hat{A}_{j-\frac{1}{2}}^{n-1}]. \end{aligned} \quad (\text{A.2.19})$$

The temperature problem is a linear one so we may immediately write

$$d'_j \hat{D}_j^n + e'_j \hat{E}_j^n + \bar{d}'_j \hat{D}_{j-1}^n + \bar{e}'_j \hat{E}_{j-1}^n = S'_{j-\frac{1}{2}} + \bar{S}'_{j-\frac{1}{2}} \quad (\text{A.2.20})$$

where

$$\begin{aligned} \bar{S}'_{j-\frac{1}{2}} = \frac{-\sigma h_j}{3\Delta_n} \xi_2^{n-\frac{1}{2}} [\hat{B}_{j-\frac{1}{2}}^n \hat{D}_{j-\frac{1}{2}}^{n-1} + \hat{E}_{j-\frac{1}{2}}^{n-1} \hat{A}_{j-\frac{1}{2}}^n] \\ d'_j = \frac{-\sigma h_j}{6} \hat{B}_j^n - \frac{\sigma h_j}{6\Delta_n} \xi_2^{n-\frac{1}{2}} (\hat{B}_{j-\frac{1}{2}}^n + \hat{B}_{j-\frac{1}{2}}^{n-1}), \quad \bar{d}'_j = \frac{-\sigma h_j}{6} \hat{B}_{j-1}^n - \frac{\sigma h_j}{6\Delta_n} \xi_2^{n-\frac{1}{2}} (\hat{B}_{j-\frac{1}{2}}^n + \hat{B}_{j-\frac{1}{2}}^{n-1}) \\ e'_j = 1 + \frac{\sigma h_j}{3} \hat{A}_j^n + \frac{\sigma h_j}{6\Delta_n} \xi_2^{n-\frac{1}{2}} (\hat{A}_{j-\frac{1}{2}}^n - \hat{A}_{j-\frac{1}{2}}^{n-1}), \quad \bar{e}'_j = -1 + \frac{\sigma h_j}{3} \hat{A}_{j-1}^n + \frac{\sigma h_j}{6\Delta_n} \xi_2^{n-\frac{1}{2}} (\hat{A}_{j-\frac{1}{2}}^n - \hat{A}_{j-\frac{1}{2}}^{n-1}). \end{aligned} \quad (\text{A.2.21})$$

The inner region recurrence relation (5.3.11) for the temperature gives

$$\hat{D}_j^n - \hat{D}_{j-1}^n = \frac{1}{2} h_j (\hat{E}_{j-1}^n + \hat{E}_j^n). \quad (\text{A.2.22})$$

For Region II, equation (5.2.27) may be written in the form

$$\begin{aligned} \hat{K}_k^n - \hat{K}_{k-1}^n - \frac{\sigma H_k}{3\Delta_n \xi_2^{n-\frac{1}{2}}} [\hat{G}_{k-\frac{1}{2}}^n (\hat{J}_{k-\frac{1}{2}}^n - \hat{J}_{k-\frac{1}{2}}^{n-1}) + \hat{G}_{k-\frac{1}{2}}^{n-1} \hat{J}_{k-\frac{1}{2}}^n - \hat{K}_{k-\frac{1}{2}}^n (\hat{F}_{k-\frac{1}{2}}^n - \hat{F}_{k-\frac{1}{2}}^{n-1}) \\ - \hat{K}_{k-\frac{1}{2}}^{n-1} \hat{F}_{k-\frac{1}{2}}^n] = R'_{k-\frac{1}{2}} \end{aligned} \quad (\text{A.2.23})$$

where

$$R'_{k-\frac{1}{2}} = -\hat{K}_k^n + \hat{K}_{k-1}^n + \frac{\sigma H_k}{3\Delta_n \xi_2^{n-\frac{1}{2}}} [-\hat{G}_{k-\frac{1}{2}}^{n-1} \hat{J}_{k-\frac{1}{2}}^{n-1} + \hat{K}_{k-\frac{1}{2}}^{n-1} \hat{F}_{k-\frac{1}{2}}^{n-1}]. \quad (\text{A.2.24})$$

Again the temperature problem is linear and we can immediately write for (A.2.23)

$$\mu'_k \hat{J}_k^\wedge + \lambda'_k \hat{K}_k^\wedge + \bar{\mu}'_k \hat{J}_{k-1}^\wedge + \bar{\lambda}'_k \hat{K}_{k-1}^\wedge = R'^{k-1} + \bar{R}'_{k-1} \quad (\text{A.2.25})$$

where

$$\bar{R}'_{k-1} = \frac{-\sigma H_R}{3\Delta_n \xi_{k-1}^2} [\hat{G}_{k-1}^\wedge \hat{J}_{k-1}^\wedge + \hat{K}_{k-1}^\wedge \hat{F}_{k-1}^\wedge]$$

$$\mu'_k = \frac{-\sigma H_R}{6\Delta_n \xi_{k-1}^2} [\hat{G}_{k-1}^\wedge + \hat{G}_{k-1}^{\wedge-1}] = \bar{\mu}'_k \quad (\text{A.2.26})$$

$$\lambda'_k = 1 + \frac{\sigma H_R}{6\Delta_n \xi_{k-1}^2} [\hat{F}_{k-1}^\wedge - \hat{F}_{k-1}^{\wedge-1}], \quad \bar{\lambda}'_k = -1 + \frac{\sigma H_R}{6\Delta_n \xi_{k-1}^2} [\hat{F}_{k-1}^\wedge - \hat{F}_{k-1}^{\wedge-1}].$$

The outer region recurrence relation (5.2.25) for the temperature gives

$$\hat{J}_k^\wedge - \hat{J}_{k-1}^\wedge = \frac{1}{2} H_R (\hat{K}_k^\wedge + \hat{K}_{k-1}^\wedge). \quad (\text{A.2.27})$$

The linear system represented by (A.2.18) - (A.2.27) with the boundary and matching conditions (5.2.28), (5.2.30), (5.2.33) consists of $2J + 2K + 4$ equations and may be assembled into a single matrix equation

$$a'_1 x = b'_1 \quad (\text{A.2.28})$$

which has the structure shown in figure A.2.2. The blocks comprising a'_1 may be treated separately from each other and are first reduced to the form

$$\begin{pmatrix} * & * & * & 0 \\ 0 & * & * & * \end{pmatrix}$$

by Gaussian elimination (* represents a non-zero value). Then the same technique was used as in the velocity problem i.e. the bottom two rows were interchanged allowing a diagonal of elements to be 'stripped off' and hence the problem to be solved.

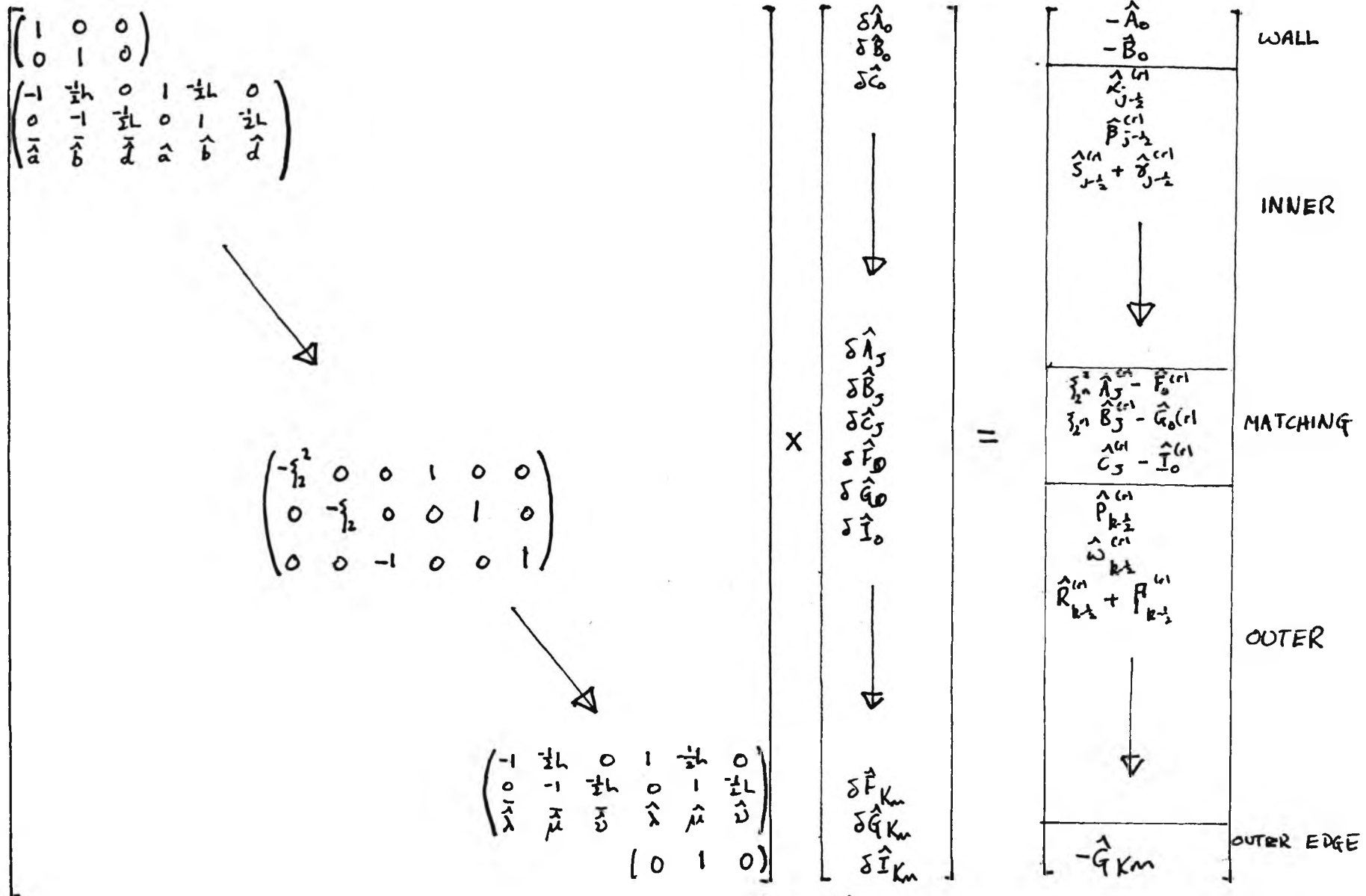


Figure A.2.1 Matrix $\hat{a}_1 x = \hat{b}_1$

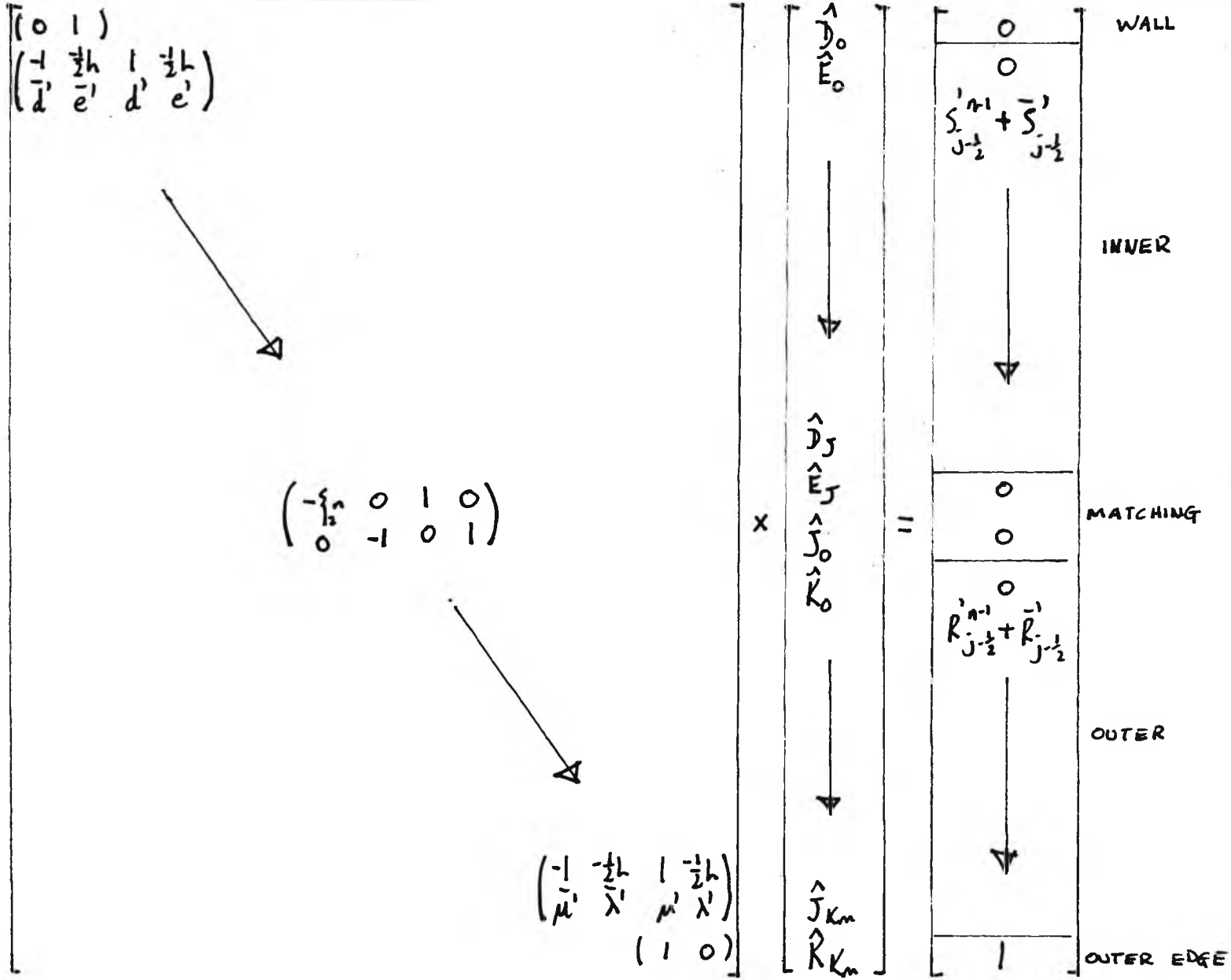


Figure A.1.2 Matrix $a'_1 x = b'_1$

Numerical Scheme for the horizontal boundary layer $x > 1$

Equation (5.3.9) may be written in the form

$$\bar{C}_j^n - \bar{C}_{j-1}^n + \frac{1}{4} h_j [\bar{A} \bar{C} + 2 \bar{B}^2]_{j-\frac{1}{2}}^n - \frac{h_j}{4 \Delta_n} \sum_{\frac{1}{2}}^n [(\bar{B}_{j-\frac{1}{2}}^n)^2 - \bar{C}_{j-\frac{1}{2}}^n (\bar{A}_{j-\frac{1}{2}}^n - \bar{A}_{j-\frac{1}{2}}^{n-1}) - \bar{C}_{j-\frac{1}{2}}^{n-1} \bar{A}_{j-\frac{1}{2}}^n] = \bar{S}_{j-\frac{1}{2}}^{n-1} \quad (\text{A.3.1})$$

where

$$\bar{S}_{j-\frac{1}{2}}^{n-1} = -\bar{C}_j^{n-1} + \bar{C}_{j-1}^{n-1} - \frac{1}{4} h_j [\bar{A} \bar{C} + 2 \bar{B}^2]_{j-\frac{1}{2}}^{n-1} + \frac{h_j}{4 \Delta_n} \sum_{\frac{1}{2}}^{n-1} [-(\bar{B}_{j-\frac{1}{2}}^{n-1})^2 + \bar{C}_{j-\frac{1}{2}}^{n-1} \bar{A}_{j-\frac{1}{2}}^{n-1}] \quad (\text{A.3.2})$$

This is a nonlinear problem so we therefore use a Newton iteration scheme by letting $\bar{A}_j^{(r)}$, $\bar{B}_j^{(r)}$, $\bar{C}_j^{(r)}$ denote the r th approximation to the true solution at step n and writing the $(r+1)$ th approximation as

$$\bar{A}_j^{(r+1)} = \bar{A}_j^{(r)} + \delta \bar{A}_j^{(r)}, \quad \bar{B}_j^{(r+1)} = \bar{B}_j^{(r)} + \delta \bar{B}_j^{(r)}, \quad \bar{C}_j^{(r+1)} = \bar{C}_j^{(r)} + \delta \bar{C}_j^{(r)} \quad (\text{A.3.3})$$

After substituting into (A.3.4) and ignoring the δ^2 terms we obtain

$$\begin{aligned} \bar{a}_j^{(r)} \delta \bar{A}_j^{(r)} + \bar{b}_j^{(r)} \delta \bar{B}_j^{(r)} + \bar{c}_j^{(r)} \delta \bar{C}_j^{(r)} + \\ \bar{a}_{j-1}^{(r)} \delta \bar{A}_{j-1}^{(r)} + \bar{b}_{j-1}^{(r)} \delta \bar{B}_{j-1}^{(r)} + \bar{c}_j^{(r)} \delta \bar{B}_{j-1}^{(r)} = \bar{S}_{j-\frac{1}{2}}^{n-1} + \bar{\gamma}_{j-\frac{1}{2}}^{(r)} \end{aligned} \quad (\text{A.3.4})$$

where

$$\begin{aligned} \bar{\gamma}_{j-\frac{1}{2}}^{(r)} = -\bar{C}_j^{(r)} + \bar{C}_{j-1}^{(r)} - \frac{1}{4} h_j [\bar{A} \bar{C} + 2 \bar{B}^2]_{j-\frac{1}{2}}^{(r)} + \frac{h_j}{4 \Delta_n} \sum_{\frac{1}{2}}^n [(\bar{B}_{j-\frac{1}{2}}^{(r)})^2 - \bar{C}_{j-\frac{1}{2}}^{(r)} \bar{A}_{j-\frac{1}{2}}^{(r)} - \bar{C}_{j-\frac{1}{2}}^{(r)} (\bar{A}_{j-\frac{1}{2}}^{(r)} - \bar{A}_{j-\frac{1}{2}}^{(r-1)})] \end{aligned} \quad (\text{A.3.5})$$

$$\bar{a}_j^{(r)} = \frac{1}{8} h_j \bar{c}_j^{(r)} + \frac{h_j}{8 \Delta_n} \sum_{\frac{1}{2}}^n [\bar{c}_{j-\frac{1}{2}}^{(r)} + \bar{c}_{j-\frac{1}{2}}^{(r-1)}] \quad (\text{A.3.6})$$

$$\bar{a}_{j-1}^{(r)} = \frac{1}{8} h_j \bar{c}_{j-1}^{(r)} + \frac{h_j}{8 \Delta_n} \sum_{\frac{1}{2}}^n [\bar{c}_{j-\frac{1}{2}}^{(r)} + \bar{c}_{j-\frac{1}{2}}^{(r-1)}] \quad (\text{A.3.7})$$

$$\tilde{b}_j^{(r)} = \frac{1}{2} h_j \bar{B}_j^{(r)} - \frac{h_j}{4\Delta_n} \sum_{\frac{1}{2}}^{\infty} \tilde{B}_{j-\frac{1}{2}}^{(r)} \quad (\text{A.3.8})$$

$$\bar{\tilde{b}}_j^{(r)} = \frac{1}{2} h_j \bar{B}_{j-1}^{(r)} - \frac{h_j}{4\Delta_n} \sum_{\frac{1}{2}}^{\infty} \bar{B}_{j-\frac{1}{2}}^{(r)} \quad (\text{A.3.9})$$

$$\tilde{c}_j^{(r)} = 1 + \frac{h_j}{8} \bar{A}_j^{(r)} + \frac{h_j}{8\Delta_n} \sum_{\frac{1}{2}}^{\infty} [\bar{A}_{j-\frac{1}{2}}^{(r)} - \bar{A}_{j-\frac{1}{2}}^{(r-1)}] \quad (\text{A.3.10})$$

$$\bar{\tilde{c}}_j^{(r)} = -1 + \frac{h_j}{8} \bar{A}_{j-1}^{(r)} + \frac{h_j}{8\Delta_n} \sum_{\frac{1}{2}}^{\infty} [\bar{A}_{j-\frac{1}{2}}^{(r)} - \bar{A}_{j-\frac{1}{2}}^{(r-1)}]. \quad (\text{A.3.11})$$

The recurrence relations (5.3.8) give

$$\delta \bar{A}_j^{(r)} - \delta \bar{A}_{j-1}^{(r)} - \frac{1}{2} h_j (\delta \bar{B}_j^{(r)} + \delta \bar{B}_{j-1}^{(r)}) = \tilde{\alpha}_{j-\frac{1}{2}}^{(r)} \quad (\text{A.3.12})$$

$$\delta \bar{B}_j^{(r)} - \delta \bar{B}_{j-1}^{(r)} - \frac{1}{2} h_j (\delta \tilde{c}_j^{(r)} + \delta \tilde{c}_{j-1}^{(r)}) = \tilde{\beta}_{j-\frac{1}{2}}^{(r)} \quad (\text{A.3.13})$$

where

$$\tilde{\alpha}_{j-\frac{1}{2}}^{(r)} = \frac{1}{2} h_j (\bar{B}_j^{(r)} + \bar{B}_{j-1}^{(r)}) + \bar{A}_{j-1}^{(r)} - \bar{A}_j^{(r)} \quad (\text{A.3.14})$$

$$\tilde{\beta}_{j-\frac{1}{2}}^{(r)} = \frac{1}{2} h_j (\bar{c}_j^{(r)} + \bar{c}_{j-1}^{(r)}) + \bar{B}_{j-1}^{(r)} - \bar{B}_j^{(r)}, \quad (\text{A.3.15})$$

For the boundary condition we have from (5.3.16)

$$\delta \bar{B}_0^{(r)} = -\bar{B}_0^{(r)}, \quad \delta \bar{A}_0^{(r)} = -\bar{A}_0^{(r)} \quad (\text{A.3.16})$$

and from (5.3.17)

$$\delta \bar{B}_J^{(r)} = -\bar{B}_J^{(r)}. \quad (\text{A.3.17})$$

The linear system represented by (A.3.2) - (A.3.17) consists of $3J + 3$ equations which may be assembled into a single matrix equation

$$\bar{a}x = \bar{b} \quad (\text{A.3.18})$$

which has the structure

$$\begin{bmatrix}
 \begin{matrix} (1 & 0 & 0) \\ (0 & 1 & 0) \\ \vdots & \vdots & \vdots \end{matrix} \\
 \tilde{P}_j \\
 \begin{matrix} \vdots \\ \vdots \\ (0 & 1 & 0) \end{matrix}
 \end{bmatrix}
 \times
 \begin{bmatrix}
 \delta A_0 \\
 \delta B_0 \\
 \delta C_0 \\
 \vdots \\
 \delta A_J \\
 \delta B_J \\
 \delta C_J
 \end{bmatrix}
 =
 \begin{bmatrix}
 -A_0 \\
 -B_0 \\
 \vdots \\
 \tilde{Q}_j \\
 \vdots \\
 -B_J
 \end{bmatrix}$$

where

$$[\tilde{P}_j] = \begin{pmatrix} -1 & -\frac{1}{2}h & 0 & 1 & -\frac{1}{2}h & 0 \\ 0 & -1 & -\frac{1}{2}h & 0 & 1 & -\frac{1}{2}h \\ \bar{a}_j & \bar{b}_j & \bar{c}_j & \bar{a}_j & \bar{b}_j & \bar{c}_j \end{pmatrix}, \quad [\tilde{Q}_j] = \begin{pmatrix} \tilde{\alpha}_{j-1/2} \\ \tilde{\beta}_{j-1/2} \\ \tilde{S}_{j-1/2}^{n-1} + \tilde{\gamma}_{j-1/2}(r) \end{pmatrix}$$

This matrix problem was solved in a similar manner to the velocity problem of Section 5.2. The three elements at the top right and bottom left corners of $[\tilde{P}_j]$ were reduced to zero by Gaussian elimination. The bottom two rows of \bar{a} were then interchanged allowing a diagonal of elements to be 'stripped off' and the increments to be found. The matrices \bar{a} and \bar{b} were then recalculated and the procedure continued until all the increments were sufficiently small.

The temperature problem is a linear one and we can immediately write equation (5.3.10) as

$$\tilde{d}_j \bar{D}_j^{\wedge} + \tilde{e}_j \bar{E}_j^{\wedge} + \tilde{d}_j \bar{D}_{j-1}^{\wedge} + \tilde{e}_j \bar{E}_{j-1}^{\wedge} = \tilde{R}_{j-1/2}^{\wedge} \tag{A.3.19}$$

where

$$\begin{aligned}
 \tilde{R}_{j-1/2}^{\wedge} = & \frac{1}{\sigma} [\bar{E}_j^{\wedge} - \bar{E}_{j-1}^{\wedge}] + \frac{1}{4} [(\bar{D}\bar{A})_j^{\wedge} - (\bar{D}\bar{A})_{j-1}^{\wedge}] - \\
 & \frac{\tilde{\gamma}_{j-1/2}}{4\Delta_n} [-\bar{D}_j^{\wedge} (\bar{A}_j^{\wedge} + \bar{A}_j^{\wedge-1}) + \bar{D}_{j-1}^{\wedge} (\bar{A}_{j-1}^{\wedge} + \bar{A}_{j-1}^{\wedge-1})] + \\
 & \frac{k_j \tilde{\gamma}_{j-1/2}}{4\Delta_n} [-(\bar{A}\bar{E})_j^{\wedge} - (\bar{A}\bar{E})_{j-1}^{\wedge}]
 \end{aligned} \tag{A.3.20}$$

$$\tilde{d}_j = \frac{1}{4} \bar{A}_j - \frac{\sum_{2^{n-1}}}{4\Delta_n} (\bar{A}_j + \bar{A}_j^{n-1}) \quad (\text{A.3.21})$$

$$\bar{d}_j = -\frac{1}{4} \bar{A}_{j-1} - \frac{\sum_{2^{n-1}}}{4\Delta_n} (\bar{A}_{j-1} + \bar{A}_{j-1}^{n-1}) \quad (\text{A.3.22})$$

$$\tilde{e}_j = \frac{1}{\sigma} + \frac{\sum_{2^{n-1}}}{4\Delta_n} \bar{A}_j \quad (\text{A.3.23})$$

$$\bar{e}_j = -\frac{1}{\sigma} + \frac{\sum_{2^{n-1}}}{4\Delta_n} \bar{A}_{j-1}. \quad (\text{A.3.24})$$

The recurrence relation (5.3.8) gives

$$\bar{D}_j - \bar{D}_{j-1} = \frac{1}{2} h_j (\bar{E}_{j-1} + \bar{E}_j). \quad (\text{A.3.25})$$

The linear system represented by (A.3.19) - (A.3.25) together with the boundary conditions (5.3.16) and (5.3.17) consists of $2J + 4$ equations and may be assembled into a single matrix equation

$$\tilde{a}^1 x = \tilde{b}^1 \quad (\text{A.3.26})$$

which has the structure

$$\begin{bmatrix} (0 & 1) \\ \left[\begin{array}{c} \tilde{P}_j^1 \\ \vdots \\ \tilde{P}_j^1 \end{array} \right] \\ (1 & 0) \end{bmatrix} \times \begin{bmatrix} \bar{D}_0 \\ \bar{E}_0 \\ \vdots \\ \bar{D}_J \\ \bar{E}_J \end{bmatrix} = \begin{bmatrix} 0 \\ \left[\begin{array}{c} \tilde{Q}_j^1 \\ \vdots \\ \tilde{Q}_j^1 \end{array} \right] \\ 0 \end{bmatrix}$$

where

$$[\tilde{P}_j^1] = \begin{pmatrix} -1 & -\frac{1}{2}h & 1 & -\frac{1}{2}h \\ \tilde{d}_j & \tilde{e}_j & \bar{d}_j & \bar{e}_j \end{pmatrix}, \quad [\tilde{Q}_j^1] = \begin{pmatrix} 0 \\ \bar{R}_{j-1/2}^{n-1} \end{pmatrix}.$$

The matrix problem was solved in the same way as the temperature problem in Section 5.2.

APPENDIX 4

Numerical Scheme for the buoyancy layer $x_3 < 1$

Equation (7.2.10) may be written in the form

$$4C_j^\wedge - 4C_{j-1}^\wedge + \frac{h_j}{\sigma} \left[-2\zeta_3^{\wedge 6} D_{j-\frac{1}{2}}^\wedge - \frac{2}{\Delta_n} \zeta_3^{\wedge 7} D_{j-\frac{1}{2}}^\wedge + 3\eta_{j-\frac{1}{2}} \zeta_3^{\wedge 6} E_{j-\frac{1}{2}}^\wedge \right] + h_j [(B_j^\wedge)^2 + (B_{j-1}^\wedge)^2] + \frac{1}{2} h_j [(AC)_j^\wedge + (AC)_{j-1}^\wedge] - \frac{\zeta_3^{\wedge 5} h_j}{\Delta_n} \times$$

$$[(B_{j-\frac{1}{2}}^\wedge)^2 - C_{j-\frac{1}{2}}^\wedge (A_{j-\frac{1}{2}}^\wedge - A_{j-1}^\wedge) - C_{j-\frac{1}{2}}^\wedge A_{j-\frac{1}{2}}^\wedge] = S_{j-\frac{1}{2}}^\wedge \quad (A.4.1)$$

where

$$S_{j-\frac{1}{2}}^{\wedge-1} = -4C_j^{\wedge-1} + 4C_{j-1}^{\wedge-1} - \frac{h_j}{\sigma} \left[-2\zeta_3^{\wedge 6} D_{j-\frac{1}{2}}^{\wedge-1} + \frac{2}{\Delta_n} \zeta_3^{\wedge 7} D_{j-\frac{1}{2}}^{\wedge-1} + 3\eta_{j-\frac{1}{2}} \zeta_3^{\wedge 6} E_{j-\frac{1}{2}}^{\wedge-1} \right] - h_j [(B_j^{\wedge-1})^2 + (B_{j-1}^{\wedge-1})^2] - \frac{1}{2} h_j [(AC)_j^{\wedge-1} + (AC)_{j-1}^{\wedge-1}] + \zeta_3^{\wedge 5} \frac{h_j}{\Delta_n} \left[-(B_{j-\frac{1}{2}}^{\wedge-1})^2 + C_{j-\frac{1}{2}}^{\wedge-1} A_{j-\frac{1}{2}}^{\wedge-1} \right] \quad (A.4.2)$$

while equation (7.2.11) may be written in the form

$$8F_j^\wedge - 8F_{j-1}^\wedge + \sigma h_j [(EB)_j^\wedge + (EB)_{j-1}^\wedge + (AF)_j^\wedge + (AF)_{j-1}^\wedge] - \frac{2\sigma h_j}{\Delta_n} \zeta_3^{\wedge 5} \left[B_{j-\frac{1}{2}}^\wedge (E_{j-\frac{1}{2}}^\wedge - E_{j-1}^\wedge) + B_{j-\frac{1}{2}}^{\wedge-1} E_{j-\frac{1}{2}}^\wedge - F_{j-\frac{1}{2}}^\wedge (A_{j-\frac{1}{2}}^\wedge - A_{j-1}^\wedge) - F_{j-\frac{1}{2}}^\wedge A_{j-\frac{1}{2}}^\wedge \right] = T_{j-\frac{1}{2}}^{\wedge-1} \quad (A.4.3)$$

where

$$T_{j-\frac{1}{2}}^{\wedge-1} = -8F_j^{\wedge-1} + 8F_{j-1}^{\wedge-1} - \sigma h_j [(EB)_j^{\wedge-1} + (EB)_{j-1}^{\wedge-1} + (AF)_j^{\wedge-1} + (AF)_{j-1}^{\wedge-1}] + \frac{2\sigma h_j}{\Delta_n} \zeta_3^{\wedge 5} \left[-B_{j-\frac{1}{2}}^{\wedge-1} E_{j-\frac{1}{2}}^{\wedge-1} + F_{j-\frac{1}{2}}^{\wedge-1} A_{j-\frac{1}{2}}^{\wedge-1} \right]. \quad (A.4.4)$$

This is a nonlinear problem so we therefore use a Newton iteration scheme by letting $A_j^{(r)}$, $B_j^{(r)}$, $C_j^{(r)}$, $D_j^{(r)}$, $E_j^{(r)}$, $F_j^{(r)}$ denote the rth approximation to the true solution at step

n and writing the (r+1)th approximation as

$$A_j^{(r+1)} = A_j^{(r)} + \delta A_j^{(r)}, \quad B_j^{(r+1)} = B_j^{(r)} + \delta B_j^{(r)}, \quad C_j^{(r+1)} = C_j^{(r)} + \delta C_j^{(r)},$$

$$D_j^{(r+1)} = D_j^{(r)} + \delta D_j^{(r)}, \quad E_j^{(r+1)} = E_j^{(r)} + \delta E_j^{(r)}, \quad F_j^{(r+1)} = F_j^{(r)} + \delta F_j^{(r)}. \quad (A.4.5)$$

After substituting into (A.4.1) and ignoring the δ^2 terms we obtain

$$\begin{aligned} a_j^{(r)} \delta A_j^{(r)} + b_j^{(r)} \delta B_j^{(r)} + c_j^{(r)} \delta C_j^{(r)} + d_j \delta D_j^{(r)} + e_j^{(r)} \delta E_j^{(r)} + \\ \bar{a}_j^{(r)} \delta A_{j-1}^{(r)} + \bar{b}_j^{(r)} \delta B_{j-1}^{(r)} + \bar{c}_j^{(r)} \delta C_{j-1}^{(r)} + \bar{d}_j \delta D_{j-1}^{(r)} + \bar{e}_j^{(r)} \delta E_{j-1}^{(r)} = S_{j-\frac{1}{2}}^{n-1} + \gamma_{j-\frac{1}{2}}^{(r)} \end{aligned} \quad (\text{A.4.6})$$

where

$$\begin{aligned} \gamma_{j-\frac{1}{2}}^{(r)} = -4 (c_j^{(r)} - c_{j-1}^{(r)}) + D_{j-\frac{1}{2}}^{(r)} \frac{2h_j}{\sigma} \left\{ \xi_3^{n-\frac{1}{2}} \left(1 + \frac{\xi_3^{n-\frac{1}{2}}}{\Delta_n} \right) - 3 \eta_{j-\frac{1}{2}} \xi_3^{n-\frac{1}{2}} \frac{h_j}{\sigma} E_{j-\frac{1}{2}}^{(r)} \right. \\ \left. - \frac{1}{2} h_j \left\{ 2(B_j^{(r)})^2 + 2(B_{j-1}^{(r)})^2 + A_j^{(r)} C_j^{(r)} + A_{j-1}^{(r)} C_{j-1}^{(r)} \right\} + \right. \\ \left. \frac{h_j}{\Delta_n} \xi_3^{n-\frac{1}{2}} \left\{ (B_{j-\frac{1}{2}}^{(r)})^2 - C_{j-\frac{1}{2}}^{(r)} (A_{j-\frac{1}{2}}^{(r)} - A_{j-\frac{3}{2}}^{(r)}) - C_{j-\frac{1}{2}}^{(r)} A_{j-\frac{3}{2}}^{(r)} \right\} \right. \end{aligned} \quad (\text{A.4.7})$$

$$a_j^{(r)} = \frac{1}{2} h_j C_j^{(r)} + \frac{1}{2} \xi_3^{n-\frac{1}{2}} \frac{h_j}{\Delta_n} (C_{j-\frac{1}{2}}^{(r)} + C_{j-\frac{3}{2}}^{(r)}) \quad (\text{A.4.8})$$

$$\bar{a}_j^{(r)} = \frac{1}{2} h_j C_{j-1}^{(r)} + \frac{1}{2} \xi_3^{n-\frac{1}{2}} \frac{h_j}{\Delta_n} (C_{j-\frac{1}{2}}^{(r)} + C_{j-\frac{3}{2}}^{(r)}) \quad (\text{A.4.9})$$

$$b_j^{(r)} = 2h_j B_j^{(r)} - \xi_3^{n-\frac{1}{2}} \frac{h_j}{\Delta_n} B_{j-\frac{1}{2}}^{(r)} \quad (\text{A.4.10})$$

$$\bar{b}_j^{(r)} = 2h_j B_{j-1}^{(r)} - \xi_3^{n-\frac{1}{2}} \frac{h_j}{\Delta_n} B_{j-\frac{1}{2}}^{(r)} \quad (\text{A.4.11})$$

$$c_j^{(r)} = 4 + \frac{1}{2} h_j A_j^{(r)} + \frac{1}{2} \xi_3^{n-\frac{1}{2}} \frac{h_j}{\Delta_n} (A_{j-\frac{1}{2}}^{(r)} - A_{j-\frac{3}{2}}^{(r)}) \quad (\text{A.4.12})$$

$$\bar{c}_j^{(r)} = -4 + \frac{1}{2} h_j A_{j-1}^{(r)} + \frac{1}{2} \xi_3^{n-\frac{1}{2}} \frac{h_j}{\Delta_n} (A_{j-\frac{1}{2}}^{(r)} - A_{j-\frac{3}{2}}^{(r)}) \quad (\text{A.4.13})$$

$$d_j^{(r)} = \frac{-h_j}{\sigma} \xi_3^{n-\frac{1}{2}} \left(1 + \frac{\xi_3^{n-\frac{1}{2}}}{\Delta_n} \right) = \bar{d}_j^{(r)} \quad (\text{A.4.14})$$

$$e_j^{(r)} = \frac{3h_j}{2\sigma} \eta_{j-\frac{1}{2}} \xi_3^{n-\frac{1}{2}} = \bar{e}_j^{(r)} \quad (\text{A.4.15})$$

Substituting (A.2.5) into (A.2.3) and again ignoring the δ^2 terms we obtain

$$\begin{aligned} \alpha_j^{(r)} \delta A_j^{(r)} + \beta_j^{(r)} \delta B_j^{(r)} + \mu_j^{(r)} \delta E_j^{(r)} + \lambda_j^{(r)} \delta F_j^{(r)} + \\ \bar{\alpha}_j^{(r)} \delta A_{j-1}^{(r)} + \bar{\beta}_j^{(r)} \delta B_{j-1}^{(r)} + \bar{\mu}_j^{(r)} \delta E_{j-1}^{(r)} + \bar{\lambda}_j^{(r)} \delta F_{j-1}^{(r)} = T_{j-\frac{1}{2}}^{n-1} + R_{j-\frac{1}{2}}^{n-1} \end{aligned} \quad (\text{A.4.16})$$

where

$$\begin{aligned} R_{j-\frac{1}{2}}^{n-1} = -8F_j^{(r)} + 8F_{j-1}^{(r)} - \sigma h_j [E_j^{(r)} B_j^{(r)} + E_{j-1}^{(r)} B_{j-1}^{(r)} + A_j^{(r)} F_j^{(r)} + A_{j-1}^{(r)} F_{j-1}^{(r)}] \\ + \frac{2\sigma h_j}{\Delta_n} \xi_3^{n-\frac{1}{2}} [B_{j-\frac{1}{2}}^{(r)} (E_{j-\frac{1}{2}}^{(r)} - E_{j-\frac{3}{2}}^{(r)}) + B_{j-\frac{1}{2}}^{(r)} E_{j-\frac{1}{2}}^{(r)} - F_{j-\frac{1}{2}}^{(r)} (A_{j-\frac{1}{2}}^{(r)} - A_{j-\frac{3}{2}}^{(r)}) - F_{j-\frac{1}{2}}^{(r)} A_{j-\frac{3}{2}}^{(r)}] \end{aligned} \quad (\text{A.4.17})$$

$$\alpha_j^{(r)} = \sigma h_j F_j^{(r)} + \sigma h_j \xi_{3^{n-k_2}} \frac{1}{\Delta_n} [F_{j-\frac{1}{2}}^{(r)} + F_{j-\frac{1}{2}}^{(r-1)}] \quad (\text{A.4.18})$$

$$\bar{\alpha}_j^{(r)} = \sigma h_j F_{j-1}^{(r)} + \sigma h_j \xi_{3^{n-k_2}} \frac{1}{\Delta_n} [F_{j-\frac{1}{2}}^{(r)} + F_{j-\frac{1}{2}}^{(r-1)}] \quad (\text{A.4.19})$$

$$\beta_j^{(r)} = \sigma h_j E_j^{(r)} + \sigma h_j \xi_{3^{n-k_2}} \frac{1}{\Delta_n} [-E_{j-\frac{1}{2}}^{(r)} + E_{j-\frac{1}{2}}^{(r-1)}] \quad (\text{A.4.20})$$

$$\bar{\beta}_j^{(r)} = \sigma h_j E_{j-1}^{(r)} + \sigma h_j \xi_{3^{n-k_2}} \frac{1}{\Delta_n} [-E_{j-\frac{1}{2}}^{(r)} + E_{j-\frac{1}{2}}^{(r-1)}] \quad (\text{A.4.21})$$

$$\mu_j^{(r)} = \sigma h_j B_j^{(r)} - \sigma h_j \xi_{3^{n-k_2}} \frac{1}{\Delta_n} [B_{j-\frac{1}{2}}^{(r)} + B_{j-\frac{1}{2}}^{(r-1)}] \quad (\text{A.4.22})$$

$$\bar{\mu}_j^{(r)} = \sigma h_j B_{j-1}^{(r)} - \sigma h_j \xi_{3^{n-k_2}} \frac{1}{\Delta_n} [B_{j-\frac{1}{2}}^{(r)} + B_{j-\frac{1}{2}}^{(r-1)}] \quad (\text{A.4.23})$$

$$\gamma_j^{(r)} = \delta + \sigma h_j A_j^{(r)} + \sigma h_j \xi_{3^{n-k_2}} \frac{1}{\Delta_n} [A_{j-\frac{1}{2}}^{(r)} - A_{j-\frac{1}{2}}^{(r-1)}] \quad (\text{A.4.24})$$

$$\bar{\gamma}_j^{(r)} = -\delta + \sigma h_j A_{j-1}^{(r)} + \sigma h_j \xi_{3^{n-k_2}} \frac{1}{\Delta_n} [A_{j-\frac{1}{2}}^{(r)} - A_{j-\frac{1}{2}}^{(r-1)}]. \quad (\text{A.4.25})$$

The recurrence relations (7.2.9) give

$$\delta A_j^{(r)} - \delta A_{j-1}^{(r)} - \frac{1}{2} h_j (\delta B_j^{(r)} + \delta B_{j-1}^{(r)}) = k_{j-\frac{1}{2}}^{(r)} \quad (\text{A.4.26})$$

$$\delta B_j^{(r)} - \delta B_{j-1}^{(r)} - \frac{1}{2} h_j (\delta C_j^{(r)} + \delta C_{j-1}^{(r)}) = L_{j-\frac{1}{2}}^{(r)} \quad (\text{A.4.27})$$

$$\delta D_j^{(r)} - \delta D_{j-1}^{(r)} - \frac{1}{2} h_j (\delta E_j^{(r)} + \delta E_{j-1}^{(r)}) = M_{j-\frac{1}{2}}^{(r)} \quad (\text{A.4.28})$$

$$\delta E_j^{(r)} - \delta E_{j-1}^{(r)} - \frac{1}{2} h_j (\delta F_j^{(r)} + \delta F_{j-1}^{(r)}) = N_{j-\frac{1}{2}}^{(r)} \quad (\text{A.4.29})$$

where

$$k_{j-\frac{1}{2}}^{(r)} = -A_j^{(r)} + A_{j-1}^{(r)} + \frac{1}{2} h_j (B_j^{(r)} + B_{j-1}^{(r)}) \quad (\text{A.4.30})$$

$$L_{j-\frac{1}{2}}^{(r)} = -B_j^{(r)} + B_{j-1}^{(r)} + \frac{1}{2} h_j (C_j^{(r)} + C_{j-1}^{(r)}) \quad (\text{A.4.31})$$

$$M_{j-\frac{1}{2}}^{(r)} = -D_j^{(r)} + D_{j-1}^{(r)} + \frac{1}{2} h_j (E_j^{(r)} + E_{j-1}^{(r)}) \quad (\text{A.4.32})$$

$$N_{j-\frac{1}{2}}^{(r)} = -E_j^{(r)} + E_{j-1}^{(r)} + \frac{1}{2} h_j (F_j^{(r)} + F_{j-1}^{(r)}). \quad (\text{A.4.33})$$

$$[Q_j] = \begin{pmatrix} m_j^{(r)} \\ k_j^{(r)} \\ n_j^{(r)} \\ L_j^{(r)} \\ T_{j-1/2}^{n-1} + R_{j-1/2}^{(r)} \\ S_{j-1/2}^{n-1} + \gamma_{j-1/2}^{(r)} \end{pmatrix} .$$

The matrix problem was solved by reducing to zero the bottom left and top right corners of $[P_j]$ (15 elements) by Gaussian elimination. NAG routine F01LBF which decomposes a general band matrix into triangular matrices using Gaussian elimination with partial pivoting and F04LDF which solves the resulting linear system were then used to solve for the Newton increments. The matrices \hat{A} and \hat{B} were then recalculated and the procedure continued until all the increments were sufficiently small.

Numerical scheme for the buoyancy layer $x_3 > 1$

Equation (7.3.10) may be written in the form

$$4\hat{C}_j^n - 4\hat{C}_{j-1}^n + \frac{h_j}{\sigma} \left[-4\frac{\hat{\xi}_3^{n-\frac{1}{2}}}{\Delta n} \hat{D}_{j-\frac{1}{2}}^n + 2\hat{\gamma}_{j-\frac{1}{2}} \hat{E}_{j-\frac{1}{2}}^n \right] + h_j [(\hat{A}\hat{C})_j^n + (\hat{A}\hat{C})_{j-1}^n] - \frac{2h_j \hat{\xi}_3^{n-\frac{1}{2}}}{\Delta n} \left[(\hat{B}_{j-\frac{1}{2}}^n)^2 - \hat{C}_{j-\frac{1}{2}}^n (\hat{A}_{j-\frac{1}{2}}^n - \hat{A}_{j-\frac{1}{2}}^{n-1}) - \hat{C}_{j-\frac{1}{2}}^{n-1} \hat{A}_{j-\frac{1}{2}}^n \right] = \hat{S}_{j-\frac{1}{2}}^{n-1} \quad (\text{A.5.1})$$

where

$$\hat{S}_{j-\frac{1}{2}}^{n-1} = -4\hat{C}_j^{n-1} + 4\hat{C}_{j-1}^{n-1} - \frac{h_j}{\sigma} \left[\frac{4\hat{\xi}_3^{n-\frac{1}{2}}}{\Delta n} \hat{D}_{j-\frac{1}{2}}^{n-1} + 2\hat{\gamma}_{j-\frac{1}{2}} \hat{E}_{j-\frac{1}{2}}^{n-1} \right] - h_j [(\hat{A}\hat{C})_j^{n-1} + (\hat{A}\hat{C})_{j-1}^{n-1}] + \frac{2}{\Delta n} \hat{\xi}_3^{n-\frac{1}{2}} h_j \left[-(\hat{B}_{j-\frac{1}{2}}^{n-1})^2 + \hat{C}_{j-\frac{1}{2}}^{n-1} \hat{A}_{j-\frac{1}{2}}^{n-1} \right]. \quad (\text{A.5.2})$$

while equation (7.3.11) may be written in the form

$$8\hat{F}_j^n - 8\hat{F}_{j-1}^n + 2\sigma h_j [(\hat{E}\hat{B})_j^n + (\hat{E}\hat{B})_{j-1}^n + (\hat{A}\hat{F})_j^n + (\hat{A}\hat{F})_{j-1}^n] - 4\sigma \frac{h_j}{\Delta n} \hat{\xi}_3^{n-\frac{1}{2}} \left[\hat{B}_{j-\frac{1}{2}}^n (\hat{E}_{j-\frac{1}{2}}^n - \hat{E}_{j-\frac{1}{2}}^{n-1}) + \hat{B}_{j-\frac{1}{2}}^{n-1} \hat{E}_{j-\frac{1}{2}}^n - \hat{F}_{j-\frac{1}{2}}^n (\hat{A}_{j-\frac{1}{2}}^n - \hat{A}_{j-\frac{1}{2}}^{n-1}) - \hat{F}_{j-\frac{1}{2}}^{n-1} \hat{A}_{j-\frac{1}{2}}^n \right] = \hat{T}_{j-\frac{1}{2}}^{n-1} \quad (\text{A.5.3})$$

where

$$\hat{T}_{j-\frac{1}{2}}^{n-1} = -8\hat{F}_j^{n-1} + 8\hat{F}_{j-1}^{n-1} - 2\sigma h_j [(\hat{E}\hat{B})_j^{n-1} + (\hat{E}\hat{B})_{j-1}^{n-1} + (\hat{A}\hat{F})_j^{n-1} + (\hat{A}\hat{F})_{j-1}^{n-1}] + \frac{4\sigma h_j}{\Delta n} \hat{\xi}_3^{n-\frac{1}{2}} \left[-\hat{B}_{j-\frac{1}{2}}^{n-1} \hat{E}_{j-\frac{1}{2}}^{n-1} + \hat{F}_{j-\frac{1}{2}}^{n-1} \hat{A}_{j-\frac{1}{2}}^{n-1} \right] \quad (\text{A.5.4})$$

This is a nonlinear problem so we therefore use a Newton iteration scheme by letting $\hat{A}_j(r)$, $\hat{B}_j(r)$, $\hat{C}_j(r)$, $\hat{D}_j(r)$, $\hat{E}_j(r)$, $\hat{F}_j(r)$ denote the r th approximation to the true solution at step

n and writing the $(r+1)$ th approximation as

$$\hat{A}_j^{(r+1)} = \hat{A}_j^{(r)} + \delta \hat{A}_j^{(r)}, \quad \hat{B}_j^{(r+1)} = \hat{B}_j^{(r)} + \delta \hat{B}_j^{(r)}, \quad \hat{C}_j^{(r+1)} = \hat{C}_j^{(r)} + \delta \hat{C}_j^{(r)}, \quad \hat{D}_j^{(r+1)} = \hat{D}_j^{(r)} + \delta \hat{D}_j^{(r)}, \quad \hat{E}_j^{(r+1)} = \hat{E}_j^{(r)} + \delta \hat{E}_j^{(r)}, \quad \hat{F}_j^{(r+1)} = \hat{F}_j^{(r)} + \delta \hat{F}_j^{(r)} \quad (\text{A.5.5})$$

After substituting into (A.5.1) and ignoring the δ^2 terms we obtain

$$\hat{a}_j^{(r)} \delta \hat{A}_j^{(r)} + \hat{b}_j^{(r)} \delta \hat{B}_j^{(r)} + \hat{c}_j^{(r)} \delta \hat{C}_j^{(r)} + \hat{d}_j^{(r)} \delta \hat{D}_j^{(r)} + \hat{e}_j^{(r)} \delta \hat{E}_j^{(r)} + \hat{a}_j^{(r)} \delta \hat{A}_{j-1}^{(r)} + \hat{b}_j^{(r)} \delta \hat{B}_{j-1}^{(r)} + \hat{c}_j^{(r)} \delta \hat{C}_{j-1}^{(r)} + \hat{d}_j^{(r)} \delta \hat{D}_{j-1}^{(r)} + \hat{e}_j^{(r)} \delta \hat{E}_{j-1}^{(r)} = \hat{S}_{j-\frac{1}{2}}^{n-1} + \delta \hat{S}_{j-\frac{1}{2}}^{(r)} \quad (\text{A.5.6})$$

where

$$\hat{\gamma}_{j-\frac{1}{2}}^{(n)} = -4\hat{c}_j^{(n)} + 4\hat{c}_{j-1}^{(n)} - \frac{h_j}{\sigma} \left\{ \frac{-4}{\Delta_n} \hat{\gamma}_{j-\frac{1}{2}}^{(n-1)} + 2\hat{\eta}_{j-\frac{1}{2}}^{(n-1)} \hat{E}_{j-\frac{1}{2}}^{(n-1)} \right\} - h_j \left\{ \hat{A}_j^{(n)} \hat{c}_j^{(n)} + \hat{A}_{j-1}^{(n)} \hat{c}_{j-1}^{(n)} \right\} + \frac{2h_j}{\Delta_n} \hat{\gamma}_{j-\frac{1}{2}}^{(n-1)} \left\{ (\hat{B}_{j-\frac{1}{2}}^{(n)})^2 - \hat{c}_{j-\frac{1}{2}}^{(n)} (\hat{A}_{j-\frac{1}{2}}^{(n)} - \hat{A}_{j-\frac{1}{2}}^{(n-1)}) - \hat{c}_{j-\frac{1}{2}}^{(n-1)} \hat{A}_{j-\frac{1}{2}}^{(n-1)} \right\} \quad (\text{A.5.7})$$

$$\hat{\alpha}_j^{(n)} = h_j \hat{c}_j^{(n)} + \frac{h_j}{\Delta_n} \hat{\gamma}_{j-\frac{1}{2}}^{(n-1)} (\hat{c}_{j-\frac{1}{2}}^{(n)} + \hat{c}_{j-\frac{1}{2}}^{(n-1)}) \quad (\text{A.5.8})$$

$$\bar{\alpha}_j^{(n)} = h_j \hat{c}_{j-1}^{(n)} + \frac{h_j}{\Delta_n} \hat{\gamma}_{j-\frac{1}{2}}^{(n-1)} (\hat{c}_{j-\frac{1}{2}}^{(n)} + \hat{c}_{j-\frac{1}{2}}^{(n-1)}) \quad (\text{A.5.9})$$

$$\hat{b}_j^{(n)} = \frac{-2h_j}{\Delta_n} \hat{\gamma}_{j-\frac{1}{2}}^{(n-1)} \hat{B}_{j-\frac{1}{2}}^{(n)} = \bar{b}_j^{(n)} \quad (\text{A.5.10})$$

$$\hat{c}_j^{(n)} = 4 + h_j \hat{A}_j^{(n)} + \frac{h_j}{\Delta_n} \hat{\gamma}_{j-\frac{1}{2}}^{(n-1)} (\hat{A}_{j-\frac{1}{2}}^{(n)} - \hat{A}_{j-\frac{1}{2}}^{(n-1)}) \quad (\text{A.5.11})$$

$$\bar{c}_j^{(n)} = -4 + h_j \hat{A}_j^{(n)} + \frac{h_j}{\Delta_n} \hat{\gamma}_{j-\frac{1}{2}}^{(n-1)} (\hat{A}_{j-\frac{1}{2}}^{(n)} - \hat{A}_{j-\frac{1}{2}}^{(n-1)}) \quad (\text{A.5.12})$$

$$\hat{d}_j^{(n)} = \frac{-2h_j}{\Delta_n \sigma} \hat{\gamma}_{j-\frac{1}{2}}^{(n-1)} = \bar{d}_j^{(n)} \quad (\text{A.5.13})$$

$$\hat{e}_j^{(n)} = \frac{h_j}{\sigma} \hat{\eta}_{j-\frac{1}{2}}^{(n-1)} = \bar{e}_j^{(n)} \quad (\text{A.5.14})$$

Substituting (A.5.5) into (A.5.11) and again ignoring the δ^2 terms we obtain

$$\hat{\alpha}_j^{(n)} \delta \hat{A}_j^{(n)} + \hat{\beta}_j^{(n)} \delta \hat{B}_j^{(n)} + \hat{\mu}_j^{(n)} \delta \hat{E}_j^{(n)} + \hat{\nu}_j^{(n)} \delta \hat{F}_j^{(n)} + \bar{\alpha}_j^{(n)} \delta \hat{A}_{j-1}^{(n)} + \bar{\beta}_j^{(n)} \delta \hat{B}_{j-1}^{(n)} + \bar{\mu}_j^{(n)} \delta \hat{E}_{j-1}^{(n)} + \bar{\nu}_j^{(n)} \delta \hat{F}_{j-1}^{(n)} = \hat{T}_{j-\frac{1}{2}}^{(n-1)} + \hat{R}_{j-\frac{1}{2}}^{(n-1)} \quad (\text{A.5.15})$$

where

$$\hat{R}_{j-\frac{1}{2}}^{(n-1)} = -8\hat{F}_j^{(n)} + 8\hat{F}_{j-1}^{(n)} - 2\sigma h_j \left\{ \hat{E}_j^{(n)} \hat{B}_j^{(n)} + \hat{E}_{j-1}^{(n)} \hat{B}_{j-1}^{(n)} + \hat{A}_j^{(n)} \hat{F}_j^{(n)} + \hat{A}_{j-1}^{(n)} \hat{F}_{j-1}^{(n)} \right\} + \frac{4\sigma h_j}{\Delta_n} \hat{\gamma}_{j-\frac{1}{2}}^{(n-1)} \left\{ \hat{B}_{j-\frac{1}{2}}^{(n)} (\hat{E}_{j-\frac{1}{2}}^{(n)} - \hat{E}_{j-\frac{1}{2}}^{(n-1)}) + \hat{B}_{j-\frac{1}{2}}^{(n-1)} \hat{E}_{j-\frac{1}{2}}^{(n)} - \hat{F}_{j-\frac{1}{2}}^{(n)} (\hat{A}_{j-\frac{1}{2}}^{(n)} - \hat{A}_{j-\frac{1}{2}}^{(n-1)}) - \hat{F}_{j-\frac{1}{2}}^{(n-1)} \hat{A}_{j-\frac{1}{2}}^{(n-1)} \right\} \quad (\text{A.5.16})$$

$$\hat{\alpha}_j^{(n)} = 2\sigma h_j \hat{F}_j^{(n)} + \frac{2\sigma h_j}{\Delta_n} \hat{\gamma}_{j-\frac{1}{2}}^{(n-1)} (\hat{F}_{j-\frac{1}{2}}^{(n)} - \hat{F}_{j-\frac{1}{2}}^{(n-1)}) \quad (\text{A.5.17})$$

$$\bar{\alpha}_j^{(n)} = 2\sigma h_j \hat{F}_{j-1}^{(n)} + \frac{2\sigma h_j}{\Delta_n} \hat{\gamma}_{j-\frac{1}{2}}^{(n-1)} (\hat{F}_{j-\frac{1}{2}}^{(n)} - \hat{F}_{j-\frac{1}{2}}^{(n-1)}) \quad (\text{A.5.18})$$

$$\hat{\beta}_j^{(n)} = 2\sigma h_j \hat{E}_j^{(n)} - \frac{2\sigma h_j}{\Delta_n} \hat{\gamma}_{j-\frac{1}{2}}^{(n-1)} (\hat{E}_{j-\frac{1}{2}}^{(n)} - \hat{E}_{j-\frac{1}{2}}^{(n-1)}) \quad (\text{A.5.19})$$

$$\bar{\beta}_j^{(n)} = 2\sigma h_j \hat{E}_{j-1}^{(n)} - \frac{2\sigma h_j}{\Delta_n} \hat{\gamma}_{j-\frac{1}{2}}^{(n-1)} (\hat{E}_{j-\frac{1}{2}}^{(n)} - \hat{E}_{j-\frac{1}{2}}^{(n-1)}) \quad (\text{A.5.20})$$

$$\hat{\mu}_j^{(n)} = 2\sigma h_j \hat{B}_j^{(n)} - \frac{2\sigma h_j}{\Delta_n} \sum_{\frac{1}{2}}^{n-\frac{1}{2}} (\hat{B}_{j-\frac{1}{2}}^{(n)} + \hat{B}_{j-\frac{1}{2}}^{(n-1)}) \quad (\text{A.5.21})$$

$$\bar{\mu}_j^{(n)} = 2\sigma h_j \hat{B}_{j-1}^{(n)} - \frac{2\sigma h_j}{\Delta_n} \sum_{\frac{1}{2}}^{n-\frac{1}{2}} (\hat{B}_{j-\frac{1}{2}}^{(n)} + \hat{B}_{j-\frac{1}{2}}^{(n-1)}) \quad (\text{A.5.22})$$

$$\hat{D}_j^{(n)} = \delta + 2\sigma h_j \hat{A}_j^{(n)} + \frac{2\sigma h_j}{\Delta_n} \sum_{\frac{1}{2}}^{n-\frac{1}{2}} (\hat{A}_{j-\frac{1}{2}}^{(n)} - \hat{A}_{j-\frac{1}{2}}^{(n-1)}) \quad (\text{A.5.23})$$

$$\bar{D}_j^{(n)} = -\delta + 2\sigma h_j \hat{A}_{j-1}^{(n)} + \frac{2\sigma h_j}{\Delta_n} \sum_{\frac{1}{2}}^{n-\frac{1}{2}} (\hat{A}_{j-\frac{1}{2}}^{(n)} - \hat{A}_{j-\frac{1}{2}}^{(n-1)}). \quad (\text{A.5.24})$$

The recurrence relations (7.3.9) give

$$\delta \hat{A}_j^{(n)} - \delta \hat{A}_{j-1}^{(n)} - \frac{1}{2} h_j (\delta \hat{B}_j^{(n)} + \delta \hat{B}_{j-1}^{(n)}) = \hat{k}_{j-\frac{1}{2}}^{(n)} \quad (\text{A.5.25})$$

$$\delta \hat{B}_j^{(n)} - \delta \hat{B}_{j-1}^{(n)} - \frac{1}{2} h_j (\delta \hat{C}_j^{(n)} + \delta \hat{C}_{j-1}^{(n)}) = \hat{l}_{j-\frac{1}{2}}^{(n)} \quad (\text{A.5.26})$$

$$\delta \hat{D}_j^{(n)} - \delta \hat{D}_{j-1}^{(n)} - \frac{1}{2} h_j (\delta \hat{E}_j^{(n)} + \delta \hat{E}_{j-1}^{(n)}) = \hat{m}_{j-\frac{1}{2}}^{(n)} \quad (\text{A.5.27})$$

$$\delta \hat{E}_j^{(n)} - \delta \hat{E}_{j-1}^{(n)} - \frac{1}{2} h_j (\delta \hat{F}_j^{(n)} + \delta \hat{F}_{j-1}^{(n)}) = \hat{n}_{j-\frac{1}{2}}^{(n)} \quad (\text{A.5.28})$$

where

$$\hat{k}_{j-\frac{1}{2}}^{(n)} = -\hat{A}_j^{(n)} + \hat{A}_{j-1}^{(n)} + \frac{1}{2} h_j (\hat{B}_j^{(n)} + \hat{B}_{j-1}^{(n)}) \quad (\text{A.5.29})$$

$$\hat{l}_{j-\frac{1}{2}}^{(n)} = -\hat{B}_j^{(n)} + \hat{B}_{j-1}^{(n)} + \frac{1}{2} h_j (\hat{C}_j^{(n)} + \hat{C}_{j-1}^{(n)}) \quad (\text{A.5.30})$$

$$\hat{m}_{j-\frac{1}{2}}^{(n)} = -\hat{D}_j^{(n)} + \hat{D}_{j-1}^{(n)} + \frac{1}{2} h_j (\hat{E}_j^{(n)} + \hat{E}_{j-1}^{(n)}) \quad (\text{A.5.31})$$

$$\hat{n}_{j-\frac{1}{2}}^{(n)} = -\hat{E}_j^{(n)} + \hat{E}_{j-1}^{(n)} + \frac{1}{2} h_j (\hat{F}_j^{(n)} + \hat{F}_{j-1}^{(n)}). \quad (\text{A.5.32})$$

At the wall from (7.3.16) we have

$$\delta \hat{A}_0^{(n)} = -\hat{A}_0^{(n)}, \quad \delta \hat{B}_0^{(n)} = -\hat{B}_0^{(n)}, \quad \delta \hat{F}_0^{(n)} = -\hat{F}_0^{(n)} \quad (\text{A.5.33})$$

while at the outer edge from (7.3.17) we have

$$\delta \hat{D}_J^{(n)} = -\hat{D}_J^{(n)}, \quad \delta \hat{B}_J^{(n)} = -\hat{B}_J^{(n)}, \quad \delta \hat{E}_J^{(n)} = -\hat{E}_J^{(n)} \quad (\text{A.5.34})$$

The matrix system represented by (A.5.6) - (A.5.34) consists of $6J + 6$ equations which may be assembled into a single matrix equation

$$\bar{A}\bar{x} = \bar{B}.$$

(A.5.35)

This has a similar structure to that obtained for the region $0 < x_3 < 1$ although the constants $\hat{a}, \bar{a}, \hat{b}, \bar{b}, \hat{c}, \bar{c}, \hat{d}, \bar{d}, \hat{e}, \bar{e}, \hat{s}, \bar{s}, \hat{\gamma}, \bar{\gamma}, \hat{\alpha}, \bar{\alpha}, \hat{\beta}, \bar{\beta}, \hat{\mu}, \bar{\mu}, \hat{\nu}, \bar{\nu}, \hat{T}$ and \hat{R} are different. The system was solved in the same way.

REFERENCES

- Bejan, A., Al-Homoud, A.A. & Imberger, J. (1981) Experimental study of high Rayleigh number convection in a horizontal cavity with different end temperatures. *J. Fluid Mech.* 109, 283.
- Bejan, A. & Rossie, A.N. (1981) Natural convection in a horizontal duct connecting two fluid reservoirs. *J. Heat Transfer* 103, 108.
- Blythe, P.A., Daniels, P.G. & Simpkins, P.G. (1981) Thermally driven cavity flows in porous media I. The vertical boundary-layer structure near the corners. *Proc. Roy. Soc. A380*, 119.
- Blythe, P.A. & Simpkins, P.G. (1977) Thermal convection in a rectangular cavity. *Physico-Chem. Hydrodynamics* 2, 511.
- Boyack, B.E. & Kearney, D.W. (1972) Heat transfer by laminar natural convection in low aspect ratio cavities. ASME Paper, 72-HT-2.
- Catton, I. (1978) Natural convection in enclosures. *Proc. 6th Int. Heat Transfer Conf., Toronto, Canada*, 13.
- Cormack, D.E., Leal, L.G. & Imberger, J. (1974a) Natural convection in a shallow cavity with differentially heated end walls. Part 1. Asymptotic theory. *J. Fluid Mech.* 65, 209.
- Cormack, D.E., Leal, L.G. & Seinfeld, J.H. (1974b) Natural convection in a shallow cavity with differentially heated end walls. Part 2. Numerical solutions. *J. Fluid Mech.* 65, 231.
- Daniels, P.G., Blythe, P.A. & Simpkins, P.G. (1982) Thermally driven cavity flows in porous media II. The horizontal boundary-layer structure. *Proc. Roy. Soc. A382*, 135.
- Daniels, P.G., Blythe, P.A. & Simpkins, P.G. (1987a) High Rayleigh number thermal convection in a shallow laterally heated cavity. AT & T Bell Laboratories TM. 11523-871019-61.
- Daniels, P.G., Blythe, P.A. & Simpkins, P.G. (1987) Onset of multicellular convection in a shallow laterally heated cavity. *Proc. Roy. Soc. A411*, 327.
- Daniels, P.G. & Wang, P. (1990) Private Communication.
- Defant, A. (1961) *Physical oceanography Vol. I* New York: Pergamon Press.
- Drummond, J.E. & Korpela, S.A. (1987) Natural convection in a shallow cavity. *J. Fluid Mech.* 182, 543.
- Eckert, E.R.G. & Carlson, W.O. (1961) Natural convection in an air layer enclosed between two vertical plates with different temperatures. *Int. J. Heat Mass Transfer* 2, 106.

- Elder, J.W. (1965) Laminar free convection in a vertical slot. *J. Fluid Mech.* 23, 77.
- Gaskell, P.H. & Wright, N.G. (1987) A multigrid algorithm for the investigation of thermal recirculating fluid flow problems. *Proc. 5th Int. Conf. on Num. Meth. for Thermal Problems*, Montreal, Canada.
- Gill, A.E. (1966) The boundary-layer regime for convection in a rectangular cavity. *J. Fluid Mech.* 26, 515.
- Gill, A.E. (1974) A theory of thermal oscillations in liquid metals. *J. Fluid Mech.* 64, 577.
- Glauert, M.B. (1956) The wall jet. *J. Fluid Mech.* 1, 625.
- Goldstein, S. (1938) *Modern developments in Fluid Dynamics*, Vol.2 §273 Oxford Univ. Press.
- Hadley, G. (1735) Concerning the cause of the general trade winds. *Phil. Trans. Roy. Soc.* 39, 58.
- Haldenwang, P. & Labrosse, G. (1986) 2-D and 3-D spectral Chebyshev solutions for free convection at high Rayleigh number. *Proc. 6th Int. Symp. on Finite Element Methods in Flow Problems*, Antibes, France.
- Hart, J.E. (1972) Stability of thin non-rotating Hadley circulations. *J. Atmos. Sci.* 29, 687.
- Hart, J.E. (1983a) A note on the stability of low Prandtl number Hadley circulations. *J. Fluid Mech.* 132, 271.
- Hart, J.E. (1983b) Low Prandtl number convection between differentially heated end walls. *Int. J. Heat Mass Transfer* 26, 1069.
- Hillman, A.P. & Salzer, H.E. (1943) Roots of $\sin z = z$. *Phil. Mag.* 34, 575.
- Hurle, D.T.J. (1966) Temperature oscillations in molten metals and their relationship to growth striae in melt-grown crystals. *Phil. Mag.* 13, 305.
- Hurle, D.T.J., Jakeman, E. & Johnson, C.P. (1974) Convective temperature oscillations in molten gallium. *J. Fluid. Mech.* 64, 565.
- Imberger, J. (1974) Natural convection in a shallow cavity with differentially heated end walls. Part 3. Experimental results. *J. Fluid Mech.* 65, 247.
- Jeffreys, (1925) On fluid motions produced by differences of temperature and humidity. *Quart. J. Roy. Met. Soc.* 51. 347.
- Kuiken, H.K. (1968) An asymptotic solution for large Prandtl number free convection. *J. Eng. Math.* 2. 355.

- Kuo, K.P., Korpela, S.A., Chait, A. & Marcus, P.S. (1986) Stability of natural convection in a shallow cavity. Proc. 8th Int. Heat Transfer Conf., San Francisco, 1539.
- Ostrach, S. (1952) An analysis of laminar free convection flow and heat transfer about a flat plate parallel to the direction of the generating body force. N.A.C.A. Rep. 1111.
- Ostrach, S. (1972) Natural convection in enclosures. Adv. Heat Transfer 8, 161.
- Ostrach, S., Loka, R.R. & Kumar, A. (1980) Natural convection in low aspect ratio rectangular enclosures. In 19th Nat. Heat Transfer Conf., Orlando, ASME Heat Transfer Division 8, 1.
- Quon, C. (1972) High Rayleigh number convection in an enclosure - a numerical study. Physics Fluids 15, 12.
- Quon, C. (1977) Free convection in an enclosure revisited. J. Heat Transfer 99, 340.
- Robbins, C.I. & Smith, R.C.T. (1948) A table of roots of $\sin z = -z$. Phil. Mag. 39, 1005.
- Rosby, H.T. (1965) On thermal convection driven by non-uniform heating from below: an experimental study. Deep Sea Res. 12, 9.
- Shiralkar, G.S. & Tien, C.L. (1981) A numerical study of laminar natural convection in shallow cavities. J. Heat Transfer 103, 226.
- Simpkins, P.G. & Chen, K.S. (1986) Convection in horizontal cavities. J. Fluid Mech. 166, 21.
- Simpkins, P.G. & Dudderar, T.D. (1981) Convection in rectangular cavities with differentially heated end walls. J. Fluid Mech. 110, 433.
- Smith, F.T. (1974) Boundary layer flow near a discontinuity in wall conditions. J. Inst. Math. Applics. 13, 127.
- Smith, F.T. (1976) On entry flow effects in bifurcating, blocked or constricted tubes. J. Fluid Mech. 78, 709.
- Smith, F.T. & Duck, P.W. (1977) Separation of jets or thermal boundary layers from a wall. Quart.J. Mech. Appl. Math. 31, 473.
- Stern, M. (1975) Ocean Circulation Physics. New York: Academic Press.
- Winters, K.H. (1983) Predictions of laminar natural convection in heated cavities. Num. Meth. in Heat Transfer, Vol.2 ,179.